Innovative Approaches To Peptide-Fatty Acid Conjugates: Towards A Novel Blood Brain Barrier Delivery Vector

Shawnm Abdullah

A thesis submitted in partial fulfilment of the requirements of Nottingham Trent University for the degree of Doctor of Philosophy

Tuesday, 11th February 2025

Copyright Notice

Acknowledgement

First of all, I would like to thank our almighty and gracious Allah. Without His perfect blessings, help, and provision of excellent health during the work on this thesis, I would not have been able to complete this project.

I would like to thank and express my gratitude and appreciation to my director of the study, Prof. Gareth Cave, who has continuously conveyed an adventurous spirit with regard to research that gave me the possibility to direct the project in a positive direction. He always motivated me when I was feeling low and when I thought that I would not be able to complete the work. Without his help (continuous support, expertise, valuable discussions, and guidance through all the meetings we had), I would not have been able to complete this project. I greatly appreciate his willingness and enthusiasm to assist me.

Thanks so much for the kind help of Prof. Rob Morries, who is my second supervisor. I never forget your advice, and it made me strong.

I am grateful to my parents (may God keep both of you in his paradise) for teaching me that I had to fight for what I wanted in life. Without their teaching and encouragement, I would not have advanced so far with regard to my academic career and my personal development. I am sure your soul is with me all the time. I lost both of you during my Ph.D. journey. God only knows how difficult that time was.

Special thanks to Prof. Carrole Perry, Dr. Waren Cross, and Prof. John Wails, whose impact on my work was beyond imagination. I never forget your kindness.

I would like to thank my friend Sheila. She is a very kind person who always trusted in me and gave me the force I needed in order to progress. I appreciate your help, and I will never forget you.

Special thanks to Dr. Biola Egbowon and Krishna, whos impact on my work was beyond imagination. They gave me all the resources and

consumables they had to help me in cell culturing. God bless both of you!

I want to express my heartfelt gratitude to everyone who has contributed to my Ph.D. experience, making it much more rewarding. Ryan Lakey, Nigel Mould, Joanny Coffey, Barbara Stevenson, and Hannah Beska, the amazing technical team at ISTeC, welcomed me into their labs and provided me with everything I required. Many thanks to my friend Asmae, who always believed in me and encouraged me to keep going. Thanks so much Krishnaperiya and Manisha for your kind help. I appreciate it.

I dedicate this thesis to my lovely husband, Sardar Hama Salih, for the unconditional support and love he provided me throughout my PhD. None of this work would have been possible without him, and I am forever grateful for his help. I also dedicate this thesis to my lovely princesses Lisa and Muhammad, who felt all my tiredness even as children; both of you are my soul.

Abstract

The human brain is protected by a semipermeable barrier, namely the blood-brain barrier (BBB). The administration of biotherapeutics across the blood-brain barrier remains a formidable challenge due to the barrier's protective nature. The intricate mechanism that drives the progression of neurodegenerative disease, for instance, Alzheimer's disease, presents significant challenges in the search for innovative therapeutic interventions. Despite these challenges, studying neurodegenerative disease remains a crucial area of scientific research, with global scientific organisations striving to develop viable therapies.

This study investigates the embedding of cationic cell-penetrating peptides (CPPs) into liposomes to create innovative vectors that penetrate the BBB and facilitate the delivery of drugs to the brain. The brain-targeted drug delivery system was produced *via* a microfluidic system. Microwave solid-phase peptide synthesis (MSPPS) was used to produce CPPs and ionic peptides, and characterisated by LC-MS, ^{1}H and ^{13}C NMR. This research also explored the possibility of linking these peptides to three distinct fatty acids (myristic acid, palmitic acid and lauric acid) to facilitate embedding them into the liposomes, while also enhancing their stability and protecting them against enzymatic degradation. The microfluidic lab-on-a-chip was used to prepare the liposomal vector and load them with the carnosine; as a model drug.

In this research, the vectors, with either cationic or ionic peptides conjugated to three distinct fatty acids embedded into liposomes, were applied to an *in vitro* human BBB model to evaluate performance and toxicity *via* live cell imaging and MTT assay, respectively. The MTT assay results demonstrated that the vectors embedded with cationic peptides conjugated to fatty acids maintained cell viability above 90% over 72 hours. Live cell imaging demonstrated that endothelial cells treated with these vectors remained viable during the observation period.

The vectors functionalised with cationic CPP-conjugated fatty acids (cationic) were able to deliver the carnosine across the BBB, however, the vectors with ionic peptides, which have a negative charge similar to the cell membrane, did not pass through.

These findings suggest that cationic peptides combined with fatty acids embedded into liposomes hold promise as vectors for the delivery of therapeutics to the brain, particularly for the treatment of neurological diseases such as Alzheimer's disease.

Table of Contents

Table Of Figures

List of Tables

Abbreviation

WHO	World Health Organisation
DNA	Deoxyribonucleic Acid
AD	Alzheimer`s disease
PD	Parkinson's disease
DALYs	Disability-Adjusted Life Years
YLDs	Years Lived with Disability
YLLs	Years of Life Lost
GBD	Global Burden of Disease
IGAP	Intersectoral Global Action Plan
Aβ	Amyloid-beta
APP	Amyloid Precursor Protein
NFTs	Neurofibrillary Tangles
ROS	Reactive Oxygen Species
NMDA	N-methyl-D-aspartate
APOE	Apolipoprotein E
EOAD	Early-Onset Alzheimer's Disease
APOEε4	Apolipoprotein E gene
FDA	Food and Drug Administration
IV	Intravenous
BBB	Blood-Brain Barrier
CNS	Central Nervous System
BCSFB	Blood-Cerebrospinal Fluid Barrier
TEER	Trans-Endothelial Electrical Resistance
NVU	Neurovascular Unit
JAMs	Junctional Adhesion Molecules
CMT	Carrier-Mediated Transport
RMT	Receptor-Mediated Transcytosis

MAOs	Mono Amine Oxidases
GSTs	Glutathione S-Transferases
PSA	Polar Surface Area
HIV	Human Immunodeficiency Virus
P-gp	P-glycoprotein
MRPs	Multidrug Resistance-associated Proteins
BCRP	Breast Cancer Resistance Protein
CPP	Cell-penetrating peptides
TAT	Trans Activator of Transcription peptide
PR	PolyArginine
SPPS	Solid Phase Peptide Synthesis
MSPPS	Microwave solid phase peptides synthesis
Boc	Tert-Butyloxycarbonyl
Fmoc	9-Fluorenylmethyloxycarbonyl
HBTU	Benzotriazole N,N,N',N'-tetrafluorophosphate
PEG	Polyethene Glycol
PS	PhosphatidylSerine
PI	Phosphatidylinositol
PC	PhosphatidylCholine
PG	PhosphatidylGlycerol
PA	Phosphatidic acid
DPPC	Dipalmitoyl phosphatidyl choline
HSPC	Hydrogenated Soy Phosphatidylcholine
POPC	1-palmitoyl-2-oleoyl-sn-glycero-3-phosphocholine
SUVs	Small unilamellar vesicles
MLVs	Multilamellar vesicles
μB	Microbubble
IN	Intranasally

MTT	5-(4,5-dimethyl-2-thiazolyl)-2,5-diphenyl-2H tetrazolium bromide
FITC	Fluorescent Isothiocyanate
LC-MS	Liquid chromatography-mass spectrometry
MeOH	Methanol
NMR	Nuclear magnetic resonance
SEM	Scanning Electron Microscopy
PDI	Polydispersity index
DLS	Dynamic light scattering
D	Aspartic acid
E	Glutamic acid
R	Arginine
K	Lysine
hCMEC/D3	human endothelial cell
hEGF	Epidermal growth factor human
DMF	Dimethyl formamide
DIPEA	Diisopropylethylamine
DCM	Dichloromethane
TFA	Trifluoroacetic acid
TIPS	Triisopropylsilane
PDCs	Peptide-drug conjugates
NOS	Nitric oxide synthase
DNS	Dansyl chloride
PBS	Phosphate-buffered saline
OCTs	Organic cationic transporters
SEC	Size exclusion chromatography

Chapter 1: Introduction

1.1 Neurological disorders

Neurological disorders encompass a wide range of conditions that affect the brain, spinal cord, and peripheral nerves, leading to various physical and cognitive impairments. There are different types of these disorders, such as neurodegenerative diseases (like Alzheimer's and Parkinson's), congenital conditions (like tuberous sclerosis and neurofibromatosis that are passed down through families and can affect brain structure and function), and traumatic injuries (like traumatic brain injury (TBI) that can cause immediate and long-term neurological deficits).[1–4]

The causes, signs, and course of these diseases differ. Certain neurological conditions have a high mortality rate; others cause persistent damage (disability). While there is no known cure for some of these diseases, others may be prevented or treated.[3,5] One of the most noteworthy outcomes of global health systems is the increase in life expectancy. However, age-related neurological conditions like Parkinson's disease (PD), stroke, Alzheimer's disease, and other dementias have also increased as a result of this increase. Therefore, global health strategies should prioritise not only survival but also the mitigation of health deterioration due to disability, by encouraging independence and functionality. The neurological load is not entirely explained by population ageing, underscoring the significance of precisely assessing the overall health impact of illnesses of the nervous system at every stage of life. The global burden of neurodegenerative diseases is significant, with varying prevalence and age distribution across different regions.[6,7] see Table 1.1. Alzheimer's disease: The incidence increased from 507.96 per 100,000 in 1990 to 569.39 per 100,000 in 2019, particularly affecting those aged 60 and above.[8] Parkinson's Disease: Increases in age-standardised incidence rates

were observed, especially in high Social Development Index (high-SDI) regions.[9] Multiple Sclerosis: Primarily affects younger adults, with a significant prevalence in women.[10]

Table 1.1: According to the WHO's data, the following table summarises key neurodegenerative diseases, their global prevalence percentages, and the age groups most affected.

Disease	Global Prevalence (%)	Age Group Most Affected
Alzheimer's Disease	0.6%	60 years and older
Parkinson's Disease	0.3%	60 years and older
Multiple Sclerosis	0.1%	20-40 years
Motor Neuron Disease	0.01%	50-70 years
Huntington's Disease	0.01%	30-50 year

Neurological disorders are the primary cause of Disability-Adjusted Life Years (DALYs) and the second most common cause of mortality worldwide, resulting in 9 million fatalities annually. In 2016, the leading causes of neurological DALYs were stroke (42.2%), migraine (16.3%), dementia (10.4%), meningitis (7.9%), and epilepsy (4.9%).[11] In 2021, neurological diseases affected over 3 billion people worldwide, constituting 43.1% of the global population. These conditions resulted in the deaths of 9 million individuals and contributed to 168 million Years Lived with Disability (YLDs) and 275 million Years of Life Lost (YLLs). According to the Global Burden of Disease (GBD) 2021, the expanded nervous system category ranked first worldwide in terms of

Disability-Adjusted Life Years (DALYs) and Years of Life Lost (YLLs), accounting for a total of 443 million DALYs. Among individuals aged 60-79 years, the prevalence of Alzheimer's disease and other dementias is 1,504.2 per 100,000 people. For those aged 80 years and above, the prevalence of Alzheimer's disease and other dementias is 13,047 per 100,000 people, along with a prevalence of Parkinson's disease of 1,773.2 per 100,000 people.[1]

In May 2022, the World Health Assembly approved the Intersectoral Global Action Plan on Epilepsy and Other Neurological Disorders 2022-2031 (IGAP) to address the increasing prevalence of nervous system illnesses and conditions globally. The primary objective of the action plan is to diminish the negative perception, consequences, and burden of neurological illnesses, including the resulting death, illness, and disability. Additionally, it strives to enhance the overall well-being of individuals with neurological disorders, their caregivers and families.[3] Neurological problems result in higher expenses for governments, communities, families, and individuals, as well as reduced economic output. In 2010, the estimated cost of brain illnesses in Europe alone was €798 billion.[12] The anticipated overall worldwide societal cost of dementia in 2019 amounted to US$1.3 trillion, which is equivalent to 1.5% of the global GDP.[11]

1.2 Alzheimer’s disease (AD)

AD is a progressive neurodegenerative disorder which bears the name of the German doctor Alois Alzheimer, and the most prevalent type of dementia is Alzheimer's disease.[13] In the United Kingdom, Alzheimer's disease accounts for about two-thirds of dementia diagnoses. The progression of Alzheimer's disease alters the structure and function of the brain, causing symptoms that commonly remain undiagnosed for many years.[4] AD is characterised by the accumulation of amyloid-beta plaques and neurofibrillary tangles composed of hyperphosphorylated tau proteins in the brain.[13–16] (See Figure 1.1) Synaptic dysfunction,

neuronal loss, and brain atrophy are all signs of a problem. This is especially true in the hippocampus and cortex, which are important for memory and thinking. Clinically, AD manifests as a gradual decline in cognitive abilities, including memory, language, executive function, and visuospatial skills, ultimately impairing daily living activities and leading to dementia. The disease predominantly affects individuals over the age of 65, with early-onset cases occurring in a minority of patients due to genetic mutations in the APP, PSEN1, and PSEN2 genes. The aetiology of AD is multifactorial, involving genetic, environmental, and lifestyle factors, with age being the most significant risk factor.[17–23]

When Alois Alzheimer examined the brain of his first patient, who exhibited behavioural changes and memory loss, he observed amyloid plaques and a significant decrease in neurons. This led him to identify the condition as a debilitating disorder affecting the cerebral cortex. Alzheimer's disease can be classified into two types based on the age of onset: early-onset and late-onset Alzheimer`s disease.[24]

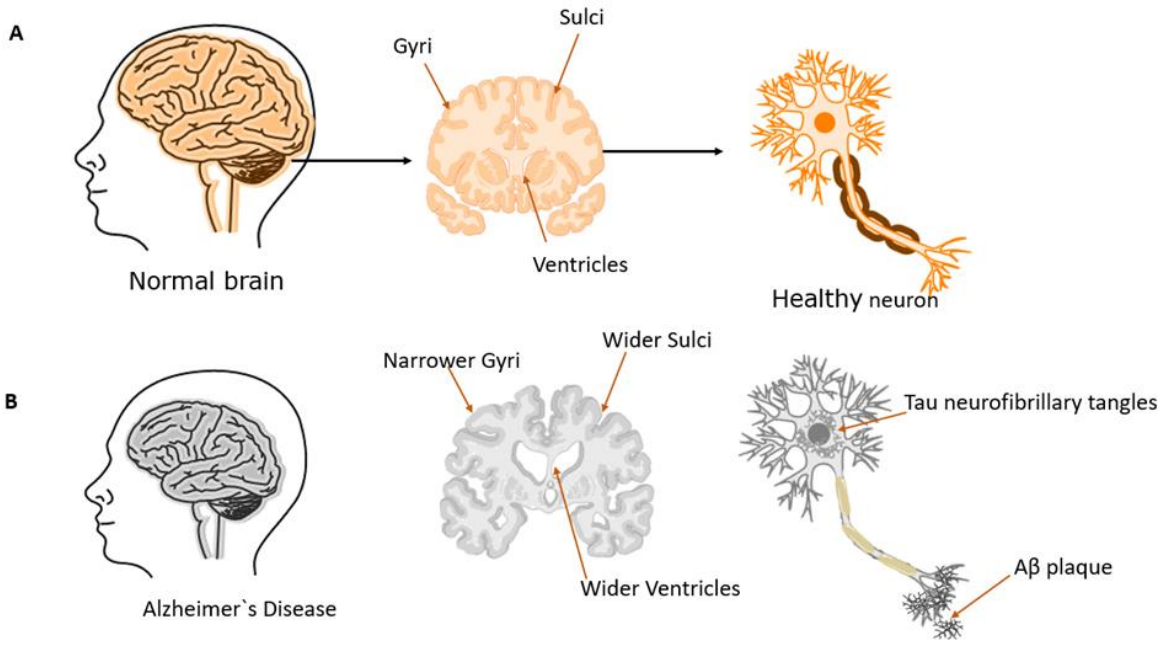

Figure 1.1: Illustrates the schematic representation of the brains of a normal individual (A) and an Alzheimer's disease patient (B); both have the same anatomical makeup of neurones and brain tissue. It illustrates the distinctions between an Alzheimer's-affected and a normal brain. Alzheimer's disease brains have wider sulci gaps, smaller gyri, and larger ventricles than those of a healthy brain when seen laterally. (Image created by BioRender.)

1.3 Cause of Alzheimer`s disease

Neurological illnesses can be caused by a variety of particular factors, including genetic disorders, birth defects or imbalances, infections, health problems in the environment or lifestyle, like not getting enough food, and brain, spinal cord, or nerve injuries. Over the years, researchers have proposed five primary hypotheses as potential causes of Alzheimer's disease. These have been summarised below.

1.3.1 Amyloid-beta (Aβ)

The amyloid cascade hypothesis implicates the amyloid precursor protein (APP) in the pathogenesis of Alzheimer's disease. This is how

the body normally works: α- and γ-secretase enzymes cut the APP gene on chromosome 21, which makes two soluble peptides called P3 and APP. These peptides are known to protect neurones from excitotoxicity and regulate neural stem cell growth. In unhealthy conditions, on the other hand, β- and γ-secretase enzymes cut APP in a certain order, creating Aβ peptides that cannot be dissolved (see Figure 1.2). These Aβ peptides exert neurotoxic effects on brain tissue, contributing to the development of dementia. The amyloid cascade hypothesis is further supported by the involvement of presenilin proteins (PSEN1 and PSEN2) in the β-secretase complex, which significantly influences the generation of Aβ from APP. Mutations in these presenilin proteins are associated with the familial transmission of Alzheimer's disease. Consequently, current research efforts are focused on developing therapeutic agents that target various aspects of Aβ pathology, including reducing Aβ production, enhancing its clearance, or inhibiting its aggregation.[25,26]

There are two primary forms of Aβ found in the brain: soluble and fibrillar forms, specifically Aβ40 and Aβ42. Due to its hydrophobic nature, Aβ42 is prone to misfolding and aggregation, transitioning from its original α-helical structure to a β-pleated sheet configuration. This structural transformation leads to the formation of neurotoxic senile plaques.[27] The degree of neurotoxicity associated with Aβ is determined by its rapid conversion to the β-pleated sheet structure.[28,29] Furthermore, β-peptides, which consist of 36–43 amino acids, play a significant role in Alzheimer's disease. The β-secretase enzyme cleaves APP to produce a C-terminal fragment (APP-CTF), which is subsequently processed by γ-secretase to form Aβ peptides. The excessive production of Aβ peptides, along with oligomer formation, disrupts proper peptide folding and leads to the accumulation of amyloid plaques and neurofibrillary tangles (NFTs). These aggregates are detrimental to neuronal health and ultimately result in neuronal death.[25–27,29]

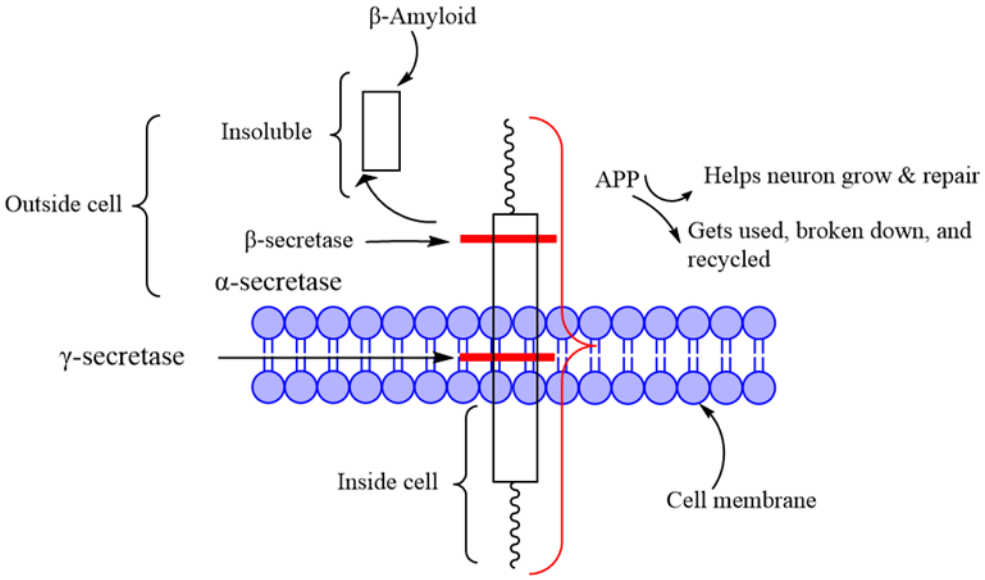

Figure 1.2: Illustrates the process that generates Aβ. (The image created by Chemdrow).

1.3.2 The dysregulation mechanism of intracellular calcium ion homeostasis in Aβ-induced neurotoxicity.

Calcium ions (Ca^{2+}) act as crucial chemical messengers for regulating homeostasis, with extracellular concentrations being higher than intracellular concentrations. The formation of Aβ plaques causes dysfunction or imbalance in the channels that transport calcium across the cell membrane. This leads to an elevated influx of Ca^{2+}, which may result in Aβ-peptide toxicity in Alzheimer's disease. Excessive intracellular calcium ions levels impair the mitochondria's ability to regulate or process Ca^{2+}, causing cellular toxicity and ultimately leading to cell death. The amyloid beta protein, a key component of senile plaques, has been shown to increase Ca^{2+} influx and produce free radicals, which may further enhance neurotoxicity. It has been reported that amyloid-beta (Aβ1–42) peptides can cause a significant influx of Ca^{2+} into neurones. This excessive accumulation of Ca^{2+} in the mitochondria within neurones eventually leads to cell death.[30] This statement is supported by research indicating that Aβ oligomers promote Ca^{2+} entry into neurones, leading to mitochondrial Ca^{2+}

overload. This overload triggers the opening of the mitochondrial permeability transition pore (mPTP), resulting in the release of apoptotic factors and ultimately causing cell death.[31]

1.3.3 The phosphorylation of tau proteins and their variants is a key aspect of the tau hypothesis.

Tau proteins, also known as τ proteins, are highly prevalent in neurones and play a crucial role in the stabilisation of neuronal microtubules. These proteins are encoded by the MAPT gene, located on the chromosome 17.[32] The tau protein hypothesis is based on the fact that the brain has intracellular neurofibrillary tangles (NFTs), which are a sign of Alzheimer's disease and look like senile plaques (See Figure 1.3). NFTs are made up of helical filaments and straight filaments that are tangled together. They are mostly caused by hyperphosphorylated tau protein. Tau protein is the most common microtubule-associated protein in neurones. It plays a significant physiological role by collaborating with microtubule proteins to facilitate the formation of microtubules. Additionally, tau protein helps stabilise microtubules and promotes their clustering. The threonine-serine kinase GSK-3β excessively phosphorylates tau protein, specifically at Ser396, Ser199, and Ser413, increasing the number of phosphate groups on the protein from 2e3 to 5e9. As a result, tau protein detaches from microtubules and forms insoluble NFTs, ultimately leading to cell death. GSK-3β can phosphorylate the tau protein. Furthermore, excessive GSK-3β activity may affect γ-secretase, which uniquely causes the production of Aβ, ultimately damaging cultured neurons.[33–36]

As individuals age, the human brain increases the activity of phosphatases, resulting in the presence of six τ-isoforms that are susceptible to phosphorylation. During the embryonic stage, a certain type of foetal protein is produced more abundantly during the phosphorylation process than in adulthood. This imbalance may lead

to the formation of neurofibrillary tangles and senile plaques, which are associated with Alzheimer's disease.[32]

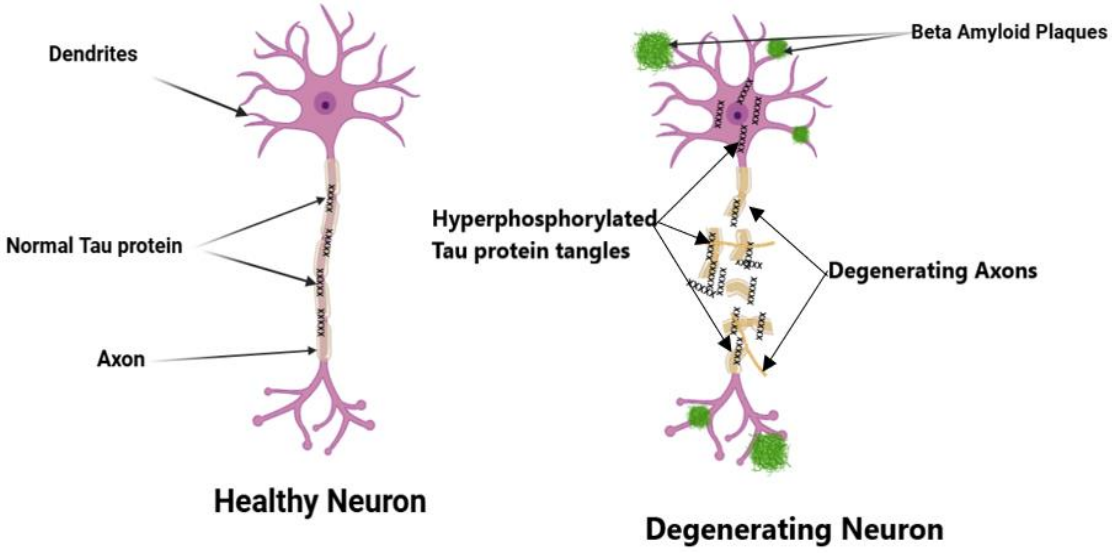

Figure 1.3: The pathological changes of neurones in Alzheimer's disease are illustrated. Healthy neurones have normal tau protein and regular axons, but in degenerating neurones the axons degenerate. (The image created by BioRender.)

1.3.4 Glycogen Synthase Kinase-3 and Alzheimer's Disease

Many individuals with Alzheimer's disease exhibit abnormalities in the enzyme glycogen synthase kinase-3 (GSK-3), which is implicated in the production of neurofibrillary tangles and the accumulation of amyloid-beta. GSK-3 actively promotes the production of Aβ and the hyperphosphorylation of tau proteins, leading to the formation of NFTs. These pathological features are central to the neurodegenerative processes observed in AD.[37,38] GSK-3 has garnered significant attention in research due to its role in various disorders, including type II diabetes, Alzheimer's disease, inflammation, cancer, bipolar disorder, glycogen metabolism, and gene transcription.[39] Clinical trials are currently underway to evaluate the therapeutic benefits of GSK-3

inhibitors for Alzheimer's disease. Lithium, a specific inhibitor of GSK-3, is administered as a mood stabiliser for individuals with bipolar disorder and is also being explored for its potential benefits in Alzheimer's disease.[26,40] Lithium's neuroprotective properties include reducing tau hyperphosphorylation, decreasing Aβ production, and mitigating neuroinflammation. [41] Despite the promising potential of GSK-3 inhibitors, there has been limited progress in developing effective medications. Ongoing research aims to identify and optimise GSK-3 inhibitors so they can provide therapeutic benefits while minimising adverse effects.[41,42]

1.3.5 Glutamate toxicity

Excessive glutamate, an amino acid heavily involved in protein synthesis, can lead to harmful effects known as glutamate neurotoxicity. Glutamate is particularly prevalent in the nervous system and acts as a neurotransmitter in over 90% of synaptic transmissions in the human brain.[43] The receptors for glutamate include AMPA receptors, NMDA receptors, and metabotropic glutamate receptors. AMPA receptors are ionotropic receptors that play a role in rapid synaptic excitation. On the other hand, N-methyl-*D*-aspartate receptor (NMDA) receptors, which are also ionotropic, help Ca^{2+} enter cells and play a role in memory and learning.[44] Mutations in glutamate transporters can lead to an increased concentration of glutamate in the blood compared to the brain. This imbalance can disrupt normal neurotransmission, potentially leading to neurological disorders. The calcium hypothesis has led to the development and testing of numerous drugs that function as NMDA receptor antagonists in clinical studies. These drugs, such as ketamine, memantine, and dextromethorphan, work by inhibiting the activity of NMDA receptors, thereby reducing the influx of Ca^{2+} and preventing the cascade of neurotoxic events.[26,45–47]

1.4 Role of biological and chemical factors in Alzheimer`s disorders

1.4.1 Malfunction of the mitochondria

Mitochondrial dysfunction in Alzheimer's disease is associated with impaired energy production, increased oxidative stress, and disrupted calcium homeostasis.[48,49] These abnormalities can lead to the degeneration of synaptic connections and neuronal death, which are critical for neurotransmitter release and synaptic transmission.[50] In particular, the less efficient electron transport chain and ATP production in mitochondria affect the energy needed for neurotransmitter production, vesicle loading, and release at synapses. Additionally, the accumulation of reactive oxygen species (ROS) and oxidative damage can further impair synaptic function and neurotransmitter release. Consequently, these mitochondrial dysfunctions contribute to the overall decline in neurotransmitter levels and synaptic transmission observed in Alzheimer's disease.[51]

1.4.2 Genetic

Apolipoprotein E (APOE) is the primary genetic factor associated with the development of Alzheimer's disease. Specific variants of the APOE gene can significantly increase an individual's susceptibility to AD. The APOE ε4 allele, in particular, is associated with a three- to four-fold increase in the risk of developing late-onset AD.[52,53] Approximately 66% of individuals in the UK who develop Alzheimer's disease possess this particular variant of APOE, making it one of the most significant factors influencing an individual's susceptibility to the LOAD. However, the APOE gene alone does not determine an individual's risk of dementia.[54] Patients with Alzheimer's disease often exhibit chromosomal mutations in chromosomes 1, 14, and 21. Mutations in the presenilin 1 (PSEN1) gene on chromosome 14 account for approximately 70% of early-onset

Alzheimer's disease (EOAD) cases, while mutations in the presenilin 2 (PSEN2) gene on chromosome 1 and the amyloid precursor protein (APP) gene on chromosome 21 are also implicated.[55,56]

Additionally, researchers have identified a strong association between mutations in chromosome 19 and late-onset Alzheimer's disease, with the APOE gene located on this chromosome.[55,57,58]

The theory of the function of APOE in Alzheimer's disease suggests that the APOE ε4 variant increases the risk of disease onset by influencing the metabolism of amyloid-beta (Aβ) peptides. APOE ε4 exhibits reduced efficacy in clearing Aβ from the brain, resulting in the formation of amyloid plaques, a hallmark of Alzheimer's disease.[59,60]

Plaque formation disrupts neuronal function and triggers a sequence of neurodegenerative events, such as inflammation and oxidative stress, ultimately leading to the memory loss associated with Alzheimer's disease.[61–64]

1.4.3 The autoimmune hypothesis

The autoimmune hypothesis posits that aberrant activation of the immune system can lead to the production of autoantibodies that target neuronal cells. This dysregulated immune response may be exacerbated by the production of amyloid-beta and the subsequent formation of amyloid plaques. These pathological processes contribute to the destruction of neurones, ultimately leading to the development of Alzheimer's disease. The hypothesis suggests that the immune system's failure to distinguish between self and non-self-antigens results in an autoimmune attack on neuronal tissues, thereby playing a critical role in the pathogenesis of AD.[65,66]

Recent studies have identified autoantibodies targeting brain proteins in patients with AD, suggesting that an autoimmune response might accelerate neuronal damage.[67] Chronic neuroinflammation, driven by

overactive microglia and astrocytes, is a hallmark of AD and is thought to be triggered by the presence of amyloid plaques and neurofibrillary tangles.[68–70]

1.4.4 The blood vessel hypothesis

Astrocytes play a crucial role in protecting neurones from oxidative stress by mitigating the effects of free radicals during the ageing process and in response to various stressors. Disruptions in cerebral blood flow can adversely affect the functioning of astrocytes, neurones, and glial cells, particularly in the hippocampus. Such vascular impairments may contribute to the pathogenesis of neurological diseases, including Alzheimer's disease. The hypothesis suggests that compromised blood flow leads to insufficient oxygen and nutrient supply, exacerbating neuronal damage and promoting the development of neurodegenerative conditions.[71]

1.4.5 Vitamin B12

Numerous studies have demonstrated a correlation between vitamin B12 deficiency and neurological disorders, including an increased susceptibility to Alzheimer's disease. Elevated homocysteine levels are a clear biomarker of insufficient vitamin B12, which may potentially cause brain damage through mechanisms such as oxidative stress, elevated intracellular calcium levels, and increased apoptosis. Vitamin B12 deficiency can be quantified through the evaluation of serum vitamin B12 levels, complete blood counts, and homocysteine assays. These diagnostic measures are essential for identifying deficiencies and mitigating the associated neurological risks.[24,72,73]

1.5 Blood-Brain Barrier

The blood-brain barrier is a critical membrane that protects the brain from harmful substances in the blood and regulates the passage of specific molecules into the central nervous system. This physical and enzymatic barrier represents the most significant challenge for the delivery of therapeutic drugs to the brain. The BBB is composed of endothelial cells connected by tight junctions, which significantly impede paracellular movement. [74–79] The brain is a highly complex and essential organ, comprising various cell types with diverse functions. Neurones are electrically excitable cells responsible for transmitting information. Endothelial cells form the cerebral micro vessels, astrocytes support neuronal activity, and microglial cells provide immunological surveillance as resident macrophages in the brain. Some brain macrophages, such as perivascular macrophages, are located on the outer (abluminal) surface of blood vessels and perform functions at the interface between the brain parenchyma and the circulatory system.[80,81]

The human brain's vascular system extends over 400 miles and includes cerebral arteries, arterioles, and capillaries. Nearly every neurone is supplied by its own cerebral capillary. There are three primary barriers to the delivery of CNS drugs to the brain: The Blood-Brain Barrier: This physiological barrier exists between blood vessels and brain parenchyma (see Figure 1.4). The Blood-Cerebrospinal Fluid Barrier (BCSFB): This barrier separates the blood circulation from the cerebrospinal fluid circulation. It is formed by choroid plexus epithelial cells facing the blood-cerebrospinal fluid. Finally, the Avascular Arachnoid Barrier: Located beneath the dura mater, this barrier completely encloses the CNS and plays a crucial role in the transfer of CNS drugs into the brain. Among these barriers, the BBB is the most significant and has the greatest impact on the immediate microenvironment of brain cells.[82–84]

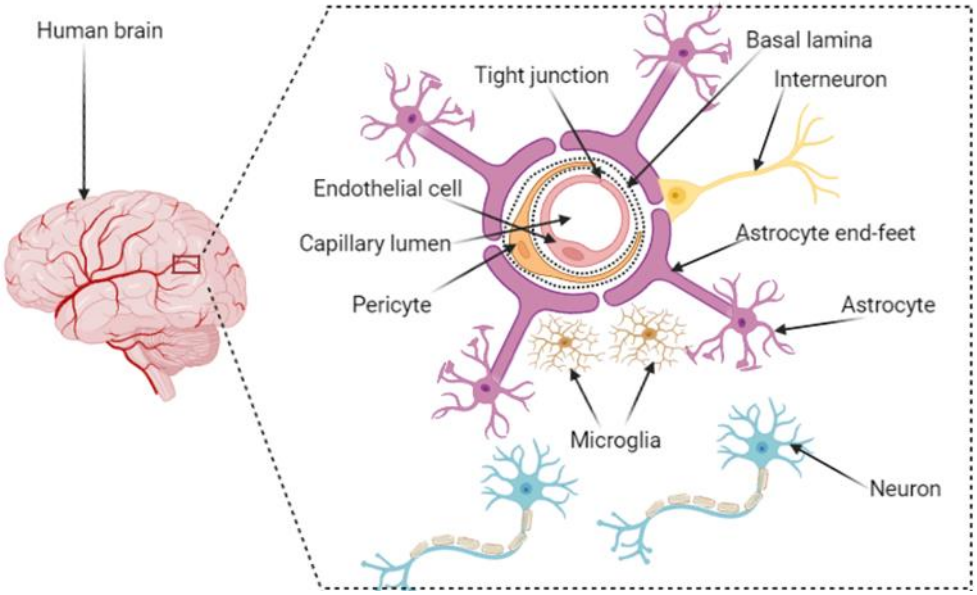

Figure 1.4: The BBB and other components of the neurovascular unit are shown schematically. The BBB is a multicellular barrier made up of a continuous brain endothelial membrane that is firmly sealed by tight junctions, pericytes, and astrocyte end feet. The BBB works as a vascular interface that facilitates communication between the CNS and periphery, separating the brain parenchyma from the peripheral blood circulation. (The image created by BioRender.)

The blood-brain barrier is a tightly controlled membrane that only allows essential substances, such as hormones, nutrients, and ions, into the brain. It stops potentially harmful xenobiotics from entering the central nervous system. The BBB is made up of endothelial cells that line the capillaries in the brain, along with the basement membrane, pericytes, and astrocyte end-feet. Brain microvascular endothelial cells utilise specialised tight junctions to fully seal the blood vessel's lumen (see Figure 1.5). Astrocytes, pericytes, endothelial cells, basal lamina, microglia, and neurones all play vital roles in maintaining the integrity of the BBB.[85,86]

In contrast to peripheral endothelial cells, brain endothelial cells lack fenestrations (pores that enable the rapid exchange of molecules between the blood and tissue), thereby restricting molecular mobility. The presence of tight junctions further limits the movement of chemicals between endothelial cells. These tight junctions are composed of a continuous network of parallel, interwoven strands of transmembrane and cytoplasmic proteins that function as paracellular gates, restricting the passage of hydrophilic molecules. These characteristics enable cerebral microcapillaries to form a dense cellular layer with a trans-endothelial electrical resistance (TEER), which is a critical parameter used to measure the integrity and permeability of cellular barriers, such as the blood-brain barrier, greater than 1000 Ωcm^2. This suggests that the endothelial cell monolayer has strong tight junctions, which effectively restrict the passage of ions and small molecules between cells.[87,88] The BBB also significantly reduces pinocytosis, the process by which live cells ingest liquid droplets, by approximately 100-fold throughout the endothelium.[89]

Several communication events happen within and between endothelial cells, astrocytes, pericytes, and neurones close to the BBB. These cells work together as the neurovascular unit (NVU) to control how easily molecules can pass through the BBB (see Figure 1.5). Specialised proteins in the luminal (blood side) and abluminal (brain side) membranes of endothelial cells govern the transport of metabolic products, such as glucose, and the movement of molecules across cell membranes.[90]

The BBB strictly controls the entry of immune cells from the periphery into the brain. Microglial cells, which are resident monocyte-derived cells in the brain parenchyma, help regulate immune responses.[91] In cases of CNS damage and disease, immune cells such as T lymphocytes can penetrate the brain.[92]

New research shows that the way certain plasma proteins get to the brain changes with age. In young, healthy mice, they get there through

ligand-specific, receptor-mediated transcytosis, but in older animals, they get there through nonspecific caveolar uptake. These attributes collectively enable the BBB to function as a physical barrier (tight junctions), a "transport barrier" (specialised transport systems), a "metabolic barrier" (specialised enzyme systems), and an "immunological barrier."

The BBB's role as a physical barrier is primarily due to the tight junctions that restrict paracellular transport. Proteins like claudins, occludins, and junctional adhesion molecules (JAMs) compose these tight junctions, creating a seal between adjacent endothelial cells. This seal prevents the free passage of ions and molecules, thereby maintaining the brain's microenvironment.[93] As a transport barrier, the BBB employs various transport systems to regulate the entry and exit of substances. Some of these systems include carrier-mediated transport (CMT) systems for amino acids and glucose, receptor-mediated transcytosis (RMT) systems for insulin and transferrin, and active efflux transporters such as P-glycoprotein (P-gp), which eliminate potentially harmful compounds and reintroduce them into the bloodstream. The metabolic barrier function of the BBB involves specialised enzyme systems that metabolise neurotoxic substances. Enzymes such as monoamine oxidases (MAOs), cytochrome P450s (CYPs), and glutathione S-transferases (GSTs) are present in the endothelial cells and contribute to the detoxification processes. Lastly, the BBB serves as an immunological barrier by regulating the entry of immune cells and maintaining immune privilege within the CNS. Microglial cells, the resident immune cells of the brain, play a crucial role in this process by monitoring the brain environment and responding to injury or infection.[82,94]

1.6 Transport routes for molecules through the blood-brain barrier

Due to the "tightness" of the BBB, the paracellular transport of molecules is modest; the majority of medications and critical chemicals reach the brain by passive diffusion, carrier-mediated transport, receptor-mediated transcytosis, adsorptive mediated transcytosis, or cell-mediated transcytosis. Transcytosis is the process by which membrane-bound vesicles transport chemicals from one side of a cell through its interior to the other side. Compared to endothelial cells in the periphery, brain endothelial cells have a characteristically slower vesicular transport rate.[95,96]

1.6.1 Passive diffusion

Passive diffusion is the unassisted movement of molecules along a concentration gradient and is not saturable.[87] This mechanism is the primary entry route for most lipophilic small-molecule CNS drugs. The maximum distance between cells and capillaries is approximately 20 μm, which can be traversed by small molecules in about half a second.[97] Diffusion of substances into the brain can be further classified as paracellular or transcellular diffusion (see Figure 1.5). Paracellular diffusion in the brain is restricted by the tight junctions between endothelial cells. These tight junctions form a continuous barrier that limits the movement of hydrophilic molecules between cells, thereby maintaining the integrity of the BBB.[97,98]

Transcellular diffusion, on the other hand, depends largely on the permeability of the molecules. Non-saturable diffusion allows small lipophilic molecules, such as alcohol and steroid hormones, to permeate cells. Several physicochemical properties of the molecules, such as molecular weight, hydrogen bonding, lipophilicity, and polar surface area, influence this process. Some factors that affect passive diffusion are: molecules with a low molecular weight (<500 Da) are more likely to diffuse across the BBB; molecules with fewer than six

hydrogen bonds are more permeable; the lipophilicity of a molecule, indicated by the water-octanol partition coefficient (LogP(oct) > 2), enhances its ability to diffuse through the lipid bilayer of endothelial cells; a lack of free rotatable bonds increases the likelihood of passive diffusion; and a Polar Surface Area (PSA) of 60 to 70 Å is generally favorable for BBB permeability.[95,99]

These factors are collectively considered when assessing a drug's permeability by passive diffusion. For instance, the highly lipid-soluble sedative diazepam quickly traverses the BBB due to its favourable physicochemical properties. Passive diffusion is relatively restricted for natural peptides unless they possess an amphipathic structure or are modified to be more lipophilic through synthetic techniques. This limitation necessitates the exploration of alternative delivery mechanisms for therapeutic peptides and proteins.[95,100–104]

Understanding the principles of passive diffusion is crucial for the design of CNS-active drugs. By optimising the physicochemical properties of drug molecules, researchers can enhance their ability to cross the BBB and achieve therapeutic concentrations in the brain. This knowledge also informs the development of novel drug delivery systems that can bypass the restrictive nature of the BBB.

1.6.2 Carrier-mediated transcytosis

Carrier-mediated transcytosis (CMT) is a crucial process for transporting essential nutrients such as glucose, amino acids, and nucleosides across the blood-brain barrier. Highly selective and stereospecific transport proteins embedded in the endothelial cell membranes of the BBB facilitate this process.[105] These transporter proteins recognise specific substrates on the luminal (blood-facing) side of the membrane, initiating a series of events that result in the substrate's translocation to the abluminal (brain-facing) side.[106]

Several transport systems for nutrients and endogenous compounds exist in the brain endothelial cell membrane. These systems include

transporter proteins that bind to substrates at the luminal side of the endothelial cell membrane. This binding is highly selective, ensuring that only specific molecules are transported. Upon substrate binding, the transporter undergoes a conformational change from an outward-facing to an inward-facing state. This change in structure makes it easier for the substrate to move across the membrane. The membrane then lets the substrate go on the abluminal side, following its concentration gradient.[107] This process can be carried out passively or actively, with ATP hydrolysis driving the transport against the concentration gradient.[108]

The carrier-mediated transcytosis of nutrients and endogenous compounds across the BBB involves several transport systems such as Glucose Transporter (GLUT1) is responsible for the transport of glucose and certain hexoses. It plays a vital role in maintaining the brain's energy supply[109], the acidic amino acid transport system facilitates the transport of acidic amino acids, such as glutamate and aspartate, which are critical for neurotransmission,[110] and Large Neutral Amino Acid Transporter (LAT1) transports phenylalanine and other essential amino acids. It also facilitates the movement of drugs like L-DOPA, gabapentin, and melphalan due to their structural and size similarities to endogenous substrates.[111]

Understanding the mechanisms of carrier-mediated transcytosis is essential for developing strategies to enhance drug delivery to the brain. By designing drugs that utilise this transport system, researchers can improve the bioavailability and therapeutic efficacy of CNS-active compounds. For example, modifying drug molecules to resemble endogenous substrates can facilitate their transport through LAT1, enhancing their ability to cross the BBB.[112]

Despite the potential of carrier-mediated transcytosis for drug delivery, several challenges remain. The specificity and selectivity of transport proteins can limit the range of molecules that can be effectively transported. Additionally, the regulation of transporter expression and

activity in pathological conditions can impact drug delivery. Future research should focus on elucidating the regulatory mechanisms of these transporters and developing novel strategies to overcome their barriers.

1.6.3 Receptor-mediated transcytosis

Brain capillary endothelial cells employ receptor-mediated transcytosis (RMT) as a critical mechanism for the selective and specific uptake of certain macromolecules. This process involves the binding of a circulating ligand on the luminal side of brain endothelial cells to its specific receptor. Vesicular trafficking machinery then internalises and transports the receptor-ligand complex through the intracellular compartment, often through the endosomal/lysosomal system. Upon reaching the abluminal side, the endothelial cells release the ligand into the extracellular space and recycle the receptor back to the luminal side. [106,113,114] (See Figure 1.5)

The mechanism of the RMT is that a ligand in the bloodstream binds to its specific receptor on the luminal (blood-facing) side of the brain endothelial cells. This binding is highly selective, ensuring that only specific macromolecules are transported. Also, the receptor-ligand complex is internalised into the endothelial cell through endocytosis. This process involves the formation of vesicles that encapsulate the complex. In addition, the vesicles containing the receptor-ligand complex are transported through the intracellular compartment, often utilising the endosomal/lysosomal system. This system facilitates the sorting and trafficking of complexes within the cell. Upon reaching the abluminal (brain-facing) side, the receptor-ligand complex is dissociated. The release of the ligand into the extracellular space allows it to influence brain tissue. The endothelial cells then recycle the receptor back to the luminal side for additional rounds of transport.[113] Examples of endogenous receptors, such as several well-characterised endogenous receptors facilitate RMT across the BBB, including mediates the transport of insulin, a hormone crucial for glucose

metabolism, The transferrin receptor facilitates the transport of transferrin-bound iron, which is essential for various cellular processes and the leptin receptor is involved in the transport of leptin, a hormone that regulates energy balance and appetite. [115]

Despite its potential, the understanding of how various CNS illnesses influence the production and regulation of receptors involved in RMT remains inadequate. Neurological diseases' impact on receptor expression and function requires further research. Additionally, developing strategies to enhance the specificity and efficiency of RMT for drug delivery remains a critical area of investigation. Receptor-mediated transcytosis is a vital mechanism for the selective transport of macromolecules across the BBB. Understanding and harnessing this process can significantly advance the development of therapeutic strategies for treating CNS disorders.[100,116]

1.6.4 Adsorptive-mediated transcytosis

Adsorptive-mediated transcytosis (AMT) represents a nonspecific transcytosis mechanism facilitated by electrostatic interactions between positively charged moieties of certain macromolecules and the negatively charged membranes of brain endothelial cells, which are rich in anionic heparin proteoglycans. The process of AMT initiates with the invagination of the electrostatic complex, leading to the formation of endosomes. The endothelial cells subsequently transport these endosomes from the luminal to the abluminal side, resulting in the release of the substrate.[112] The process of AMT initiates with the invagination of the electrostatic complex, leading to the formation of endosomes. The endothelial cells subsequently transport these endosomes from the luminal to the abluminal side, resulting in the release of the substrate. Polycationic proteins, like protamine, or cell-penetrating cationic peptides, like SynB peptides, are often used in the AMT-facilitated central nervous system drug delivery strategy. (see

Figure 1.5). However, a significant limitation to utilising cationic proteins or peptides in this context is their indiscriminate distribution, which results in a lack of brain selectivity; additionally, the use of these cationic agents is associated with potential toxicity due to endothelial damage.[112,117]

1.6.5 Cell-mediated transcytosis

Cell-mediated transcytosis represents a relatively novel mechanism for drug transport across the blood-brain barrier.[106] Certain pathogens exploit monocytes as "Trojan horses" to infiltrate the central nervous system through this process.[118]

For instance, the human immunodeficiency virus (HIV) exploits this pathway to enter the brain, where HIV-infected monocytes and/or macrophages traverse the BBB during routine immune surveillance or in response to the production of proinflammatory mediators that enhance vascular permeability.[118,119] (See Figure 1.5) Several neurological disorders, including Alzheimer's, Parkinson's, brain tumours, and dementia, exhibit an inflammatory component. During the inflammatory phase, leukocytes such as monocytes and neutrophils are recruited in substantial numbers. These cells demonstrate exceptional capabilities in migrating to sites of inflammation through processes such as diapedesis and chemotaxis. Cell-mediated transcytosis has emerged as an innovative strategy for therapeutic delivery across the BBB. Research has explored the use of immune cells, neural stem cells, and mesenchymal stem cells as carriers for therapeutic agents targeting brain malignancies. This method uses the cells' natural ability to move and return home to deliver drugs directly to diseased areas in the CNS. This could make treatments for a number of neurological conditions more effective and targeted.[120–122]

1.6.6 Active efflux transport

Drug efflux transporters are found on brain capillary endothelial cells, which makes it much harder for many therapeutic agents to get into the brain. These efflux transporters actively push drugs out of the endothelial cells, which stops them from getting into the brain and makes it even harder for them to cross the blood-brain barrier.[123] (See Figure 1.5)

The primary efflux transporters involved in this process include P-glycoprotein (P-gp), multidrug resistance-associated proteins (MRPs), and breast cancer resistance protein (BCRP). P-glycoprotein (P-gp) is a well-characterised efflux transporter that plays a crucial role in the pharmacokinetics of various drugs by pumping them out of cells. Similarly, MRPs are a family of transporters that contribute to the efflux of a wide range of substrates, including drugs and endogenous compounds. BCRP, another key efflux transporter, is known for its role in multidrug resistance and its ability to limit drug accumulation in the brain. Collectively, these efflux transporters are integral components of the BBB, which regulates the entry and exit of essential chemicals and signalling molecules, such as peptides. This regulatory function of the BBB serves as a critical communication link between the brain and the systemic circulation, maintaining the homeostasis of the central nervous system. The presence of these efflux transporters poses a significant challenge for CNS drug delivery, as they can reduce the efficacy of therapeutic agents intended to treat neurological disorders. Understanding the mechanisms of active efflux transport and developing strategies to overcome these barriers are essential for improving drug delivery to the brain and enhancing the treatment of CNS diseases.[100,124]

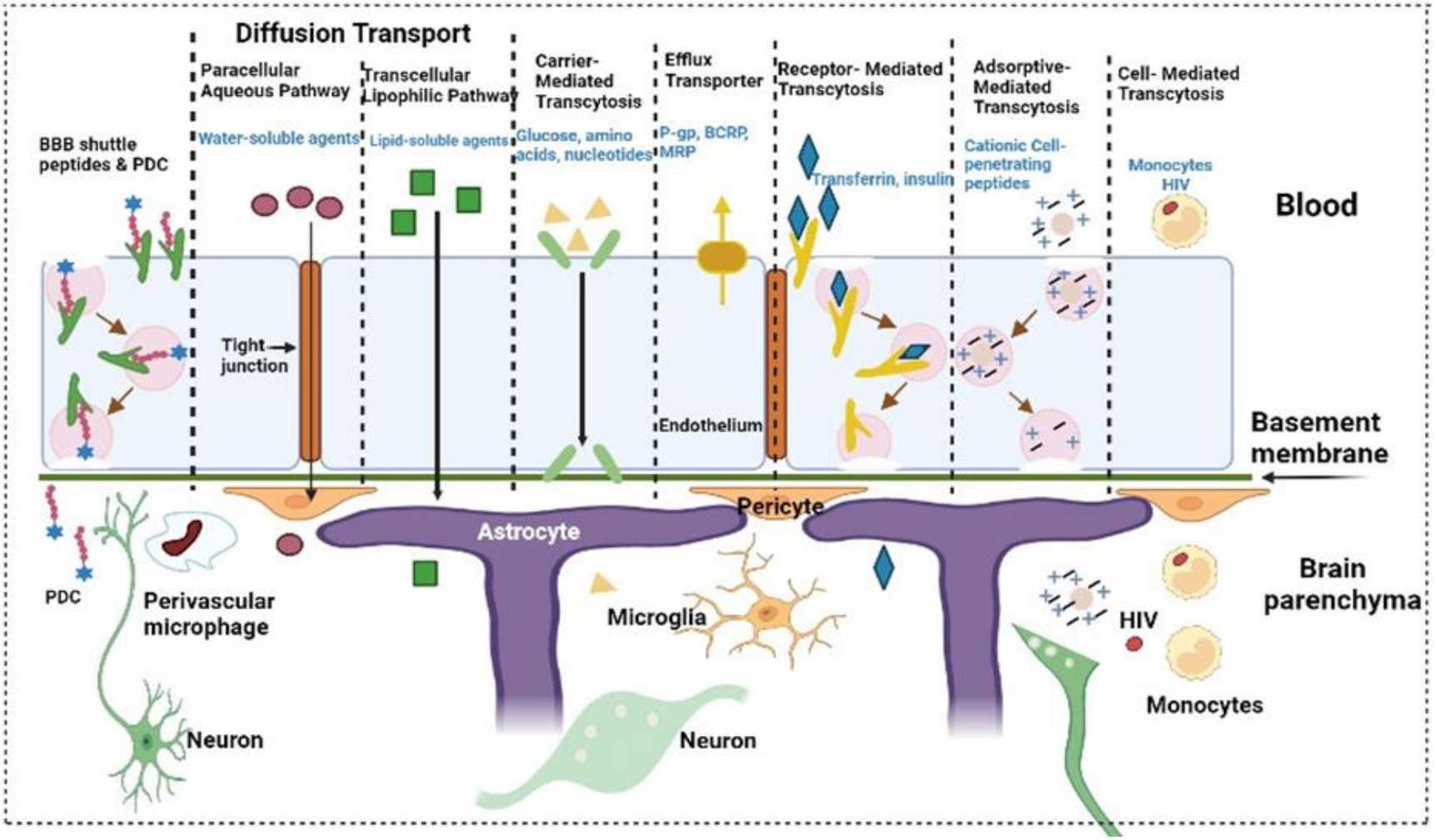

Figure 1.5: The blood-brain barrier, a structural barrier between blood vessels and brain parenchyma, is depicted as a diagram of the principal transport routes for molecular traffic. (The image created by BioRender.)

1.7 Electrostatic Interactions Between cationic CPPs and the BBB for the Treatment of Neurological Diseases

The electrostatic interactions between cationic cell-penetrating peptides (CPPs) and the blood-brain barrier are crucial for the effective delivery of therapeutic agents targeting neurological diseases such as Alzheimer's disease. CPPs facilitate the transport of drugs across the BBB by exploiting their positive charge, which enhances binding to the negatively charged components of the BBB, thereby promoting transcytosis. This mechanism is essential for overcoming the BBB's restrictive nature and ensuring that therapeutic agents reach the central nervous system.[125] (See Figure 1.6)

Cationic CPPs interact with the anionic surface of endothelial cells, enhancing their ability to cross the BBB.[126] They use receptor-mediated transcytosis to transport drugs across the BBB effectively (see Figure 1.6). Researchers have combined CPPs with nanoparticles such as liposomes to enhance drug delivery efficiency for AD treatments, specifically targeting amyloid-beta and tau proteins. Multifunctional delivery systems that incorporate CPPs have shown enhanced therapeutic effects, including reduced neuroinflammation and improved cognitive function in AD models.[127]

Despite the promise of CPPs, challenges remain in optimising their delivery systems to ensure specificity and minimise off-target effects. Additionally, the long-term safety and efficacy of these approaches require further investigation.[126]

In contrast, while CPPs represent a viable strategy for drug delivery across the BBB, alternative methods, such as transient BBB opening techniques, are also being explored. These methods try to improve drug delivery without relying only on peptide interactions. This suggests that treating CNS disorders may need more than one approach to work.

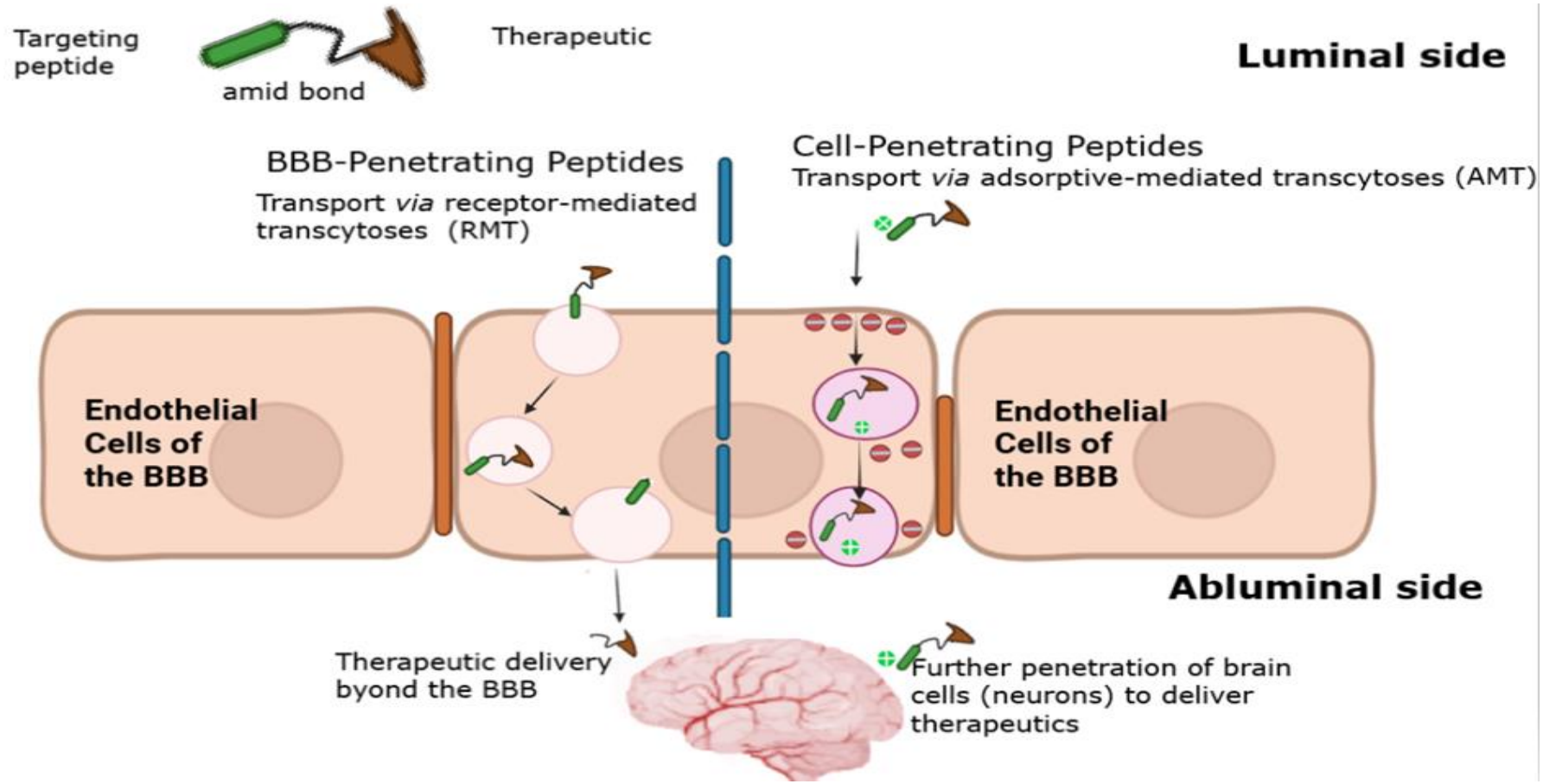

Figure 1.6: The diagram shows how BBB-penetrating and cell-penetrating peptides help therapeutics (cargos) move across the endothelial cells of the blood-brain barrier. (Biorender was used to draw this image.

1.8 BBB disruption

Researchers have developed several mechanisms to disrupt the blood-brain barrier. One notable method involves the use of acoustic radiation to open the BBB by placing microbubbles against the vessel walls (see Figure 1.7). Typically, a shell of polymers, lipids, or proteins stabilises a gas core, such as air or perfluorocarbon in these microbubbles. Short pulses of acoustic radiation have been found effective in opening the BBB. Therefore, radiation force is not the only way to disrupt the BBB; it is one of the mechanisms for increasing opening with increasing pulse length.[128] Microbubble (μB) oscillation can induce shear stress and circumferential stress in the microvasculature, potentially disrupting the BBB. The size of microbubbles ranges between 1 and 10 μm, with the gas core stabilised by a polymer, lipid, or protein shell.[129, 130] The mechanism of ultrasound's effect occurs when the microbubbles within the vessels expand and contract, causing movement in the vessel walls and inducing circumferential stress.[131] This stretching of the vessel wall temporarily opens the tight junctions of the BBB. [132] The duration of BBB opening primarily depends on the size of the microbubbles. Larger microbubbles result in larger pores. For instance, when the size of microbubbles is 2 μm (polydisperse commercial formulation), the duration for the BBB to close is approximately between 24 and 48 hours. However, when the size of microbubbles increases to 4 μm or 6 μm, the BBB requires more than five days to close.[133, 134]

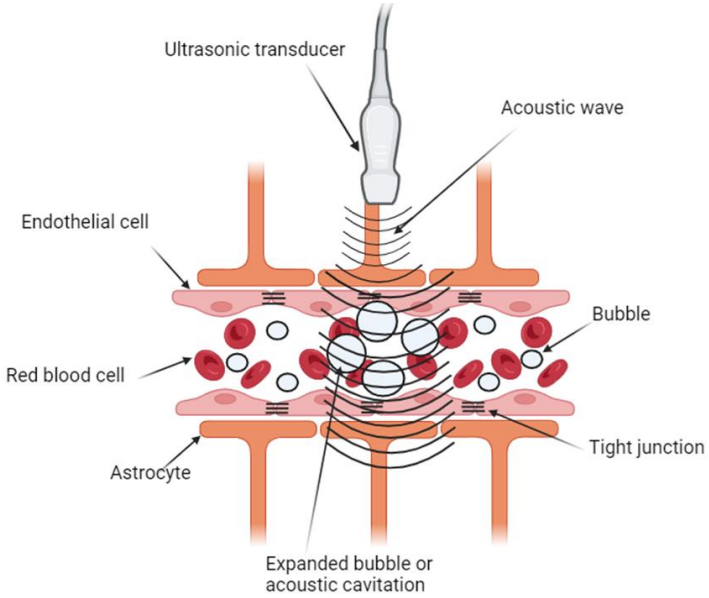

Figure 1.7: The disruption of the blood-brain barrier leads to the creation of acoustic cavitation. The nano and microbubbles are administered intravenously. When bubbles come into contact with the ultrasonic field, they vibrate at the same frequency as the ultrasonic waves. The bubbles undergo expansion and engage in interactions with the endothelial cells, disrupting the blood-brain barrier. (The image created by BioRender.)

1.9- Alzheimer`s Disease Treatments

Researchers have identified several potent and efficacious pharmacological agents for the therapeutic management of Alzheimer's disease, with a particular emphasis on targeting specific molecular sites. These targets include cholinesterase, amyloid-beta plaques, and NMDA receptors. Among these agents, donepezil, galantamine, rivastigmine, memantine, aducanumab, lecanemab, and donanemab are the only drugs that have received FDA approval for the treatment of Alzheimer's disease. These therapies specifically target distinct pathological mechanisms and have the potential to significantly ameliorate cognitive decline and memory loss in patients. However, it is important to acknowledge that these medications are not capable of completely

eradicating the disease.[33] The treatments for Alzheimer's disease reflect a range of approaches, from symptomatic relief to disease modification. However, the efficacy and safety of newer agents like aducanumab and lecanemab remain subjects of ongoing debate, particularly regarding their clinical benefits versus side effects.[135,136] (See table 1.2.)

Table 1.2: Treatments of AD approved by the FDA.

Drug	Mechanism of Action	Type of Administration	Year Approved by FDA
Donepezil	Cholinesterase inhibitor, increases acetylcholine levels	Oral	1996 [137,138]
Galantamine	Cholinesterase inhibitor, enhances cholinergic function	Oral	2001[139,140]
Rivastigmine	Cholinesterase inhibitor, increases acetylcholine levels	Oral	2001

Drug	Mechanism of Action	Type of Administration	Year Approved by FDA
Memantine	NMDA receptor antagonist, regulates glutamate	Oral	2003 [141–144]
Aducanumab	Monoclonal antibody targeting amyloid-beta plaques	IV infusion	2021 [145,146]
Lecanemab	Monoclonal antibody targeting amyloid-beta plaques	IV infusion	2022 [147–150]
Donanemab	Monoclonal antibody targeting amyloid-beta plaques	IV infusion	2023 [151,152]

1.10 Cell Penetrating Peptides

The systemic administration of drugs involves several critical steps, each presenting its own challenges. These include how the drug is given (by mouth or injection), how long it stays in the bloodstream, how to get around biological barriers, how cells take it up, and how it gets to the cytosol. Many bioactive molecules encounter difficulties accessing their target sites and must penetrate the cell membrane to exert their therapeutic effects. Plasma membranes play a crucial role in preventing exogenous invasion as they function as effective biochemical barriers. Cell-penetrating peptides have emerged as promising tools to facilitate these processes, particularly in delivering therapeutic agents across cell membranes.[153,154]

Cell-penetrating peptides, also known as CPPs, are short cationic or neutral peptides that have the potential to transport their associated molecular payloads (such as peptides, proteins, oligonucleotides, nanoparticles, bacteriophages, and so on) into the cells.[155] Biological evolution has endowed certain proteins with the ability to penetrate the cell membrane, thanks to the inclusion of specific peptide sequences known as protein transduction domains.[156] This capacity is essential for the transmission of information across the membrane. These domains are called cell-penetrating domains because the peptide sequences that make up these domains include basic amino acids and have the ability to enter cells; as a result, these peptides are referred to as cell-penetrating peptides.

Cell-penetrating peptides (CPPs) are short peptides that facilitate the transport of various molecules across cellular membranes. CPPs can carry diverse bioactive substances into cells due to their cationic or hydrophobic nature. At physiological pH, the positive charge of CPPs encourages electrostatic interactions with the negatively charged cell membrane, thereby accelerating transport. Hydrophobic interactions help increase the speed at which peptides with hydrophobic features move across membranes. The order of amino acids in CPPs affects how

they interact with cell membranes and how well they can transport drugs. Cationic peptide sequences, such as those containing arginine and lysine, are particularly efficient at interacting with cell membranes. Consequently, CPPs can traverse the blood-brain barrier (BBB) without the need for receptor-mediated mechanisms. [157,158]

The molecules transported by CPPs can include drugs, proteins, peptides, and nucleic acids, such as multi-arginine peptides or peptides containing cationic amino acids like lysine and arginine. CPPs can enter cells through direct translocation, absorptive-mediated transcytosis, or endocytosis. As a result, they are increasingly valuable in treating a wide range of diseases, including neurological disorders such as Alzheimer's and Parkinson's diseases. This is due to their ability to facilitate the passage of therapeutic agents across cellular membranes. These peptides are particularly advantageous in overcoming biological barriers like the BBB, which poses significant challenges in the treatment of central nervous system (CNS) disorders. Current applications of CPPs span several therapeutic domains, leveraging their unique properties to enhance drug delivery and efficacy.[159,160]

In a general sense, CPPs are diverse peptides with a maximum length of 40 amino acid monomers. They are positively charged and contain a high concentration of fundamental amino acids. CPPs are known for being able to enter cells quickly and easily, passing through the membranes of different types of cells without hurting them or triggering an immune response.[161]

CPPs can efficiently internalise associated biomolecules without compromising their biocompatibility. This means that cell-penetrating peptides can effectively transport and incorporate biomolecules into cells while remaining safe and non-toxic for biological systems. Their ability to maintain biocompatibility is crucial for potential therapeutic applications. Their ability to cross the cell membrane via receptor- and energy-independent processes has garnered significant interest in the scientific community.[162–165] Studies have demonstrated that CPPs can

transport nanoparticles, peptides, proteins, nucleic acids (DNA, RNA), and other molecules into cells. Cargo molecules can form covalent conjugations or non-covalent associations with CPPs.[154,166] Many CPPs, including PolyArginine (PR) and the Trans Activator of Transcription peptide (TAT), have been attached to delivery vectors to optimise the distribution of medicinal compounds and avoid unwanted side effects. This optimisation enhances the therapeutic efficacy of the compounds while minimising their potential toxicity, leading to more effective and safer treatment options.[167–169]

The blood-brain barrier obstruction often limits the therapeutic efficacy of treatments for central nervous system disorders.[170] Therapeutic compounds could be brought into the brain by CPPs using an adsorptive-mediated transcytosis pathway across the BBB. They were able to do this effectively at concentrations as low as submicromolar levels without harming cells.[171] Also, CPPs have the potential to circumvent P-glycoprotein in order to boost drug accumulation in the brain and hence enhance the therapeutic impact. However, the ability of diverse CPPs to penetrate the BBB barriers varies considerably. Cho *et al.* 2017 created a multicellular BBB spheroids model in culture that can be used to quickly test brain-penetrating CPPs. This model has repeatable BBB functions and characteristics.[172] This was attributed to the BBB spheroids model being modelled with CPPs. The next generation could use this robust BBB model as a platform *in vitro*, accelerating the discovery of treatments for diseases affecting the central nervous system. The modified method of CPPs played a crucial role in bypassing the BBB and enhancing the therapeutic effect.

1.10.1 Peptide production by Solid-Phase Peptide Synthesis (SPPS)

Solid Phase Peptide Synthesis is a pivotal technique in the field of peptide chemistry, revolutionising the synthesis of peptides and

proteins. This method, pioneered by Robert Bruce Merrifield in the 1960s, involves the stepwise assembly of peptide chains on a solid support, typically a resin bead.[173] The innovation of SPPS has significantly streamlined peptide synthesis, enabling the rapid and efficient production of peptides with high purity and yield. The SPPS process begins with the attachment of the C-terminal amino acid of the target peptide to a solid resin support. This resin is functionalised with reactive groups, such as amine or hydroxyl groups, which form covalent bonds with the amino acid. The peptide chain is then elongated by sequentially adding protected amino acids. Each amino acid is protected at its N-terminus and side chains to prevent undesirable side reactions. Common protecting groups include the acid-labile tert-butyloxycarbonyl (Boc) and the base-labile 9-fluorenylmethyloxycarbonyl (Fmoc) groups.[174] (See Figure 1.8)

The synthesis cycle involves several key steps: deprotection, coupling, and washing. Deprotection removes the protecting group from the growing peptide chain's N-terminus, revealing a free amine group for the subsequent coupling reaction. Coupling involves the addition of the next amino acid, activated by coupling reagents such as HBTU, HATU, or DIC, to form a peptide bond. Washing the resin removes excess reagents and by-products, ensuring the purity of the synthesised peptide.

One of the major advantages of SPPS is the ability to automate the synthesis process. Automated peptide synthesisers can perform the repetitive cycles of deprotection, coupling, and washing, allowing for the efficient production of peptides with minimal manual intervention. This automation has facilitated the synthesis of complex peptides and proteins, including those with post-translational modifications and non-natural amino acids.[173]

SPPS also offers significant advantages over traditional solution-phase synthesis. The solid support allows for the easy removal of excess reagents and by-products through simple filtration, eliminating the

need for laborious purification steps after each reaction. Additionally, the solid-phase approach minimises the loss of intermediates, improving the overall yield of the synthesis.[174]

Despite its advantages, SPPS is not without limitations. The synthesis of very long peptides can be challenging due to incomplete reactions and side reactions that accumulate over multiple cycles. Moreover, the choice of protecting groups and coupling reagents can impact the efficiency and fidelity of the synthesis. Researchers continue to develop new strategies and reagents to address these challenges and improve the robustness of SPPS.[174]

In conclusion, solid-phase peptide synthesis is a cornerstone technique in peptide chemistry, enabling the efficient and high-yield production of peptides and proteins. Its development has had a profound impact on the field, facilitating advances in drug discovery, biochemistry, and molecular biology. Ongoing research aims to further refine SPPS methodologies, expanding their applicability and enhancing their efficiency for the synthesis of increasingly complex peptide structures.

1.10.2 Peptide production by Microwave Solid-Phase Peptide Synthesis (MSPPS)

Microwave solid-phase peptide synthesis is considered the most widely used method for peptide preparation due to its efficiency, speed, and ability to produce high-purity products. This technique uses microwave energy to enhance reaction rates during peptide bond formation, significantly reducing the overall synthesis time. As a result, it allows for the rapid generation of peptides with minimal impurities, making it a preferred choice in many research and industrial applications. MSPPS substantially reduces reaction times in both coupling and deprotection stages, often completing these procedures in minutes instead of hours. Coupling reactions generally take about 7 minutes, although some specific sequences may require longer times, such as 12 to 14 minutes

for coupling Arginine.[175,176] Therefore, in this research, those peptides that have an arginine double coupling process are used. MSPPS improves the quality and amount of produced peptides. The use of microwave energy provides more complete reactions, minimising the risk of incomplete coupling and side reactions. This method improves quality control in the production process, reducing the risk of synthesis errors. MSPPS decreases the need for harmful reagents and solvents such as DMF compared to traditional procedures, making it more environmentally friendly.[177] The successful use of carbodiimide activation alongside microwave heating reduces solvent usage while maintaining increased crude purities. MSPPS is flexible and suitable for the synthesis of various peptides, including small, medium, large, and cyclic peptides. It has been successfully used in the synthesis of bioactive peptides, including cell-penetrating peptides, which are essential for drug delivery applications. [178,179] Related to the above benefits, MSPPS was chosen to prepare all the peptides in this research.

A half-automated microwave peptide synthesiser (Biotage) was used in this research on all produced peptides to ensure consistency and uniformity across different peptide productions.

Microwave-assisted solid-phase peptide synthesis is a great method for peptide production due to its combination of faster reaction rates, better results and purity, decreased epimerisation process, energy efficiency, scalability, decreased solvent consumption and automation.

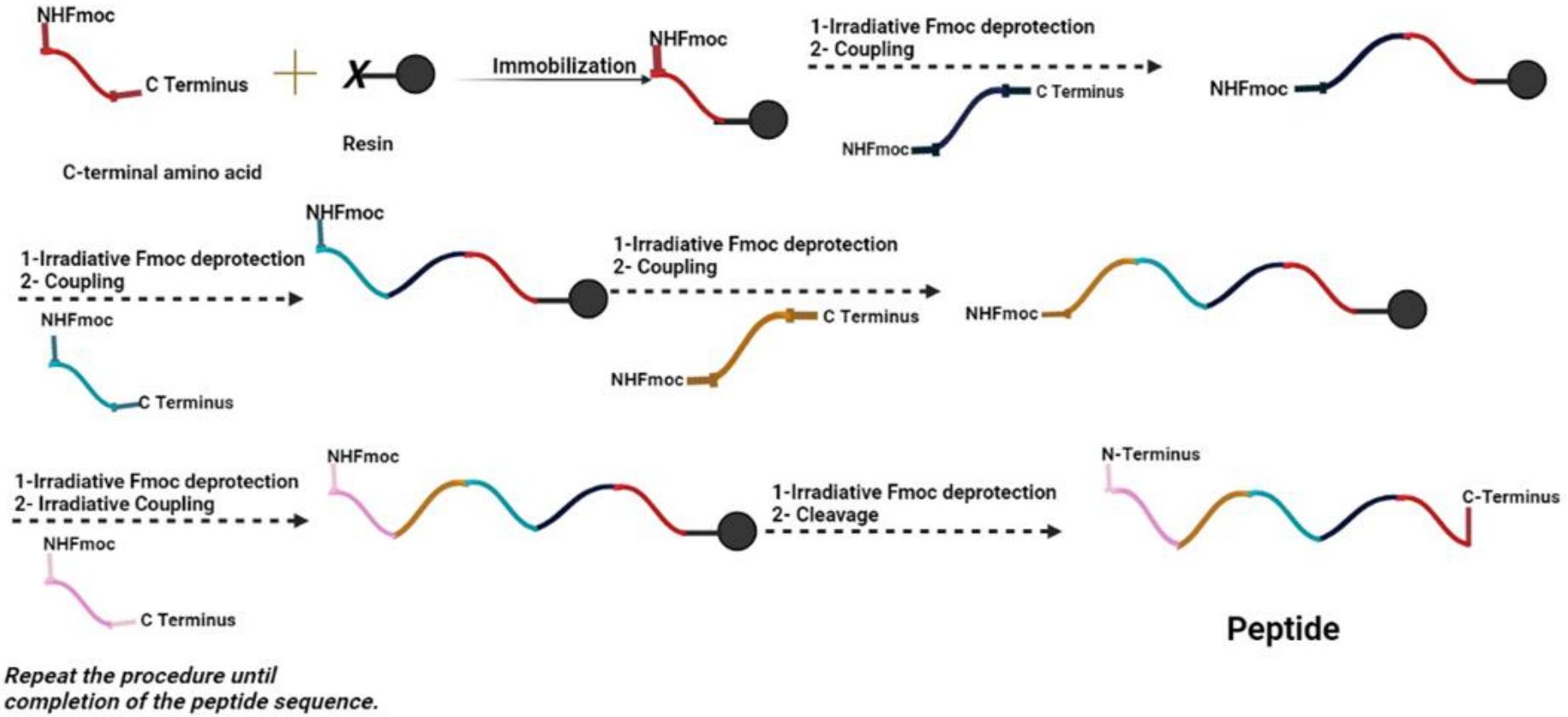

Figure 1.8: Illustrates the standard schematic of the solid-phase peptide synthesis (SPPS). (The image created by BioRender.)

1.11 Liposomes

Liposomes are typically spherical, formed by one or more phospholipid bilayers, analogous to those composing cell membranes. There is an aqueous core inside these bilayers, which lets hydrophilic (water-soluble) molecules join the core and hydrophobic (fat-soluble) atoms join the bilayer itself (see Figure 1.9). This structural configuration enables liposomes to protect encapsulated drugs from environmental and chemical changes, including enzymatic degradation and pH fluctuations. The lipid composition of liposomes can be modified to target specific organs and tissues, thereby enhancing the specificity and efficacy of drug delivery. This site-targeting capability allows for the direct delivery of therapeutic agents to the affected area, minimising systemic side effects. By encapsulating drugs, liposomes can reduce the toxicity of certain pharmaceuticals, thereby improving patient safety during treatment. One significant advancement in liposome technology is PEGylation, which involves the attachment of polyethene glycol (PEG) chains to the liposome surface. PEGylation increases the time that liposomes stay in the bloodstream and gives them controlled release properties, which makes the drugs inside them more effective in therapy. Various fields, such as pharmaceuticals, cosmetics, and food industries, utilise liposomes due to their ability to encapsulate a wide range of compounds. Advances in liposome technology have led to the development of multifunctional liposomes, which can be tailored for specific therapeutic applications, such as cancer treatment, central nervous system disorders, and vaccine delivery.[180–183]

Thus, compared to conventional drug delivery methods, liposomes offer several advantages. They enable targeted drug delivery to specific sites, ensure controlled release, and protect drugs from degradation, thereby enhancing therapeutic efficacy and minimising side effects. Extensive preclinical and clinical studies have demonstrated the

effectiveness of liposomes as drug carriers. However, ongoing research continues to address challenges related to stability and effective targeting. Liposomes can be produced to deliver medications directly to particular target areas, minimising systemic exposure and side effects. For example, Doxil is a liposome-encapsulated form of the chemotherapy drug doxorubicin. It is designed to deliver the drug directly to cancer cells, minimising systemic exposure and reducing side effects. The liposomal formulation allows Doxil to circulate in the bloodstream for an extended period, enhancing its accumulation in tumour tissues due to the enhanced permeability and retention (EPR) effect. This targeted delivery prevents the harmful effects of doxorubicin from reaching healthy tissues. This lowers common side effects like cardiotoxicity.

Liposomes provide extended or controlled drug release, improving therapeutic outcomes.[180] The development of robust liposome formulations continues to be a focus of research, aiming to improve their stability, targeting efficiency, and therapeutic efficacy.

1.11.1 Liposome components

Liposomes are round, bubble-like structures made up of phospholipids and cholesterol. They are the building blocks of flexible drug delivery systems.

Phospholipids are the fundamental building blocks of liposomes. These amphipathic molecules consist of a glycerol or sphingosine backbone connected to a phosphate head group, which is further bound to an alcohol. One or two fatty acid chains are attached to this head group. The amphipathic nature of phospholipids enables them to spontaneously assemble into bilayers in aqueous environments, resulting in the primary spherical structure of liposomes. Natural phospholipids, derived from sources such as soybeans or egg yolks,

include phosphatidylcholine (PC), phosphatidylserine (PS), phosphatidylinositol (PI), phosphatidylglycerol (PG), and phosphatidic acid (PA). These natural phospholipids, often composed of unsaturated hydrocarbon chains, exhibit lower stability in liposome formulations compared to their synthetic counterparts (see Figures 1.8 and 1.9). Synthetic phospholipids are produced through organic chemical reactions or enzymatic modifications that alter the nonpolar and polar regions of the molecules. Dipalmitoyl phosphatidylcholine (DPPC), hydrogenated soy phosphatidylcholine (HSPC), and 1-palmitoyl-2-oleoyl-sn-glycero-3-phosphocholine (POPC) are all examples of synthetic phospholipids. The specific type of phospholipid used in liposome formulation can significantly influence their properties, such as charge, mobility, and interactions with cells and biological components. For instance, anionic lipids like phosphatidylserine (PS) and phosphatidylglycerol (PG) create negatively charged liposomes, which affect their interactions with positively charged molecules and their behaviour in biological systems.[184,185]

The chemical structure of L-alpha-phosphatidylcholine (PC) has a significant effect on its ability to combine with cholesterol to form liposomes. This is mainly due to the fact that PC is amphipathic, which helps form the two layers. Phosphatidylcholine and cholesterol interact in a way that is necessary for liposomes to stay stable and work properly. This is because cholesterol controls the fluidity, permeability, and structural integrity of membranes. Adding cholesterol to the phosphatidylcholine bilayer makes it easier for stable liposomal structures to form, which can be useful for many things, like taking medications. L-alpha-phosphatidylcholine has a hydrophilic head and hydrophobic tails, allowing the formation of bilayers that can accept cholesterol. Cholesterol integrates into the bilayer by rotating its hydroxyl group toward the hydrophilic head of phosphatidylcholine, forming hydrogen bonds with the polar head groups of phospholipids.

The hydrophobic side of cholesterol, which includes its hydrocarbon tail, interacts with the hydrophobic tails of phospholipids *via* van der Waals forces. These interactions contribute to the overall stability and fluidity of the membrane; thus, they increase membrane packing and stability. (See Figure 1.10). It is important for liposome stability that cholesterol raises the packing density of the phosphatidylcholine bilayer. This lowers the membrane's fluidity and permeability. Furthermore, research demonstrates that the presence of cholesterol can shield liposomes from destabilising chemicals, as cholesterol-rich liposomes require higher surfactant concentrations to prevent their leakage. Cholesterol can produce superlattices inside the phospholipid bilayer, influencing its distribution and the kinetics of cholesterol removal. Rising cholesterol levels in liposomes result in increased vesicle sizes, which can be beneficial or harmful based on the specific application (see figures 1.9 and 1.10). Medication delivery systems, where controlled release and stability are important, use phosphatidylcholine's capacity to create stable liposomes with cholesterol. Certain biomedical applications customise the targeted liposome properties, such as size and fluidity, to determine the ideal cholesterol content. The addition of cholesterol to phosphatidylcholine liposomes improves stability and performance, but it presents difficulties in identifying the ideal cholesterol concentration for particular applications. Excessive cholesterol may result in excessively rigid membranes, possibly blocking the release of encapsulated drugs. Therefore, a balance must be found to achieve the necessary liposomal characteristics for efficient application in various fields.[185–188]

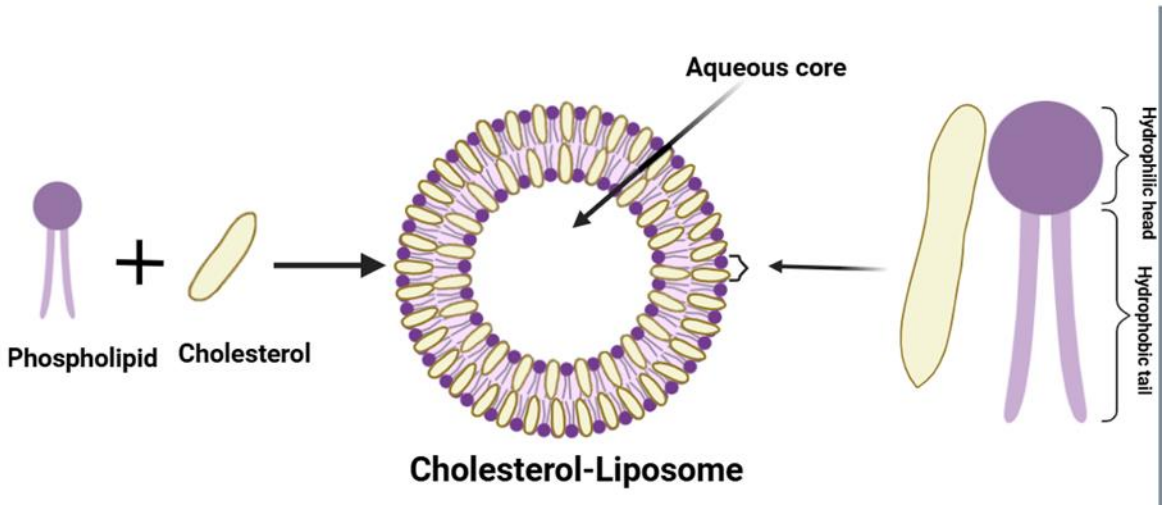

Figure 1.9: Illustrates the schematic draw of a liposome bilayer that incorporating with cholesterol. The image created by Biorender

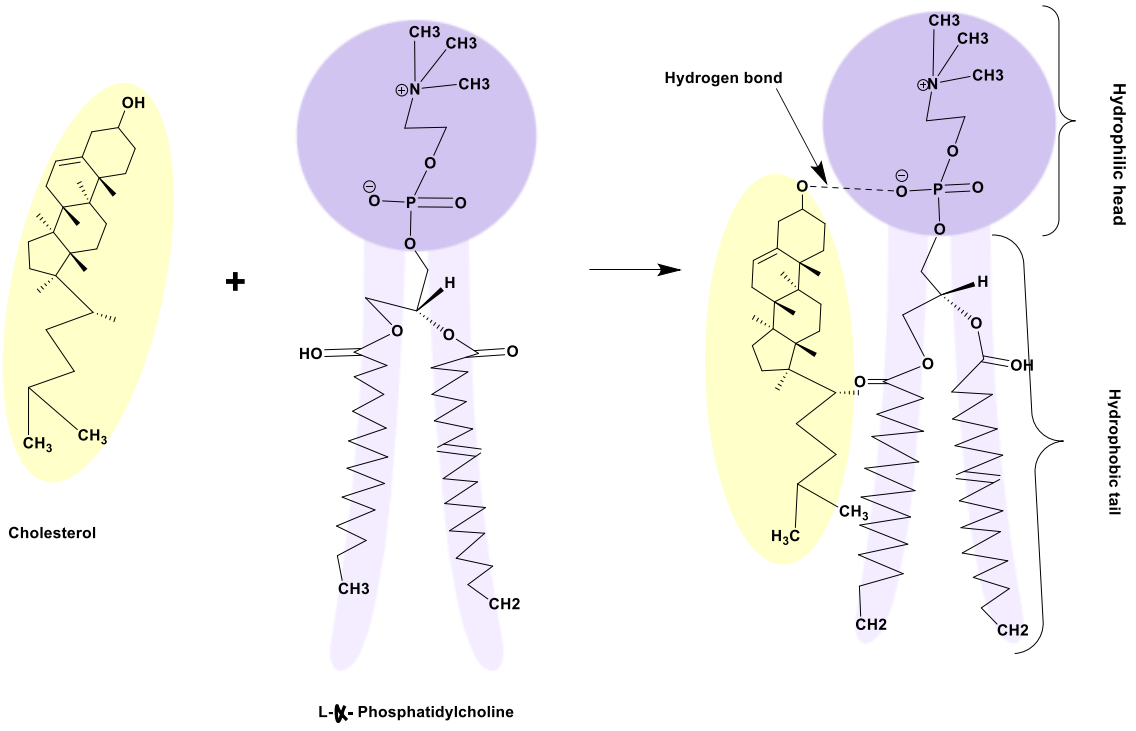

Figure 1.10: Shows the chemical reaction between cholesterol and L-Alpha-phosphatidylcholine to form liposomes. (The image created by BioRender and ChemDraw.)

1.11.2 Methods for liposome synthesis

Various methods exist for synthesising liposomes, with the thin film hydration technique being one of the most commonly employed. This method involves the dehydration of organic solvents containing phospholipids, resulting in the dispersion of phospholipids throughout a thin film layer. The formation of bilayer sheets necessitates the addition of a hydrophobic substance to an aqueous mixture, followed by the application of sufficient heat and agitation, such as mechanical shaking, sonication, or a combination of both. To create liposomes, the bilayer sheets must be isolated from the bulk material, which is then separated into two layers or bilayers.[189,190] Encapsulation techniques, such as active or passive loading, can be applied during liposome production. Active loading encapsulation involves the insertion of bioactive substances into intact vesicles using a driving force potential generated by agents like calcium acetate and ammonium sulphate. However, to enhance the solubility of both hydrophilic and hydrophobic components, these preparation methods often require potentially harmful solvents, including, ether, methanol, and chloroform.[189,191]

Hydration of lipid films using mechanical means such as sonication, French pressure cells, membrane extrusion, freeze-thaw liposomes, micro emulsification, and desiccated reconstituted vesicles, as well as freeze-drying and freeze-agitation, are all examples of mechanical dispersion methods. Additionally, lipid-film hydration is the most common type of mechanical dispersion. This technique involves the development of a thin film that is made up of a phospholipid and cholesterol membrane. This membrane is formed from the evaporation of the organic solvent that was present in the solution including phospholipids and cholesterol. The evaporated fluid is rehydrated with a phosphate buffer solution; this procedure, coupled with vortexing, and sometimes sonication, results in the production of liposomes. In addition, this method may be combined with membrane extrusion in order to make small unilamellar vesicles (SUVs) from multilamellar

vesicles (MLVs). However, there is a possibility that this procedure may leave behind some residue of the organic solvent in the finished product.[192]

Sonication is a straightforward method for preparing liposomes, particularly for creating SUVs from MLV. During this process, MLV are either dispersed using a sonicator probe or placed in a sonicator bath to be fragmented. Ultrasonic irradiation reduces the size of the vesicles by providing energy to the lipid suspension of MLV, causing them to become smaller. This method has some problems, such as low encapsulation efficiency because the internal volume is small, the possibility that phospholipids and encapsulated compounds will break down, the removal of large molecules, and the presence of residual MLV.[193,194]

Microfluidic systems are now recognised as an effective technique for liposome production, enabling fine control over the synthesis process and producing liposomes with appropriate properties for drug delivery applications. These methods provide substantial benefits for scalability, repeatability, and control of liposome characteristics, including size, shape, and encapsulation efficiency. Microfluidic systems provide the precise control of fluids at the microscale, allowing better control over the sizes, shapes, and size distribution of liposomes. This accuracy is necessary for guaranteeing excellent repeatability across groups, which is essential for pharmaceutical applications. The capacity to regulate flow rate ratios and overall flow rates in microfluidic systems significantly influences encapsulation efficiency and lipid retention in liposomes, as shown by research on various flow rate ratios and solvent extraction techniques. Furthermore, microfluidic technologies make it possible to synthesise liposomes on a high throughput, a challenge that traditional methods often find difficult. The use of design-of-experiments (DoE) methodologies in microfluidic systems facilitates the optimisation and validation of process parameters, thereby ensuring reliable and scalable liposome production. Also, high-

throughput microfluidic technologies make it possible to make liposomes of exact size and with good drug encapsulation, which is not possible with traditional methods because they are not scalable or reproducible.[195–197] In this research, a microfluidic system was used to prepare liposomes, encapsulated and embedded liposomes; see the results in the following chapters.

1.12 Aim and objectives

1.12.1 Aim

The aim of this research is to develop and evaluate an alternative vector for crossing the blood-brain barrier (BBB) and delivering therapeutic agents for neurological disorders, specifically Alzheimer's disease.

1.12.2 Objectives

- **Synthesis and characterisation of CPP-Fatty Acid Conjugates:**
  - Develop cell-penetrating peptides (CPP) conjugated with fatty acids (palmitic acid, myristic acid, and lauric acid).
  - Characterise the conjugates using appropriate biochemical techniques, such as mass spectrometry and nuclear magnetic resonance (NMR) spectroscopy.

- **Formulation and characterisation of a liposomal drug delivery system:**
  - Embed the liposomal formulation with CPP-conjugated fatty acids.
  - Characterise the liposomal formulation in terms of size, charge, and morphology using techniques such as dynamic light scattering (DLS), nanosizer (ZetaView), and scanning electron microscopy (SEM).

- **Evaluation of Cytotoxicity of CPP-Fatty Acid Liposomal Formulation:**
  - Assess cell viability via MTT assays in blood-brain barrier endothelial cells.

- **To investigate the penetration ability of CPP-fatty acid conjugates**

- Evaluate the ability of CPP-fatty acid conjugate-embedded and encapsulated liposomes to penetrate an artificial BBB model.
- Characterise the eluent using appropriate biochemical techniques, such as LC-MS.

Chapter 2: Experimental Methodology

2.1 Chapter Overview

This chapter provides a comprehensive description of the methodologies used in this research. It consists of the following key areas:

Chemical Reagents and Instrumentation: All chemicals used to produce compounds are listed comprehensively. The instruments and techniques used for characterising all produced compounds.

Peptide Synthesis and Conjugation: The synthesis of peptides follows detailed procedures. Methods for conjugating peptides with fatty acids.

Liposome Preparation: Preparing liposomes involves using drug encapsulation compounds. Methods for embedding liposomes with peptides conjugated to fatty acids.

Human Endothelial Cell Culture: Protocols for cell culture.

Toxicity Assessment of Vectors: Evaluation of the toxicity of vectors on endothelial cells *via* MTT assay and real-time cellular analysis (IncuCyte).

Application on Artificial Blood-Brain Barrier (BBB): Experimental procedures for applying the prepared vectors on an artificial BBB model.

2.2 Chemicals and Instruments

The compounds were used in their original form as provided by the vendors (Sigma-Aldrich, UK, a subsidiary of Merck KGaA, Darmstadt, Germany, Acros Organics, a brand of Thermo Fisher Scientific based in Geel, Belgium., Alfa Aesar, a Thermo Fisher Scientific brand based in Heysham, UK) unless specified differently. All other solvents were used

in their original form without undergoing further purification since they were obtained in laboratory, analytical, or LC-MS grades.

The Biotage® Initiator+ Microwave System with Robot Eight, Biotage AB, Sweden was used to conduct microwave-assisted synthesis to prepare peptides in the solid phase. The system has dynamic temperature and pressure control and a 30-second pre-stirring time.

Mass spectrometric analysis was conducted using a Waters MS XVEOG2XS qTOF with the direct mass spectrometric infusion spray technique.

The ^{1}H and ^{13}C NMR spectra were obtained using a Jeol ECZ 400S operating at 400 MHz at a temperature of 25 °C.

The Biotage® Isolera flash chromatography, Biotage AB, Sweden.

A Dolomite Microfluidic System, Dolomite, UK; including two pumps, a microfluidic chip (Droplet junction chip 100 µm etch depth, hydrophobic, part No.: 3000301) with chip interface H, and a pressure supplier.

Joel JSM-7100F A Field Emission Scanning Electron Microscope (SEM) was utilised to examine the liposomes' morphology and size.

The concentration of liposomes was measured at room temperature (24 degrees) by using a nanosizer machine, ZetaView PMX120 (Particle Metrix, Germany).

To measure the absorbance of viable cells of the hCMEC/D3 a at 570 nm using a SYNERGY|LX spectrophotometer multi-mode plate reader (BioTek, USA).

To monitor the hCMEC/D3 cells the Incucyte® S3, S4, and S5 Live Cell Analysis Systems (Essen BioScience, Germany) was used.

In this study, all of the Fmoc amino acids and resins were acquired from Merck4Biosciences and utilised without any additional purification process. Used amino acids, their abbreviations, and chemicals:

Arginine (R), Fmoc-Arg(Pbf)-OH, and Fmoc-Arg(Pbf)-Wang resin (100-200 mesh).

Aspartic acid (D), Fmoc-Asp(OtBu)-OH

Glutamic acid (E), Fmoc-Glu(OtBu)-OH and Fmoc-Glu(OtBu)-Wang resin (100-200 mesh), Fmoc-

Lysine (K), Fmoc-Lys(Boc)-OH, and Lys(Boc)-Wang resin (100-200 mesh),

To visualise and track the embedded liposomes by fluorophore-peptide-fatty acid, the fluorescence microscopy, Leica Thunder Microscope with an LED8 light engine, Leica Microsystems, Germany was used.

Material and reagents for the human endothelial cell (hCMEC/D3)culture.

hCMEC/D3 culture medium Lonza EGM-2 Single Quots, catalogue No.: cc-4147, Lot No.: 0001226248, USA. Its media (foetal bovine serum (FBS). 25 mL, hydrocortisone. 0.2 mL, human fibroblast growth factor (hFGF-B). 2 mL, R3- IGF-1. 0.5 mL, ascorbic acid. 0.5 mL, epidermal growth factor human hEGF. 0.5 mL, and GA-1000. 0.5 mL).

Collagen type 1, Rat Tail, from Millipore, USA, Merck KGaA, Germany used as coating solution, Sterilised phosphate buffered saline (PBS), Trypsin-EDTA solution, sterile culture flasks P75. CO_2 incubator set at 37^0C, centrifuge, microscope and hood.

2.3 Methodology

2.3.1 Peptide Synthesis

Microwave-assisted solid-phase peptide synthesis (MSPPS) was used for the production of all peptides. The Wang resin, for instance, Fmoc-Lys(Boc)-Wang (100–200 mesh) (0.2 mmol, 0.298 g), was wetted with dimethylformamide (DMF, 1.5 mL) in a 10 mL MSPPS reaction vessel.

The mixture was then placed in the half-automated Biotage® Initiator+ SP Microwave Peptide Synthesiser and allowed to swell for 30 minutes at room temperature with stirring at 500 RPM. Subsequently, the resin was drained and washed automatically with DMF (4 x 5 mL) with stirring at 600 RPM.

The resin was deprotected from the Fmoc protecting group by adding piperidine (20% in DMF, 4 mL) in a two-stage process. The first stage involved allowing the reaction to proceed for (3 minutes at 75 ± 2 °C) with stirring at 500 RPM, followed by draining and the addition of fresh piperidine (20% in DMF, 4 mL) for the second stage. The second stage involved allowing the reaction to proceed for (10 minutes at 75 ± 2 °C) with stirring at 500 RPM. At the end of this process, the deprotected resin was washed with DMF (4 x 4 mL).

To elongate the peptide chain, the coupling agent O-(benzotriazol-1-yl)-N,N,N’,N’-tetramethyluronium hexafluorophosphate (HBTU) (0.6 mmol, 0.227 g) was dissolved in 1.5 mL of DMF, along with diisopropylethylamine (DIPEA) (0.4 mL, 0.3 mmol, 2.58 M), and the second amino acid of the peptide sequence, Fmoc-Lys(Boc)-OH (0.287 g, 0.6 mmol). This mixture was vortexed for 3-5 minutes to produce an activated ester solution. The solution was then added to the deprotected resin and exposed to microwave irradiation for double coupling. The first stage of the reaction was conducted for (5 minutes at 75 ± 2 °C) with stirring at (500 RPM), followed by draining. The same solution of the protected amino acid was prepared again and added to the resin for the second stage of the reaction, which also proceeded for (5 minutes at 75 ± 2 °C) with stirring at (500 RPM). Afterwards, the mixture was drained and washed with DMF (4 x 5 mL) at (1200 RPM).

The Fmoc deprotection of the amino acid was achieved by adding piperidine (20% in DMF, 4 mL) in a two-stage process. The first stage involved allowing the reaction to proceed for (3 minutes at 75 ± 2 °C) with stirring at (500 RPM), followed by draining. Fresh piperidine (20%

in DMF, 4 mL) was then added for the second stage, which proceeded for (10 minutes at 75 ± 2 °C) with stirring at (500 RPM). At the end of this process, the deprotected amino acid was washed with DMF (4 x 4 mL) at (500 RPM). Peptide elongation was performed by repeatedly removing the Fmoc group and coupling new amino acids until the desired sequence was obtained.

For further purification of the peptide after elongation, the resin was prepared for subsequent coupling with fatty acids. The resin underwent three additional washing stages using DMF, dichloromethane (DCM), and methanol (MeOH) (4 x 5 mL each) in that order. See Figure 2.1 for an example of the prepared peptides.

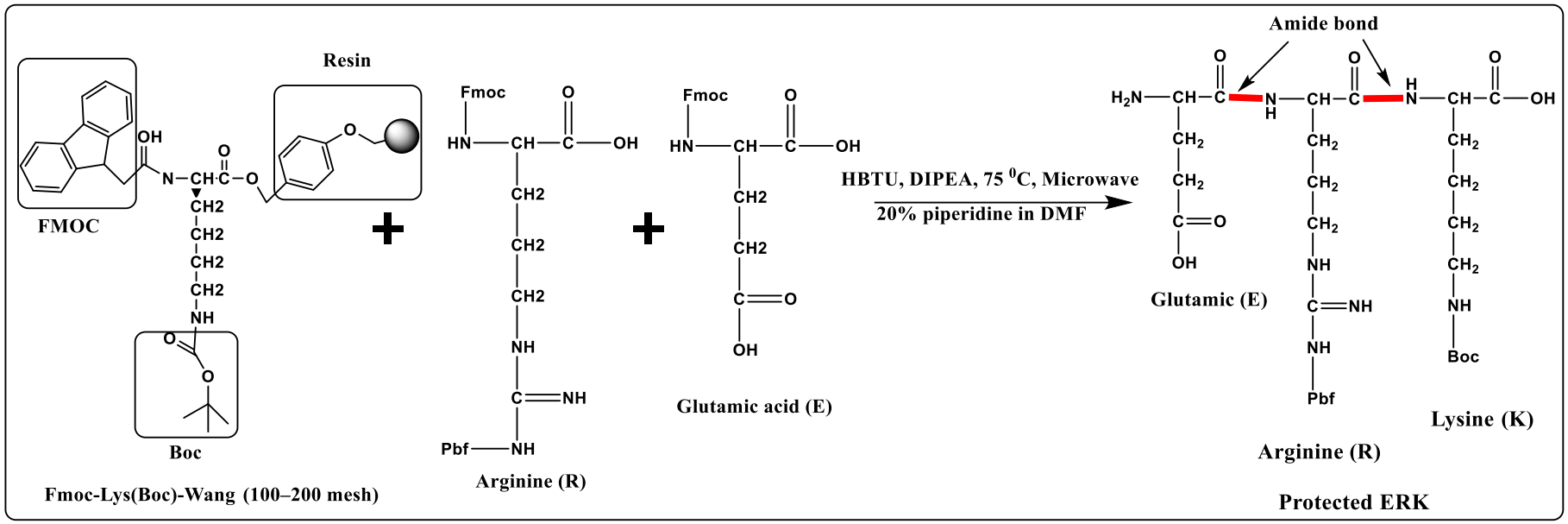

Figure 2.1: The chemical reaction to produce cationic tripeptide (ERK) contains glutamic acid (E), arginine (R), and lysine (K).

2.3.2 Coupling peptide with fatty acids

The peptide was then conjugated with three fatty acids: lauric acid (C_{12}) (CH_3-$(CH_2)_{10}COOH$), myristic acid (C_{14}) (CH_3-$(CH_2)_{12}COOH$), and palmitic acid (C_{16}) (CH_3-$(CH_2)_{14}COOH$) (see Figure 2.2). The peptide was combined with lauric acid (C_{12}) (0.04 g, 0.2 mmol), myristic acid (C_{14}) (0.046 g, 0.2 mmol), and palmitic acid (C_{16}) (0.051 g, 0.2 mmol) in a 1:1 molar ratio to the Wang resin. This combination of the peptide with the fatty acids in a 1:1 ratio to the Wang resin facilitates the attachment of the hydrophobic components, which can enhance the solubility and stability of the peptide in various applications. A balanced interaction is achieved by using specific amounts of each fatty acid, potentially optimising the peptide's functional properties. Additionally, four times the amount of coupling reagents, HBTU (2.4 mmol, 0.91 g) and DIPEA (1.2 mmol, 1.6 mL), were added. Then it was filtered and purified by washing using dimethylformamide (3 x 10 mL). The filtration and purification process with dimethylformamide helps remove unreacted materials and by-products, ensuring the final peptide product is high purity. This step is crucial for obtaining reliable results in subsequent applications or experiments.

The cleavage solution was made by mixing a cocktail solution (10 mL) that contains water (2.5% mL), triisopropylsilane (2.5% mL), ethylenedioxy diethanethiol (5% mL), and trifluoroacetic acid (90% mL) and stirring it at room temperature for 2.5 hours. This specific combination of ingredients is designed to create an effective cleavage solution, which facilitates the removal of protective groups (the bead of resin) from synthesised peptides. The careful proportions and mixing duration are crucial for achieving optimal results in the cleavage process.

After 2.5 hours, the mixture was filtered using a vacuum into diethyl ether (100 mL, -20 ^{o}C). The resin was washed with trifluoroacetic acid (TFA) (3 x 3 mL). The mixture was left to precipitate overnight in the

freezer (-20 °C). After the precipitation had happened, the mixture was separated into four 50-mL falcon tubes, with about 25 mL in each tube. Next, the tubes underwent centrifugation (5000 rpm, 4 °C) for 10 min. The diethyl ether was extracted and substituted with a fresh solvent at a temperature of -20 °C. The method was conducted three times, with each repetition including the sequential combining of two peptide pellets. As a consequence, the number of tubes decreased from 4 to 2 and finally to 1. The waxy white product was dried by using a vacuum, directing nitrogen gas or freeze drier.

The above protocol was repeated for all prepared peptides conjugated with fatty acids.

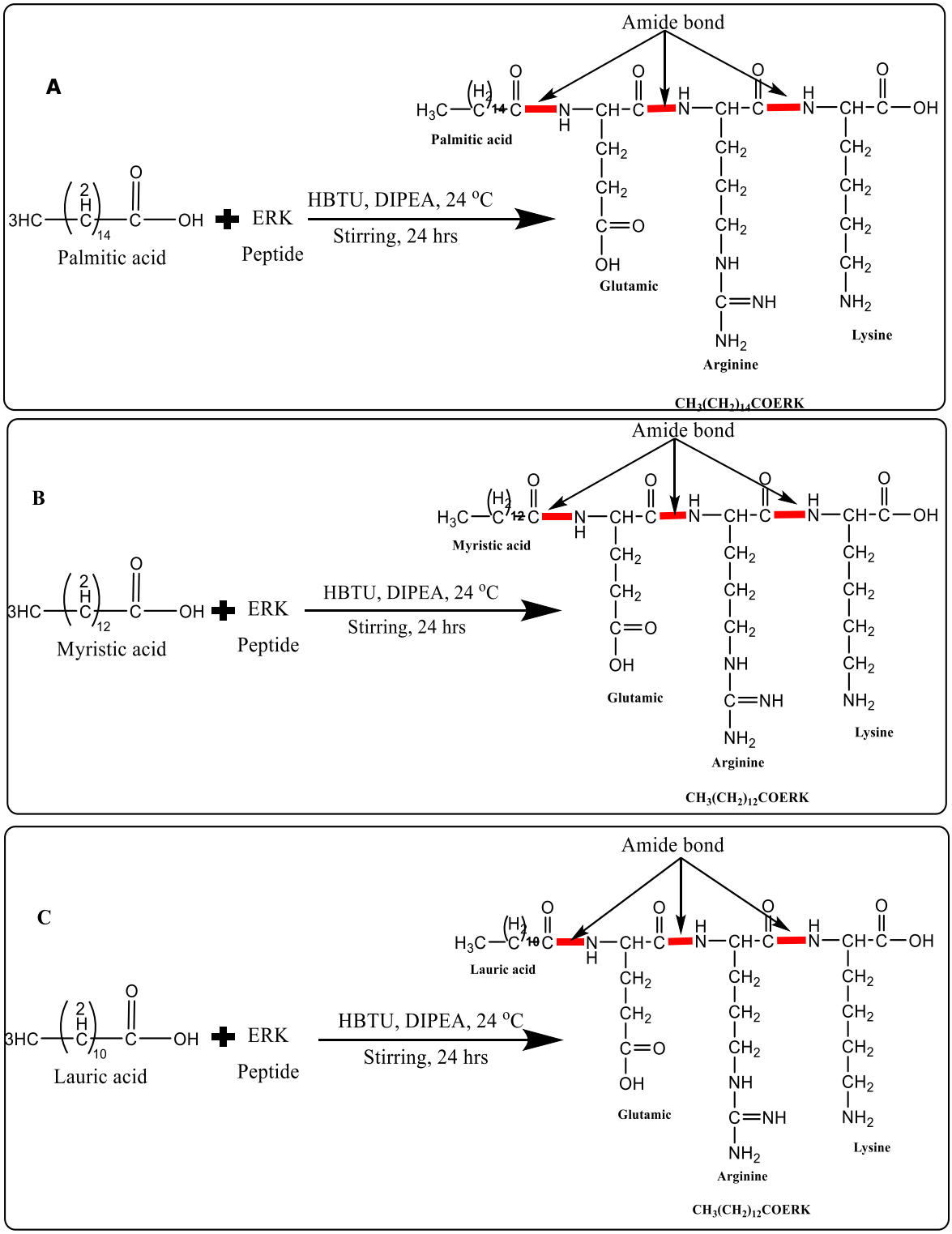

Figure 2.2: The chemical reaction of coupling peptide (ERK) with Fatty acids {**A**- Palmitic acid (C_{16}), **B**-Myristic acid (C_{14}), **C**- Lauric acid (C_{12})}

2.4 Characterisation of the prepared peptides coupled to fatty acids

The peptide-fatty acid was characterised using MALDI-TOF LC/MS to determine the produced peptides and their purity. The samples, mixed with MeOH LC-MS grade (0.2 mg in 1 mL), were introduced into the source at a flow rate of 0.3 µL min^{-1}. The LC criteria were as follows: The Eksigentekspert nanoLC 425 system was separated using an ACE raptor C18 column (100 x 2.1 mm, 2.7 µm) from ACE chromatography. At 45 ^{o}C, the mobile phase consists of MS-grade water containing 0.1% formic acid (solvent A) and methanol containing 0.1% formic acid (solvent B), provided by Merck, UK. The LC separation used a standardised gradient elution program with the following parameters: at 0 min, 1% B; at 1 min, 1% B; at 3 min, 50% B; at 10 min, 100% B; at 20 min, re-equilibration for 5 min. Mass Lynx software processes the LCMS/MS data that was collected.

Additionally, for further characterisation, ^{1}H- and ^{13}C NMR (JOEL ECZ 400 MHz) were used by dissolving (2 mg) of the result in methanol-D4 (1 mL) as the solvent. The chemical shift is expressed in parts per million (ppm) and is calibrated using the remaining solvent peak.

Then, all produced peptides conjugated fatty acids were purified by using the Biotage® Isolera flash chromatography, to purify coupled peptides with fatty acids at room temperature and using the Sfar C_{18} column (12 gm, flow rate 25 mL min^{-1}) as a stationary phase and methanol (B) and ultra-pure water (A) as a mobile phase. Their mobile phase gradient condition follows:

Time (min)	Solvent A	Solvent B
0-5	90%	5%
5-10	70%	30%
10-15	50%	50%
15-20	30%	70%
20-25	5%	90%

All prepared peptides that were conjugated with three distinct fatty acids were fully characterised by using LC-MS, ^{1}H NMR, ^{13}C NMR, and flash chromatography. The peptide names, their chemical structure, and the ^{1}H NMR, ^{13}C NMR, and LC-MS results are shown below. These show that all of the peptides were successfully made and with high purity. The flash chromatography methods were also used to make sure that each result was clean. This thorough characterisation confirms the successful synthesis and high purity of the peptides, indicating that conjugation with fatty acids was effective. The results from various analytical techniques provide a comprehensive validation of the peptides' structural integrity and purity.

2.5 Labelling peptide-fatty acid by Dansyl Chloride (5-(dimethylamino)naphthalene-1-sulfonyl chloride) and FITC (Fluorescein isothiocyanate)

The peptide-fatty acid was dissolved in acetone (1 mL), specifically cationic CPP conjugated palmitic acid ($CH_3(CH_2)_{14}CORRR$) (0.092 mmol). Then, 30% potassium carbonate (K_2CO_3) was added to the peptide-fatty acid mixture. This step is crucial for advancing the understanding of how these molecules interact at a biochemical level. Afterwards, in two separate tubes, mix dansyl chloride and FITC (fluorescein isothiocyanate) at a concentration 10% greater than that of the peptide-fatty acid. This change makes sure that the labelling agents are reactive enough to bind completely to the peptide-fatty acid complexes. Consequently, this enhances the detection and analysis of these interactions in subsequent experiments. Continue stirring and allow the mixture to develop at room temperature for two nights. This prolonged stirring and development period allows the reactive labelling agents to fully engage with the peptide-fatty acid complexes.

2.5.1 Characterisation of labelled peptides conjugated fatty acids

Confocal microscopy was used to analyse the primary results, revealing the presence of dansyl chloride (blue), and FITC (green). Both coupled fluorophores were characterised by LC-MS and NMR.

MALDI-TOF LC/MS to determine the produced labelled peptide conjugated fatty acid and their purity. The samples, mixed with MeOH LC-MS grade (0.2 mg in 1 mL), were introduced into the source at a flow rate of 0.3 µL min^{-1}. The LC criteria were as follows: The Eksigentekspert nanoLC 425 system was separated using an ACE raptor C18 column (100 x 2.1 mm, 2.7 µm) from ACE chromatography. At 45 ^{0}C, the mobile phase consists of MS-grade water containing 0.1% formic acid (solvent A) and methanol containing 0.1% formic acid (solvent B), provided by Merck, UK. The LC separation used a standardised gradient elution program with the following parameters: at 0 min, 1% B; at 1 min, 1% B; at 3 min, 50% B; at 10 min, 100% B; at 20 min, re-equilibration for 5 min. Mass Lynx software processes the LC-MS/MS data that was collected.

Additionally, for further characterisation, ^{1}H- and ^{13}C NMR (JOEL ECZ 400 MHz) were used by dissolving (2 mg) of the result in methanol-D4 (1 mL) as the solvent. The chemical shift is expressed in parts per million (ppm) and is calibrated using the remaining solvent peak.

2.6. Liposome preparation

Before beginning to prepare liposomes, the microfluidic system (Dolomite) was calibrated. Empty and clean vials (10 mL) were used and subsequently weighed. The basic pressure pump and pump 1 were turned on, and the pressure supplier was connected to both pumps to maintain the appropriate pressure of them. After that, the system was accessed. Pump 1 and the basic pressure pump were filled with distilled water, and a microfluidic chip (100 µm) was connected to them. This

chip has three inputs and one output. With an initial value of 200 mbar, the pressure increased by 200 mbar at each subsequent interval until it reached 6000 mbar. Each pressure increase continued for 5 min.

Following the established liposome production protocol by the Dolomite company for their microfluidic system (see Figures 2.3 and 2.4), the phosphatidylcholine (10 mg/mL) was dissolved in methanol. Then, another solution was produced by dissolving cholesterol (3 mg/mL) in methanol. Incorporate the previously stated solutions into Pump A, which is connected to the central line of the microfluidic chip (Droplet junction chip, 100 µm etch depth, hydrophobic, part No.: 3000301) with chip interface H, and a pressure supplier. Meanwhile, load Pump B with distilled water, which functions as a scissor to cleave the lipid molecules, resulting in the production of liposomes. Subsequently, the established flow rate was used to generate the requisite liposome sizes. Pump A with a flow rate of 11.618 µL/min (pressure = 2 bar) and a water pump flow rate of 24.93 µL/min (pressure = 2.6 bar). This method enables precise control over the liposome formation process, ensuring the desired characteristics and uniform size. The combination of lipid solutions with distilled water in a microfluidic environment enhances the efficiency of liposome production.

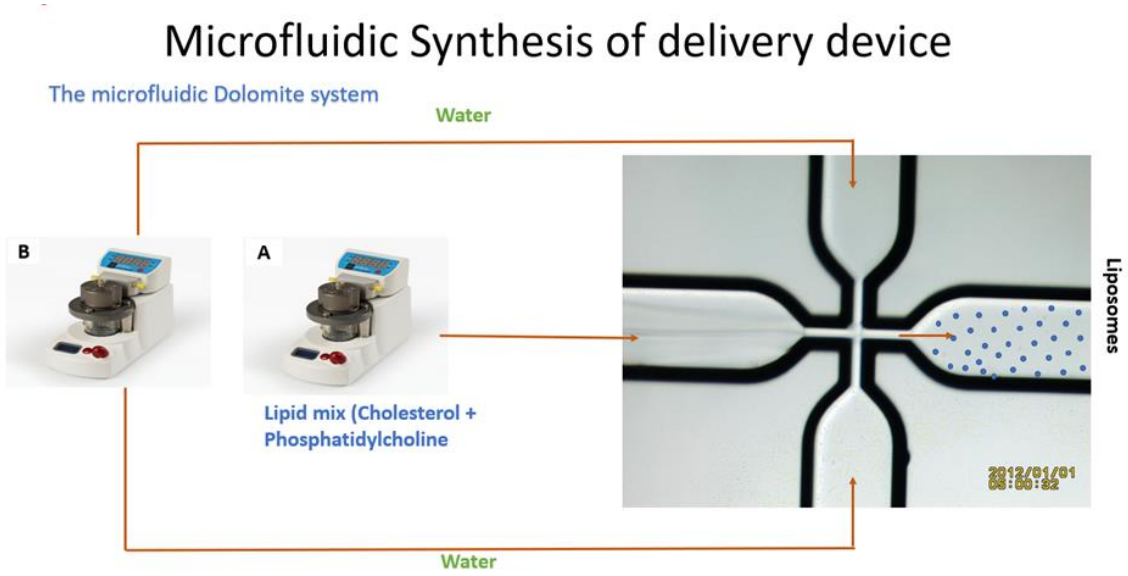

Figure 2.3: Illustrates the dolomite microfluidic system, which comprises two pressure pumps and a microfluidic chip.

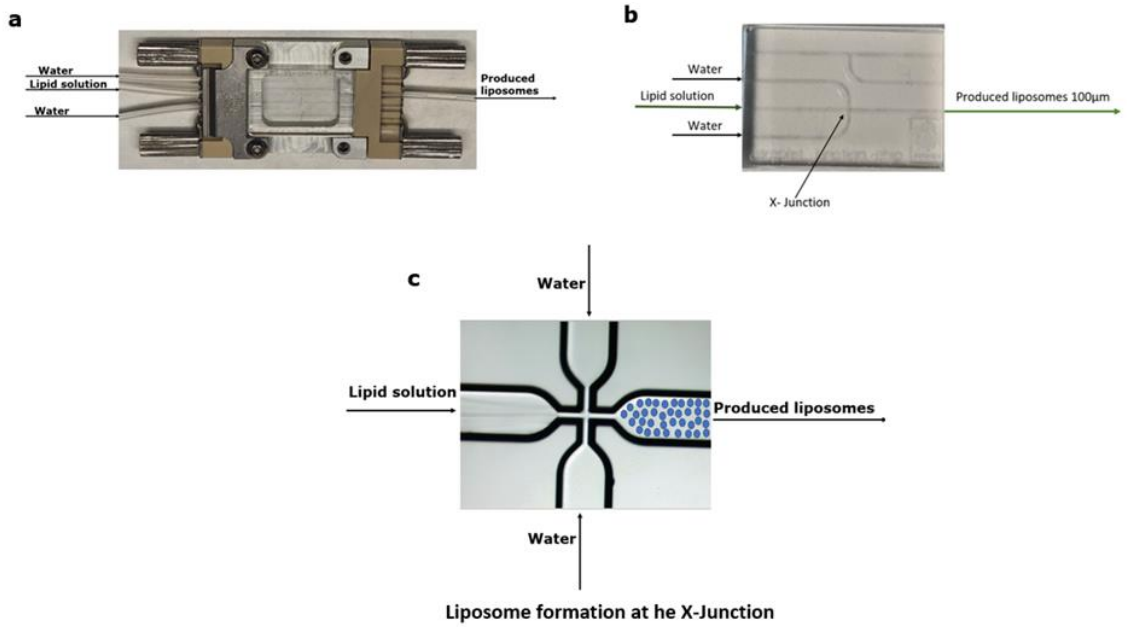

Figure 2.4: Illustrates the most important parts of the microfluidic system: a) the chip interface H; b) the hydrophobic microfluidic chip (Droplet junction hydrophobic chip (100 µm) etch depth, Part No.: 3000301); and c) the liposome formation at the X-junction, which is used to make liposomes, encapsulated liposomes, and embedded liposomes.

2.6.1 Liposome characterisation

The size and polydispersity index (PDI) of the liposomes were measured using dynamic light scattering (DLS) with a NanoPlus Zeta/Nanoparticle Analyser, Otsuka Electronics, Japan. The measurements were conducted at 4 °C using low-volume sizing cuvettes (0.5 mL).

Scanning electron microscopy (SEM) was used to confirm the size and morphology of the produced liposomes.

To further characterise the produced vectors in terms of concentration and charge, a nanosizer machine, ZetaView PMX120 (Particle Metrix, Germany), was used. Polystyrene (diluted in ultra-pure water in a 1:1 ratio) was used as a standard bead solution, pin: 750009-03. The beads (polystyrene) were used as a reference (blank) at a dilution ratio of 1/300,000. The software ZetaView 8.04.02 was used to analyse the data.

2.7 Encapsulating Rhodamine B Dye into Liposomes.

In compliance with the designated technique for liposome production using the microfluidic system (see Figures 2.3 and 2.4), the phosphatidylcholine (10 mg/mL) was solubilised in methanol. A subsequent solution was created by dissolving cholesterol (3 mg/mL) in methanol and Rhodamine B dye (2.5 µg/mL in distilled water). Once the solutions had been mixed, they were put into Pump A and connected to the microfluidic chip's central channel (Droplet junction chip 100 µm etch depth, hydrophobic). This setup makes sure that the phosphatidylcholine and cholesterol are mixed perfectly in a controlled setting, which makes it easier to make liposomes with the properties that are wanted. The other pump B, contains distilled water and connects to both sides of the chip's X-shaped inlet. The determined

flow rate produced encapsulated liposomes of the necessary size (*ca.* 100 nm).

2.7.1 Characterisation of Encapsulated Rhodamine B Dye into Liposomes

Dynamic light scattering (DLS) measured the size and polydispersity index (PDI) of the encapsulated liposomes with Rhodamine B dye. To determine their morphology, scanning electron microscopy (SEM) was used.

2.8 Embedded fluorophore-peptide-fatty acid into liposomes

Both fluorophores were embedded into liposomes separately by using the same concentration and microfluidic system. In accordance with the specified method for liposome production, the microfluidic system was used (see Figures 2.3 and 2.4); phosphatidylcholine (10 mg/mL) was solubilised in methanol. Another solution was prepared by dissolving cholesterol (3 mg/mL) in methanol. The previously mentioned solutions were mixed with the coupled dansyl chloride to the multi-arginine peptide-palmitic acid (2.5 mg/mL). Then, the solution was placed into Pump A, which was then connected to the central channel of the microfluidic chip (droplet junction chip, 100 µm etch depth, hydrophobic). Meanwhile, Pump B, used distilled water and cleaves lipid molecules, facilitating the formation of embedded liposomes by fluorophores that are coupled to the triple arginine peptide-fatty acid molecules. The specified flow rate generated liposomes of the required size (*ca.*100 nm). The product was analysed using a fluorescent microscope (100X).

Repeating the above procedure to embed FITC-peptide-fatty acid instead of the dansyl chloride and using the same concentration (2.5 mg/mL).

2.8.1 Characterisation of embedded dansyl chloride-RRR-palmitic acid and FITC-ERK-palmitic acid into liposomes

Both fluorophores were embedded into liposomes separately. Their products were characterised using scanning electron microscopy and fluorescence microscopy (100X).

2.9 Human hCMEC/D3 cell culture

The P75 flask with collagen (10 µL) in sterile PBS (7 mL) was coated. The flask was incubated overnight at 37 °C and then rinsed with PBS before use. The medium for hCMEC/D3 was prepared, and it was Lonza EGM-2 Single Quots, USA (500 mL), and its supplements were (foetal bovine serum (FBS) (25 mL), hydrocortisone (0.2 mL), human fibroblast growth factor (hFGF-B) (2 mL), R3-IGF-1 (0.5 mL), ascorbic acid (0.5 mL), epidermal growth factor human hEGF (0.5 mL), and GA-1000 (0.5 mL). The hCMEC/D3 cells in Crovial, which were frozen, were quickly thawed in a water bath (37 °C) to bring them back to a liquid state. Then, the hCMEC/D3 cells were transferred into pre-warmed culture medium (10 mL) and centrifuged for 5 min at 3000 RPM. After that, the supernatant was aspirated, and the cell pellet was resuspended in a fresh pre-warmed culture medium (500 µL). The cells were then seeded into the coated P75 flask that had fresh pre-warmed medium (10 mL) and incubated at 37 °C. This step ensures that the hCMEC/D3 cells are evenly distributed in a suitable environment for growth and further experimentation. Incubating at (37 °C) mimics physiological conditions, promoting optimal cell viability and function. The medium was changed after 24 hours, and the cells were sub-cultured for 2-3 days. Cell confluence and morphology were monitored under a microscope until their confluence reached 90% (see Figure 2.5).

After confluency of the cells, they were rinsed with PBS 3 times, and then trypsin-EDTA solution was added, and the cells were incubated at

37 °C for 5 min until the cells detached from the bottom of the P75 flask. This process ensures the cells are properly detached for further experimentation without compromising their viability. Trypsin-EDTA facilitates the gentle release of cells from the culture surface, allowing for accurate assessment and manipulation in subsequent steps. After that, 5 mL of culture medium was added to neutralise the trypsin-EDTA and incubated at 37 °C for 5 min. The mixture was then moved to a 15-mL Falcon tube and centrifuged at 3000 RPM for 5 min. This centrifugation step helps to pellet the detached cells at the bottom of the tube, separating them from the trypsin-EDTA solution. Following this, the supernatant was typically discarded, leaving the concentrated cell pellet ready for resuspension or further analysis. Next, discarded the solvent and resuspended them in 1 mL of freshly pre-warmed medium. To count the cells, 10 µL was taken from above and transferred to 100 µL of trypan blue, mixed thoroughly, and left for 2–3 min. Next, add 10 µL to the cell counting chamber and appeared that the number of live cells was 50,000 live cells/mL. This process ensures that the cells are properly stained with trypan blue, which allows for the differentiation between viable and non-viable cells. The cell counting chamber facilitates an accurate assessment of cell concentration and viability.

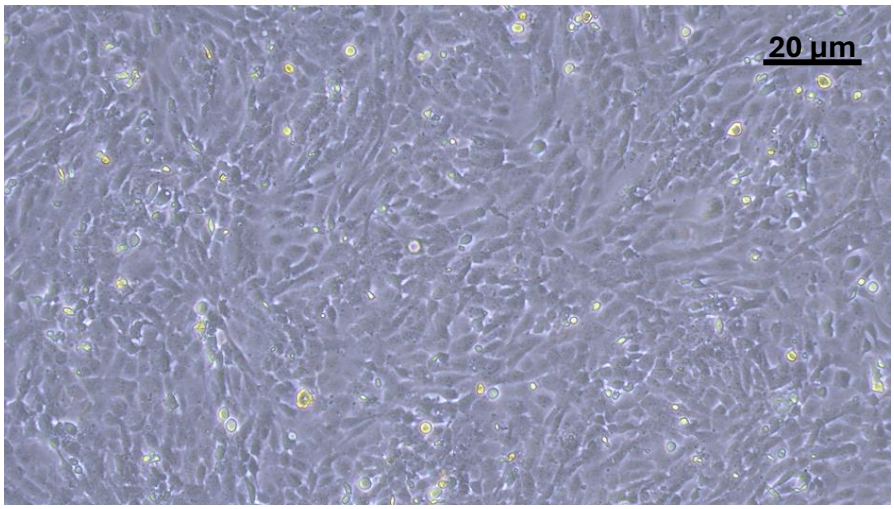

Figure 2.5: hCMEC/D3 cells grown on the surface forming a BBB model.

2.10.1 Evaluation of the cytotoxicity of produced vectors using the MTT assay in the hCMEC/D3 cell line.

The MTT assay was used to evaluate the impact of the vectors on the viability of hCMEC/D3 cells. A total of 8000 hCMEC/D3 cells were seeded per well in 96-well plates, each containing 200 µL of growth medium. The cells were allowed to recover from handling stress for 24 hours before the introduction of vectors. This recovery period ensures that the cells are in optimal condition to respond accurately to the vectors, minimising any potential confounding effects from the initial handling. By allowing the cells to stabilise, the experiment aims to obtain reliable data on the vector's influence on cell viability. Subsequently, the medium was carefully aspirated and replaced with fresh medium containing varying concentrations of vectors, specifically peptide-fatty acid embedded in liposomes. The serial vector concentrations were (0, 3.6 X 10^2, 3.6 X 10^3, 3.6 X 10^4, and 3.6 X 10^5 particles/mL or nanomoles per litre (nM/L), with three replicates for each condition. This step ensures that any initial disturbances are minimised, allowing for a more accurate assessment of how different concentrations of the vectors affect cell viability. By using multiple replicates for each condition, the experiment enhances the reliability of the results obtained. The control was cells alone with their medium, and the blank was just medium; both were in triplicate wells as cells with vectors.

After 24, 48, and 72 hours of treatment, 20 µL of 5-(4,5-dimethyl-2-thiazolyl)-2,5-diphenyl-2H-tetrazolium bromide (MTT) solution (5 mg/mL in PBS) was added to each well until the final concentration reached 0.5 mg/mL (see Figure 2.6). The cells were then incubated at 37°C for 40 minutes. This incubation period allows the MTT to be metabolically reduced by viable cells, resulting in the formation of a purple formazan product. The intensity of the colour produced is directly proportional to the number of live cells, thus providing a

quantitative measure of cell viability across different vector concentrations. The MTT solution was carefully taken out after the incubation, and 200 µL of dimethyl sulfoxide (DMSO) was added to each well. This addition of DMSO serves to solubilise the purple formazan crystals formed during the MTT reduction process, enabling accurate measurement of absorbance. The resulting absorbance values can then be analysed to determine the viability of cells at varying concentrations of the tested vectors. This resulted in the appearance of a pink colour, which intensified over time (see Figure 2.7). The plate was subsequently kept in the dark for 10 minutes to facilitate the formation of formazan crystals. This step is crucial, as it prevents any light exposure that could potentially interfere with the reaction and ensures that the formazan crystals fully develop. The darkness allows for a more consistent and accurate assessment of cell viability when measuring the absorbance.

Absorbance measurements were performed by using a spectrophotometer at 570 nm using a SYNERGY|LX multi-mode plate reader (BioTek, USA) and analysed with Gen5 3.11 software. The use of a specific wavelength at 570 nm is essential for accurately quantifying the formazan crystals, as it corresponds to the peak absorbance of these compounds. This precise measurement, combined with the analysis software, allows for a reliable interpretation of cell viability results.

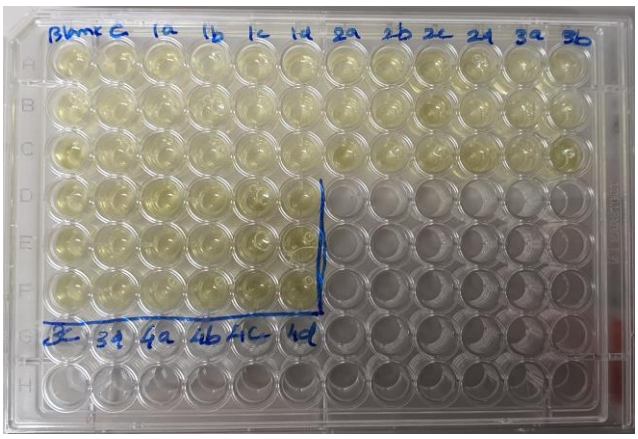

Figure 2.6: Shows the effect of the blood-brain barrier human endothelial cells after adding different concentrations of produced vectors to find the cells' viability by using the MTT assay.

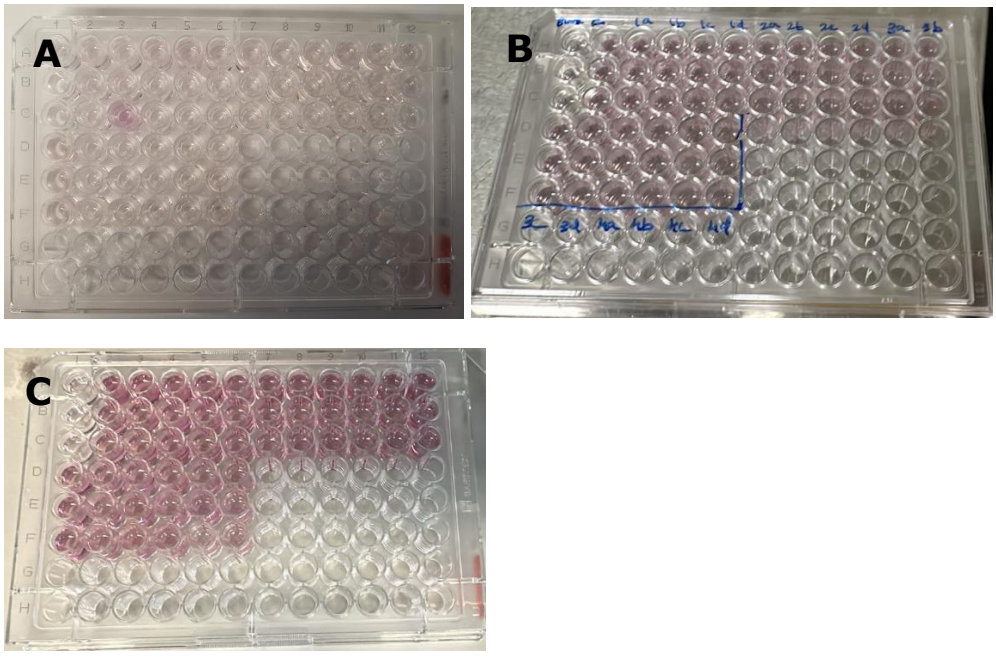

Figure 2.7: Shows the effect of produced vectors on the endothelial cells. As the time increased, the formation of formazan crystals increased, as evidenced by the MTT's colour changing from light pink (24 hrs) to dark pink (72 hrs). The figures A), B), and C) illustrate the impact of varying vector concentrations after 24 hours, 48 hours, and 72 hours, respectively.

2.11 Application of innovative vectors on an artificial BBB that contains only hCMEC/D3

Preparation of transwell inserts for hCMEC/D3

The transwell inserts were prepared by electrospinning nanofiber scaffolds at the bottom of the inserts, replacing the commercially available membrane. The electrospun nanofibers were then coated with collagen type I (20 µg/ml; 08-115, Sigma). The excess collagen was removed after a 1 h incubation period to allow for collagen attachment, leaving a collagen-coated surface on the (growing endothelial cells on a PAN–Jeffamine electro spun nanofiber as a 3D scaffold). The prepared inserts were placed into 24-well plates, ready for hCMEC/D3 (SCC066, Sigma) cell seeding.

BBB development using HCMEC/D3 cell lines

hCMEC/D3 cells were cultured in EndoGRO™-MV complete media kit (CC-3156, Lonza), supplemented with EndoGRO™-MV growth supplement (CC-4147, Lonza). The cells were seeded at a density of 200,000 cells on the apical side of the nanofiber inserts, which mimic a 3D environment. The cells were cultured for 9 days to promote barrier formation, during which they developed a monolayer and formed tight junctions, mimicking the blood-brain barrier characteristics. (See Figure 2.8).

Paracellular Permeability Assay

Barrier function across the monolayer was assessed using drug-loaded liposomes on nanofiber scaffolds electrospun to the bottom of transwell inserts, seeded with endothelial cells. The inserts were placed in 24-well plates, with endothelial growth medium added to the basal side (950 µl) and apical side (250 µl). The medium (250 µl) in the apical chamber was taken out for medium containing liposomes (250 µl) to use the final concentration of embedded liposomes by cationic tripeptide conjugated fatty acids $(CH_3CH_2)_{14}$CORRK and ionic tripeptide conjugated fatty acids ($(CH_3CH_2)_{14}$CODDK) (3.6×10^2, 3.6

× 10^3, and 3.6 10^4 particles/mL mg/ml) and encapsulated the same liposomes by L-carnosine (2.5 mg/mL). From the basal chamber, samples (250 µl) were collected at regular intervals each hour until 6 hours and transferred to a centrifuge tube, with the medium replaced by fresh medium (250 µl).

To find the amount of penetrated carnosine, all collected eluent was characterised by using Waters qTof LC-MS.

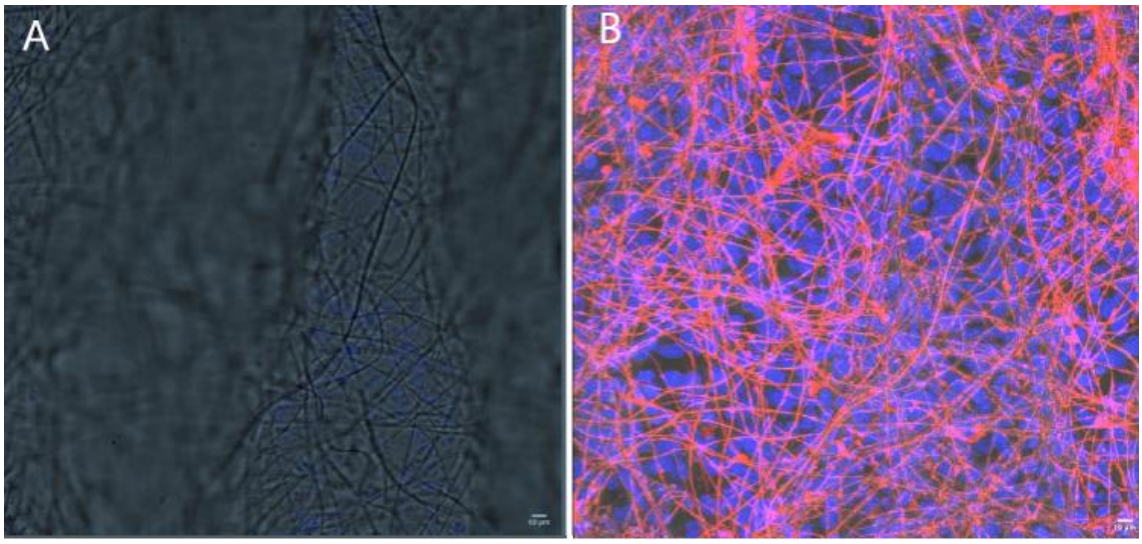

Figure 2.8: Illustrates **A-** transmittance microscopy images of the nanofiber scaffold. **B**- Rowing endothelial cells on a PAN–Jeffamine electro-spun nanofiber as a 3D scaffold.

Chapter 3: Cell-penetrating peptides

3.1 Summary

This chapter describes the synthesis of cationic cell-penetrating peptides and ionic peptides. Solid-phase peptide synthesis via a microwave synthesiser was used to prepare both types of peptides. Using solid-phase peptide synthesis with microwaves makes it faster and easier to produce peptides, improving their use in medical research and drug delivery. This method streamlines the process while ensuring high purity and yield of the synthesised peptides. The CPPs and ionic peptides were conjugated with three different types of fatty acids: palmitic acid, myristic acid, and lauric acid, in order to improve their stability, cellular absorption, and embedding in the liposomes. This conjugation enhances the peptides' properties by facilitating their incorporation into cellular membranes and thus improving their effectiveness in targeted drug delivery systems. As a result, the modified peptides exhibit increased stability and bioavailability, which are crucial for their practical applications in therapeutics. In addition, two of those CPPs were further modified with fluorescent biomarkers, dansyl chloride, and fluorescein isothiocyanate for the aim of enhancing the visualisation and tracking of the peptides conjugated to fatty acids during their embedding into liposomes and application to grow endothelial cells on a nanofiber 3D scaffold. Liquid chromatography-mass spectrometry (LC-MS), proton nuclear magnetic resonance (^{1}H NMR), and carbon nuclear magnetic resonance (^{13}C NMR) were used to completely characterise the synthesised peptides. To clean up all the cationic and ionic peptides that were made, Biotage flash chromatography with a reverse-phase C18 column was used.

3.2 Results and Discussion

3.2.1 Result

In this study, four cationic tripeptides were prepared (see Table 1). The peptides listed in Table 1 have been synthesised and purified by using flash chromatography and a reversed-phase (C_{18}) column, and synthesised *via* solid-state using a semi-autonomous microwave peptide synthesiser (Biotage) using a double coupling process (see below section). The results from LC-MS, ^{1}H NMR, and ^{13}C NMR tests verified that their synthesis was successful, with a purity percentage above 95%.

Table 3.1: Shows all produced and targeted triple peptides in this research, and they were conjugated with three distinct fatty acids: lauric acid (C_{12}), myristic acid (C_{14}), and palmitic acid (C_{16}).

No	**CPPs**	**CPPs+Palmitic acid**	**CPPs+Myristic acid**	**CPPs+Lauric acid**
1	RRR	$CH_3(CH_2)_{16}CORRR$	$CH_3(CH_2)_{14}CORRR$	$CH_3(CH_2)_{12}CORRR$
2	RRK	$CH_3(CH_2)_{16}CORRK$	$CH_3(CH_2)_{14}CORRK$	$CH_3(CH_2)_{12}CORRK$
3	ERK	$CH_3(CH_2)_{16}COERK$	$CH_3(CH_2)_{14}COERK$	$CH_3(CH_2)_{12}COERK$
4	RK	$CH_3(CH_2)_{16}CORK$	$CH_3(CH_2)_{14}CORK$	$CH_3(CH_2)_{12}CORK$
5	DDK	$CH_3(CH_2)_{16}CODDK$	$CH_3(CH_2)_{14}CODDK$	$CH_3(CH_2)_{12}CODDK$
6	EEE	$CH_3(CH_2)_{16}COEEE$	$CH_3(CH_2)_{14}COEEE$	$CH_3(CH_2)_{12}COEEE$

The first tripeptide was a triple arginine peptide (RRR), which was the strongest cationic tripeptide, and was made by using a microwave solid-phase peptide synthesis method *via* a Biotage microwave peptide synthesiser. To produce it started with Fmoc-Arg(Pbf)-Wang resin (100-200 mesh) and then coupled with two molecules of arginine that were

protected by Fmoc and Pbf groups (Fmoc-Arg(Pbf)-OH). (See Figure 3.1)

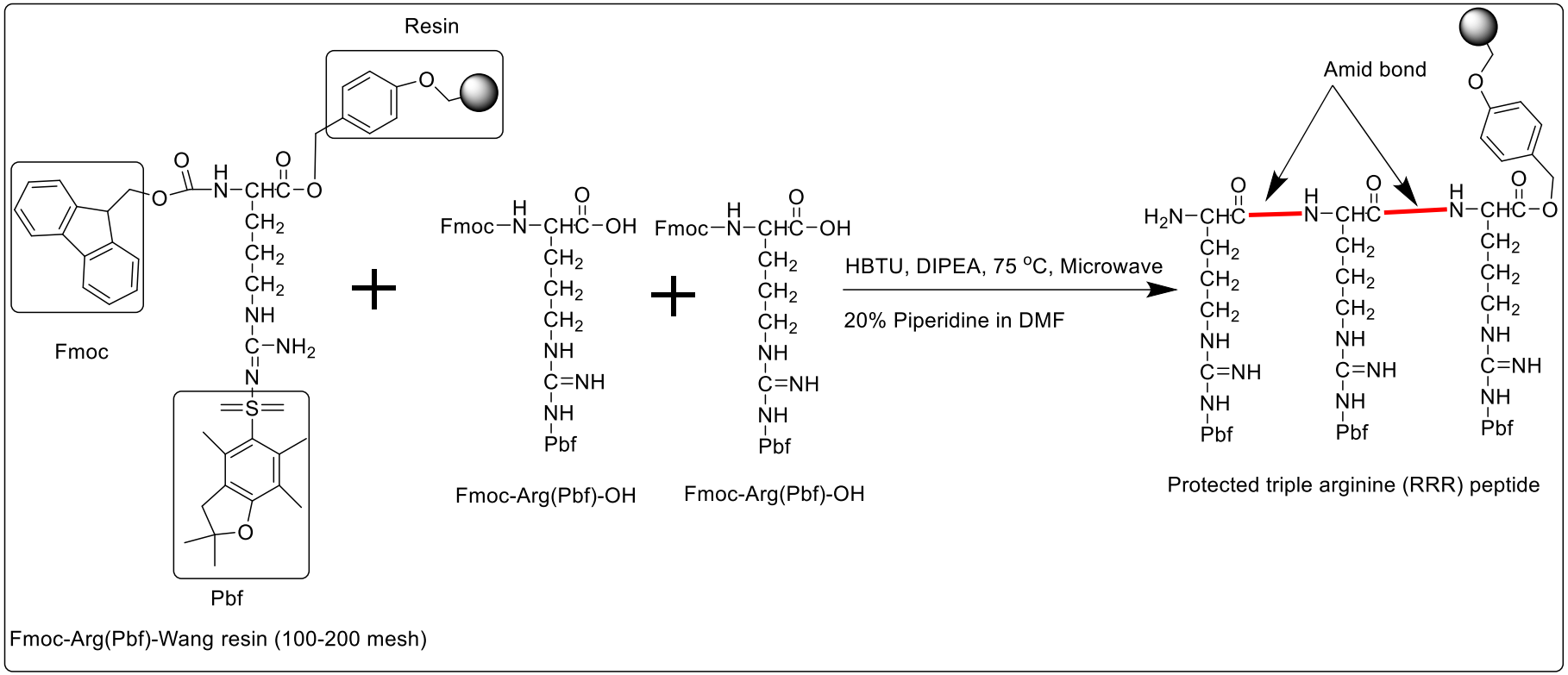

Figure 3.1: Shows how to produce the triple arginine peptide, and the arginine molecules were linked by an amide bond.

After producing the protected triple arginine peptide, it was coupled with three different fatty acids through amide bonds: palmitic acid ($CH_3(CH_2)_{14}CORRR$), myristic acid ($CH_3(CH_2)_{12}CORRR$), and lauric acid ($CH_3(CH_2)_{10}CORRR$) by using HBTU and DIPEA as coupling agents with continuous stirring overnight at room temperature. See Figure 3.2.

An amide bond couples the fatty acids with the peptides. The amide bond between fatty acids and peptides was formed by using HBTU as a coupling agent dissolved in DMF, and DIPEA was added to make it a basic solution. To create the same amide bond between fatty acids and peptides, the coupling process required four times more coupling agents than when using microwaves. This is because, in solid-phase peptide synthesis, microwaves were used as a source of energy to provide similar and high temperature (75°C) for the reaction mixture, while coupling fatty acids was done at room temperature and needed to stir overnight.

Then, cleavage cocktail (10 mL) that contains (90% TFA, 2.5% water, 2.5% TIPS and 5% ethylenedioxy diethanethiol) was added with stirring at room temperature for 2.5 hours. This specific combination of ingredients is designed to create an effective cleavage solution, which facilitates the removal of protective groups.

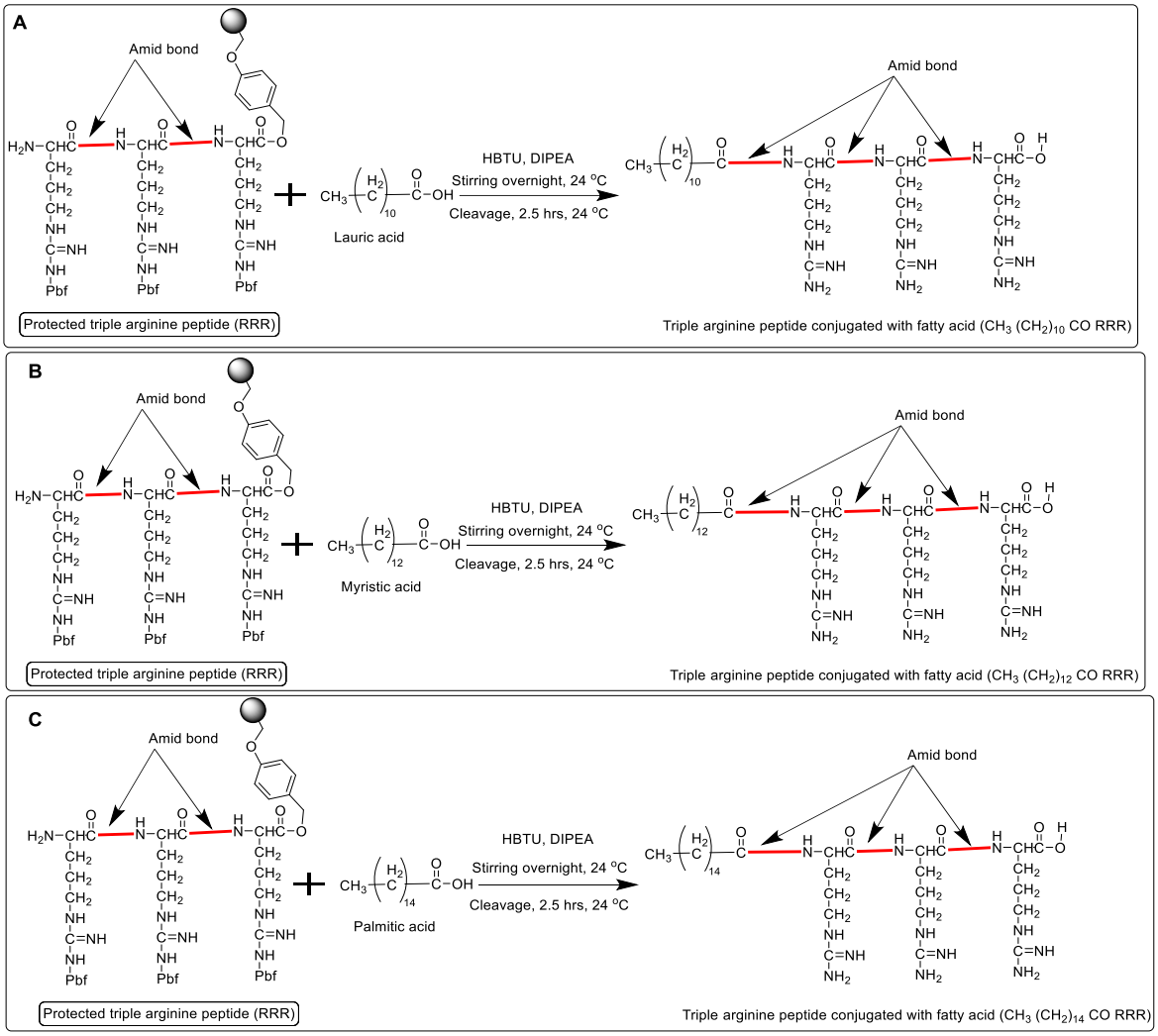

Figure 3.2: The diagram illustrates the chemical reactions that produce conjugated triple arginine peptide with three different fatty acids (**A-** lauric acid, **B-** myristic acid, and **C-** palmitic acid). An amide bond linked them together.

The conjugated triple arginine peptides with fatty acids ($CH_3(CH_2)_{10}CORRR$, $CH_3(CH_2)_{12}CORRR$, and $CH_3(CH_2)_{14}CORRR$) were fully characterized using WATERS LC-MS, ^{1}H NMR, and ^{13}C NMR. Flash chromatography also was used to purify them.

The LC-MS machine data shows that the combination of triple arginine and lauric acid has a molar mass-to-charge ratio (M/Z) of 668, which was exactly the same as theoretical. It was also, detected at a retention time of 7.51 minutes and had a purity greater than 96%.

Also, the product's weight was 0.52 g, which is equivalent to 7.8 x 10^{-4} mol.

The ^{1}H NMR and ^{13}C NMR confirmed that $CH_3(CH_2)_{10}CORRR$ was produced, and it has high purity because all the peaks of its atoms (H, C) could be found, and the results are as follows.

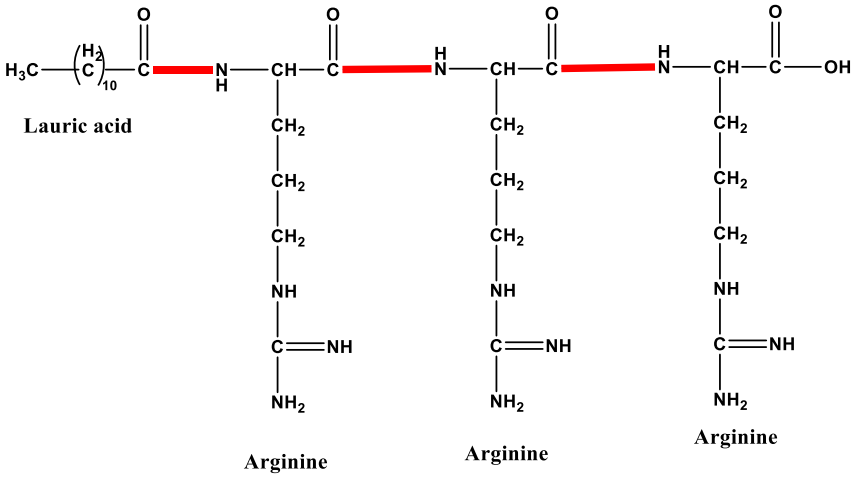

^{1}H NMR spectrum for triple arginine peptide that coupled with lauric acid: (400 MHz, CD_3OD, 25 °C) δ = 0.87 (t,^{3}J = 8.00 Hz, 3H), 1.27 (m, 16H), 1.55 (m, 8H), 1.79 (m, 6H), 2.1 (t, ^{3}J= 8.00 Hz, 2H), 2.6 (t, ^{3}J = 8.00 Hz, 3H), 3.4 (t, ^{3}J = 8.00 Hz, 6H), 4.5 (t, ^{3}J= 8.00 Hz, 2H), 6.7 (s, 6H), 7.9 (s, 3H), 8.4 (s, 3H) ppm.

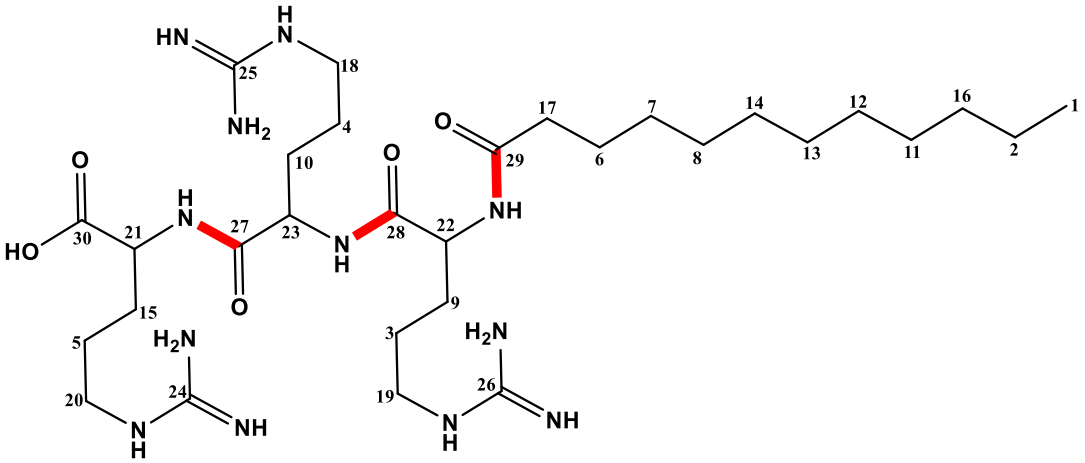

^{13}C NMR (100 MHz, CD_3OD, 25 °C) δ = 13.1, 22.4, 23.4, 23.5, 24.8, 24.9, 25.6, 28.2, 28.3, 28.6, 28.9, 29.2, 29.3, 29.4, 33.9, 35.5, 35.6, 36.5, 39.2, 40.7, 51.8, 53.1, 53.3, 157.2, 157.3, 157.4, 172.8, 173.2, 173.45, 175.5 ppm.

The LC-MS machine data shows that the combination of triple arginine and myristic acid was produced successfully with a high purity ratio. Its molar M/Z= 696 which was exactly the same as theoretical, retention time: 8.55 min, purity: >96%. Product: 0.53 g, 7.6 x 10^{-4} mol.

The ^{1}H NMR and ^{13}C NMR confirmed that $CH_3(CH_2)_{12}CORRR$ was produced, and it has high purity because all the peaks of its atoms (H, C) could be found, and the results are as follows.

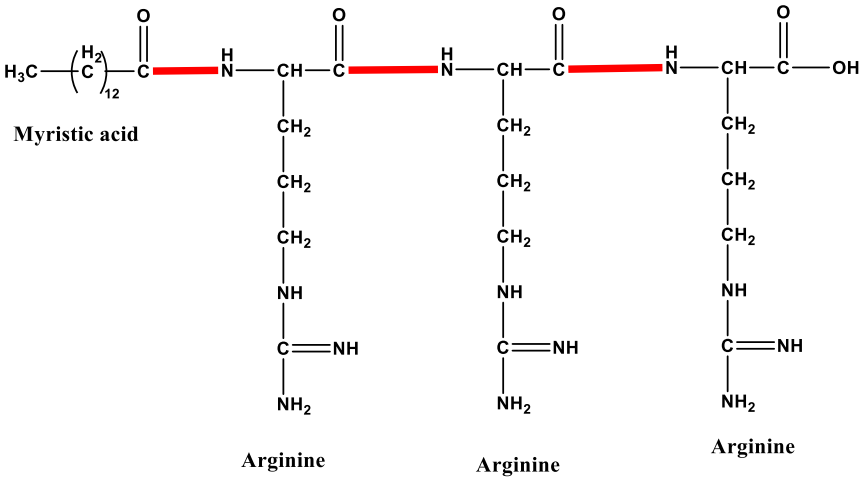

^{1}H NMR spectrum for triple arginine peptide that coupled with myristic acid: (400 MHz, CD_3OD, 25 °C) δ= 0.86 (t,^{3}J = 7.60 Hz, 3H), 1.27 (m, 20H), 1.55 (m, 8H), 1.79 (m, 6H), 2.1 (t, ^{3}J = 7.60 Hz, 2H), 2.6 (t, ^{3}J = 7.60 Hz, 3H), 3.4 (t, ^{3}J = 7.60 Hz, 6H), 4.5 (t, ^{3}J = 7.60 Hz, 2H), 6.7 (s, 6H), 7.9 (s, 3H), 8.4 (s, 3H) ppm.

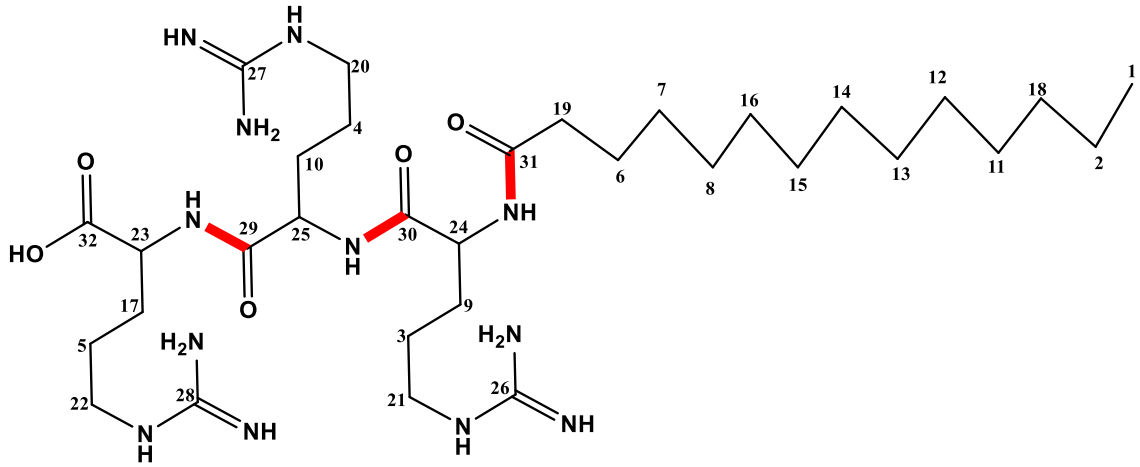

^{13}C NMR (100 MHz, CD_3OD, 25 °C) δ= 13.1, 22.4, 23.4, 23.5, 24.8, 25.0, 25.7, 28.3, 28.6, 28.7, 29.1, 29.2, 29.4, 29.5, 30.4, 31.8, 34.0, 35.5, 35.8, 38.26, 39.2, 40.7, 51.9, 53.1, 53.3, 157.2, 157.3, 157.3, 172.8, 173.2, 173.5, 175.5 ppm.

The LC-MS machine data also showed that the combination of triple arginine and palmitic acid was produced successfully with a high purity ratio. Its molar M/Z= 724 which was exactly the same as theoretical. Retention time: 9.59 min. Purity: >96%. Product: 0.53 g, 7.32 x 10^{-4} mol.

The ^1H NMR and ^{13}C NMR confirmed that $CH_3(CH_2)_{14}CORRR$ was produced, and it has high purity because all the peaks of its atoms (H, C) could be found, and the results are as follows.

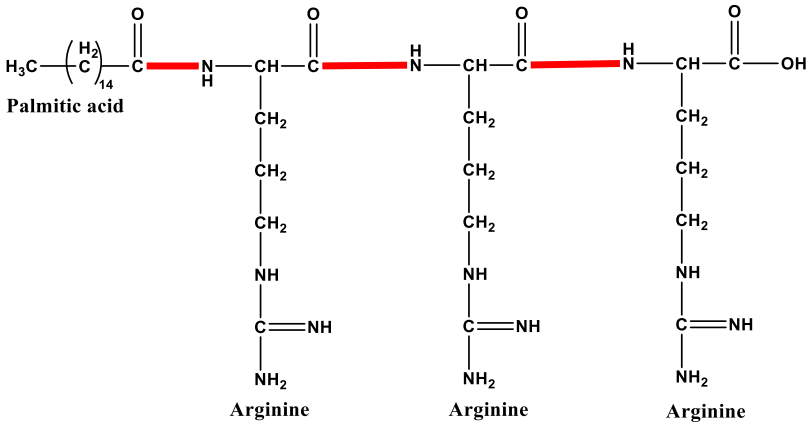

^1H NMR spectrum for triple arginine peptide that coupled with palmitic acid: (400 MHz, CD_3OD, 25 °C) δ= 0.85 (t,^3J = 7.20 Hz, 3H), 1.27 (m, 24H), 1.55 (m, 8H), 1.79 (m, 6H), 2.1 (t, ^3J = 7.20 Hz, 2H), 2.6 (t,^3J = 7.20 Hz, 3H), 3.4 (t, ^3J = 7.20 Hz, 6H), 4.5 (t, ^3J = 7.20 Hz, 2H), 6.7 (s, 6H), 7.9 (s, 3H), 8.4 (s, 3H) ppm.

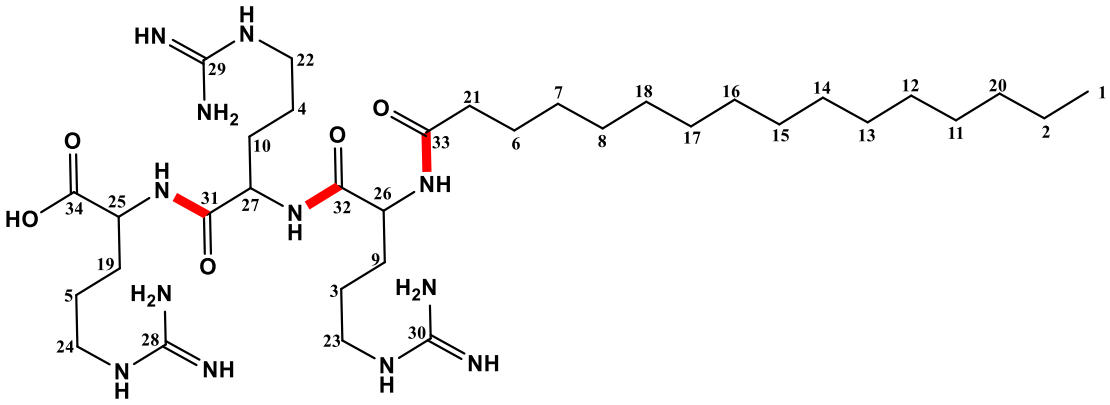

^{13}C NMR (100 MHz, CD_3OD, 25 ^oC) δ= 13.2, 22.4, 23.4, 23.5, 24.8, 25.0, 25.7, 27.5, 28.3, 28.6, 28.7, 29.1, 29.4, 29.6, 30.0, 31.5, 32.4, 32.5, 33.8, 35.0, 35.5, 35.8, 39.2, 40.7, 51.9, 53.1, 53.3, 157.2, 157.3, 157.3, 172.9, 173.2, 173.5, 175.5 ppm.

In this research, another cationic triple cell-penetrating peptide was produced, containing two molecules of arginine (Fmoc-Arg(Pbf)-OH) and lysine. Lysine was the first sequence of the produced peptide. Therefore, the Wang resin of lysine was used as a starting chemical (Lys(Boc)-Wang resin (100-200 mesh). This tripeptide was produced by using the microwave solid-phase peptide synthesis *via* the Biotage microwave peptide synthesiser. The microwave was used as a source of energy, HBTU as a coupling agent, and DIPEA as a basic media for coupling amino acids by an amide bond. (See Figure 3.3.)

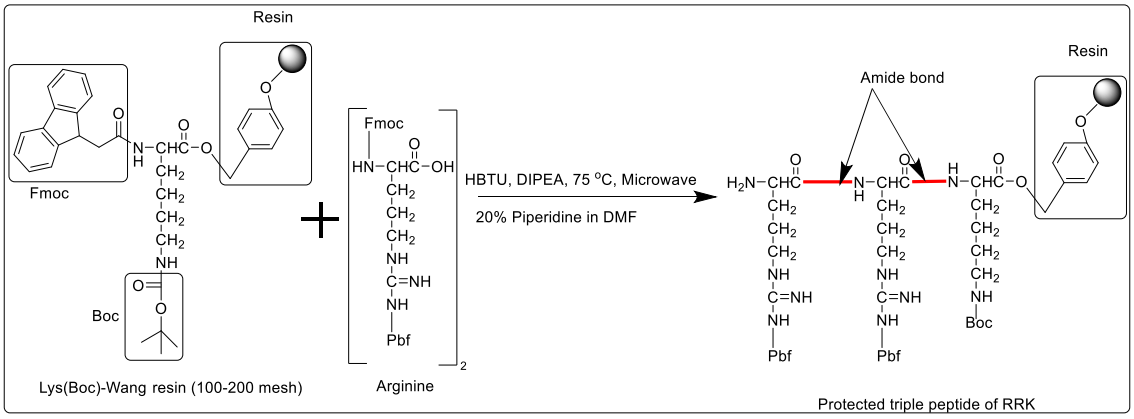

Figure 3.3: Illustrates the chemical reaction to produce the protected triple peptide of two molecules of arginine and lysin (RRK).

Similar to the previous peptide, this tripeptide also underwent conjugation with three different fatty acids. An amide bond couples the fatty acids with the peptides. The amide bond between fatty acids and peptides was formed by using HBTU as a coupling agent dissolved in DMF, and DIPEA was added to make it a basic solution. This coupling happened at room temperature under stirring overnight. (See figure 3.4.)

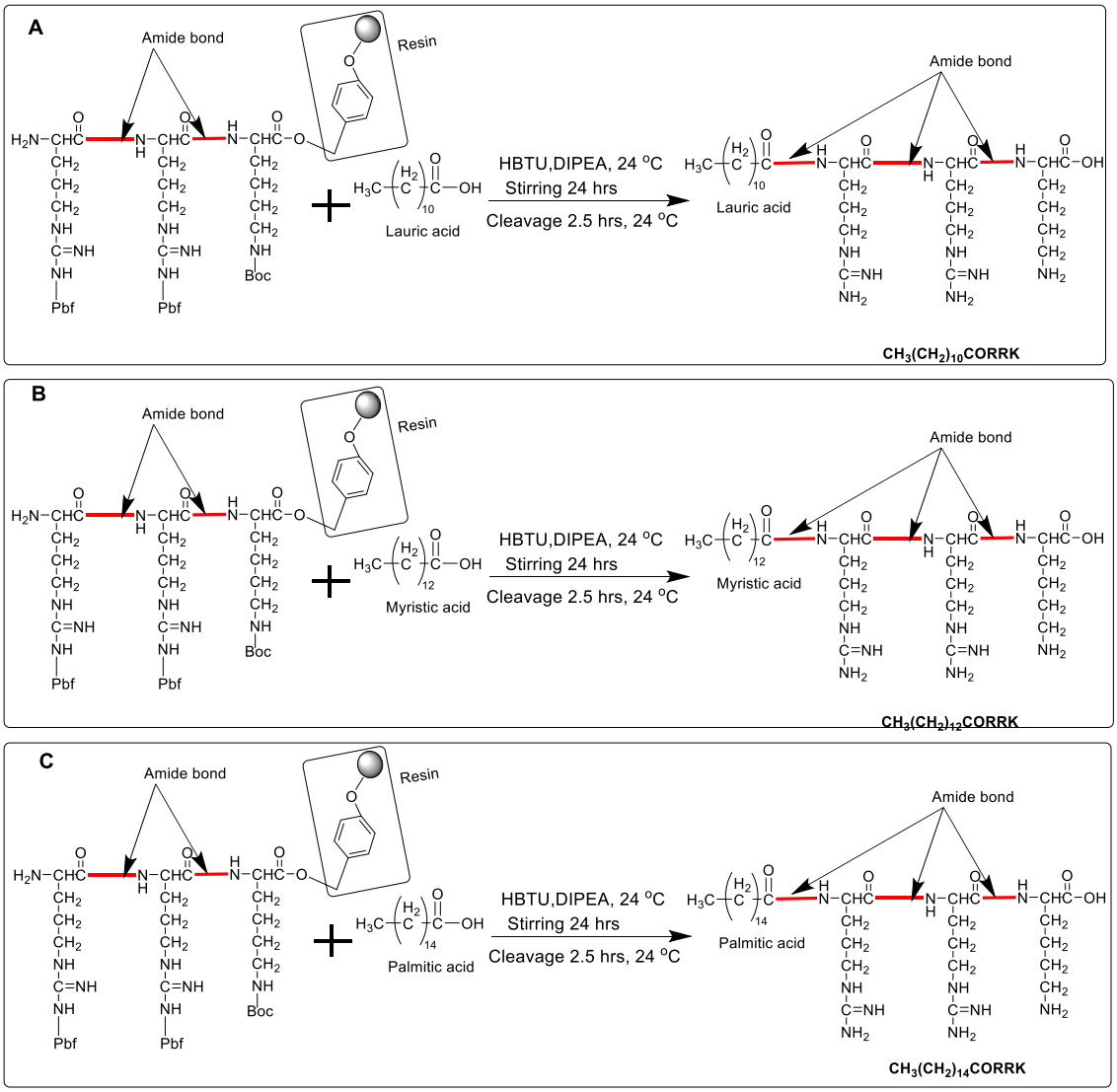

Figure 3.4: Illustrates the chemical reactions that produce conjugated triple peptide (RRK) with three different fatty acids (A- lauric acid, B- myristic acid, and C- palmitic acid). An amide bond linked them together.

The LC-MS machine data showed that the combination of two arginine molecules with lysine in this tripeptide and lauric acid was produced successfully with a high purity ratio. Its molar M/Z was 640 which was exactly the same as theoretical. Retention time: 7.11 min. Purity: >96%. Product: 0.49 g, 7.65 x 10^{-4} mol.

The ^{1}H NMR and ^{13}C NMR also confirmed that $CH_3(CH_2)_{10}CORRK$ was produced, and it has high purity because all the peaks of its atoms (H, C) could be found, and the results are as follows.

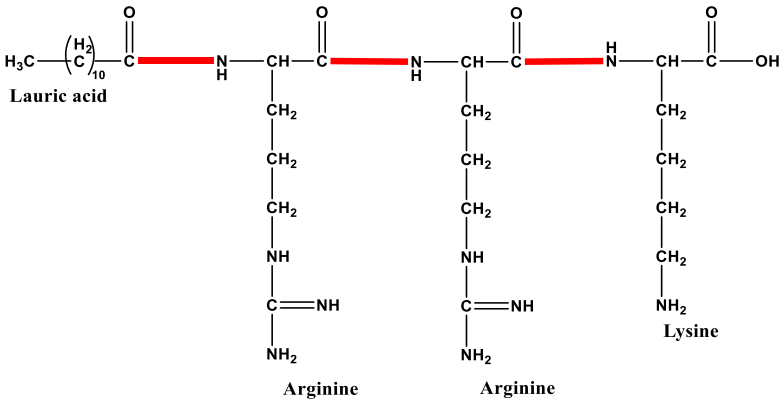

^{1}H NMR spectrum for a triple peptide that contains two molecules of arginine and one lysine and coupled with lauric acid (400 MHz, CD_3OD, 25 °C) δ= 0.85 (t, ^{3}J = 8.00 Hz, 3H), 1.25(m,18H), 1.51 (m, 10H), 1.75 (m, 6H), 2.0 (t, ^{3}J= 8.00 Hz, 2H), 2.4 (t, ^{3}J = 8.00 Hz, 2H), 2.66 (m, 2H), 3.31 (m, 4H), 4.3 (m, 2H), 4.54 (m, 1H), 6.61 (s, 4H), 7.81 (s, 2H), 8.29 (s, 3H) ppm.

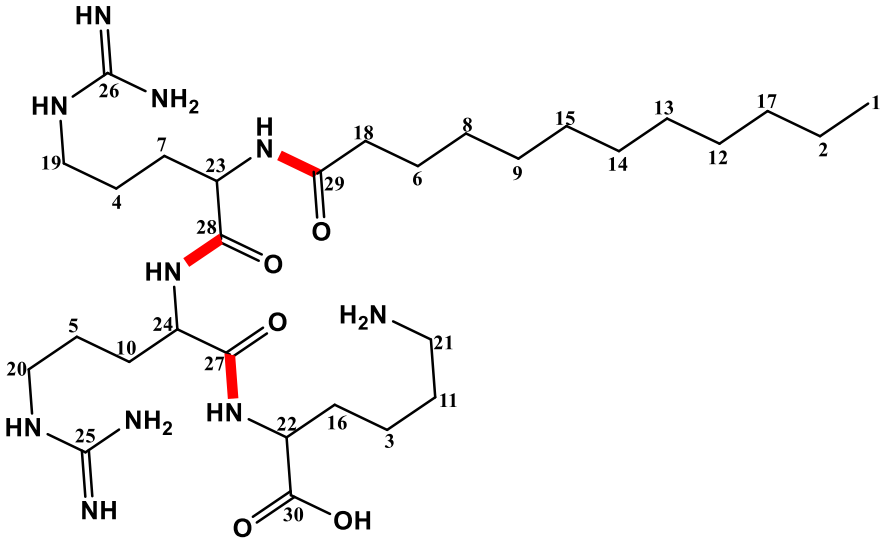

^{13}C NMR (100 MHz, CD_3OD, 25 °C): δ= 13.2, 22.4, 22.5, 23.3, 24.3, 24.9, 25.6, 26.5, 28.6, 29.0, 29.1, 29.2, 29.3, 29.4, 30.6, 34.1, 35.4, 35.7, 39.0, 39.3, 40.6, 52.0, 52.9, 53.2, 157.3, 157.5, 172.7, 173.2, 173.8, 175.4 ppm.

The LC-MS machine data showed that the combination of two arginine molecules with lysine in this tripeptide and myristic acid was produced successfully with a high purity ratio. Its molar M/Z= 668 which was

exactly the same as theoretical. Retention time: 8.11 min. Purity: >95%. Product: 0.51 g, 7.63 x 10^{-4} mol.

The ^{1}H NMR and ^{13}C NMR also confirmed that $CH_3(CH_2)_{12}CORRK$ was produced, and it has high purity because all the peaks of its atoms (H, C) could be found, and the results are as follows.

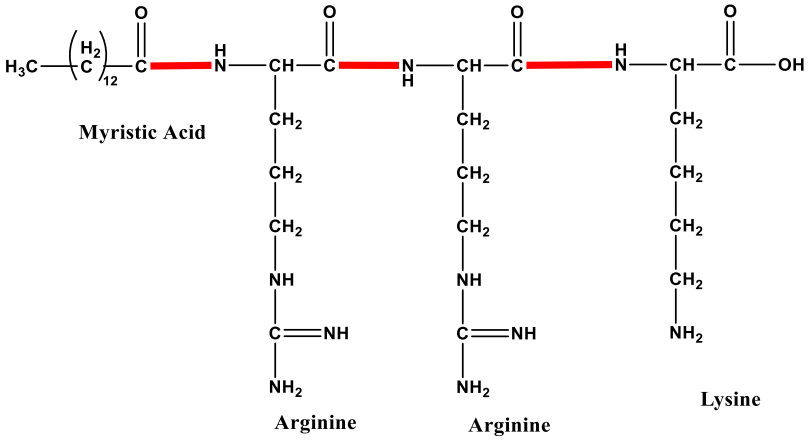

^{1}H NMR spectrum for a triple peptide that contains two molecules of arginine and one lysine and coupled with myristic acid (400 MHz, CD_3OD, 25 °C) δ= 0.84 (t, ^{3}J = 8:00 Hz, 3H), 1.25(m, 22H), 1.51 (m, 10H), 1.75 (m, 6H), 2.0 (t. 2H), 2.4 (t, 2H), 2.66 (m, 2H), 3.31 (m, 4H), 4.3 (m, 2H), 4.54 (m, 1H), 6.61 (s, 4H), 7.81 (s, 2H), 8.29 (s, 3H) ppm.

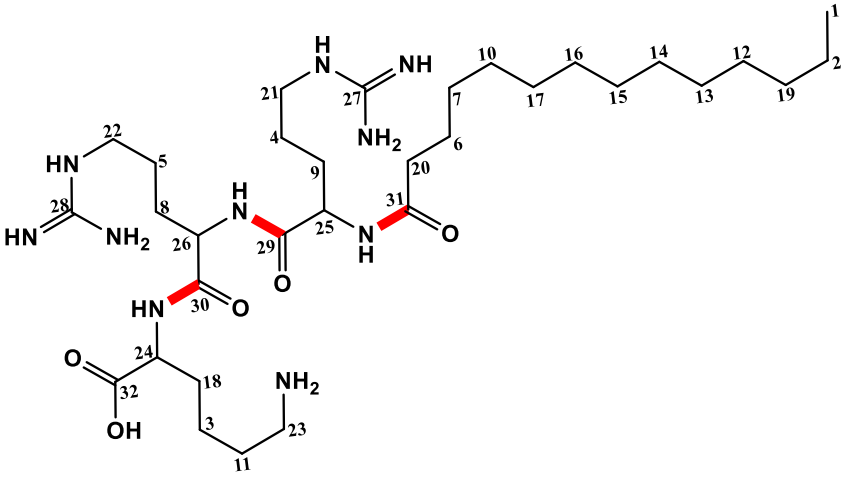

^{13}C NMR (100 MHz, CD_3OD, 25 °C): δ= 13.1, 22.4, 22.5, 23.6, 24.32, 25.0, 25.6, 26.6, 28.6, 29.0, 29.1, 29.2, 29.3, 29.4, 30.4, 30.5, 31.8, 34.0, 35.5, 35.7, 39.1, 39.2, 40.6, 52.0, 53.0, 53.20, 157.2, 157.3, 172.7, 173.2, 173.7, 175.4 ppm.

The LC-MS machine data also showed that the combination of two arginine molecules with lysine in this tripeptide and palmitic acid was produced successfully with a high purity ratio. Its molar M/Z= 696 which was exactly the same as theoretical. Retention time: 9.77 min. Purity: >96%. Product: 0.53 g, 7.61 x 10^{-4} mol.

The ^{1}H NMR and ^{13}C NMR also confirmed that $CH_3(CH_2)_{14}CORRK$ was produced, and it has high purity because all the peaks of its atoms (H, C) could be found, and the results are as follows.

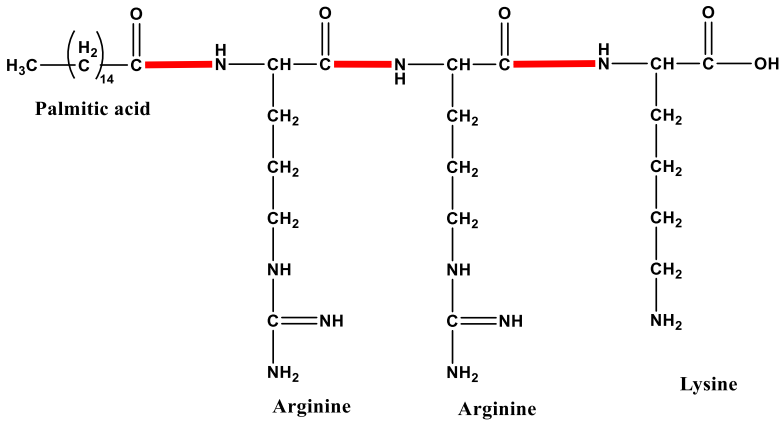

^{1}H NMR spectrum for a triple peptide that contains two molecules of arginine and one lysine and coupled with palmitic acid: (400 MHz, CD_3OD, 25 °C) δ= 0.84 (t, ^{3}J = 7.92.00 Hz, 3H), 1.25 (m,26H), 1.51 (m, 10H), 1.75 (m, 6H), 2.0 (t, ^{3}J = 7.92 Hz, 2H), 2.4 (t, ^{3}J = 7.92 Hz, 2H), 2.66 (m, 2H), 3.31 (m, 4H), 4.3 (m, 2H), 4.54 (m, 1H), 6.61 (s, 4H), 7.81 (s, 2H), 8.29 (s, 3H) ppm.

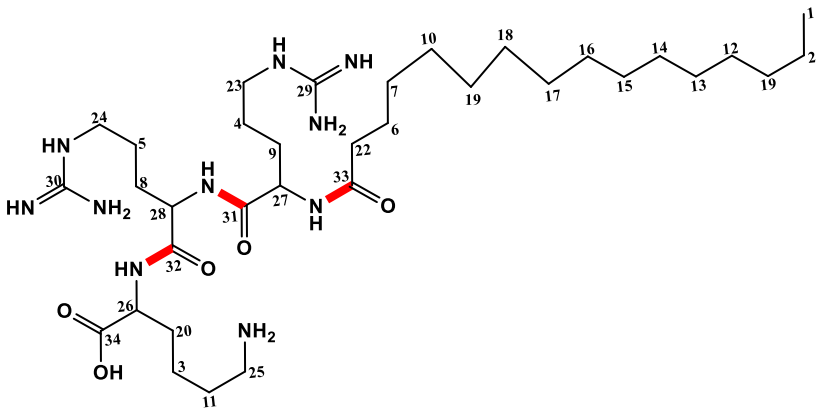

^{13}C NMR (100 MHz, CD_3OD, 25 ^{o}C): δ= 13.1, 22.4, 22.5, 23.4, 24.4, 25.0, 25.7, 26.6, 28.6, 29.0, 29.1, 29.2, 29.3, 29.4, 29.5, 30.1, 30.4, 30.5, 31.8, 34.05, 35.5, 35.8, 39.1, 39.2, 40.7, 52.0, 53.0, 53.2, 157.3, 157.4, 172.7, 173.2, 173,7, 175.4 ppm.

In this research, another cationic triple cell-penetrating peptide was produced, containing three different amino acids a molecule of glutamic acid (Fmoc-Glu(OtBu)-OH), arginine (Fmoc-Arg(Pbf)-OH) and lysine. Lysine was the first sequence of the produced peptide. Therefore, the Wang resin of lysine was used as a starting chemical (Lys(Boc)-Wang resin (100-200 mesh)). This tripeptide was produced by using the microwave solid-phase peptide synthesis *via* the Biotage microwave peptide synthesiser. The microwave was used as a source of energy, HBTU as a coupling agent, and DIPEA as a basic solution for coupling amino acids by an amide bond. (See Figure 3.5.)

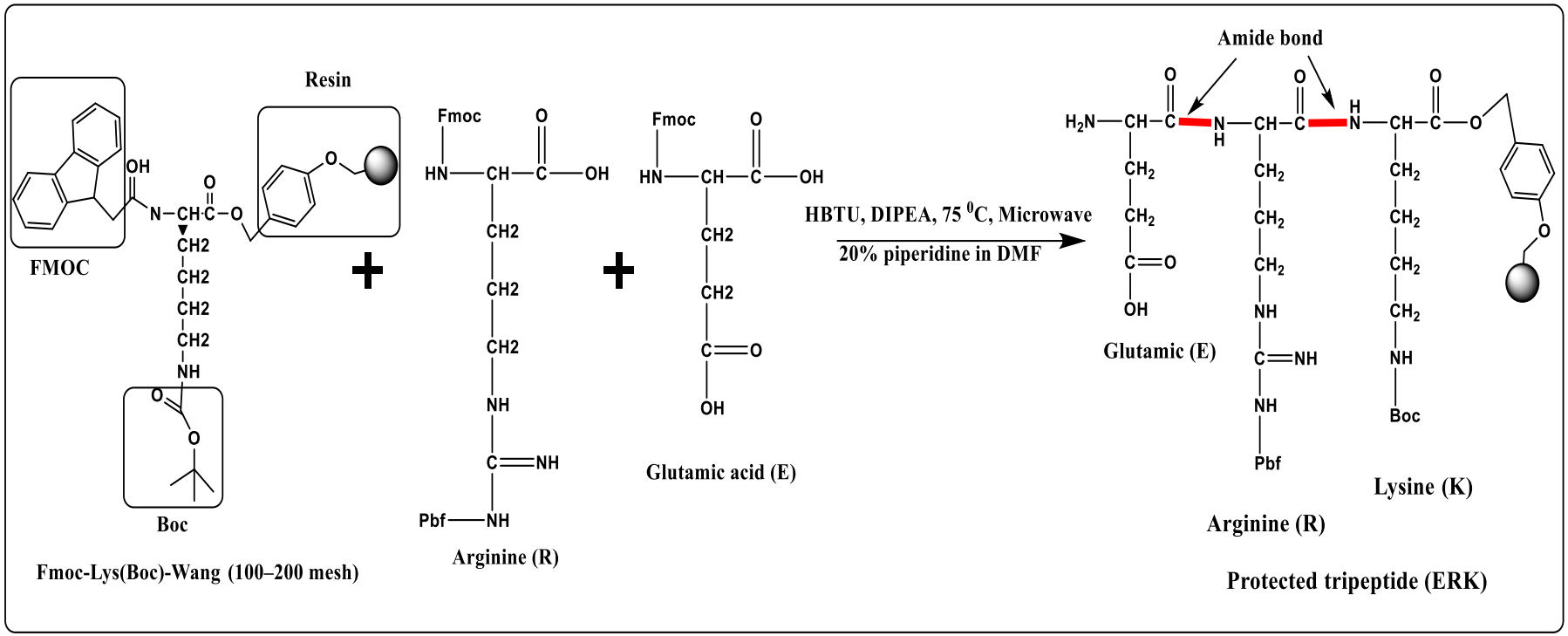

Figure 3.5: Shows how to produce the triple peptide by using two molecules of arginine and lysine. The amino acid molecules were linked by an amide bond.

Similar to the previous peptide, this tripeptide also underwent conjugation with three different fatty acids. An amide bond couples the fatty acids with the peptides. The amide bond between fatty acids and peptides was formed by using HBTU as a coupling agent dissolved in DMF, and DIPEA was added to make it a basic solution. This coupling happened at room temperature under stirring overnight. (See figure 3.6.)

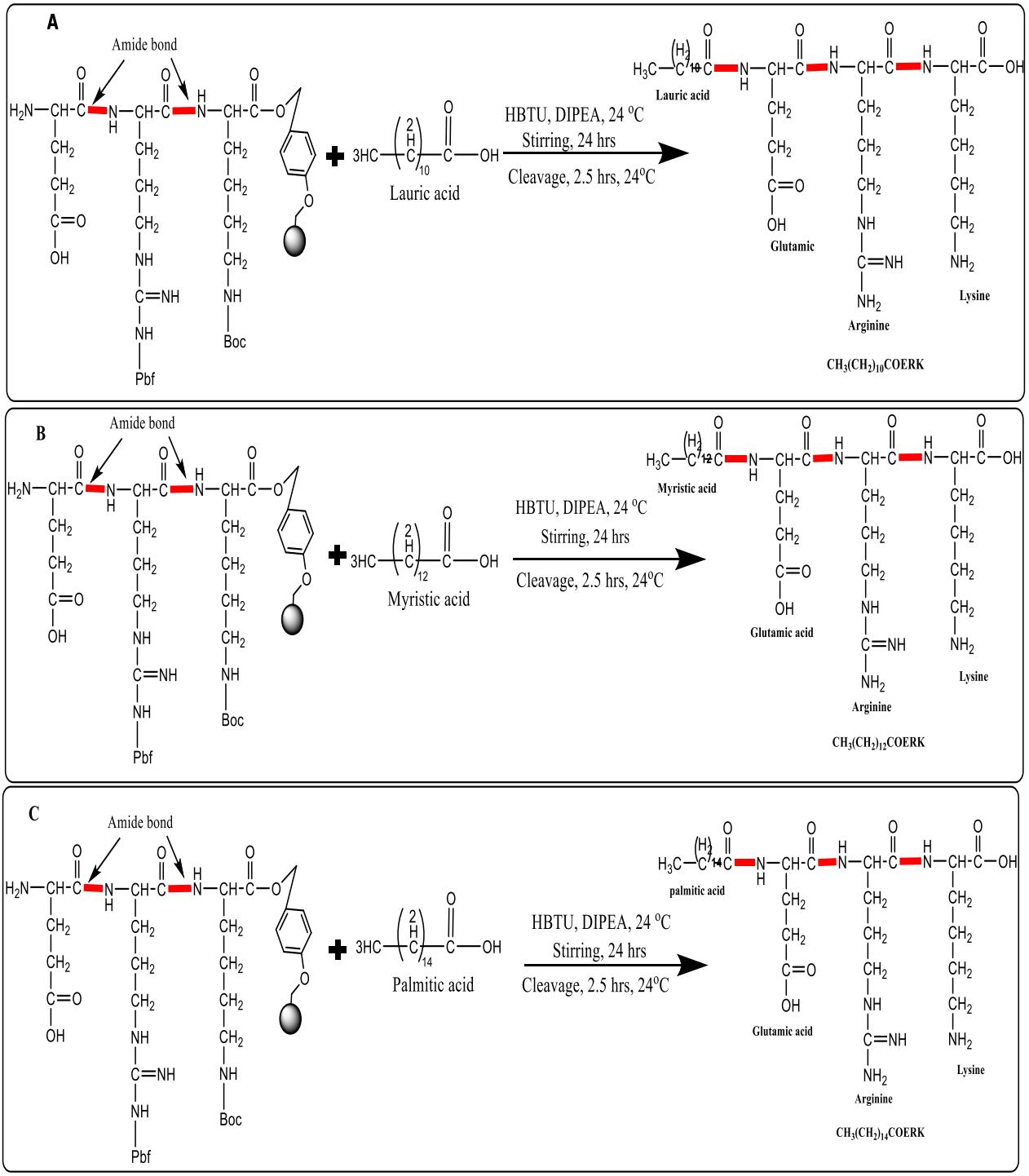

Figure 3.6: Illustrates the chemical reactions that produce conjugated triple peptide (ERK) with three different fatty acids (**A-** lauric acid, **B-** myristic acid, and **C-** palmitic acid). An amide bond linked them together.

The conjugated triple peptides with fatty acids ($CH_3(CH_2)_{10}$COERK, $CH_3(CH_2)_{12}$COERK, and $CH_3(CH_2)_{14}$COERK) were fully characterized

using WATERS LC-MS, ^{1}H NMR, and ^{13}C NMR. Flash chromatography also was used to purify them.

The LC-MS machine data indicates that a peptide with two arginine molecules combined with lysine and attached to lauric acid has M/Z= 613, matching the theoretical value. It was also detected at a retention time of 8.92 min and had a purity greater than 96%. Also, the product's weight was 0.55 g, which is equivalent to 8.97 x 10^{-4} mol.

The ^{1}H NMR and ^{13}C NMR confirmed that $CH_3(CH_2)_{10}COERK$ was produced, and it has high purity because all the peaks of its atoms (H, C) could be found, and the results are as follows.

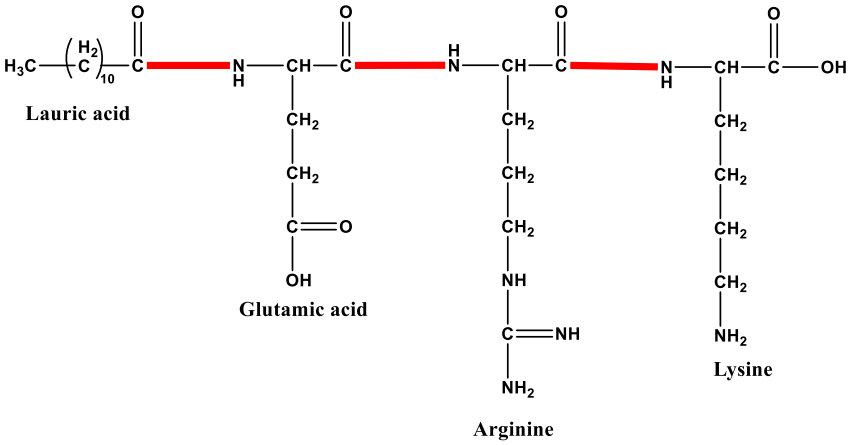

^{1}H NMR spectrum for a triple peptide that contains glutamic acid, arginine and lysine and coupled with lauric acid (400 MHz, CD_3OD, 25 ^{o}C) δ= 0.87 (t, ^{3}J = 7.96 Hz, 3H), 1.27(m, 18H), 1.52 (m, 8H), 1.75 (m, 4H), 2.0 (m, 4H), 2.31 (t, ^{3}J = 7.96 Hz, 2H), 2.46 (s, 1H), 2.67 (t, ^{3}J = 7.96 Hz, 2H), 3.32 (t, ^{3}J = 7.96 Hz, 2H), 4.41 (m, 2H), 4.42 (m, 1H), 6.6 (s, 2H), 7.82 (s, 1H), 8.3 (s, 3H) ppm.

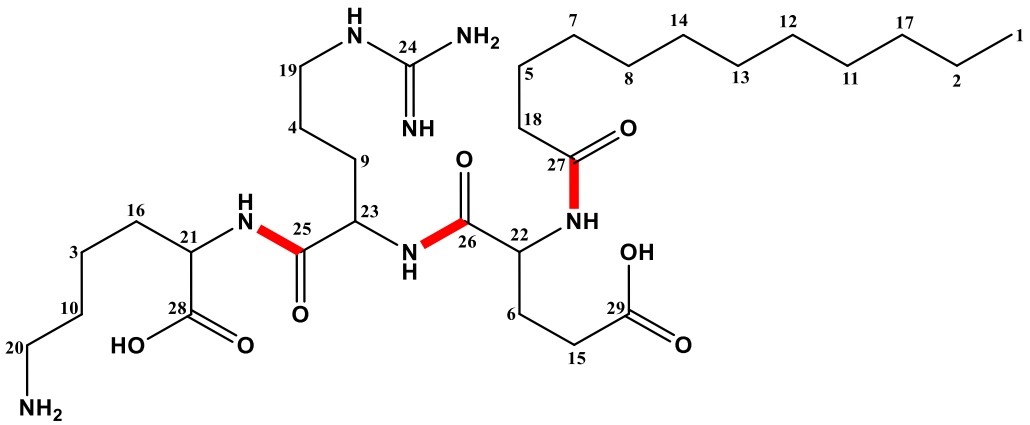

^{13}C NMR (100 MHz, CD_3OD, 25 ^oC) δ= 13.1, 22.4, 24.8, 25.6, 26.5, 26.6, 28.7, 29.0, 29.2, 29.3, 29.4, 29.9, 30.3, 30.4, 31.7, 34.0, 35.4, 35.7, 39.2, 40.7, 51.8, 52.8, 53.1, 157.3, 163.6, 172.5, 172.9, 173.7, 175.3 ppm.

The LC-MS machine data indicates that a tripeptide contains glutamic acid and arginine molecules combined with lysine and attached to myristic acid has M/Z= 641, matching the theoretical value. It was also detected at a retention time of 9.92 min, and had a purity >96%.

Also, the product's weight was 0.548 g, which is equivalent to 8.55 x 10^{-4} mol.

The ^1H NMR and ^{13}C NMR confirmed that $CH_3(CH_2)_{12}COERK$ was produced, and it has high purity because all the peaks of its atoms (H, C) could be found, and the results are as follows.

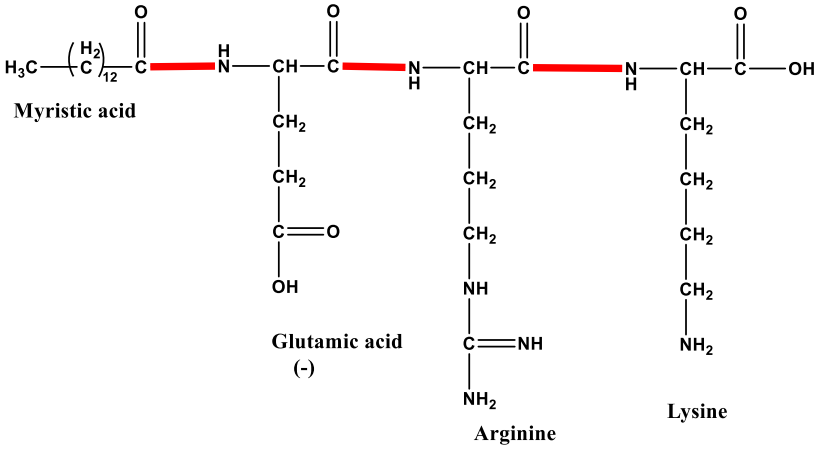

^1H NMR spectrum for a triple peptide that contains glutamic acid, arginine and lysine and coupled with myristic acid (400 MHz, CD_3OD, 25 ^oC) δ= 0.88(t, ^3J = 7.92 Hz, 3H), 1.27(m, 22H), 1.52 (m, 8H), 1.75 (m, 4H), 2.0 (m, 4H), 2.31 (t, ^3J = 7.92 2H), 2.46 (s, 1H), 2.67 (t, ^3J = 7.92 Hz, 2H), 3.32 (t, ^3J = 7.92 Hz, 2H), 4.41 (m, 2H), 4.42 (m, 1H), 6.6 (s, 2H), 7.82 (s, 1H), 8.3 (s, 3H) ppm.

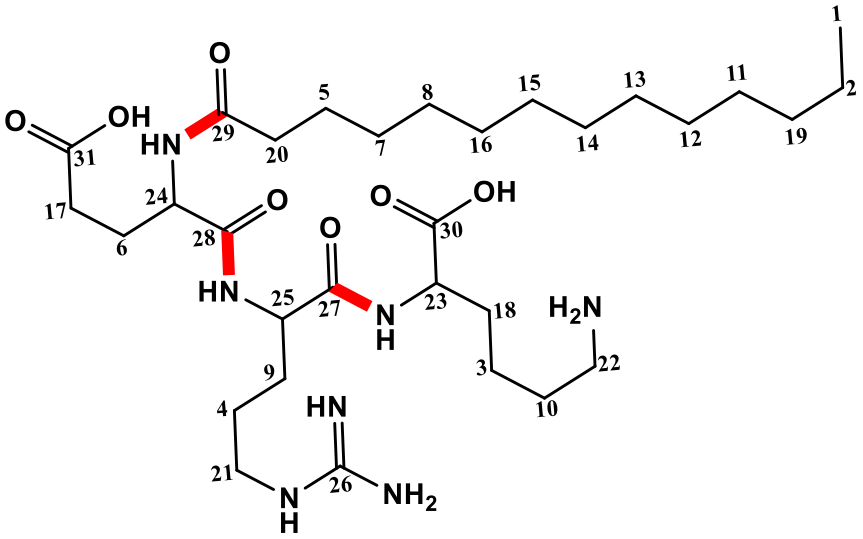

^{13}C NMR (100 MHz, CD_3OD, 25 °C): δ= 13.1, 22.4, 23.3, 24.8, 25.6, 26.5, 26.6, 27.4, 28.7, 29.0, 29.2, 29.3, 29.4, 29.9, 30.6, 31.8, 33.9, 35.4, 35.7, 39.0, 39.2, 40.7, 51.7, 52.8, 53.1, 157.3, 172.4, 172.9, 173.6, 175.1, 175.3 ppm.

The LC-MS machine data indicates that a tiple peptide with glutamic and arginine molecules combined with lysine and attached to palmitic acid has M/Z= 669 , matching the theoretical value. It was also detected at a retention time of 11.02 min, and had a purity >97%.

Also, the product's weight was 0.0.56 g, which is equivalent to 8.4 x 10^{-4} mol.

The ^1H NMR and ^{13}C NMR confirmed that $CH_3(CH_2)_{14}COERK$ was produced, and it has high purity because all the peaks of its atoms (H, C) could be found, and the results are as follows.

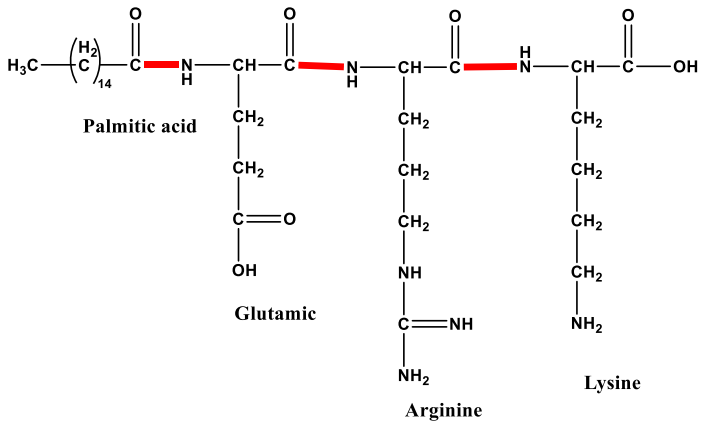

^{1}H NMR spectrum for a triple peptide that contains glutamic acid, arginine and lysine and coupled with palmitic acid (400 MHz, CD_3OD, 25 ^{o}C) δ= 0.86(t, ^{3}J = 8.00 Hz, 3H), 1.27(m, 26H),1.52 (m, 8H), 1.75 (m, 4H), 2.0 (m, 4H), 2.31 (t, ^{3}J= 8.00 Hz, 2H), 2.46 (s, 1H), 2.67 (t, ^{3}J = 8.00 Hz, 2H), 3.32 (t,^{3}J = 8.00 Hz, 2H), 4.41 (m, 2H), 4.42 (m, 1H), 6.6 (s, 2H), 7.82 (s, 1H), 8.3 (s, 3H) ppm.

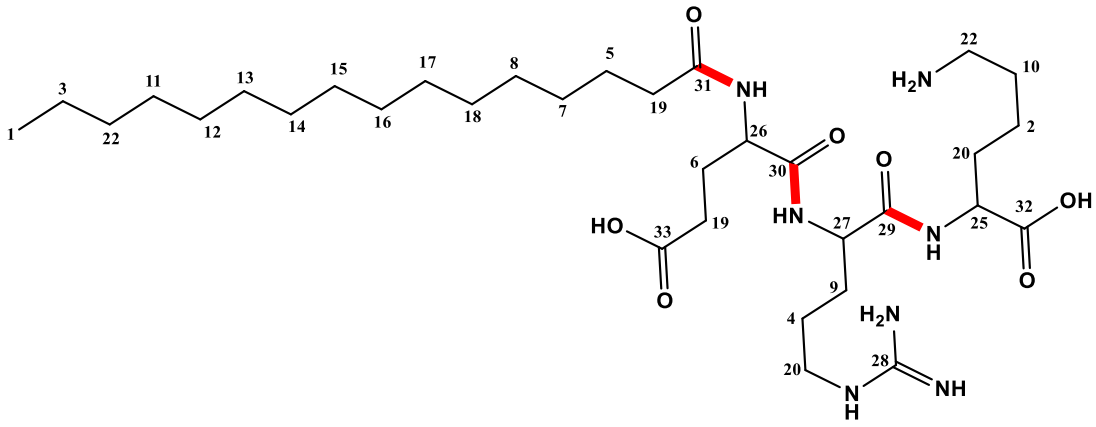

^{13}C NMR (100 MHz, CD_3OD, 25 ^{o}C): δ= 13.1, 22.4, 22.4, 23.3, 24.8, 25.6, 26.5, 28.5, 28.7, 28.9, 29.0, 29.1, 29.2, 29.3, 29.4, 29.5, 29.9, 30.3, 30.6, 31,8, 34.0, 35.4, 35.7, 39.0, 39.2, 40.7, 163.5, 172.4, 172.9, 173.6, 175.1, 175.3 ppm.

In this research, another cationic peptide was produced, but this peptide was composed of two molecules of amino acids which are arginine (Fmoc-Arg(Pbf)-OH) and lysine . Lysine was the first sequence of the produced dipeptide. Therefore, the Wang resin of lysine was used as a starting chemical (Lys(Boc)-Wang resin (100-200 mesh)). This dipeptide was produced by using the microwave solid-phase peptide synthesis *via* the Biotage microwave peptide synthesiser. The microwave was used as a source of energy, HBTU as a coupling agent, and DIPEA as a basic solution for coupling amino acids by an amide bond. (See Figure 3.7.)

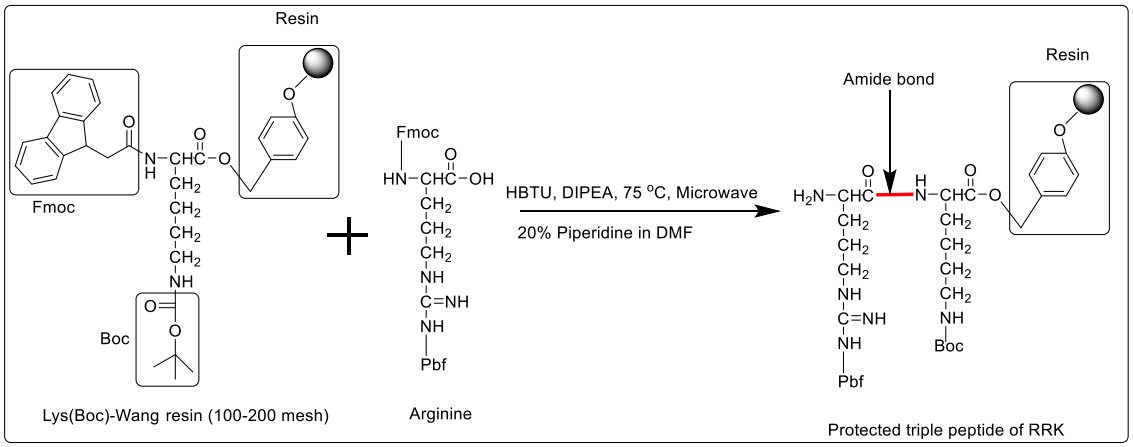

Figure 3.7: Shows the chemical reaction of producing protected dipeptides that contain arginine and lysine.

Similar to the previous peptide, this dipeptide also underwent conjugation with three different fatty acids. An amide bond couples the fatty acids with the peptides. The amide bond between fatty acids and peptides was formed by using HBTU as a coupling agent dissolved in DMF, and DIPEA was added to make it a basic solution. This coupling happened at room temperature under stirring overnight. (See figure 3.8.)

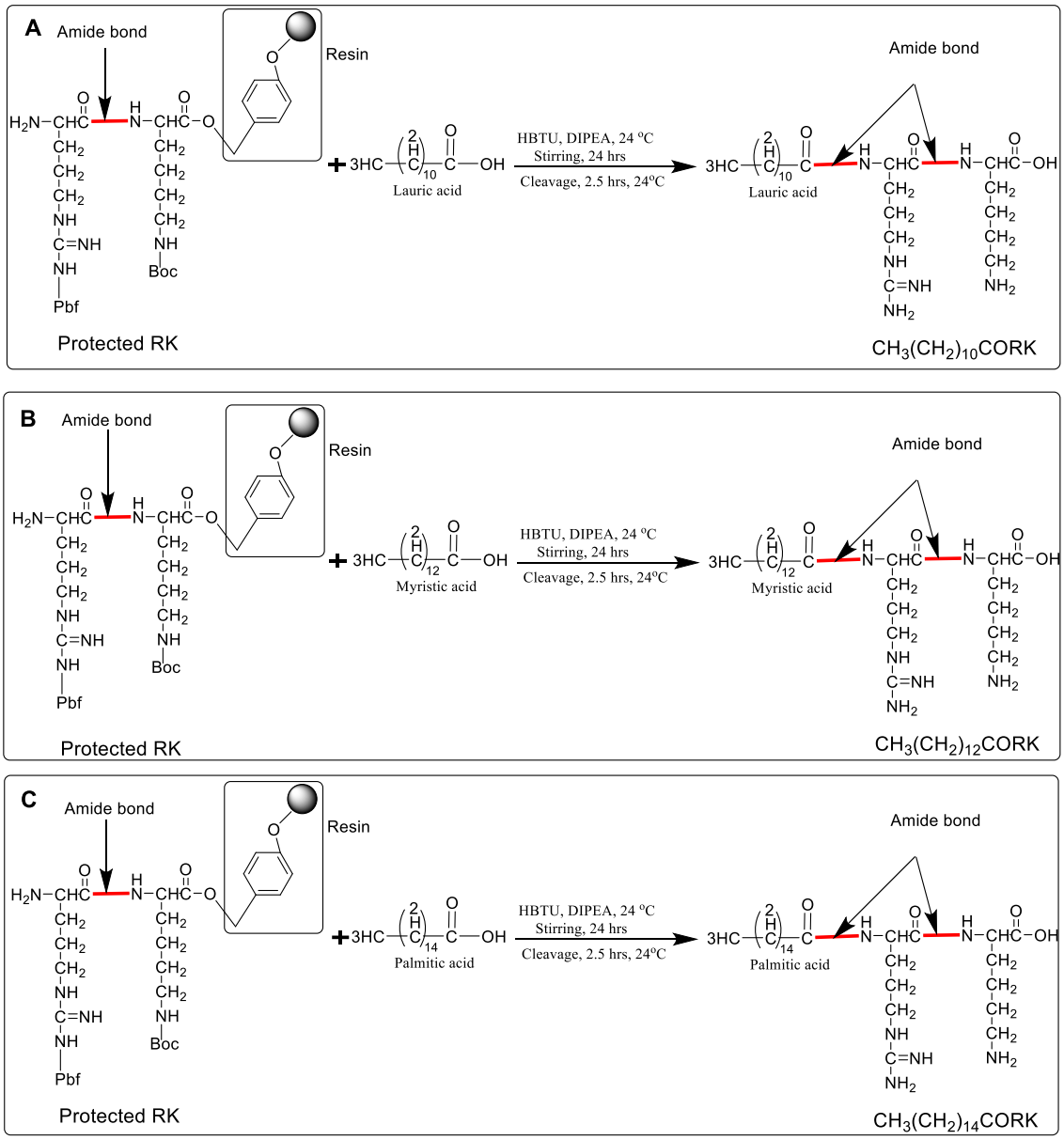

Figure 3.8: Demonstrates the chemical reactions to produce conjugating dipeptides with three distinct fatty acids coupled with RK *via* amid bond. **A-** coupling lauric acid *via* amid bond to RK, **B-** coupling myristic acid with RK by amide bond, **C-** coupling palmitic acid *via* amide bond with RK.

The LC-MS machine data indicates that a dipeptide that contained arginine combined with lysine molecule and attached to lauric acid has M/Z= 484 , matching the theoretical value. It was also detected at a retention time of 8.54 min, and had a purity >96%. Also, the product's weight was 0.0.52 g, which is equivalent to 1.1 x 10^{-3} mol.

The ^{1}H NMR and ^{13}C NMR confirmed that $CH_3(CH_2)_{10}CORK$ was produced, and it has high purity because all the peaks of its atoms (H, C) could be found, and the results are as follows.

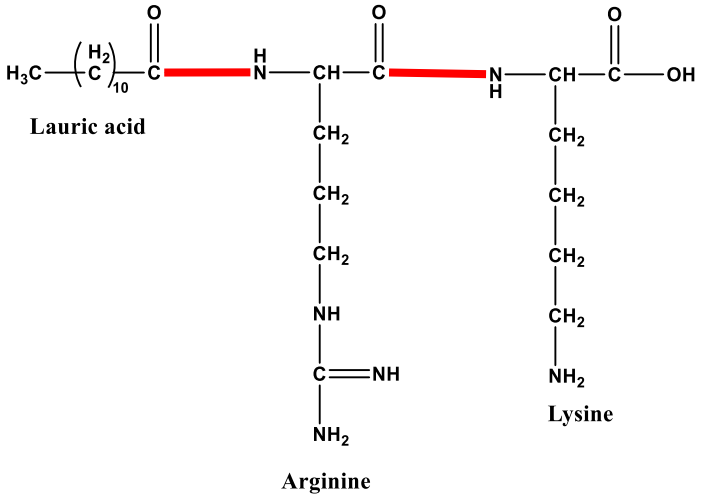

^{1}H NMR spectrum for a dipeptide that contains a molecule of arginine and lysine and is coupled with lauric acid (400 MHz, CD_3OD, 25 °C): δ= 0.87 (t, ^{3}J = 8.92 Hz, 3H), 1.28 (m, 18H), 1.52 (m, 8H), 1.75 (m, 4H), 2.03 (t, 2H), 2.4 (t, ^{3}J = 8.92 Hz, 1H), 2.68 (m, 2H), 3.32 (m, 2H), 4.43 (t, ^{3}J = 8.92 Hz, 1H), 6.61 (s, 2H), 7.81 (s, 1H), 8.2 (d, ^{3}J = 8.92 Hz, 2H) ppm.

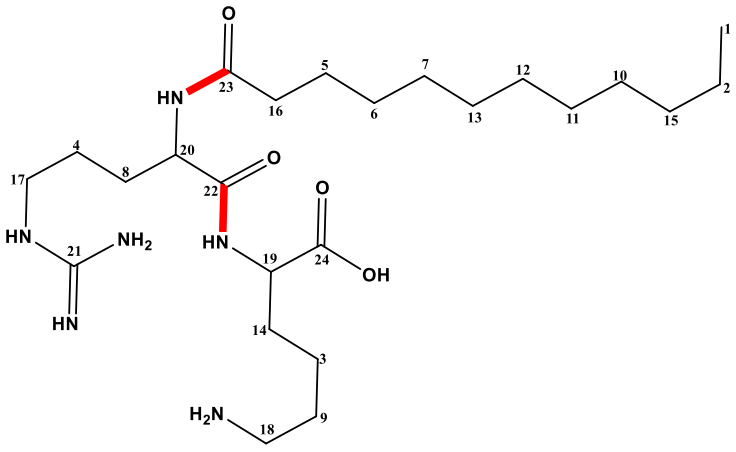

^{13}C NMR (100 MHz, CD_3OD, 25 °C): δ= 13.1, 22.4, 23.3, 24.5, 24.9, 25.6, 26.5, 28.7, 29.0, 29.1, 29.3, 29.5, 29.6, 30.5, 31.7, 33.9, 35.4, 39.0, 39.2, 40.7, 53.1, 57.5, 157.3, 173.2, 173.6, 175.1 ppm.

The LC-MS machine data indicates that a dipeptide that contained arginine combined with lysine molecule and attached to myristic acid has M/Z= 512 , matching the theoretical value. It was also detected at a retention time of 9.72 min, and had a purity >96%. Also, the product's weight was 0.54 g, which is equivalent to 1.055 x 10^{-3} mol.

The ^{1}H NMR and ^{13}C NMR confirmed that $CH_3(CH_2)_{12}CORK$ was produced, and it has high purity because all the peaks of its atoms (H, C) could be found, and the results are as follows.

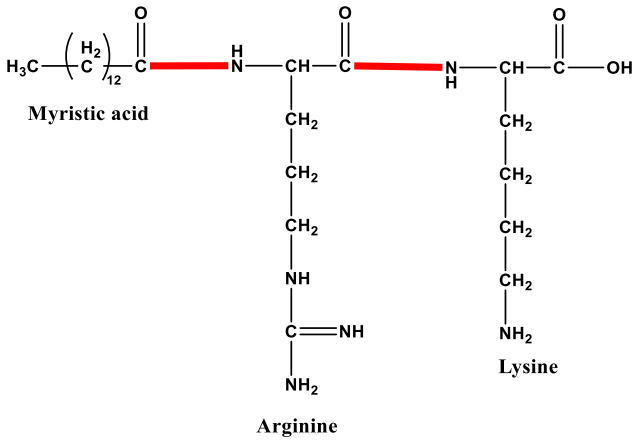

^{1}H NMR spectrum for a dipeptide that contains a molecule of arginine and lysine and is coupled with myristic acid: (400 MHz, CD_3OD, 25 ^{o}C) δ= 0.86 (t, ^{3}J = 7.92 Hz, 3H), 1.28 (m, 22H), 1.52 (m, 8H), 1.75 (m, 4H), 2.03 (t, ^{3}J = 7.92 Hz, 2H), 2.4 (t, ^{3}J = 7.92 Hz, 1H), 2.68 (m, 2H), 3.32 (m, 2H), 4.43 (t, ^{3}J = 7.92 Hz, 1H), 6.61 (s, 2H), 7.81 (s, 1H), 8.2 (d, ^{3}J = 7.92 Hz, 2H) ppm.

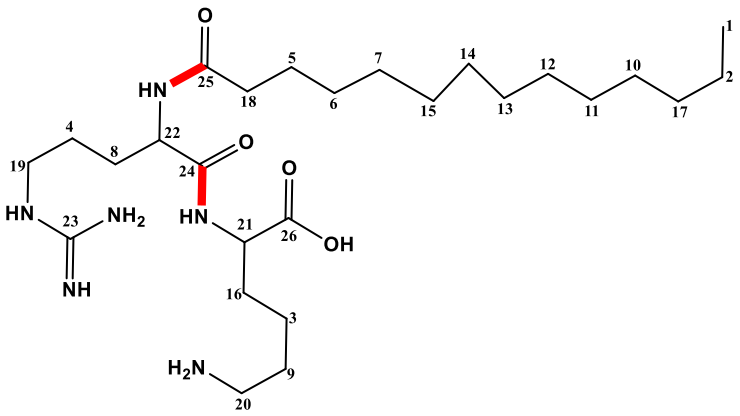

^{13}C NMR (100 MHz, CD_3OD, 25 °C): δ= 13.1, 22.4, 22.8, 23.4, 24.5, 24.9, 25.6, 26.5, 28.7, 29.0, 29.2, 29.3, 29.4, 30.6, 31.7, 34.0, 35.4, 39.0, 39.2, 40.7, 53.1, 57.6, 157.3, 173.0, 173.7, 175.2 ppm.

The LC-MS machine data indicates that a dipeptide that contained arginine combined with a lysine molecule and attached to palmitic acid has M/Z= 540, matching the theoretical value. It was also detected at a retention time of 10.87 min, and had a purity >96%. Also, the product's weight was 0.55 g, which is equivalent to 1.02 x 10^{-4} mol.

The ^{1}H NMR and ^{13}C NMR confirmed that $CH_3(CH_2)_{14}CORK$ was produced, and it has high purity because all the peaks of its atoms (H, C) could be found, and the results are as follows.

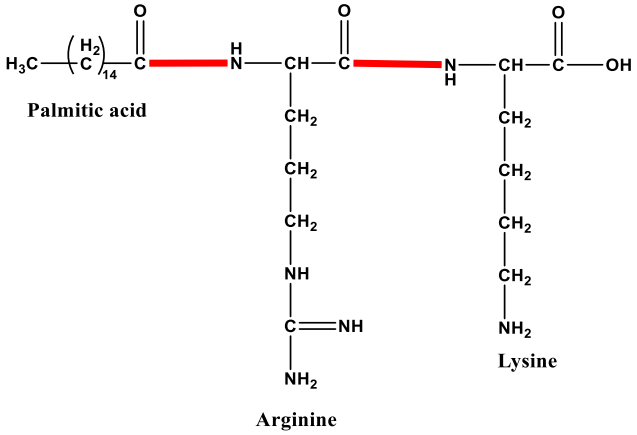

^{1}H NMR spectrum for a dipeptide that contains a molecule of arginine and lysine and is coupled with palmitic acid: (400 MHz, CD_3OD, 25 °C)

δ= 0.87 (t, ^{3}J = 7.96 Hz, 3H), 1.28 (m, 26H), 1.52 (m, 8H), 1.75 (m, 4H), 2.03 (t, ^{3}J = 7.96 Hz, 2H), 2.4 (t, ^{3}J = 7.96 Hz, 1H), 2.68 (m, 2H), 3.32 (m, 2H), 4.43 (t, ^{3}J = 7.96 Hz, 1H), 6.61 (s, 2H), 7.81 (s, 1H), 8.2 (d, ^{3}J = 7.96 Hz, 2H) ppm.

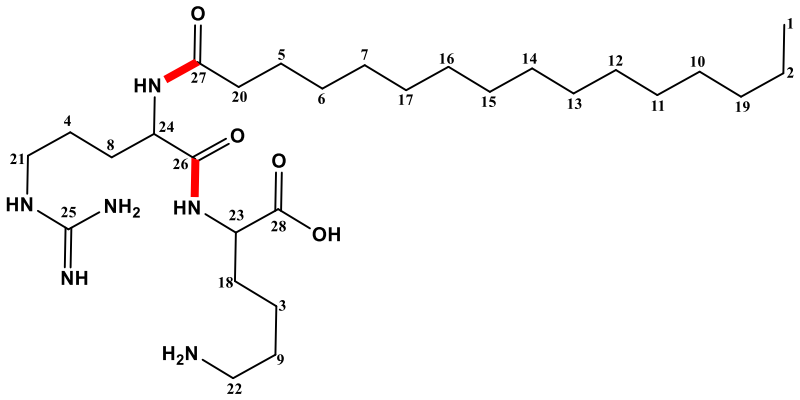

^{13}C NMR (100 MHz, CD_3OD, 25 °C): δ= 13.1, 22.4, 23.3, 24.5, 24.9, 25.7, 26.5, 28.8, 29.0, 29.1, 29.3, 29.4, 29.5, 30.3, 30.6, 34.0, 35.4, 39.0, 39.2, 40.7, 53.1, 57.6, 157.3, 173.7, 175.7, 175.2, 175.4 ppm.

In this research, another triple peptide was produced, but this peptide was composed of two molecules of the amino acids, which are aspartic acid (Fmoc-Asp(OtBu)-OH) and lysine. Lysine was the first sequence of the produced dipeptide. Therefore, the Wang resin of lysine was used as a starting chemical (Lys(Boc)-Wang resin (100-200 mesh)). This dipeptide was produced by using the microwave solid-phase peptide synthesis via the Biotage microwave peptide synthesiser. The microwave was used as a source of energy, HBTU as a coupling agent, and DIPEA as a basic solution for coupling amino acids by an amide bond. (See Figure 3.9.)

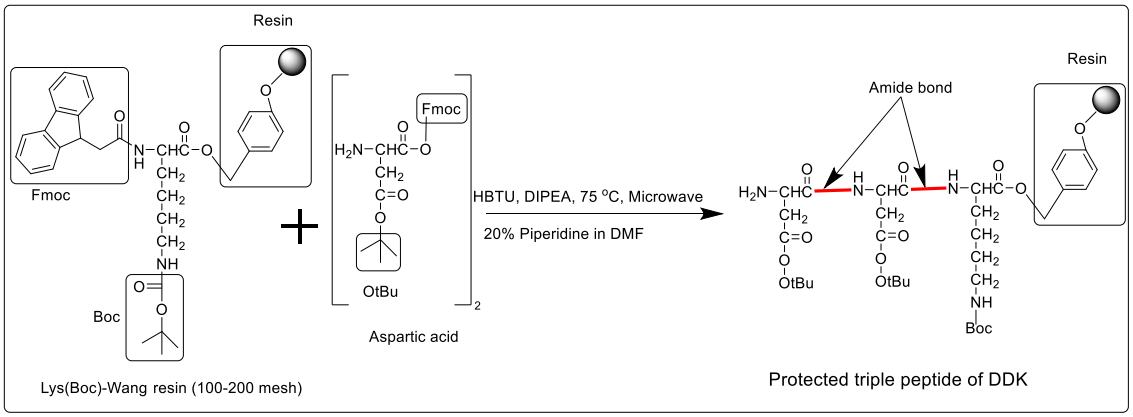

Figure 3.9: Illustrates the chemical reaction of producing protected tripeptides that contain two molecules of aspartic acid and lysine.

Similar to the previous cationic peptides, this triple ionic peptide also underwent conjugation with three different fatty acids. An amide bond couples the fatty acids with the peptides. The amide bond between fatty acids and peptides was formed by using HBTU as a coupling agent dissolved in DMF, and DIPEA was added to make it a basic solution. This coupling happened at room temperature under stirring overnight. (See Figure 3.10.)

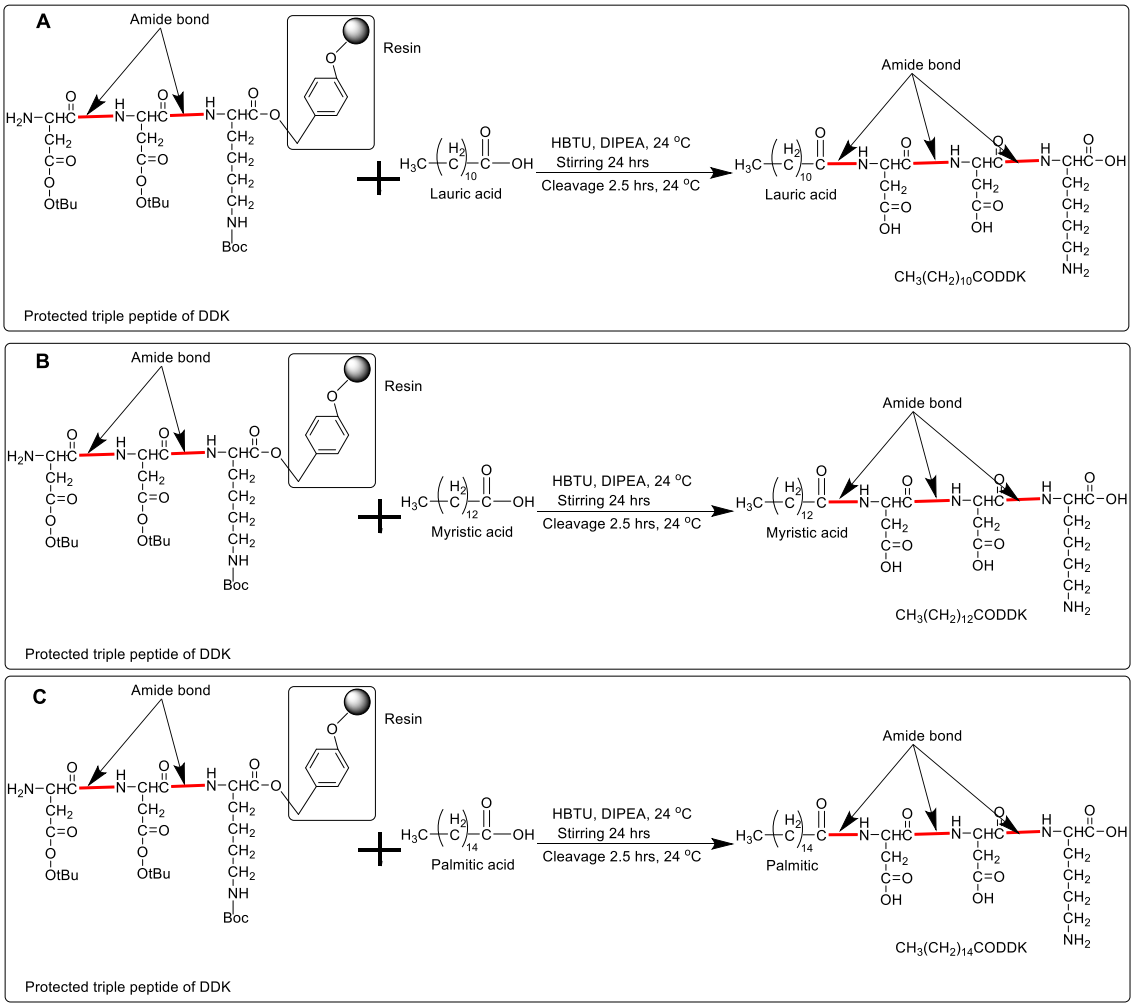

Figure 3.10: Shows the chemical reactions to produce conjugating tripeptides with three distinct fatty acids coupled with DDK *via* an amide bond. **A-** coupling lauric acid *via* amid bond to DDK, **B-** coupling myristic acid with DDK by amide bond, **C-** coupling palmitic acid *via* amide bond with DDK.

The LC-MS machine data indicates that a dipeptide that contained two molecules of aspartic acid combined with a lysine molecule and attached to lauric acid has M/Z= 558, matching the theoretical value. It was also detected at a retention time of 10.35 min, and had a purity >97%. Also, the product's weight was 0.5 g, which is equivalent to 8.96 x 10^{-4} mol.

The ^{1}H NMR and ^{13}C NMR confirmed that $CH_3(CH_2)_{10}CODDK$ was produced, and it has high purity because all the peaks of its atoms (H, C) could be found, and the results are as follows.

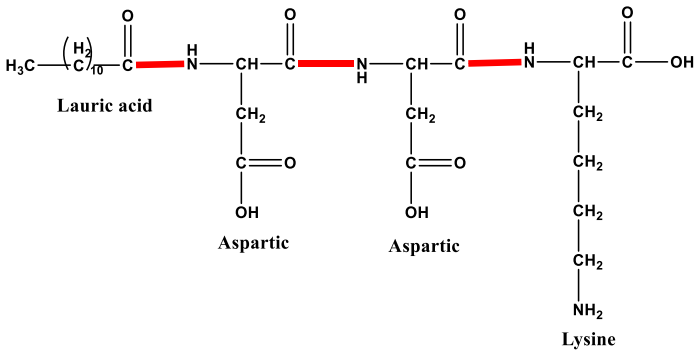

^{1}H NMR spectrum for a triple peptide that contains two molecules of aspartic acid and one lysine and was coupled with lauric acid (400 MHz, CD_3OD, 25 °C): δ= 0.85 (t, ^{3}J = 7.96 Hz, 3H), 1.27 (m, 18H), 1.52 (m, 6H, 1.74 (m, 2H), 2.1 (t, ^{3}J = 7.96 Hz, 2H), 2.65 (m, 2H), 2.85 (d, ^{3}J = 7.96 Hz, 4H), 4.5 (m, 1H), 4.84 (m, 2H), 8.1 (s, 3H) ppm.

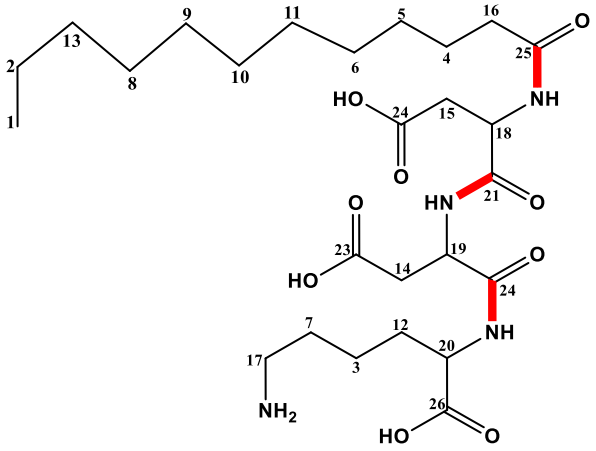

^{13}C NMR (100 MHz, CD_3OD, 25 °C): δ= 13.1, 22.4, 22.5, 25.1, 25.2, 26.3, 26.5, 30.5, 30.7, 30.9, 34.8, 35.2, 35.5, 39.1, 39.3, 52.0, 52.1, 52.2, 53.4, 172.2, 172.3, 173.2, 173.3, 174.0, 174.6, 175.2 ppm.

The LC-MS machine data indicates that a tripeptide that contained two molecules of aspartic acid combined with a lysine molecule and attached to myristic acid has M/Z= 586, matching the theoretical value. It was also detected at a retention time of 11.61 min, and had a purity >97%. Also, the product's weight was 0.509 g, which is equivalent to 8.7 x 10^{-4} mol.

The ^{1}H NMR and ^{13}C NMR confirmed that $CH_3(CH_2)_{12}CODDK$ was produced, and it has high purity because all the peaks of its atoms (H, C) could be found, and the results are as follows.

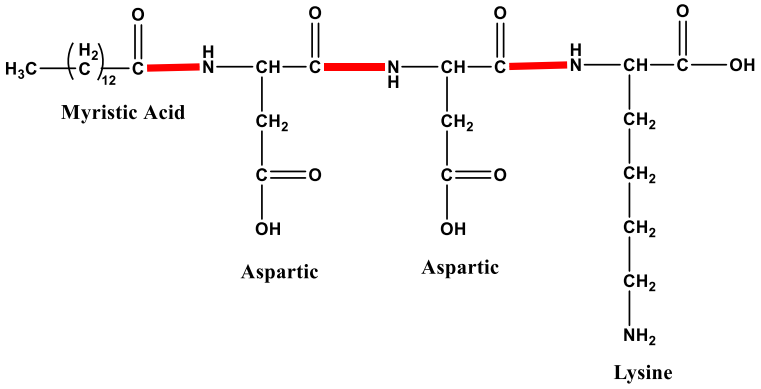

^{1}H NMR spectrum for a triple peptide that contains two molecules of aspartic acid and one lysine and coupled with myristic acid (400 MHz, CD_3OD, 25 °C): δ= 0.89 (t, ^{3}J = 7.96 Hz, 3H), 1.27 (m, 22H), 1.52 (m, 6 H, 1.74 (m, 2H), 2.1 (t, ^{3}J = 7.96 Hz, 2H), 2.65 (m, 2H), 2.85 (d, ^{3}J = 7.96 Hz 4H), 4.5 (m, 1H), 4.84 (m, 2H), 8.1 (s, 3H).

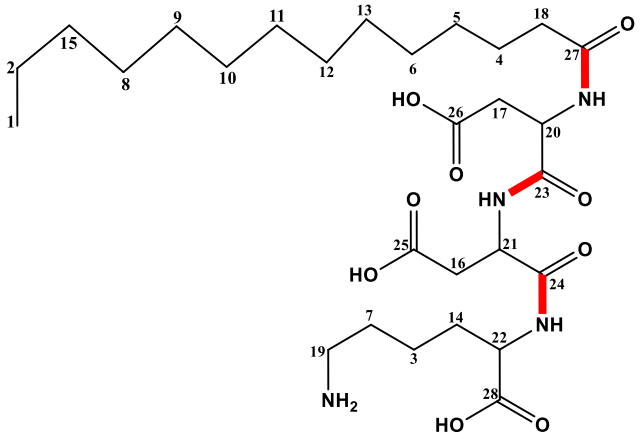

^{13}C NMR (100 MHz, CD_3OD, 25 °C): δ= 13.3, 22.5, 22.7, 25.7, 25.8, 26.6, 26.7, 30.6, 30.7, 31.0, 34.8, 34.9, 35.2, 35.6, 35.8, 39.6, 39.9, 52.0, 52.2, 52.4, 53.6, 172.6, 172.7, 173.2, 173.8, 174.5, 174.9, 175.3 PPM.

The LC-MS machine data indicates that a tripeptide that contained two molecules of aspartic acid combined with a lysine molecule and

attached to palmitic acid has M/Z= 514, matching the theoretical value. It was also detected at a retention time of 12.58 min, and had a purity >97%. Also, the product's weight was 0.53 g, which is equivalent to 8.63 x 10^{-4} mol.

The ^{1}H NMR and ^{13}C NMR confirmed that $CH_3(CH_2)_{14}CODDK$ was produced, and it has high purity because all the peaks of its atoms (H, C) could be found, and the results are as follows.

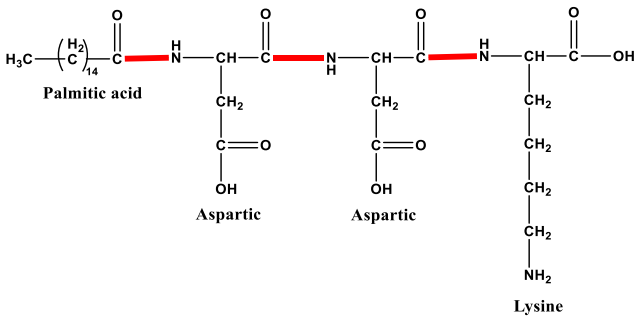

^{1}H NMR spectrum for a triple peptide that contains two molecules of aspartic acid and one lysine and coupled with palmitic acid (400 MHz, CD_3OD, 25 °C): δ= 0.85 (t, ^{3}J = 7.92 Hz, 3H), 1.27 (m, 26H), 1.52 (m, 6H, 1.74 (m, 2H), 2.1 (t, ^{3}J = 7.92 Hz, 2H), 2.65 (m, 2H), 2.85 (d, ^{3}J = 7.92 Hz, 4H), 4.5 (m, 1H), 4.84 (m, 2H), 8.1 (s, 3H).

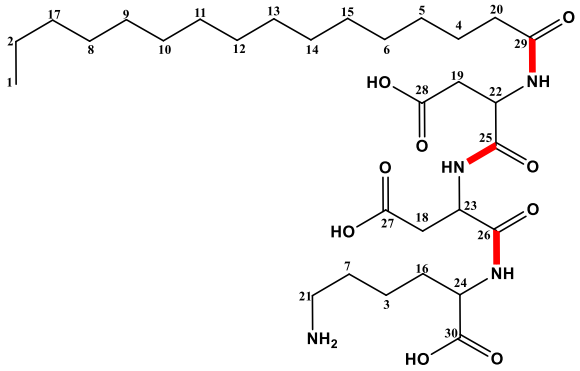

^{13}C NMR (100 MHz, CD_3OD, 25 °C): δ=13.1, 22.2, 22.4, 25.5, 25.8, 26.4, 26.7, 30.5, 31.0, 31.8, 34.8, 35.2, 35.2, 35.3, 35.4, 35.5, 35.6, 39.7, 40.2, 51.8, 52.1, 52.3, 53.8, 172.6, 172.8, 173.5, 173.7, 174.7, 174.9, 175.3 ppm.

In this study, the final triple peptide was produced, but this peptide was composed of three molecules of glutamic acid (Fmoc-Glu(OtBu)-OH). Glutamic acid was the first sequence of the produced tripeptide. Therefore, the Wang resin of glutamic acid was used as a starting chemical (Fmoc-Glu(OtBu)-Wang resin (100-200 mesh). This tripeptide was produced by using the microwave solid-phase peptide synthesis *via* the Biotage microwave peptide synthesiser. The microwave was used as a source of energy, HBTU as a coupling agent, and DIPEA as a basic solution for coupling amino acids by an amide bond. See Figure 3.11.

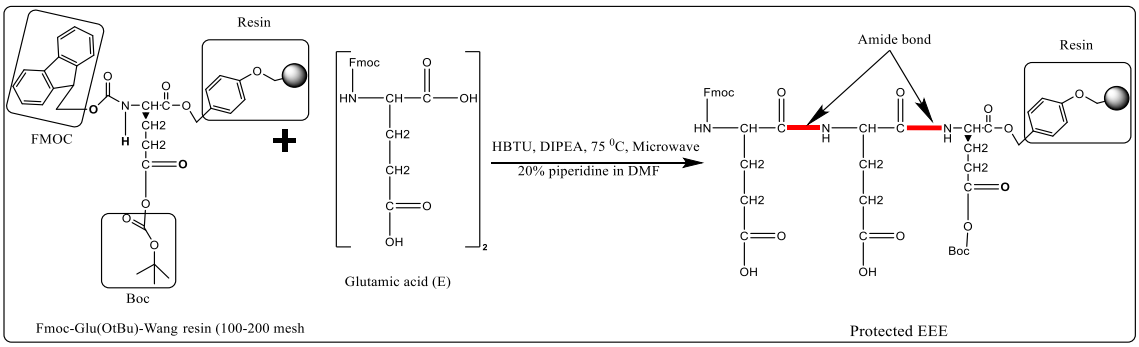

Figure 3.11: Shows the chemical reaction of producing protected triple glutamic acid peptide.

Similar to the previous ionic peptides, this triple ionic peptide also underwent conjugation with three different fatty acids. An amide bond couples the fatty acids with the peptides. The amide bond between fatty acids and peptides was formed by using HBTU as a coupling agent dissolved in DMF, and DIPEA was added to make it a basic solution. This coupling happened at room temperature under stirring overnight. (See Figure 3.12.)

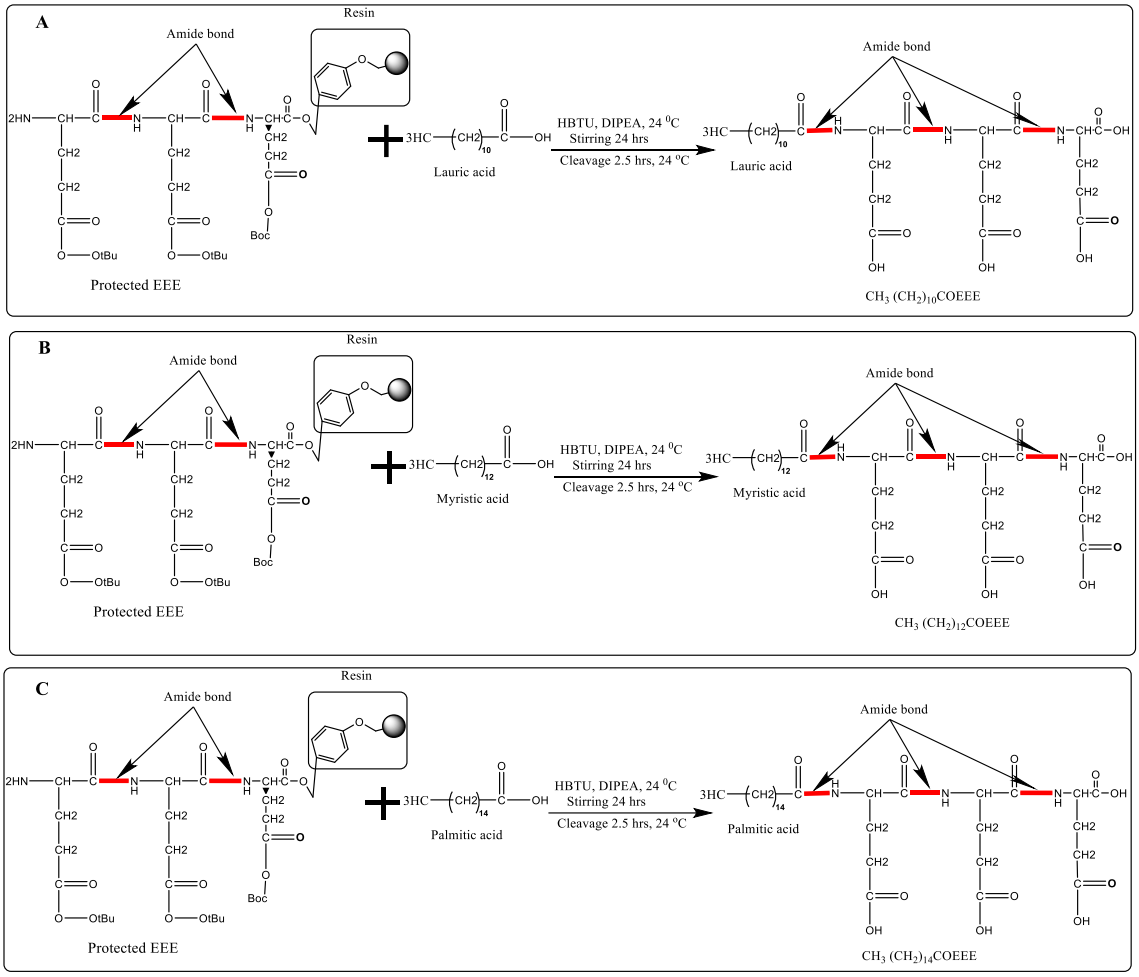

Figure 3.12: Shows the chemical reactions to produce conjugating tripeptides with three distinct fatty acids coupled with EEE *via* an amide bond. **A-** coupling lauric acid *via* an amide bond to EEK, **B-** coupling myristic acid with EEE by an amide bond, **C-** coupling palmitic acid *via* an amide bond with EEE.

The LC-MS machine data indicate that a tripeptide that contained three molecules of glutamic acid and was attached to lauric acid *via* an amide bond has M/Z= 587, matching the theoretical value. It was also detected at a retention time of 11.98 min, and had a purity >96%. Also, the product's weight was 0.48 g, which is equivalent to

8.2×10^{-4} mol.

The ^{1}H NMR and ^{13}C NMR confirmed that $CH_3(CH_2)_{10}COEEE$ was produced, and it has high purity because all the peaks of its atoms (H, C) could be found, and the results are as follows.

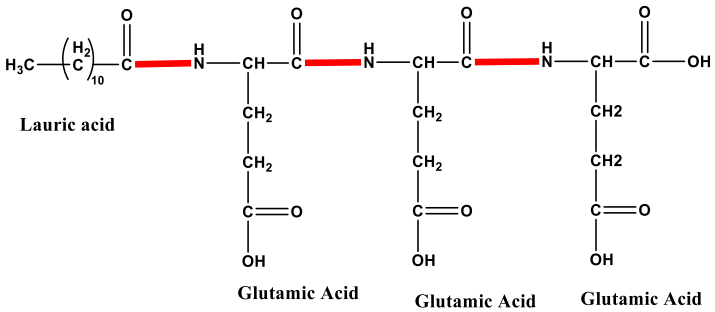

^{1}H NMR spectrum for a triple peptide that contains three molecules of glutamic acid and is coupled with lauric acid (400 MHz, CD_3OD, 25 °C): δ= 0.88 (t, ^{3}J = 7.92 Hz, 3H), 1.25 (m, 16H), 1.48 (m, 2H), 2.4 (m, 6H), 2.31 (t, ^{3}J = 7.92 Hz, 4H), 2.45 (t, ^{3}J = 7.92 Hz, 2H), 4.43 (m, 2H), 4.53 (m, 1H), 8.1 (s, 3H) ppm.

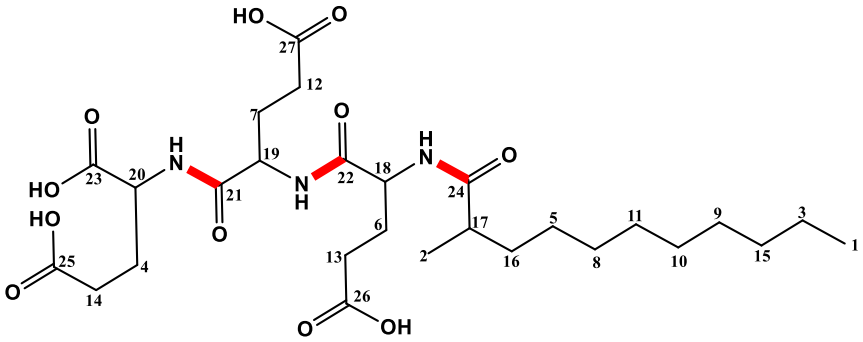

^{13}C NMR (100 MHz, CD_3OD, 25 °C): δ=13.1, 16.4, 22.3, 25.6, 25.7, 26.8, 26.9, 29.5, 30.4, 30.9, 31.6, 34.5, 34.5, 34.6, 34.7, 34.9, 35.3, 51.3, 51.6, 52.6, 168.0, 168.3, 172.7, 172.9, 175.2, 175.3, 175.4 ppm.

The LC-MS machine data indicate that a tripeptide that contained three molecules of glutamic acid and was attached to myristic acid *via* an amide bond has M/Z= 615, matching the theoretical value. It was also detected at a retention time of 11.36 min, and had a purity >96%. Also, the product's weight was 0.49 g, which is equivalent to

7.97 x 10^{-4} mol.

The ^{1}H NMR and ^{13}C NMR confirmed that $CH_3(CH_2)_{12}COEEE$ was produced, and it has high purity because all the peaks of its atoms (H, C) could be found, and the results are as follows.

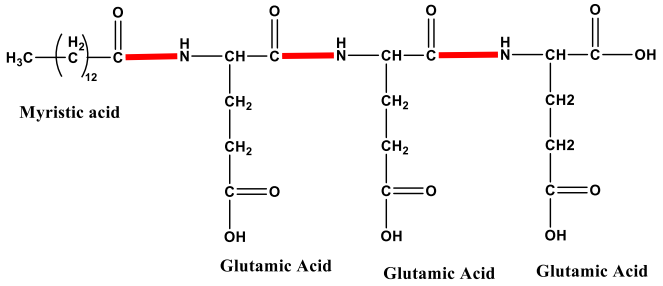

^{1}H NMR spectrum for a triple peptide that contains three molecules of glutamic acid and is coupled with myristic acid (400 MHz, CD_3OD, 25 ^{o}C): δ= 0.87 (t, ^{3}J = 7.94 Hz, 3H), 1.25 (m, 20H), 1.48 (m, 2H), 2.4 (m, 6H), 2.31 (t, ^{3}J = 7.94 Hz, 4H), 2.45 (t, ^{3}J = 7.94 Hz, 2H), 4.43 (m, 2H), 4.53 (m, 1H), 8.1 (s, 3H) ppm.

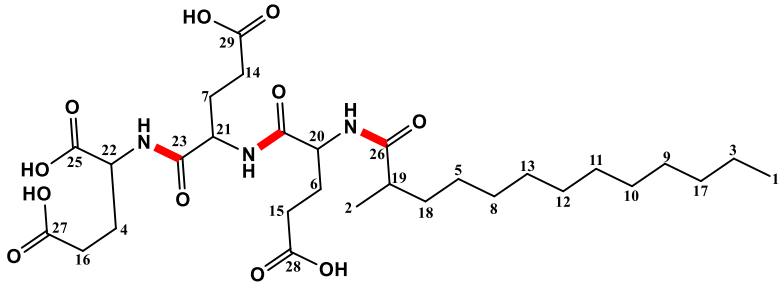

^{13}C NMR (100 MHz, CD_3OD, 25 ^{o}C): δ= 13.1, 16.5, 22.4, 25.8, 25.9, 26.9, 27.1, 29.7, 30.5, 30.9, 31.7, 32.2, 32.9, 34.6, 34.7, 34.7, 34.8, 35.0, 35.4, 51.5, 52.0, 52.8, 168.1, 168.4, 172.8, 172.9, 175.3, 175.4, 175.4 ppm.

The LC-MS machine data indicates that a tripeptide that contained three molecules of glutamic acid and attached to palmitic acid *via* an amide bond has M/Z= 643, matching the theoretical value. It was also detected at a retention time of 11.95 min, and had a purity >96%. Also, the product's weight was 0.507 g, which is equivalent to

7.9 x 10^{-4} mol.

The ^{1}H NMR and ^{13}C NMR confirmed that $CH_3(CH_2)_{14}COEEE$ was produced, and it has high purity because all the peaks of its atoms (H, C) could be found, and the results are as follows.

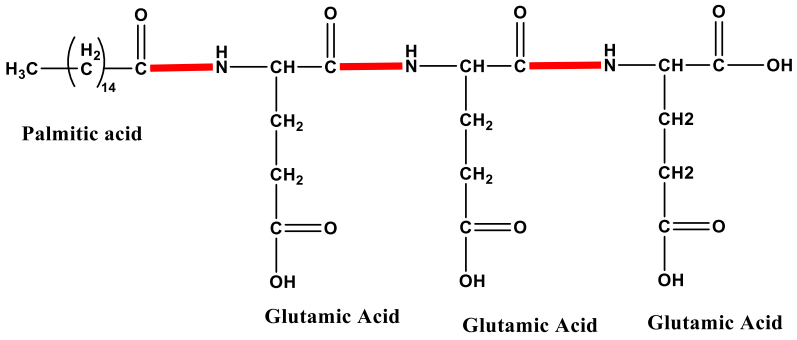

^{1}H NMR spectrum for a triple peptide that contains three molecules of glutamic acid and is coupled with palmitic acid (400 MHz, CD_3OD, 25 ^{o}C): δ= 0.85 (t, ^{3}J= 7.88 Hz, 3H), 1.25 (m, 24H), 1.48 (m, 2H), 2.4 (m, 6H), 2.31 (t, ^{3}J= 7.88 Hz, 4H), 2.45 (t, ^{3}J= 7.88 Hz, 2H), 4.43 (m, 2H), 4.53 (m, 1H), 8.1 (s, 3H) ppm.

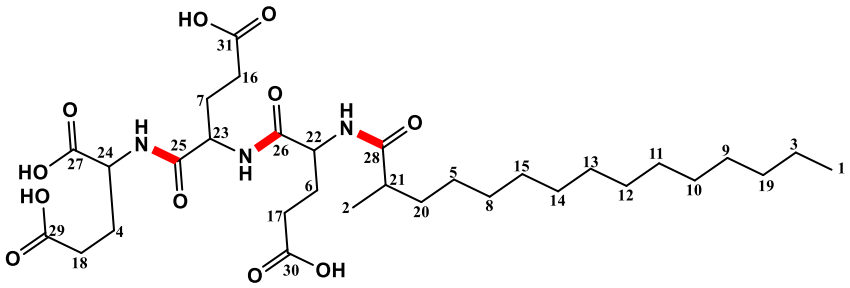

^{13}C NMR (100 MHz, CD_3OD, 25 ^{o}C): δ= 13.1, 16.6, 22.5, 25.8, 26.0, 27.0, 27.2, 29.8, 30.6, 31.0, 31.8, 32.3, 32.9, 33.3, 33.8, 34.7, 34.8, 34.9, 35.0, 35.10, 35.4, 51.6, 52.2, 52.9, 168.2, 168.6, 172.8, 173.1, 175.4, 175.5, 175.6 ppm.

3.3.2 Discussion

The microwave solid phase peptide synthesis (MSPPS) method was used to produce cationic tripeptides containing cationic amino acids (arginine and lysine). These cationic amino acids are known for their ability to enhance cellular uptake, making the peptide potentially more

effective in delivering therapeutic agents into cells. This modification aims to improve the peptide's efficiency in penetrating cell membranes.

The first tripeptide that was produced in this research was a triple arginine peptide. This type of CPP can easily pass through cell membranes because arginine has a guanidinium group. Guanidinium has a high positive charge. This nitrogen-rich group connects to a carbon chain. When the body's pH level is around 7.4, the guanidinium group can take in a proton (H^+) and make a positively charged guanidinium ion (NH_2^+-C(=NH)-NH_2). Thus, this protonation gives arginine its positive charge (see Figure 3.13). The positive charge of arginine interacts strongly with the negatively charged (phosphate, sulphate) cell membrane of the endothelial cells that make up the blood-brain barrier. In addition to embedding it in the liposomes and increasing its stability and permeability, it was conjugated with three different fatty acids: lauric acid, myristic acid, and palmitic acid.

This research produced another triple peptide that contained two molecules of arginine and a lysine (RRK). Lysine possesses a side chain with a terminal amino group (NH_2) attached to a carbon chain. This structure allows lysine to interact more effectively with negatively charged cell membranes, facilitating the peptide's entry into cells. Consequently, the incorporation of lysine alongside arginine is strategically designed to optimise the peptide's cellular penetration capabilities. (See Figure 3.13.)

Additionally, the production of another triple peptide included a molecule of glutamic acid, arginine, and lysine. The properties of each amino acid guided the selection of the sequences for this tripeptide. The specific characteristics of glutamic acid, arginine, and lysine, such as their charge and hydrophilicity, influenced how they were arranged in the tripeptide. This careful selection is crucial for determining the peptide's overall function and stability. Glutamic acid is one of the ionic amino acids and is essential for normal synaptic transmission and neuronal communication in the brain, significantly helping to regulate

neuroplasticity, the brain's capacity for adaptation and self-recognition, as well as cognitive functions, including learning and memory. The enzyme glutaminase synthesises glutamic acid from glutamine in the brains of patients with Alzheimer's disease, following the same metabolic pathway as in healthy brains. This cycle includes the transformation of glutamic acid to glutamine in astrocytes, which is then transported back to neurones and reconverted to glutamic acid.[198] Glutamic acid may also be synthesised by transamination processes, in which an amino group is transferred from another amino acid to alpha-ketoglutarate, resulting in the formation of glutamic acid. Changes in brain energy metabolism in Alzheimer's disease can influence glutamic acid levels. Decreased glucose usage may reduce glutamic acid synthesis, thereby affecting brain function.[199,200] This led to the selection of glutamic acid. Glutamic acid has a side chain including a carboxylic group (-COOH) (see Figure 3.14), which, at physiological pH (*ca.* 7.4), undergoes deprotonation, producing a negatively charged carboxylate group (-COO-). This deprotonation is significant as it affects the molecule's chemical properties and interactions within the brain. Consequently, the negatively charged carboxylate group plays a crucial role in the function of glutamic acid as a neurotransmitter. The selection of the additional two amino acids, arginine and lysine in this tripeptide is dependent upon the previously stated reasons for selecting the other two peptides mentioned that contained arginine and lysine. These amino acids are chosen based on their complementary properties and roles in enhancing the overall functionality of the peptides. Their inclusion is essential for optimising interactions and ensuring effective signalling within neural pathways. The net charge of the produced peptide (ERK) is positive because glutamic acid is an ionic amino acid, and the other two are cationic amino acids. This positive net charge enhances the peptide's ability to interact with negatively charged molecules in the cell membranes, facilitating better binding and signalling. Consequently, these properties contribute to the peptide's overall effectiveness in biological processes. This lets it work

as a cell-penetrating peptide (CPP) and interact with the cell membrane through electrostatic forces.

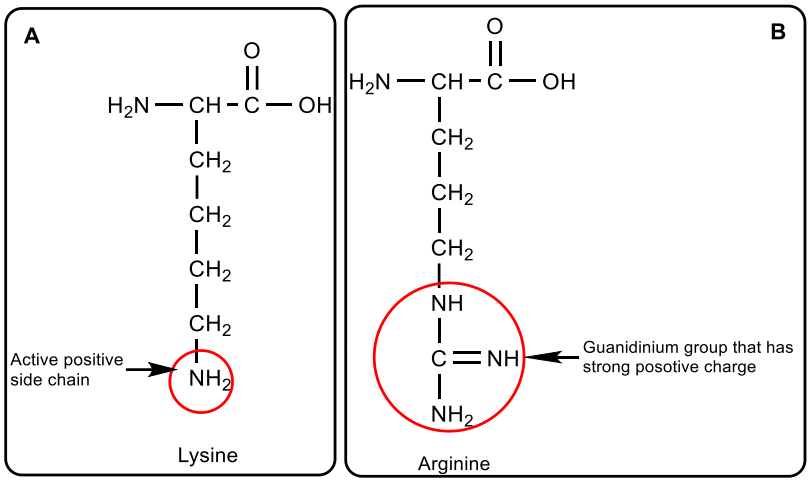

Figure 3.13: Shows the chemical structure of arginine and lysine with their selected active group that gives a positive charge at physiological conditions.

This research prepared a final cationic peptide, a dipeptide containing arginine and lysine (RK). This dipeptide is important because both amino acids have a positive charge, which helps it have a strong interaction with negatively charged molecules in cell membranes. Such properties make RK a valuable candidate for using it as a valuable CPP. The aim behind making this peptide was to make it the smallest and work as a blood-brain barrier-penetrating peptide; also, the properties of arginine and lysine were important in that decision. This strategic design allows RK to potentially facilitate the delivery of therapeutic agents across the blood-brain barrier, overcoming a significant challenge in treating central nervous system disorders, especially AD. By leveraging the unique characteristics of arginine and lysine, this study hopes to improve drug efficacy and targeting. Similar to other peptides, it conjugates with all three fatty acids (see Table 1). This conjugation enhances the stability and bioavailability of the peptides, thereby optimising their ability to transfer drugs to the brain. By

incorporating fatty acids, the study aims to further improve the ability of RK to penetrate cellular membranes effectively.

In this study, two ionic tripeptides were prepared, the first one of them which contained two molecules of aspartic acid (an ionic amino acid) coupled with lysine (EEK), and the other ionic tripeptide was triple glutamic acid (EEE). See Table 1. Both of them were synthesised through MSPPS via the Biotage microwave peptide synthesiser. Both ionic tripeptides were coupled with three distinct fatty acids as cationic peptides. The aim behind producing them was to use them as a control because they have a side chain including a carboxylic group (-COOH) (see Figure 3.14), which, at physiological pH (around 7.4), undergoes deprotonation, producing a negatively charged carboxylate group (-COO-). Due to their negative charge, and when they reach the cell membrane, repulsion will happen between these triple ionic peptides and cell membrane because of the negative charge of the phosphate and sulphate groups of the cell membrane.

In this study, all produced cationic peptides were linked to three different fatty acids through amide bonds: palmitic acid ($CH_3(CH_2)_{14}COOH$), myristic acid ($CH_3(CH_2)_{12}COOH$), and lauric acid ($CH_3(CH_2)_{10}COOH$), so that they would be ready to be embedded in liposomes for the next step of producing innovative vectors. These three fatty acids were chosen because they have different properties. Lauric acid is a 12-carbon saturated fatty acid that is known for its antimicrobial properties and has a moderate ability to pass through cell membranes. Myristic acid is a 14-carbon saturated fatty acid that is a little longer than lauric acid and may have better membrane integration properties. Palmitic acid is a 16-carbon saturated fatty acid that is even longer than the first two and may have stronger and enhanced hydrophobic interactions with cell membranes. These longer-chain fatty acids, such as palmitic acid, typically exhibit greater hydrophobicity, which can improve their ability to embed within and

influence the structure of cellular membranes. This characteristic can potentially enhance their biological activity and efficacy in various applications. Those fatty acids were chosen to be coupled with all produced peptides due to the above reasons. This coupling aims to improve the peptides' membrane permeability, facilitating their potential effectiveness in biological applications. By selecting fatty acids of varying chain lengths, the integration and interaction with cellular structures can be optimised.

Comparing the results of conjugated cationic peptides with fatty acids to previous research, it is evident that the selection of fatty acids significantly influences the effectiveness of cell-penetrating peptides (CPPs). Li *et al.* (2013) demonstrated that the incorporation of fatty acids into CPPs enhances their ability to cross cell membranes. Myskova *et al.* (2023) investigated how lipid modifications improve the stability and delivery efficiency of CPPs. Studies show that acylated CPPs such as polyarginine peptides exhibit significantly higher cellular uptake compared to their non-acylated polyarginine, with enhancements of up to 13.7 fold.[201]

This research corroborates previous findings but with higher purity due to the accuracy in preparing and using the microwave-assisted solid-phase peptide synthesis (MSPPS) method for cationic peptides.

In this research, all produced conjugated peptides with fatty acids have a high purity due to the accuracy in preparing and using the MSPPS method to prepare cationic peptides. Furthermore, using four folds of the coupling agents (HBTU, DIPEA) to couple the fatty acids with the peptides *via* amide bond and leaving the reaction to be processed overnight with continuous stirring gave a chance to couple all produced peptide molecules with the applied fatty acid molecules. Other two researches by showing that attaching fatty acids to cationic peptides such as polyarginine peptides makes them more stable and permeable, which makes them to produce innovative vectors for drug delivery. This improvement in stability and permeability helps these modified

peptides to effectively carry medications across biological barriers, making drug delivery systems more effective. Consequently, this approach could significantly improve the efficacy of drug delivery systems by enabling more reliable and efficient drug transportation to targeted areas of the body.

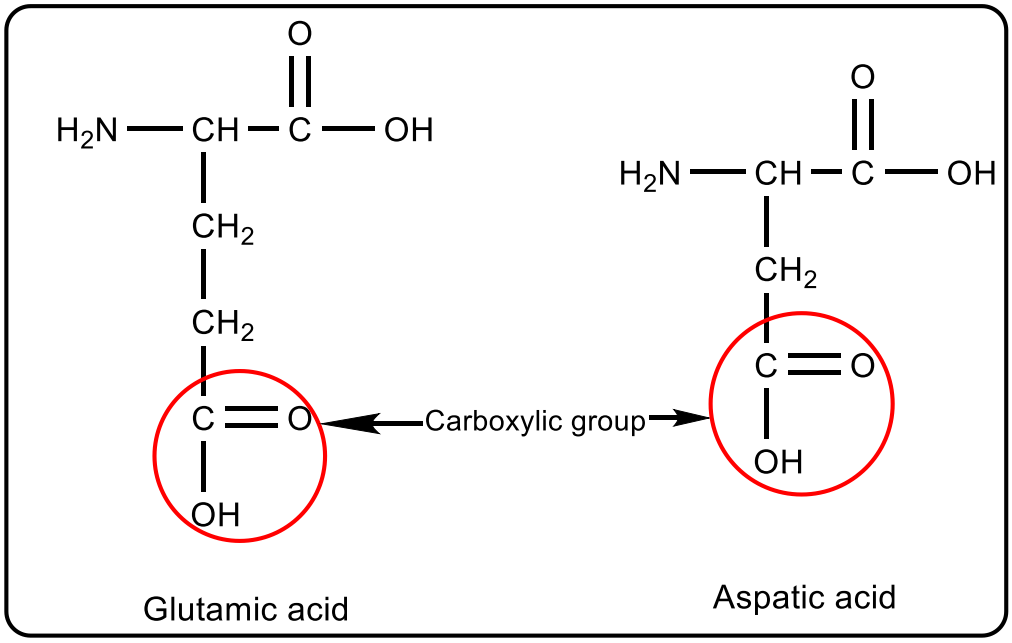

Figure 3.14: Shows the chemical structure of arginine and lysine with their selected active group that gives a positive charge at physiological conditions.

3.4 Peptide synthesis

All the peptides in this research were produced by microwave solid-phase peptide synthesis (MSPPS) using the semi-automated Biotage microwave peptide synthesiser. This method allows for efficient and rapid synthesis of peptides by using microwave energy to facilitate the chemical reactions involved. The semi-automated nature of the Biotage synthesiser also enhances reproducibility and ease of use in peptide

production. The Wang resin was wetted, for instance, Fmoc-Lys(Boc)-Wang (100–200 mesh) (0.2 mmol, 0.298 g), with dimethylformamide in a 10 mL SPPS reaction vessel to improve swallowing. Then it placed the mixture in the Biotage Initiator+ SP Microwave Peptide Synthesiser, allowing it to swell at room temperature with stirring. This step is crucial for ensuring that the resin is properly activated and ready to bond with the peptide sequences during synthesis after deprotected it by removing the (Fmoc) *via* using 20% piperidine in DMF.

This deprotection step is crucial as it allows the amino group of the peptide to become active for subsequent coupling reactions. By removing the protecting group, the synthesis process can continue efficiently, leading to a more refined and effective peptide product. By controlling both temperature and stirring speed, the process promotes uniform mixing and enhances product formation. In the end, the deprotected resin was washed with DMF to eliminate the unwanted protecting group (Fmoc). This washing step is crucial for removing the Fmoc protecting group, which can hinder further reactions. By using DMF, a polar solvent, the process effectively cleans the resin, preparing it for subsequent steps in synthesis. To further lengthen the peptide chain by coupling the second amino acid, the coupling agent 2-(1H-benzotriazole-1-yl)-1,1,3,3-tetramethylaminium hexafluorophosphate (HBTU) was dissolved in DMF. The use of HBTU in DMF facilitates the activation of the second amino acid for coupling, ensuring a more efficient and effective peptide chain extension. This step is essential for maintaining the integrity of the synthesis process as it allows for precise bond formation between amino acids.

The reaction must occur under basic conditions. These basic conditions facilitate the activation of the amino acid for coupling, ensuring that the reaction proceeds efficiently. This step is essential for successfully elongating the peptide chain and advancing the synthesis process. Consequently, diisopropylethylamine (DIPEA) was incorporated into the mixture to make a basic solution. Then the second amino acid was

added to the peptide sequence, such as Fmoc-Arg(Boc)-OH and vortexed for 3-5 minutes to generate an activated ester solution. The solution was subsequently added to the deprotected resin and placed in microwave irradiation, using double coupling due to the basic structural and chemical properties of arginine that make its binding with other molecules difficult. The guanidinium group of arginine can form strong electrostatic and hydrogen-bonding interactions; however, it is located at the end of a flexible hydrocarbon chain. This flexibility can result in entropic penalties that slow down binding, as the side chain fails to have additional functional groups to improve specific interactions. The double coupling process consists of two stages of reaction.

The first reaction time was 5 minutes at 75 ± 2 °C and 500 RPM. The tube was eventually drained. The same solution of the protected amino acid was prepared similarly and introduced to the resin to start the second stage of the reaction (5 minutes, 75 +/- 2°C, 500 RPM). The mixture was afterwards drained and washed with DMF. The Fmoc deprotection of the amino acid was carried out by adding a solution of piperidine. This entailed a two-phase procedure: The initial stage consisted of permitting the reaction to occur for 3 minutes at 75 ± 2 °C with agitation at 500 RPM, followed by drainage. Following that, piperidine was introduced for the second stage. The second stage consisted of permitting the reaction to proceed for 10 minutes at 75 ± 2 °C and 500 RPM. After that, the deprotected amino acid was washed with DMF (4 x 4 mL, 500 RPM). Peptide elongation can be achieved through the removal of the Fmoc protected group followed by the addition of a new amino acid until the desired amino acid sequence is attained.

To enhance the purification of the peptide following its elongation, it was readied for the next phase of coupling with fatty acids. The component was put through three additional washing stages, using (4x5 mL) of DMF, dichloromethane (DCM), and methanol (MeOH)

repeatedly. These washing stages are crucial for removing any unreacted reagents and by-products that may interfere with the subsequent coupling process. By ensuring a clean peptide substrate, the efficiency and purity of the final product are significantly improved.

All the peptides that were produced in this research were characterised by LC-MS and NMR machines and purified by using flash chromatography, reverse phase C18 Sfar column.

3.5 Coupling CPP-fatty acid with fluorophores

Two cationic cell-penetrating peptides were conjugated with two distinct fluorophores, dansyl chloride and fluorescent isothiocyanate (FITC). A triple cationic peptide, including arginine, previously conjugated with palmitic acid, was further linked with the dansyl chloride fluorophore through a sulfonamide bond (See Figure 3.15).

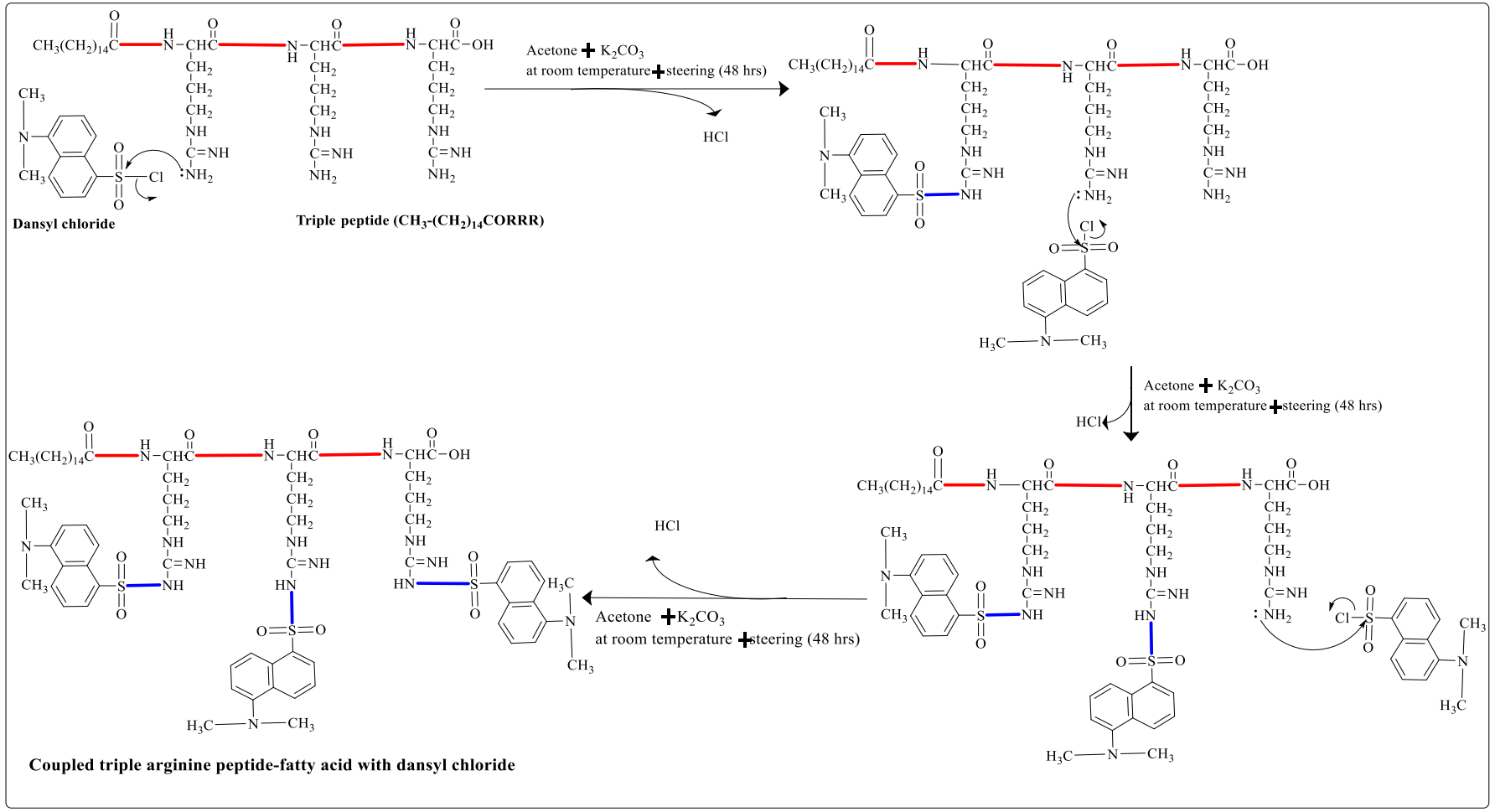

Figure 3.15: Illustrates the mechanism of the chemical reaction between the triple arginine peptide-palmitic acid and dansyl chloride fluorophore, which occurs through a sulphonamide bond (blue bonds); all red bonds are amide bonds between amino acids and the fatty acid.

To confirm that the linkage between dansyl chloride and triple arginine-conjugated palmitic acid was successfully coupled through a sulfonamide bond, ultraviolet light was used as a primary analysis of the result. This analysis showed that dansyl chloride was present and had a blue colour. Further characterisation was done by using LC-MS, 1H NMR, and 13C NMR to determine the produced labelled peptide-conjugated fatty acid and their purity. These advanced characterisation techniques provide a more comprehensive analysis of the chemical structures and interactions involved, ensuring that the experimental results are accurate and reliable.

The LC-MS machine data indicates that a tripeptide that contained three molecules of arginine conjugated palmitic acid *via* an amide bond and coupled with dansyl chloride through sulphonamide bond has M/Z= 1423, matching the theoretical value. It was also detected at a retention time of 14.96 min, and had a purity >94%. Also, the product's weight was 0.35 g, which is equivalent to 2.46 x 10^{-4} mol.

The ^{1}H NMR and ^{13}C NMR confirmed that $CH_3(CH_2)_{14}CORRR$ was successfully coupled to dansyl chloride with high purity because all the peaks of its atoms (H, C) could be found. The results are as follows.

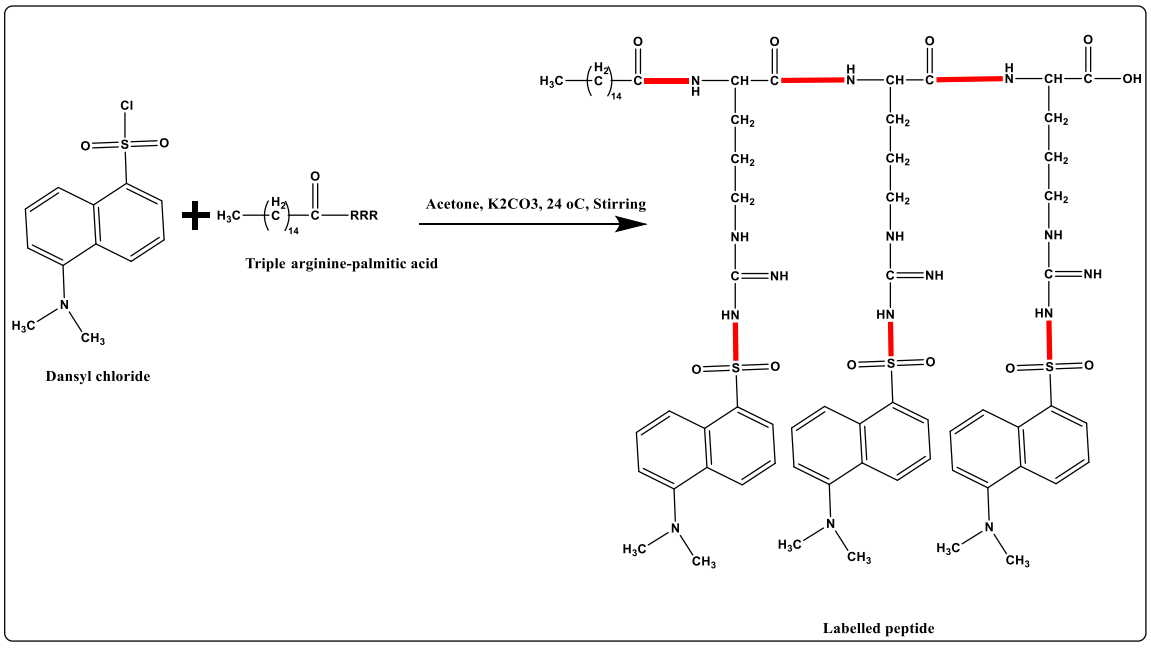

^{1}H NMR spectrum for a triple peptide that contains three arginine and was coupled with palmitic acid and dansyl chloride fluorophore (400 MHz, CD_3OD, 25 °C) δ= 0.87 (t, ^{3}J = 7.96 Hz, 3H), 1.25 (m, 24H), 1.63 (m, 8H), 1.87 (m, 6H), 2.04 (s, 3H), 2.20 (t, ^{3}J = 7.96 Hz, 3H), 2.86 (s, 18H), 3.32 (m, 4H), 4.29 (m, 2H), 4.4 (m, 1H), 7. 18 (d, ^{3}J = 7.96 Hz, 3H), 7.47 (t, ^{3}J = 7.96 Hz, 3H), 7.95 (s, 3H), 8.13 (t, ^{3}J = 7.96 Hz, 3H), 8.29 (d, ^{3}J = 7.96 Hz, 3H), 8.32 (d, ^{3}J = 7.96 Hz, 3H), 8.38 (d, ^{3}J= 7.96 Hz, 3H), 8.50 (d, ^{3}J = 7.96 Hz, 3H) ppm.

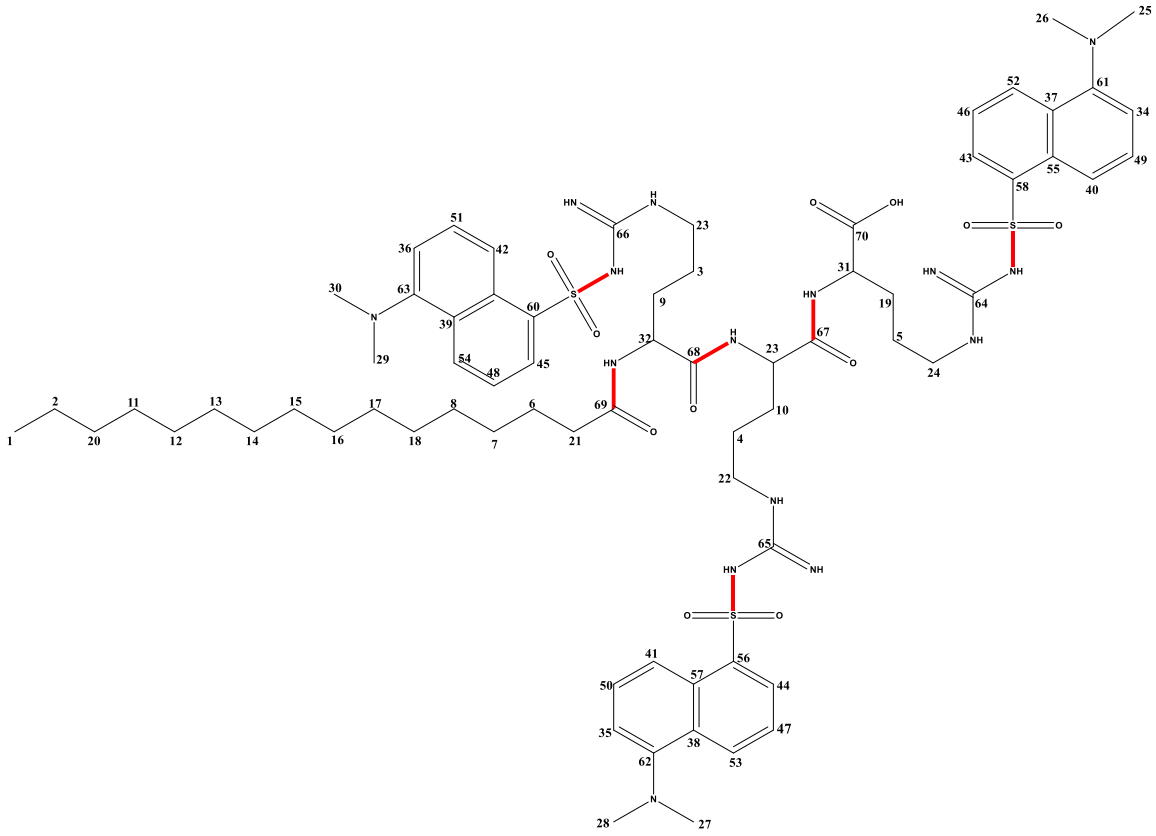

^{13}C NMR (100 MHz, CD_3OD, 25 °C): δ= 13.2, 22.4, 23.9, 24.3, 24.9, 25.6, 25.7, 27.4, 28.5, 28.6, 28.8, 29.1, 29.3, 29.4, 29.5, 31.2, 31.8, 32.6, 33.6, 35.4, 35.4, 35.7, 38.9, 40.5, 45.7, 45.8, 45.9, 46.0, 46.1, 46.2, 53.2, 53.3, 53.44, 114.0, 114.4, 114.6, 115.0, 115.4, 115.5, 118.1, 118.3, 118.7, 121.1, 121.2, 121.3, 123.1, 123.2 123.3, 125.4, 125.5, 126.4, 127.3, 129.6, 130.5, 140.4, 140.6, 140.7, 143.2, 143.4, 143.4, 157.1, 157.3, 157.6, 161.6, 161.9, 162.3, 172.1, 173.3, 175.3, 176.0 ppm.

Another cationic triple cell-penetrating peptide, including one molecule each of glutamic acid, arginine, and lysine, was conjugated with palmitic acid and then labelled with fluorescent isothiocyanate (FITC) through amide bond (See Figure 3.16).

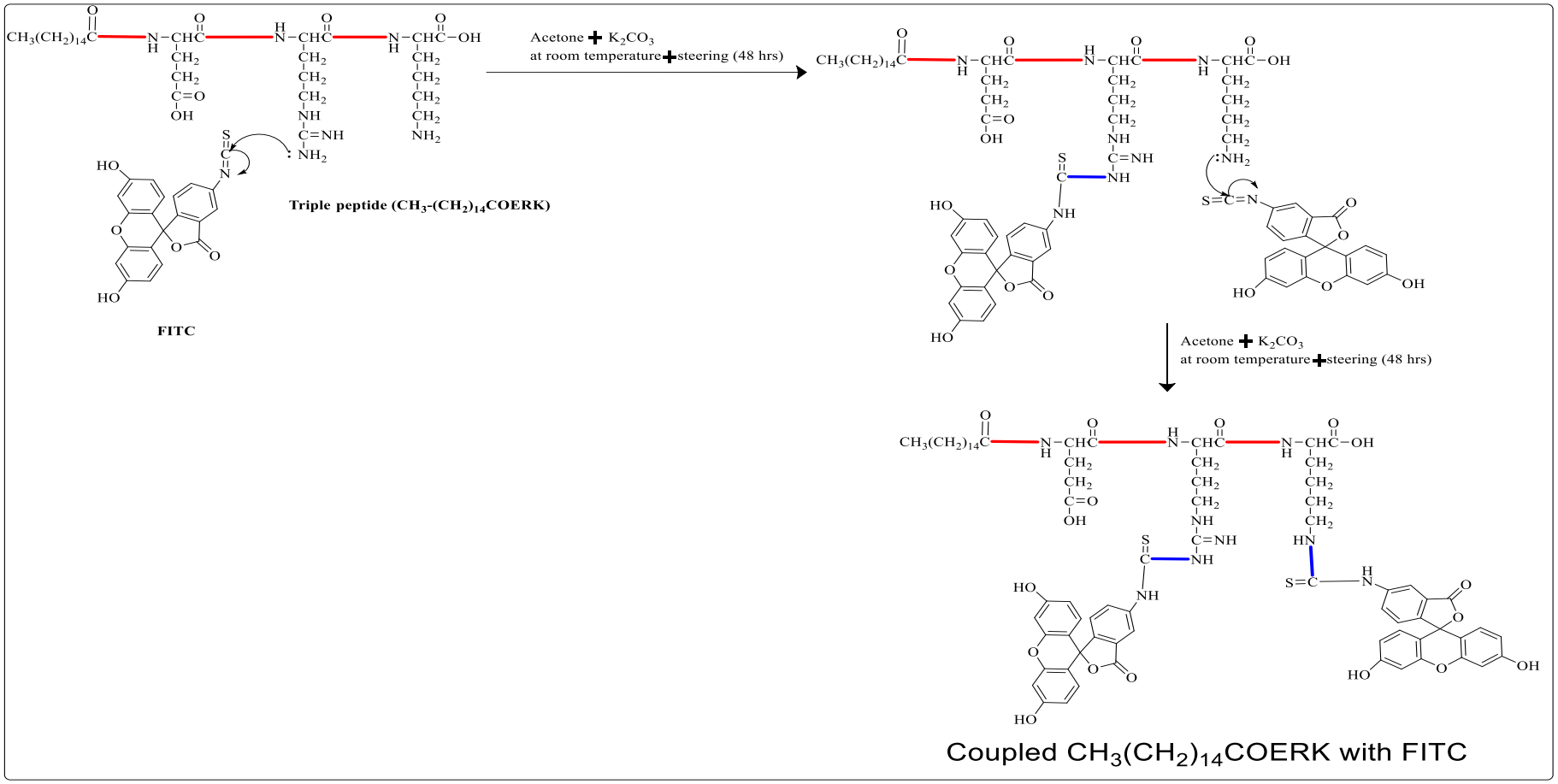

Figure 3.16: Illustrates the chemical reaction between a triple peptide containing lysine, arginine, and glutamic acid, coupled with palmitic acid, and then coupled with fluorescein isothiocyanate (FITC) fluorophore. This reaction occurs through carbonamide bond (blue bonds); all red bonds are amide bonds between amino acids and fatty acids.

The LC-MS machine data indicate that a tripeptide that contained glutamic acid, arginine, and lysine conjugated palmitic acid *via* an amide bond and coupled with FITC through carbonamide bond has M/Z= 1475, matching the theoretical value. It was also detected at a retention time of 15.05 min, and had a purity >95%. Also, the product's weight was 0.32 g, which is equivalent to 2.17 x 10^{-4} mol.

The ^{1}H NMR and ^{13}C NMR confirmed that $CH_3(CH_2)_{14}COERK$ was successfully coupled FITC with high purity because all the peaks of its atoms (H, C) could be found. The results are as follows.

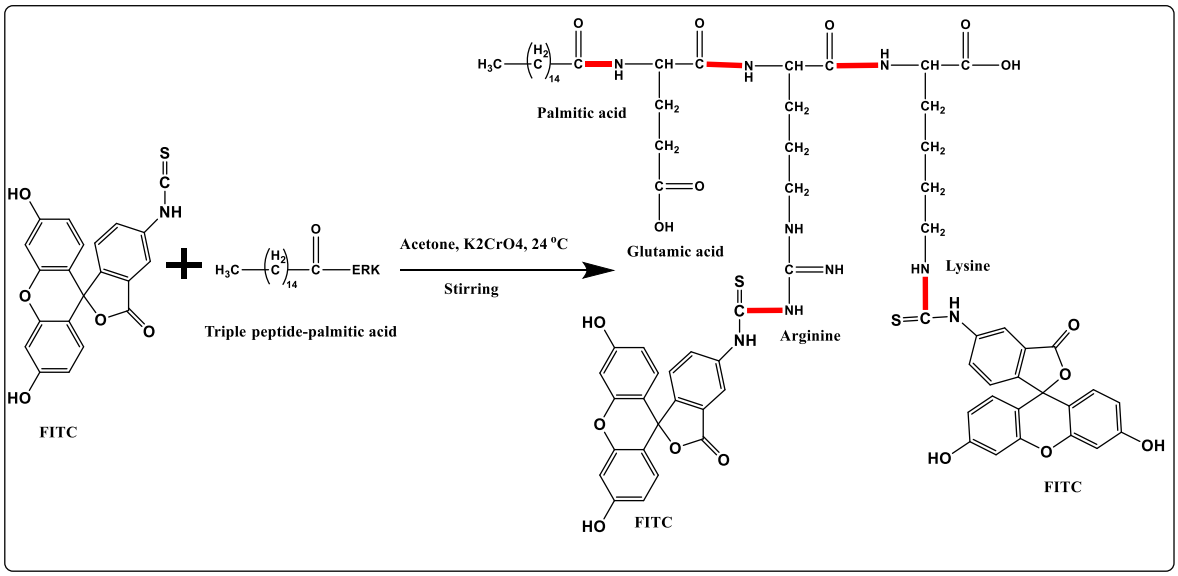

^{1}H NMR spectrum for a triple peptide that contains lysine, arginine, and glutamic acid conjugated with palmitic acid and FITC (400 MHz, CD_3OD, 25 °C) δ= 0.85(t, ^{3}J = 7.96 Hz, 3H), 1.26(m, 26H),1.51 (m, 8H), 1.74(m, 4H), 2.01 (m, 4H), 2.30 (t, ^{3}J= 8.00 Hz, 2H), 2.44 (s, 1H), 2.65 (t, ^{3}J = 7.96 Hz, 2H), 3.30 (t,^{3}J = 7.96 Hz, 2H), 4.41 (m, 2H), 4.42 (m, 1H), 6.41 (d, ^{3}J = 7.96 Hz, 4H), 6.3 (s, 2H), 6.5 (s, 4H), 7.05 (d, ^{3}J = 7.96 Hz, 4H), 7.3 (t, 1H), 7.43 (d, ^{3}J = 7.96 Hz, 2H), 7.64 (d, ^{3}J = 7.96 Hz, 2H), 7.82 (s, 1H), 8.1 (s, 2H), 8.3 (s, 3H), 12.6 (s, 1H), 13.01 (s, 1H) ppm.

^{13}C NMR (100 MHz, CD_3OD, 25 ^{o}C): δ= **^{13}**C NMR (100 MHz, CD_3OD, 25 ^{o}C): δ= 13.1, 22.4, 22.4, 23.3, 24.8, 25.6, 26.5, 28.5, 28.7, 28.9, 29.0, 29.1, 29.2, 29.3, 29.4, 29.5, 29.9, 30.3, 30.6, 31,8, 34.0, 35.4, 35.7, 39.0, 39.2, 40.7, 84.5, 84.8, 105, 105.1, 105.5, 105.7, 107.1, 107.5, 107.8, 108, 109, 109.2, 109.5, 109.8, 124, 124.5, 127, 127.4, 128,9, 129, 129.1, 129.6, 131, 131.4, 133.9, 134.3, 146.95, 147.5, 151.9, 152, 152.4, 152.8, 153.5, 155.1, 155.4, 156.1, 165.7, 163.5, 168.9, 169.5, 172.4, 172.9, 173.6, 175.1, 175.3 ppm.

Coupling dansyl chloride with a triple arginine peptide conjugated to palmitic acid and FITC with a triple peptide of glutamic acid, arginine, and lysine conjugated to palmitic acid involves complex peptide synthesis techniques. The resulting conjugates were ready to be used for the next step, which was encapsulating them within liposomes.

The coupling of dansyl chloride with a triple arginine peptide conjugated to palmitic acid and FITC with a triple peptide of glutamic acid, arginine, and lysine conjugated to palmitic acid demonstrates the versatility of peptide modification. These conjugates can enhance the delivery and visualisation of peptides in biological systems, offering the potential for targeted therapeutic and diagnostic applications.

3.6 Conclusion

The main purpose of combining cell-penetrating peptides (CPPs) with fatty acids like palmitic acid, myristic acid, and lauric acid was to embed the CPPs into the liposome, which has the potential to improve their capacity to pass across the blood-brain barrier. Combining fatty acids with CPPs can significantly increase their hydrophobicity, a crucial component for their ability to penetrate lipid membranes like the BBB wall and increase stability. [202–204]

The lipophilic characteristics of peptides changed with fatty acids, significantly improving their capacity to pass through the blood-brain barrier. The modifications improve the hydrophobicity of peptides, encouraging their interaction with lipid membranes, which is essential for moving across the blood-brain barrier. Peptide-fatty acid uses the natural ability of lipophilic molecules to bind with lipid bilayers of the cell membrane, increasing the transport of therapeutic agents to the brain. Fatty acids improve the hydrophobicity of peptides, enabling their interaction with lipid bilayers, an important step for passing through cellular barriers such as the blood-brain barrier. The improved lipophilicity allows the electrostatic interaction of peptides through biological barriers, such as the blood-brain barrier. [205–207]

The choice of fatty acids may affect the ability of CPPs to deliver therapeutic drugs to the brain, with each fatty acid presenting a unique set of benefits. Fatty acids increase the hydrophobicity of CPPs, a crucial factor in their ability to cross the blood-brain barrier.[203,208] This change could make it much easier for CPPs to interact with the lipid-rich environment of the BBB, which could greatly improve how well CPPs work during the transition process. Additionally, the incorporation of fatty acids has the potential to improve the cellular absorption of CPPs, therefore making them more efficient in transporting medicines across the blood-brain barrier. This is especially important when targeting brain tissues, where effective delivery can sometimes be challenging. Fatty acid-modified CPPs may also adapt to specific cell types, potentially enabling more focused delivery of therapeutic drugs to the brain.

The solid phase peptide synthesis (SPPS) method has been used to produce cationic tripeptides containing cationic amino acids (arginine and lysine) and then coupled with fatty acids *via* amide bond. The fatty acids associated with peptides are palmitic acid, myristic acid, and lauric acid, the main aim of coupling those fatty acids was to incorporate (embed) the peptides into liposomes. Also, it has several

advantages, particularly concerning the transport of drugs across the blood-brain barrier. One of the most well-known characteristics of cationic peptides is their capacity to interact with negatively charged cell membranes. Coupling these cell-penetrating peptides with fatty acids by a strong bond, which is an amide bond, which could further boost their hydrophobic strength could improve their ability to pass through biological membranes, including the blood-brain barrier. Additionally, fatty acids such as palmitic acid can stabilise the peptides, preventing them from being degraded by enzymes and increasing the amount of time they may be used effectively. Palmitic acid, which is well-known for its high hydrophobicity, can dramatically improve the membrane penetrating capacities of CPPs, which makes it a beneficial choice for BBB penetration. [202] Myristic acid strikes a balance between being hydrophobic and being flexible, which could be useful for keeping the structure of CPPs intact while also making them more effective at delivering drugs. [202] Lauric Acid, despite being less hydrophobic than palmitic and myristic acids, lauric acid can still enhance CPP penetration, albeit to a lesser extent than the other acids. Also, lauric acid has anti-inflammatory properties.[202]

Furthermore, fatty acids can increase the solubility of peptides in lipid environments, which in turn makes them more suited for encapsulation (embed) in liposomes. These advantages make this technique especially beneficial for transporting therapeutic drugs across the blood-brain barrier, potentially leading to an improvement in the treatment of neurological illnesses such as Alzheimer`s disease. Palmitic acid is often considered the best option for improving BBB penetration due to its high hydrophobicity. This is because it corresponds well with the physicochemical qualities necessary for optimal brain targeting. It is possible that the decision was changed based on the particular therapeutic setting and the desired balance between the risk of side effects and the effectiveness of the treatment. The use of fatty acid-modified CPPs has several larger consequences,

including the possibility of toxicity and the need for precision targeting to prevent off-target effects. Although palmitic acid shows promise, it is vital to consider these consequences.[209] In addition, coupling CPP-conjugated fatty acid with fluorophores facilitates the tracking and visualisation of embedded peptide-fatty acid complexes inside liposomes using fluorescence microscopy or other imaging methods. This assists in examining the distribution and dynamics of the loaded liposomes and tracking them to the targeted area. Dansyl chloride is an important tool for end-group analysis of peptides due to its binding capacity to primary and secondary amines. Dansyl chloride's fluorescence properties enable the visualisation of peptide localisation and distribution within the complicated biological environments of endothelial cells.

Their maximum absorption wavelengths are 335 nm and 498 nm, and their maximum emission wavelengths are 500 nm and 517 nm, respectively. Both fluorophore-CPPs-fatty acid compounds were incorporated into the liposomes *via* a microfluidic system (dolomite), with the optimal concentration determined to be 2.5 mg/mL of the formulated liposome solvent.

Chapter 4: Vectors

4.1 Summary

This chapter discusses the production of liposomes composed of 70% L-alpha-phosphatidylcholine and 30% cholesterol by the microfluidic system (Dolomite). The liposomes were characterised using dynamic light scattering (DLS) to determine their size in solution, polydispersity, and diffusion constant; scanning electron microscopy (SEM) to assess their morphology; and a nanosizer (Zetaview) to evaluate their concentration, charge, and size. Initially, the liposomes were encapsulated with rhodamine B dye as model drugs. However, fluorescence microscopy revealed that rhodamine B did not remain encapsulated within the liposomes, as it could diffuse through the lipid bilayer. Then, dansyl chloride was coupled with a triple arginine-conjugated fatty acid and fluorescein isothiocyanate was coupled with a triple peptide of glutamic acid, arginine, and lysine-conjugated fatty acid to find its characterisation before being applied as a delivery vector on an artificial BBB for the aim of tracking the effect and movement of the functionalised liposomes.

Subsequently, two distinct peptide-fatty acids were embedded within the liposome membrane and fully characterised to be ready for the next step of this research, which is applying a functionalised produced vector on the artificial BBB to penetrate drugs.

This chapter also talks about how the microfluidic system can be used to make liposomes, which are made up of L-alpha-phosphatidylcholine and cholesterol. The liposomes were characterised with dynamic light scattering (DLS) to determine their size and polydispersity in solution, SEM to determine their morphology and size, and a nanosizer (Zetaview) to check their concentration, charge, and size. The liposomes were initially loaded with a fluorophore (dansyl chloride and fluorescent isothiocyanate)-conjugated cationic peptide fatty acid for the purpose of tracking and visualising innovatively produced vectors

before their application to the artificial blood-brain barrier (growing endothelial cells on the nanofiber 3D scaffold). They were characterised by SEM and fluorescent microscopy. The produced liposomes were also encapsulated with rhodamine B dye for the purpose of using it instead of the drug and visualising its movement. The encapsulated liposomes with the rhodamine B dye were characterised by size exclusion chromatography, DLS, SEM, and fluorescent microscopy.

4.2 Overview

Microfluidic systems are quickly becoming known as the most accurate way to prepare lab-on-a-chip liposomes because they can make formulations that are very consistent and can be used again and again. This consistency in formulation is crucial for ensuring reliable results in experiments and applications. Additionally, the ability to reuse the system enhances efficiency and reduces waste in the liposome preparation process. This method enables precise control over various parameters, resulting in improved encapsulation efficiency and scalability, which is necessary for pharmaceutical applications.[210,211] The improved encapsulation efficiency allows for a higher concentration of active ingredients within the liposomes, making them more effective in delivering therapeutic compounds. Scalability ensures that this reliable preparation method can be adapted for both small-scale research and larger industrial production. Microfluidics allows the production of monodisperse liposomes, providing uniform size and distribution, which improves the success of drug delivery. This uniformity is crucial because it enhances the predictability of how the liposomes will behave in biological systems, leading to better therapeutic outcomes.[212] Consequently, the combination of improved encapsulation and scalability positions these liposome formulations as highly effective tools in drug delivery for pharmaceutical applications.[210] The microfluidic method could potentially be scaled up without compromising quality, as proven by research that effectively moved from laboratory settings to larger-scale production. Careful

modification of the flow rate ratios and lipid concentrations enables real-time optimisation of liposome properties. This adaptability ensures that the liposome formulations maintain their efficacy and safety even when produced in larger quantities, making them suitable for widespread clinical use. As a result, this method not only enhances the manufacturing process but also supports the development of more effective drug delivery systems.[213]

Microfluidic methods have demonstrated the ability to improve drug loading and reduce lipid loss, which is essential for maintaining therapeutic efficacy. Microfluidics-generated liposomes can be produced for both passive and active targeting in neurological treatments, increasing drug delivery to the brain and minimising systemic toxicity. This targeted approach is particularly valuable in treating neurological disorders, where precise drug delivery is crucial for maximising therapeutic effects while minimising side effects.[211] By optimising the delivery mechanism, microfluidics advances the overall efficacy and safety of treatments aimed at the central nervous system.

4.3 Results and Discussion

This section presents the findings of a study on liposomes made with L-alpha-phosphatidylcholine and cholesterol using a microfluidic system. Before starting to prepare liposomes, the microfluidic system was calibrated carefully to find the accurate flow rate to produce the desired liposome, which is their size of around 100 nm. After calibration, the unfunctionalized liposomes were produced in a microfluidic system with a lipid solution pump flow rate of 11.618 µL/min (pressure = 2 bar) and a water pump flow rate of 24.93 µL/min (pressure = 2.6 bar) using a hydrophilic droplet junction chip (100 µm) at room temperature. The produced liposomes were characterised by DLS to find their size and polydispersity index (similarity in their size). See Figure 4.1.

According to the DLS result the mean diameter size liposomes (average diameter) of the generated liposomes was 97.9 nm. The polydispersity index was 0.09. The Diffusion coefficient was 1.504 x 10^{-8} cm^2/sec.

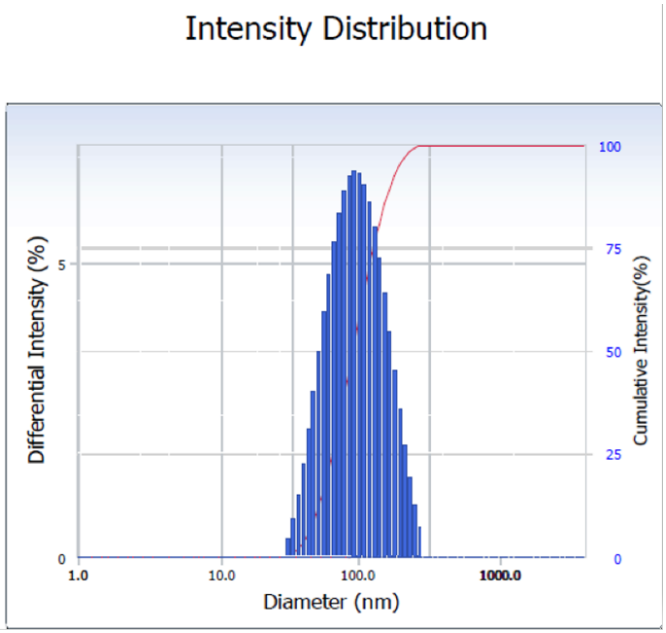

Figure 4.1: Demonstrates the intensity-weighted distribution of the unfunctionalised liposomes by DLS.

SEM was used to find their morphology and size. It confirmed that the produced unfunctionalized liposomes had 100 nm in size. See Figure 4.2.

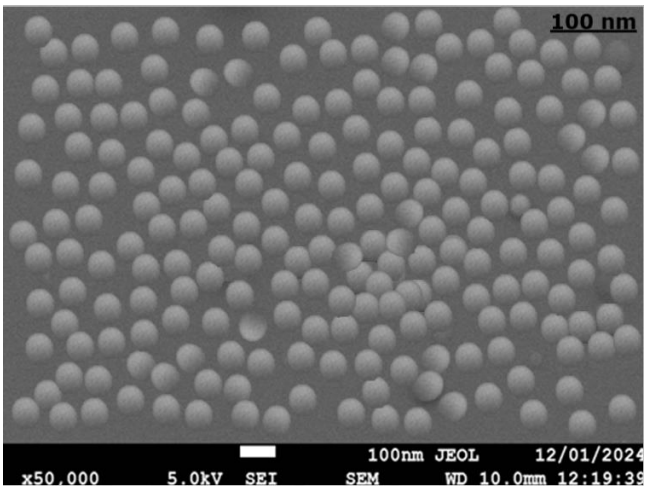

Figure 4.2: Illustrates the size of the produced liposomes *via* SEM.

The unfactionalized liposomes also, characterised by a nanosizer (ZetaView) to find the concentration, charge and size. See figure 4.3 used to find the concentration of the produced liposomes, size, and charge. According to the results of the nanosizer (ZetaView), the concentration of the produced liposomes was 3.6 × 10^15 particles/mL, and the median of their size was 95.9 nm. Also, the charge of the produced liposomes was found by the same machine, and it was neutral.

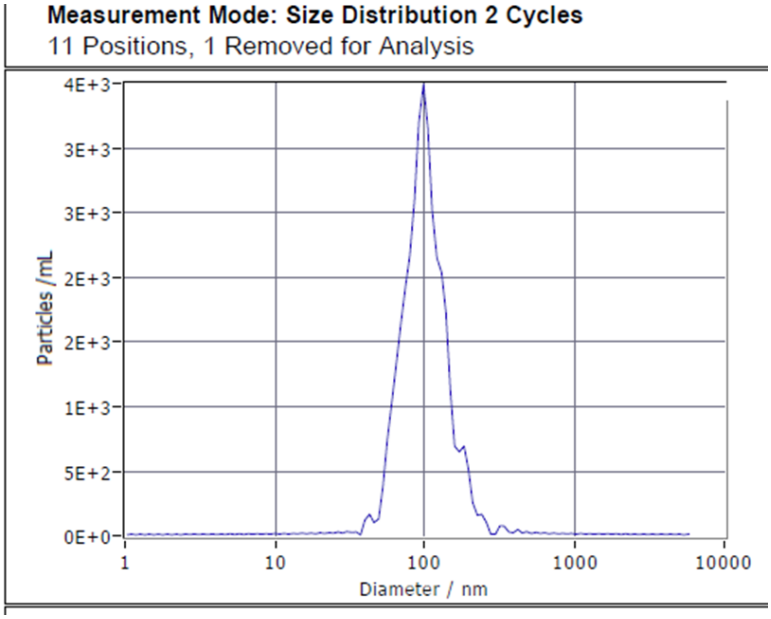

Figure 4.3: Shows the nanosizer (ZetaView) data in finding the concentration and size of the produced liposomes by the microfluidic system.

The microfluidic technique enabled the production of liposomes with a controlled size distribution. This controlled size distribution is crucial for optimising the liposomes' performance in drug delivery, as it can influence their circulation time, cellular uptake, and overall therapeutic efficacy. Consequently, the findings of this study highlight the advantages of using microfluidic methods in developing more effective liposomal formulations. The dynamic light scattering (DLS) results showed that the particles had a diameter of 97.9 nm and a low polydispersity index (PDI) of 0.09, which means they were similar. This

similarity in size distribution, indicated by the low PDI, is essential because it suggests that the liposomes behave consistently in biological systems, enhancing their reliability for targeted drug delivery. Such precise control over particle size can lead to improved drug delivery outcomes by ensuring a more predictable therapeutic response. Also, the diffusion constant of the produced liposomes was very low (1.504 x 10^{-8} cm^2/sec), this indicates larger or more viscous liposomes.

The SEM also, confirms the produced liposomes that were made microfluidic system that their size was 100 nm and according to the SEM image they were spherical and similar. This measurement indicates that the liposomes are within a desirable size range for effective cellular uptake and distribution. Consequently, this size contributes to their potential efficacy in delivering therapeutic agents to specific targets within the body.

A nanosizer machine (Zeta View) was confirmed the Median size of the 98.2% of the produced liposomes was 95.9 nm , their concentration was (3.6x10^{15} particles/mL), and charge of the liposomes that were made was neutral. This indicates a high yield of liposomes that are similar in size, which is crucial for ensuring consistent behaviour in biological systems. The neutral charge further suggests minimised interactions with unintended targets, enhancing their delivery efficacy. This result matches what was found in a previous study, which showed that microfluidic techniques could make liposomes with controlled sizes and a low polydispersity index (PDI).[214] This consistency in size and charge is essential for optimising the performance of liposomes in drug delivery applications. By achieving a low PDI, Diffusion constant and high concentration of the liposomes with their neutral charge can behave predictably within biological environments, leading to improved delivery of therapeutic outcomes.

4.4 Stability of liposomes

The stability of the liposomes was monitored after producing them and full characterisation to the desired size (*ca*. 100 nm) for this research using a microfluidic system. This monitoring ensured that the liposomes maintained their structural integrity and functionality, which is crucial for their intended applications in drug delivery and other biomedical uses. By confirming their stability, the reliability of the experimental results can be proved. Therefore, before encapsulation, the liposomes were stored at room temperature and in the fridge (4 °C), and their diameter was monitored with DLS.

4.4.1 Liposome stability at 24 °C

The liposomes were produced *via* a microfluidic system (Dolomite) with a lipid solution (70% L-α phosphatidylcholine and 30% cholesterol). After its production, the size was measured by DLS at regular intervals, every hour, until the liposomes fused. (See Figure 4.4.)

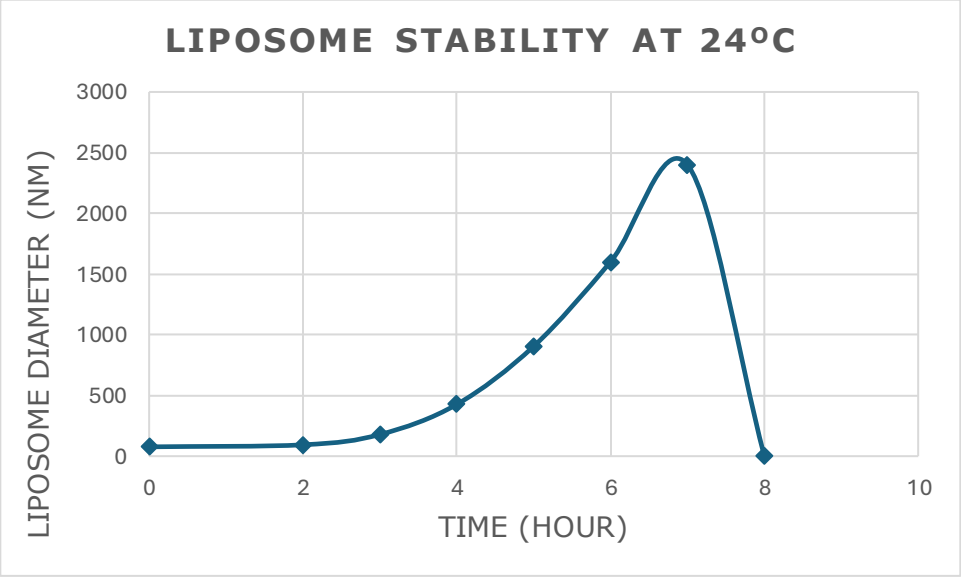

Figure 4.4: Illustrates the average stability of the liposomes at 24 °C for six times.

During the initial two hours, there was no significant change in the unfunctionalized liposomes` diameter. Afterwards, their size increased dramatically, and after 8 hours, all the produced liposomes were fused. This dramatic increase in size indicates that the liposomes underwent a process of aggregation, which typically occurs when they come into close proximity, leading to their merging into larger structures. By the end of the 8 hours period, this fusion resulted in a complete transformation of the initial liposome into larger aggregates. This process not only alters the physical characteristics of the liposomes but also may impact their functionality and interactions with other biological components.

4.4.2 Liposome stability at 4 ^{o}C

The liposomes were made from a mixture of L-α phosphatidylcholine and cholesterol. This was done using a microfluidic system. After their production was kept under 4°C for the first 8 hours, the size was measured by DLS at regular intervals, each for every hour, and then after 24 hours and until 120 hours, all liposomes were fused. See Figure 4.5. This careful monitoring allowed for an assessment of the liposome size and stability over time, ensuring that any changes could be promptly identified. By maintaining controlled conditions and measuring at set intervals, the aim is to optimise the liposome formulation for its intended application.

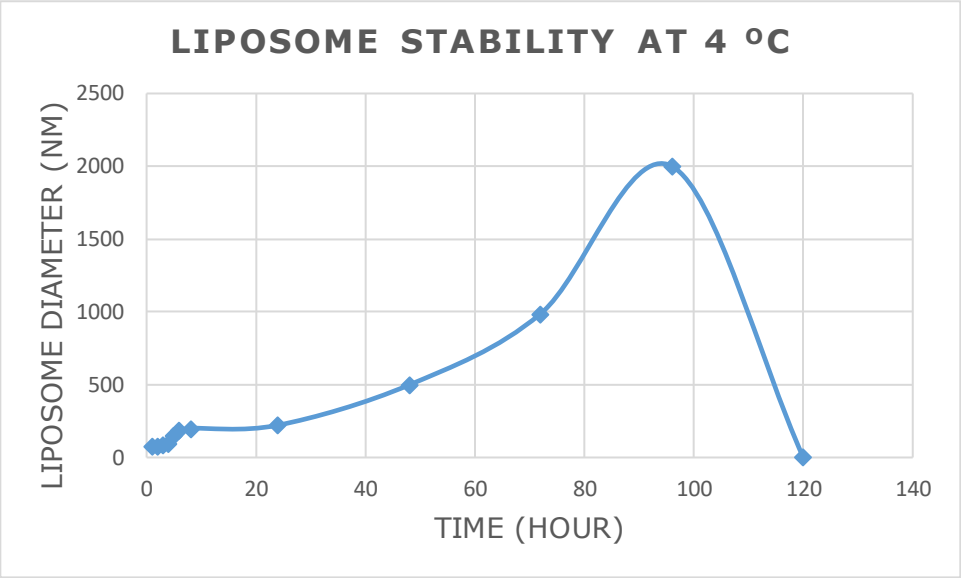

Figure 4.5: Shows the stability of the liposomes at 4°C. The liposomes can withstand a longer duration at lower temperatures. During the initial hours, there was minimal alteration in their diameter. Subsequently, they grew in size, and by day four, they had fused all the liposomes produced.

The liposomes can remain for much shorter durations at room temperature (24 °C) than at lower temperatures. The liposomes made at room temperature were not as stable as the ones stored in the fridge, even though they were constantly mixed using a vortex. This comparison highlights the importance of temperature control in preserving liposome integrity, especially as the produced liposomes in this research were not PEGylated. According to this result, maintaining the liposomes at lower temperatures ensures their stability and enhances the reliability of subsequent experimental outcomes. The liposomes at 24°C rapidly grew in size as the first two hours remained the same, and then after 3 hours, their size increased dramatically, and the maximum remaining time was up to 7 hours, and after that time, all the produced liposomes fused together, leading to a loss of their individual characteristics. On the other hand, when liposomes were kept at 4 °C, there was no significant change in their size. This emphasises the need for strict time management during the

experiment to maintain liposome functionality and prevent unwanted aggregation. (See Figure 4.4.) At room temperature, increased kinetic energy may result in increased rates of liposome coalescence, which reduces stability.[215] The cholesterol in the liposomes maintained the membrane's stability. However, as the temperature rose, the cholesterol's effectiveness decreased because the lipids were more likely to move around, which could lead to phase transitions.[216] Increasing temperatures speed up chemical decomposition processes, possibly resulting in a shorter storage period and reduced liposome stability.[217] The liposomes were made up of 70% L-alpha-phosphatidylcholine and 30% cholesterol in methanol and stored in the fridge (4 °C). The produced liposomes at 4 °C remained much longer than those stored at room temperature. The size of the liposomes did not appear to change significantly in the first 8 hours but gradually increased each day until they fused on day four (120 hours) (see Figure 4.5). Many factors, including the lipids they contain and their storage, affect their stability. Cholesterol plays an important role in increasing the stability of liposomal bilayers by regulating membrane fluidity and decreasing permeability, which is critical for preserving structural integrity over time. It is essential for stabilising liposomes because it fills the spaces between phospholipid molecules; thus, it decreases membrane fluidity and permeability.[216] This indicates that the composition and environmental conditions of the liposomes are crucial for maintaining their structural characteristics. As such, understanding these factors can help optimise liposome formulations for various applications. However, the absence of polyethylene glycol (PEG) may pose challenges to stability, as PEG molecules typically offer enhanced protection against degradation and fusion. The usage of L-alpha-phosphatidylcholine creates a natural phospholipid environment, advantageous for biocompatibility, although susceptible to oxidation and hydrolysis over time. Keeping liposomes at 4°C reduces oxidative and hydrolytic breakdown, which becomes worse at higher temperatures.[215] Therefore, careful consideration of storage conditions

is needed to maintain the integrity of liposomal formulations. This ensures that their therapeutic efficacy is preserved while minimising their potential degradation. As a solvent, methanol might affect the stability of liposomes by changing the structure and mobility of the lipid bilayer. This uncertainty arises because the behaviour of liposomes in methanol has not been as extensively studied, leaving gaps in our understanding of how this solvent influences their stability compared to water or cell culture medium. Consequently, further research is needed to fully elucidate the implications of using methanol on liposomal formulations.

4.5 Rhodamine B Dye Encapsulation

Rhodamine B dye encapsulated into the liposomes using a microfluidic system. This process allows for the precise control of liposome formation. The functionalised liposomes were characterised by DLS, SEM, and fluorescence microscopy. While the use of a microfluidic system enhances the similarity and size distribution of the resulting liposomes according to the DLS data, the size of encapsulated liposomes did not have a significant change, the polydispersity index (P.I.) rose to 0.154, and the diffusion coefficient also increased to 2.807 x 10^{-7}. (See Figure 4.6.)

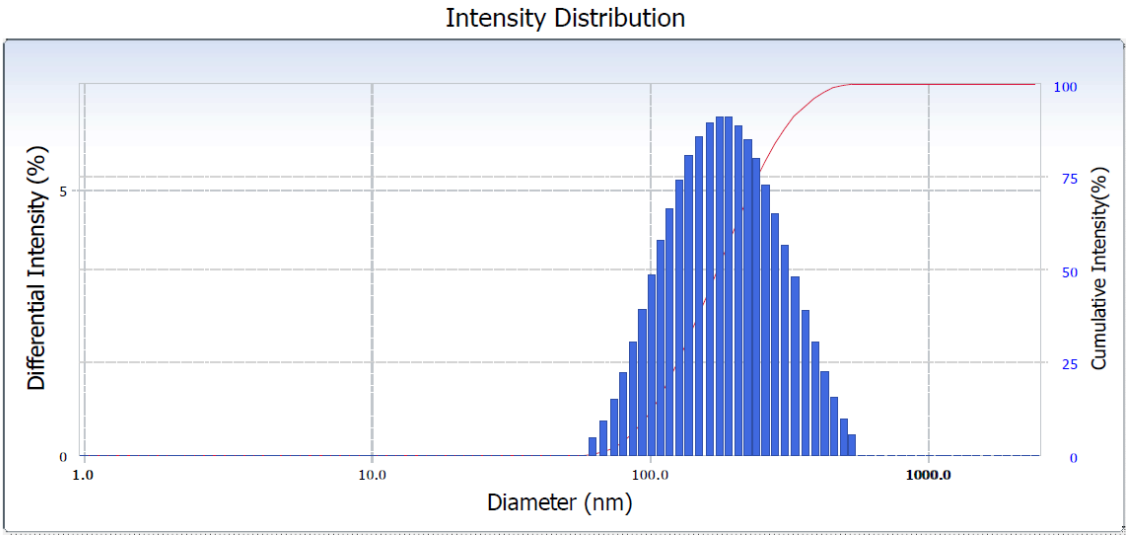

Figure 4.6: Demonstrates the intensity-weighted distribution of the rhodamine B dye encapsulated into liposomes by DLS.

The encapsulated liposomes were characterised by SEM; their size was also checked. (See Figure 4.7.) While for SEM the sample must be dry and by this process the liposomes shrink, which is why their size became smaller.

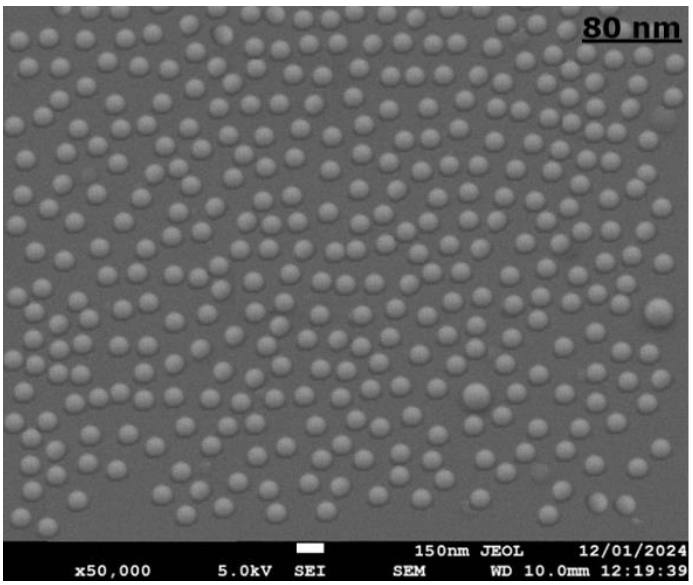

Figure 4.7: Illustrates *via* SEM that rhodamine B dye was encapsulated in liposomes that were produced in a microfluidic system.

Fluorescence microscopy characterised the functionalised liposomes under two conditions. The first condition involved encapsulating rhodamine B dye into liposomes and checking their brightness. Fluorescent microscopy showed that the rhodamine B dye can move freely in and out of the liposomes because it was spread randomly (see Figure 4.8). The second step involved making liposomes with rhodamine B dye. However, the solvent changed from methanol to phosphate buffer saline (PBS) because methanol is harmful to endothelial cells (hCMEC/D3). After encapsulating rhodamine B dye within the liposome and using the PBS solution, it was then applied to the cells. See Figure 4.9. The results confirmed the movement of rhodamine B dye by observing its clear movement towards the low concentration.

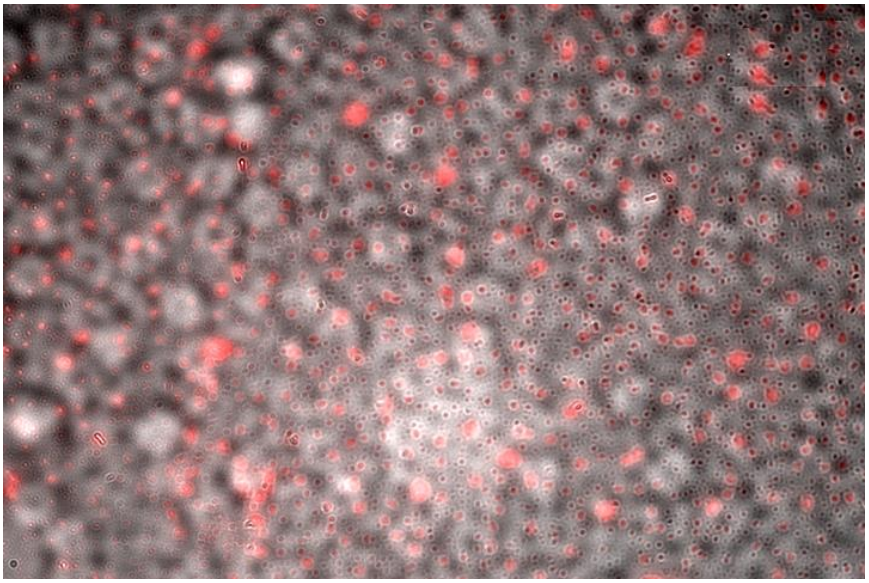

Figure 4.8: Illustrates the distribution of rhodamine B dye everywhere where liposomes after purification by size exclusion chromatography.

The results of both experiments clearly showed that the rhodamine B dye could move freely. This shows that the dye can move freely through the liposomal structure, meaning it can easily pass through both the liposome and cell membranes. This shows the dye's ability to penetrate the liposomal layer (see Figure 4.8). The findings in this study also

demonstrated that rhodamine B can move through the cellular environment (human BBB endothelial cells). The restricted entry of the dye into the nucleus is probably due to its molecular size, charge, and the way the nuclear membrane allows certain substances to pass through. (See Figure 4.9.)

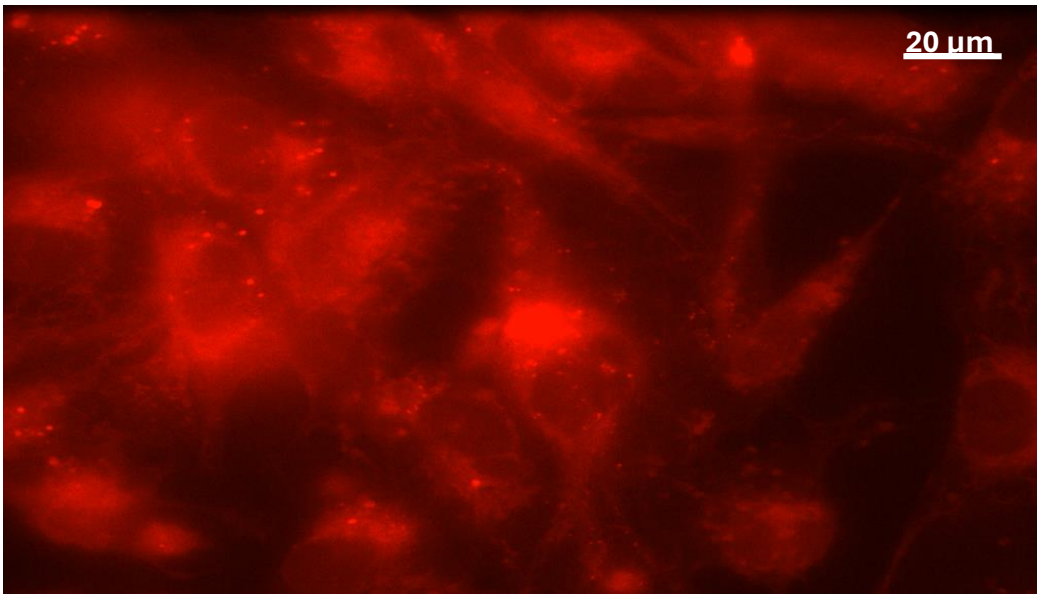

Figure 4.9: Shows the mobility of rhodamine B dye after purification by size exclusion chromatography, and was applied to the human blood-brain barrier endothelial cells.

The zwitterionic composition of rhodamine B dye aids this movement by promoting its solubility and diffusion in aquatic conditions [218] (See Figure 4.10.) This characteristic enables interaction with both hydrophilic and hydrophobic domains inside liposomes and cells. Molecular dynamics models show that rhodamine B can diffuse in different polyelectrolyte solutions. This shows that it can move through complex environments.[219] For these reasons, we were unable to encapsulate the rhodamine B dye in the aqueous core of the liposome instead of the drug, which would have allowed it to penetrate the human blood-brain barrier endothelial cells.

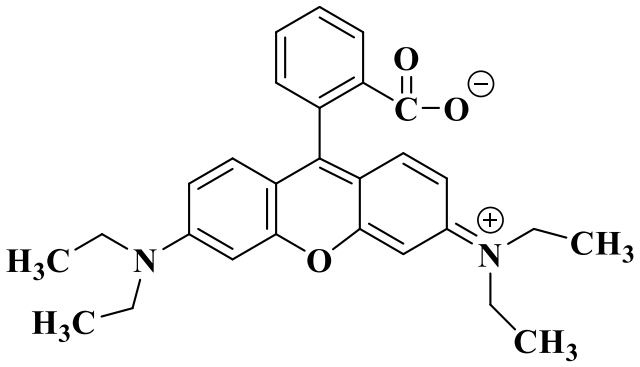

Picture 4.10: Illustrates the chemical structure of Rhodamine B dye, showing its zwitterionic characteristics, which include both positive and negative charges within a single molecule.

4.6 Vectors embedded by CPP conjugated fatty acid

The cationic cell-penetrating peptides (CPPs) coupled with fatty acid ($CH_3(CH_2)_{14}CORRK$) and the ionic tripeptide coupled with fatty acid ($CH_3(CH_2)_{14}CODDK$) were embedded into liposomes using a microfluidic system. The produced liposomes, containing both peptide-conjugated fatty acids, were characterised using dynamic light scattering (DLS) and scanning electron microscopy (SEM). These analyses were performed to ensure the liposomes were suitable for subsequent applications to endothelial cells, with the aim of studying their drug penetration ability.

The cationic tripeptide-conjugated fatty acid ($CH_3(CH_2)_{14}CORRK$) and ionic tripeptide-conjugated fatty acid ($CH_3(CH_2)_{14}CODDK$) were embedded into the liposomes separately using a microfluidic system. The liposomes were composed of L-alpha-phosphatidylcholine and cholesterol, with 2.5 mg/mL of both conjugated tripeptides and fatty acids.

The DLS results for liposomes embedded with cationic tripeptide and palmitic acid showed that the size of the embedded liposomes

increased slightly from 97.9 nm to 106.1 nm compared to unfunctionalised liposomes. (See Figure 4.11) This increase in size suggests that the incorporation of cationic tripeptides and palmitic acid alters the liposome structure, potentially enhancing their stability or functionality. The polydispersity index and diffusion coefficient of the functionalised liposomes also increased from 0.09 and 1.51 × 10^{-8} cm^2/sec to 0.106 and 2.827 × 10^{-8} cm^2/sec, respectively, compared to the unfunctionalised liposomes. SEM also confirmed that the functionalised liposome size increased slightly. (See Figure 4.12)

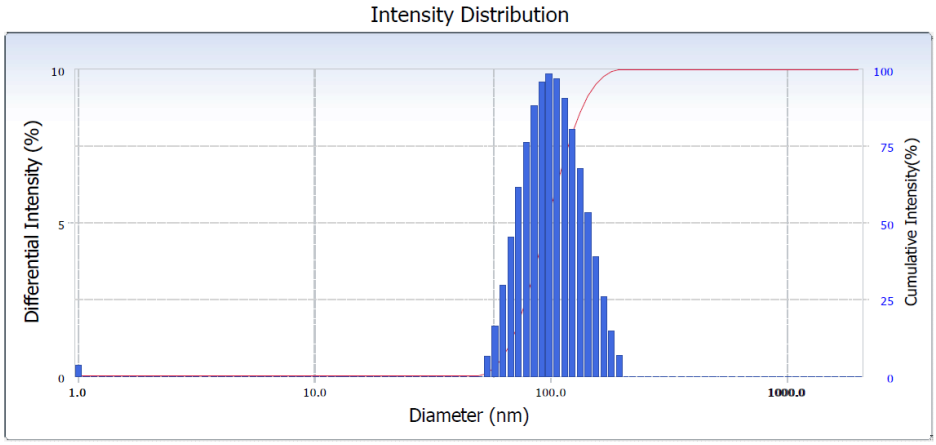

Figure 4.11: Demonstrates the intensity-weighted distribution of the cationic CPP conjugated fatty acid ($CH_3(CH_2)_{14}$CORRK) encapsulated into liposomes by DLS.

For embedding the ionic tripeptide-conjugated fatty acid ($CH_3(CH_2)_{14}$CODDK), the same process was used. The functionalised liposomes were characterised by DLS and SEM. The DLS results demonstrated that the size of the functionalised liposomes increased slightly compared to the unfunctionalised liposomes, changing from 97.9 nm to 113.0 nm. The polydispersity index and diffusion coefficient of the functionalised liposomes also increased slightly, from 0.09 and 1.51 × 10^{-8} cm^2/sec to 0.19 and 4.44 × 10^{-8} cm^2/sec, respectively (see Figure 4.15).

These similarities indicate that while functionalisation has led to some changes in size and properties, the overall characteristics of the liposomes remain comparable. This suggests that the cationic and ionic tripeptides attached to the fatty acids did not significantly alter the basic structure of the liposomes. The results showed that both types of tripeptide-linked fatty acids can be effectively applied to an artificial blood-brain barrier (BBB) model (growing endothelial cells on a PAN–Jeffamine electro spun nanofiber as a 3D scaffold).

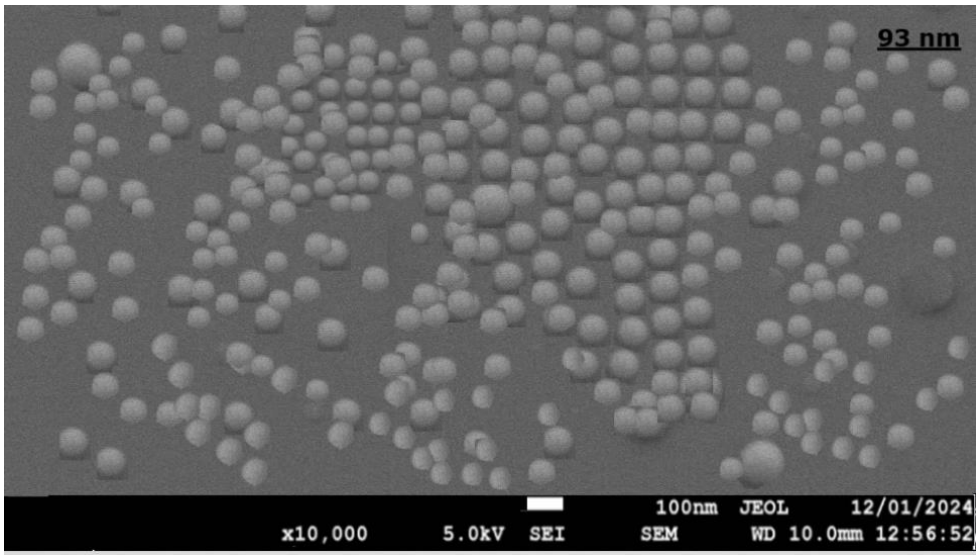

Figure 3.12: Illustrates *via* SEM that embedded liposomes by $CH_3(CH_2)_{14}CORRK$ were produced in a microfluidic system. The diameter of the generated functionalised vectors was (*ca.* 100 nm).

For embedding the ionic tripeptide conjugated fatty acid ($CH_3(CH_2)_{14}CODDK$), the same process was used to embed it within the liposomes. The functionalised liposomes by ionic tripeptide-conjugated fatty acid were characterised by DLS and SEM. The DLS results demonstrated that the size of the functionalised liposome increased slightly compared to the unfunctionalised liposomes, changing from 97.9 nm to 113.0 nm. Also, the polydispersity and diffusion constant of the functionalised liposomes were only slightly

greater than unfunctionalised liposomes (0.09 and 1.51 × 10^{-8} cm^2/sec to 0.11 and 2.52 × 10^{-8} cm^2/sec, respectively). (See Figure 4.13). SEM also showed that the size of the embedded liposomes by ionic peptide-conjugated fatty acid was marginally increased (*ca.* 100 nm). (See Figure 4.14.)

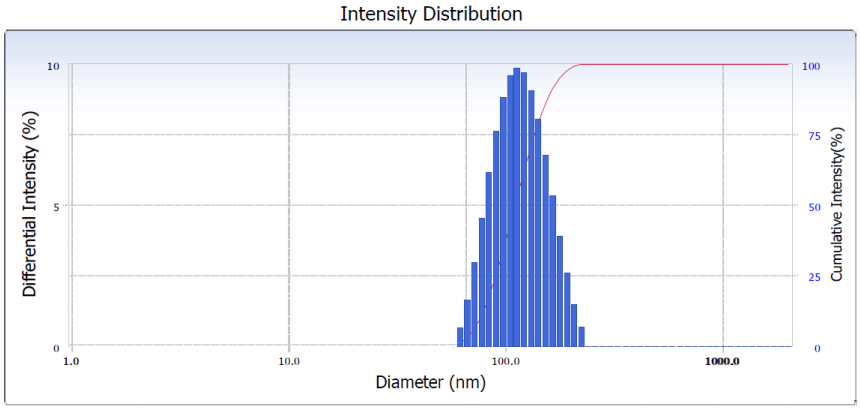

Figure 4.13: Demonstrates the intensity-weighted distribution of the ionic tripeptide conjugated fatty acid ($CH_3(CH_2)_{14}CODDK$) encapsulated into liposomes by DLS.

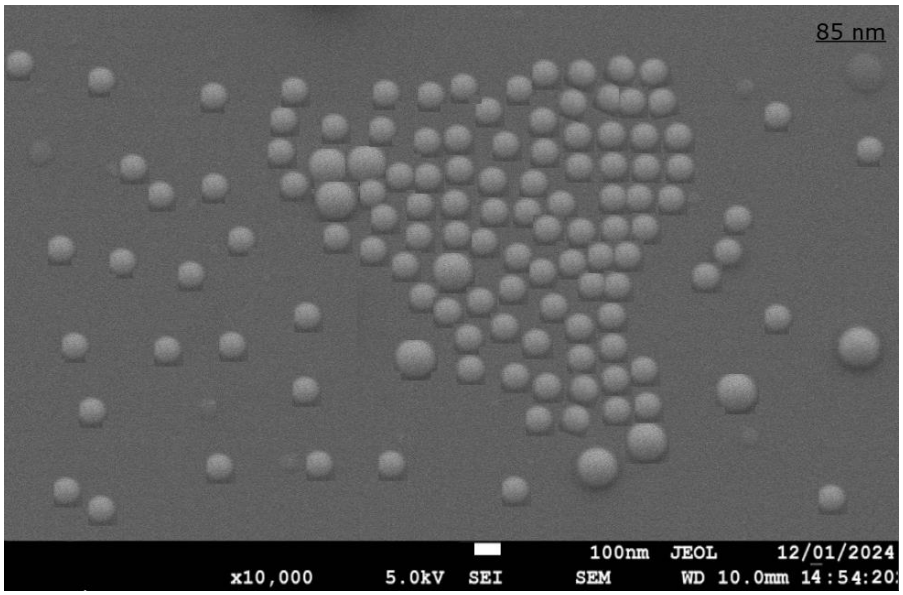

Figure 4.14: Illustrates *via* SEM that embedded liposomes by $CH_3(CH_2)_{14}CODDKD$ were produced in a microfluidic chip system. The diameter of the generated functionalised vectors (*ca.* 100 nm.)

These similarities indicate that while the functionalisation has led to some changes in size and properties, the overall characteristics of the liposomes remain comparable. This means that the cationic and ionic tripeptides that were attached to the fatty acids did not significantly change the liposomes' basic structure. The results showed that both types of tripeptide-linked fatty acids can be effectively applied to an artificial blood-brain barrier (BBB) model (growing endothelial cells on a PAN–Jeffamine electrospun nanofiber as a 3D scaffold). In order to penetrate the drug after encapsulation in liposomes and embed them within tripeptides conjugated to fatty acids.

Recently, studies have similarly explored the functionalisation of liposomes with CPPs and fatty acids to enhance their stability and drug delivery capabilities. For example, Bangera *et al.* looked at how polymer-lipid hybrid nanoparticles (PLHNs) modified with CPPs could be used to deliver drugs more precisely, showing better uptake by cells and better therapeutic effectiveness.[220] This aligns with the findings of the current study, which also observed enhanced stability and functionality of liposomes upon conjugation with CPPs and fatty acids. Additionally, research by Ouyang *et al.* reviewed the progress of molecular dynamics simulations of CPP-membrane interactions, emphasising the importance of peptide-lipid interactions in enhancing CPP-mediated delivery.[221] This study's findings on the increased size and altered properties of functionalised liposomes are consistent with these observations, suggesting that peptide–lipid interactions play a crucial role in modulating liposome characteristics.

In conclusion, functionalising liposomes with cationic and ionic tripeptide-conjugated fatty acids enhances their stability and penetration ability, consistent with recent literature on CPP-based drug delivery systems. These findings contribute to a growing body of research on liposome functionalisation for improved therapeutic applications.

4.7 Fluorophores-peptide-fatty acid embedded liposomes

The FITC-peptide (ERK)-palmitic acid and the dansyl chloride-triple arginine-palmitic acid conjugates were both attached to fatty acids and encapsulated into liposomes using a Dolomite microfluidic system. The resulting liposomes, containing both fluorophore and peptide-conjugated fatty acids, were characterised using dynamic light scattering (DLS), scanning electron microscopy (SEM), and fluorescence microscopy at 100x magnification. These characterisations were performed to ensure the liposomes were suitable for subsequent applications to endothelial cells, with the aim of studying their movement during drug penetration.

The fluorophores-CPP-fatty acids ($CH_3(CH_2)_{14}$CORRR-Dansyl chloride and $CH_3(CH_2)_{14}$COERK-FITC) were embedded into the liposomes separately using a microfluidic system and its chip (Dolomite droplet junction chip, 100 µm etch depth, hydrophobic). The flow rate for the lipid and fatty acids-tripeptides-fluorophores solutions was 11.618 µL/min, and the flow rate for the water solution was 24.93 µL/min. The liposomes were made up of 70% L-alpha-phosphatidylcholine and 30% cholesterol. There were 2.5 mg/mL of both fluorophores coupled with CPP-fatty acids. DLS, SEM, and fluorescence microscopy have characterised the size and brightness of embedded liposomes. The DLS result for embedded liposomes by dansyl chloride triple arginine coupled with palmitic acid confirmed that the size of the embedded liposomes was slightly increased from 97.9 nm to 117.1 nm compared to unfunctionalized liposomes. The polydispersity index and diffusion constant of the functionalised liposomes also, increased from 0.09 and 1.505×10^{-8} cm²/sec to 0.107 and 4.442×10^{-8} cm²/sec, respectively, compared to the unfunctionalized liposomes. SEM, also, confirmed that the functionalised liposome size increased slightly. (See Figures 4.15 and 4.16.) The fluorescence microscopy confirmed that dansyl chloride coupled with triple arginine peptide conjugated palmitic acid has a clear brightness and can be used to track and visualise them when applied

to the artificial BBB (growing endothelial cells on ZO-1 electrospinning nanofiber 3D scaffold) while its brightness slightly less than FITC. (See Figures 4.17 and 4.20.)

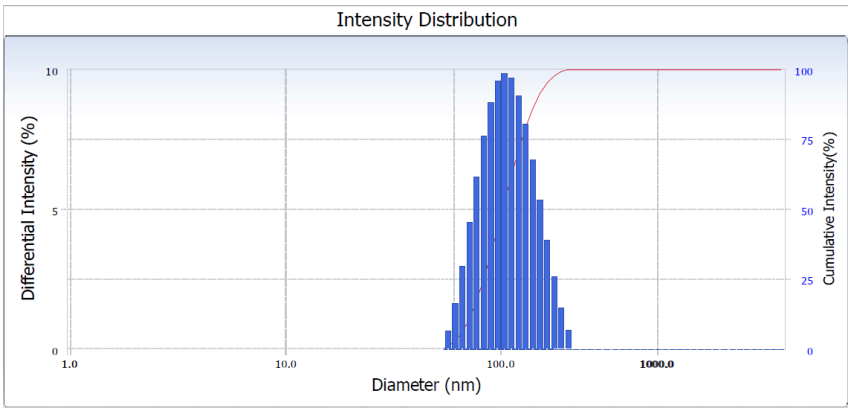

Figure 4.15: Demonstrates the intensity-weighted distribution of the cationic CPP conjugated fatty acid ($CH_3(CH_2)_{14}$CORRR-Dansyl chloride) encapsulated into liposomes by DLS.

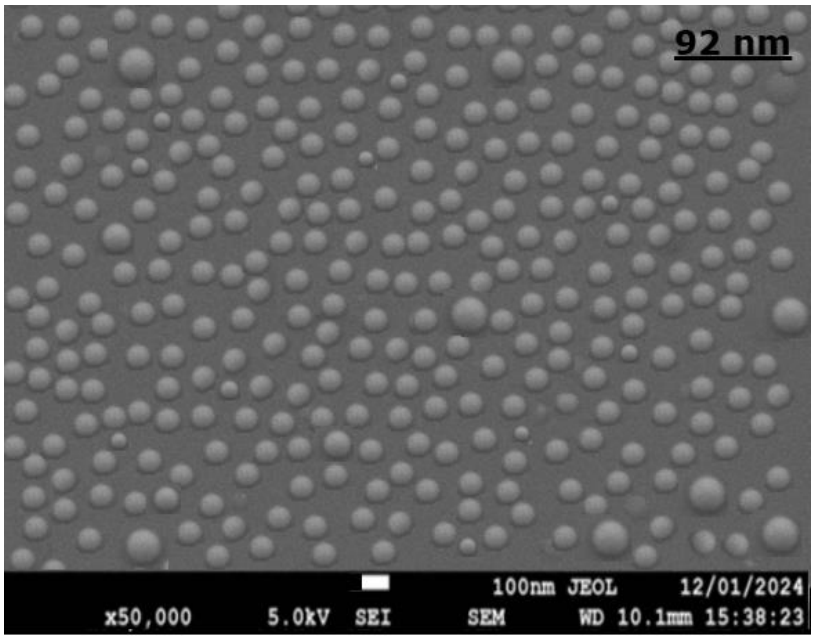

Figure 4.16: Illustrates *via* SEM that embedded liposomes by $CH_3(CH_2)_{14}$CORRR-Dansyl chloride were produced in a microfluidic system. The diameter of the generated functionalised vectors *ca.* 100 nm.

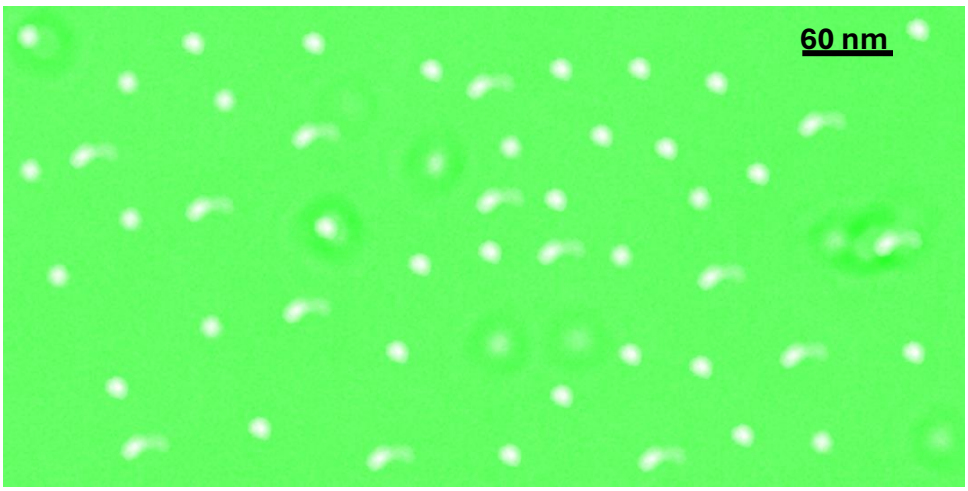

Figure 4.17: Illustrates the brightness of the dansyl chloride after coupling with the triple arginine peptide-palmitic acid and then embedding it in the liposomes.

The DLS results for embedding liposomes by $CH_3(CH_2)_{14}$COERK-FITC also showed that the size of the embedded liposomes was 113.4 nm bigger than functionalized liposomes. The polydispersity and diffusion constant also increased and changed to 0.104, 4.338×10^{-8} cm^2/sec, respectively. (See Figure 4.18.)

The SEM results showed that produced embedded liposomes by $CH_3(CH_2)_{14}$COERK-FITC measuring 100 nm in size. (See Figure 4.19). Fluorescence microscopy showed a clear brightness when coupled dansyl chloride with triple arginine peptide conjugated palmitic acid, and confirmed that the embedded liposomes by FITC coupled to cationic cell-penetrating peptides were properly embedded in the liposomes. The data also clearly demonstrate that the FITC fluorophore exhibits superior brightness compared to dansyl chloride. This is attributed to the higher maximum excitation level of FITC, resulting in a more pronounced fluorescence signal in our microscopy analysis. (See Figure 4.20.)

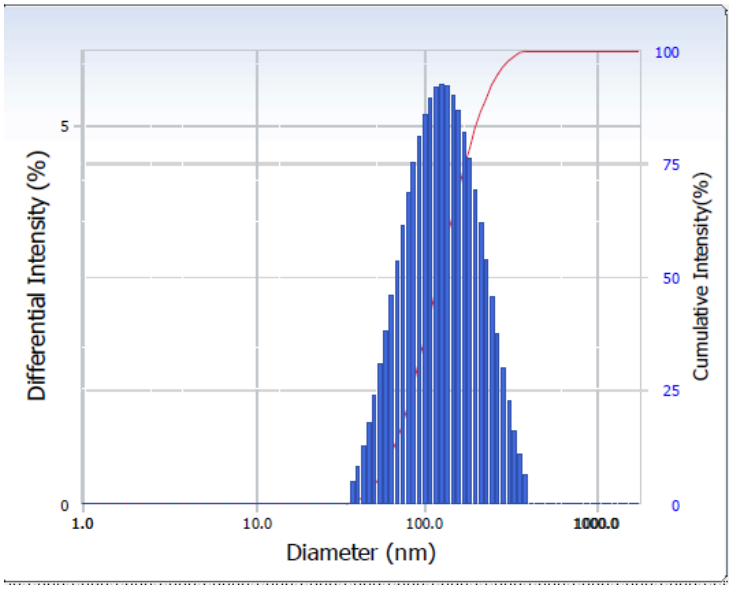

Figure 4.18: Demonstrates the intensity-weighted distribution of the cationic CPP conjugated fatty acid $CH_3(CH_2)_{14}$CORRR-FITC encapsulated into liposomes by DLS.

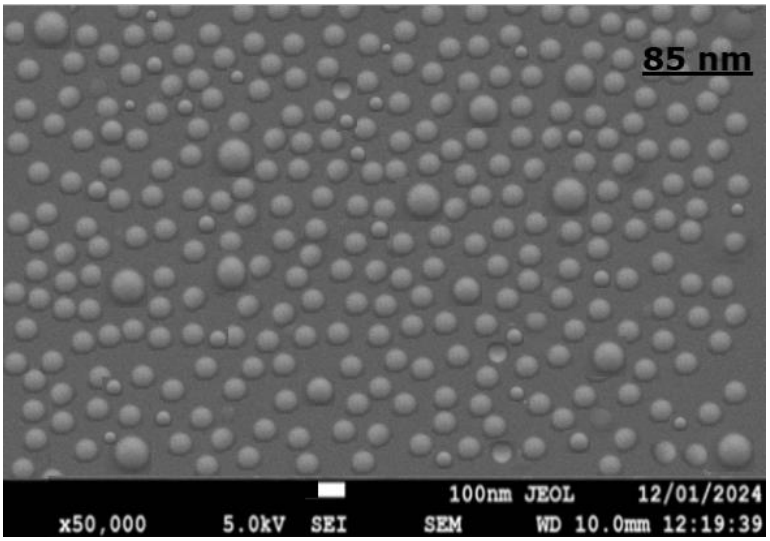

Figure 4.19: Illustrates *via* SEM that embedded liposomes by $CH_3(CH_2)_{14}$COERK-FITC were produced in a microfluidic system. The diameter of the generated functionalised vectors *ca.* 100 nm.

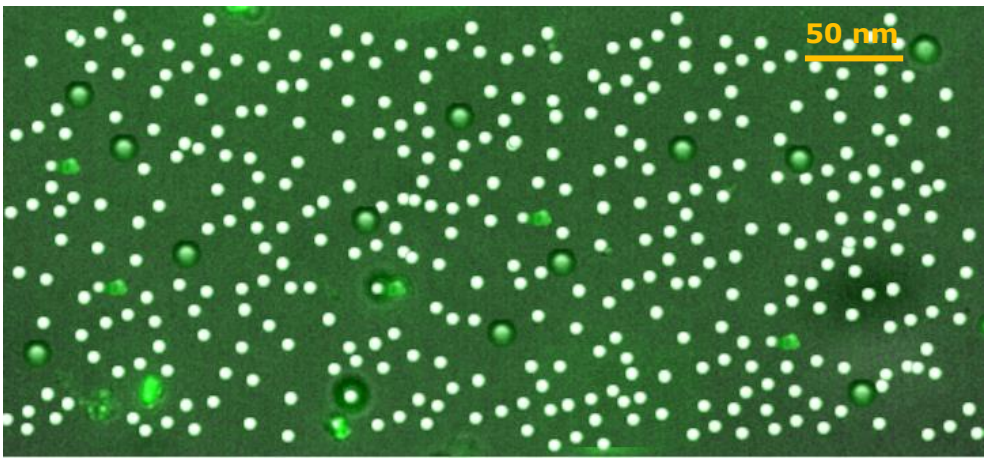

Figure 4.20: Illustrates the fluorescence intensity of the FITC fluorophore following its conjugation with a tri-peptide-fatty acid complex, specifically glutamic acid, arginine, and lysine-palmitic acid ($CH_3(CH_2)_{14}COERK$), and subsequent embedding into liposomes.

The fluorophore-CPP-fatty acid embedded into the liposomes before being characterised had been purified by using size exclusion chromatography (SEC) using Sephadex G-50 as a stationary phase. The size exclusion chromatography (SEC) is a method that differentiates molecules according to their sizes, which is especially advantageous for isolating fluorophore-CPP-fatty acid complexes embedded into liposomes from unembedded molecules and contaminants. The process depends on the varying capacity of molecules to enter the pores of the stationary phase, which consists of porous beads (Sephadex G-50). Smaller contaminants penetrate the pores and elute later, while larger molecules like the fluorophore-CPP-fatty acid complexes embedded into liposomes, excluded from entering the pores and therefore elute quicker. Size-based separation happens without chemical contact between the solutes and the stationary phase. This makes SEC a gentle method that maintains the integrity of the complexes.

The study successfully demonstrated the encapsulation of FITC-peptide (ERK)-palmitic acid and dansyl chloride-triple arginine-palmitic acid

conjugates into liposomes using a Dolomite microfluidic system. Characterisation of the resulting liposomes using dynamic light scattering (DLS), scanning electron microscopy (SEM), and fluorescence microscopy confirmed their suitability for application to endothelial cells. The DLS results indicated a slight increase in the size of functionalised liposomes compared to unfunctionalised ones, with corresponding increases in the polydispersity index and diffusion constant. SEM analysis corroborated the size increase, while fluorescence microscopy demonstrated the clear brightness of the fluorophores, with FITC exhibiting superior brightness compared to dansyl chloride. These findings suggest that the functionalised liposomes are effective carriers for drug delivery across biological barriers, such as the blood-brain barrier (BBB).

Recent research has similarly highlighted the potential of liposome-based delivery systems for enhancing drug delivery efficacy. For instance, studies have shown that the incorporation of fluorophores and peptides into liposomes can significantly improve their stability and permeability, aligning with the findings of this study.[222] Also, improvements in liposomal nanotechnology have made it possible to create targeted and stimuli-responsive liposomes, which make drug delivery even more precise and effective.[223] These advancements underscore the importance of continued innovation in the design and application of liposome-based delivery systems for overcoming biological barriers and improving therapeutic outcomes.

In conclusion, the encapsulation of fluorophore-CPP-fatty acid conjugates into liposomes using microfluidic systems represents a promising approach for enhancing drug delivery across the BBB. The findings of this study are consistent with recent literature, highlighting the potential of liposome-based systems to improve the stability, permeability, and overall efficacy of therapeutic agents.

4.8 Conclusion

For liposome production using the microfluidic system, the L-α-phosphatidylcholine was solubilised in methanol. A second solution was created by dissolving cholesterol in methanol. After mixing the first and second solutions, they were transferred to Pump A, which is linked to the central conduit of the microfluidic chip (droplet junction chip, 100 µm etch depth, hydrophobic). At the same time, Pump B was primed with distilled water and served to cut the liposome to size. The flow rate was optimised to produce the necessary liposome sizes. This careful optimisation of flow rates ensures that the liposomes formed are similar in size, which is crucial for their intended applications in drug delivery and other biomedical uses. Controlling the mixing and cutting processes is a precise achievement of liposome characteristics tailored to specific needs. In order to find the best flow rate, the size of the liposomes that were made was measured at many different flow rates.

It was found that using 11.6 µL/min (pressure: 2 bar) for the lipid pump and 24.9 µL/min (2.6 bar) for the aqueous solution pump made liposomes that were about 100 nm in size, with a low polydispersity index (0.09) and low diffusion coefficient (1.504×10^{-8} cm^2/sec). This was achieved by dynamic light scattering (DLS), also scanning electron microscopy (SEM) confirms the morphology (size and spherical shape) of the produced liposomes (100 nm). The nanosizer (ZetaView) illustrated that the median of the produced liposomes was 95.9 nm, and their concentration was $3.6x10^{15}$ particles/mL, and their net charge was 97.9% neutral. Therefore, this specific flow rate combination was crucial in optimising the liposome size, demonstrating the importance of precise control in the formulation process. These characterisation techniques allowed for a comprehensive assessment of the liposomes' size, shape, and stability, ensuring they met the intended specifications for their application. Ultimately, this thorough analysis confirms the success of the formulation process in producing high-quality liposomes.

This is excellent for stability and compatibility in a wide range of applications. The measurements showed that the vectors that were made are about the same size and ready to be used as innovative vector for drug delivery.

Chapter 5: *In Vitro* Cell Culture Study

5.1 Summary

This chapter outlines the results from the use of embedded liposomes, including cell-penetrating peptide (CPP)-fatty acid conjugates, on the model blood-brain barrier (BBB) human endothelial cells. It also evaluates the toxicity and penetration capacity of CPP-fatty acids, specifically palmitic acid, myristic acid, and lauric acid, using MTT tests and live cell image analysis (Incucyte) at various concentrations (3.6 x 10^2, 3.6 x 10^3, 3.6x10^4, 3.6 x10^5 particles/mL). The toxicity of the CPP-fatty acid conjugates was measured using the MTT test. Different concentrations of the conjugates were tested to evaluate their cytotoxic effects on human blood-brain barrier endothelial cells (same concentration used for live cell image analysis). The results indicated that CPP fatty acids (palmitic acid, myristic acid, and lauric acid) were non-toxic at all tested concentrations.

The cell viability was above 95%, indicating the safety of these conjugates for blood-brain barrier applications. The Incucyte machinery was used to observe the real-time effects of CPP-fatty acid conjugates on human blood-brain barrier endothelial cells. The investigation confirmed the conjugates' non-toxic characteristics by observing no significant changes in cell shape or growth over the 48-hour experimental duration. The cells maintained their integrity and functioned properly, hence confirming the safety of the CPP-fatty acid conjugates. Furthermore, the penetration ability of the CPP-fatty acid conjugates was determined by applying different concentrations of vectors embedded by cationic peptide fatty acids and encapsulated by L-carnosine as a drug to cross the blood-brain barrier model. The results showed that the conjugates were able to penetrate the model BBB endothelial cells and be taken up by those cells in a big way and

could penetrate the encapsulated drug. The liposomal delivery system made this possible by making the CPP-fatty acids more bioavailable.

The findings of this study show that liposomes embedded by CPP-fatty acid conjugates have a lot of potential as reliable and innovative vectors for drug delivery involving the blood-brain barrier. MTT tests showed that the conjugates are not toxic, which means they could be used to improve drug delivery systems for the brain in the future. The liposomal embedding method works well to improve the transport of therapeutic drugs to the brain for treating Alzheimer's disease because it can fuse through the artificial blood-brain barrier and transport carnosine.

5.2 Overview of drug delivery to the brain

The main problem in neurological research is getting medicines across the blood-brain barrier (BBB). This is because the BBB protects the central nervous system (CNS) but makes it hard to get medicines into the CNS. The blood-brain barrier is a selective permeability barrier that allows only certain substances to pass while blocking others, which complicates the delivery of therapeutic agents. Consequently, developing effective treatments for neurological conditions becomes challenging, researchers must find innovative ways to cross this barrier. Researchers are looking into several techniques to optimise medication delivery to the brain with the objective of enhancing treatment results for central nervous system illnesses. These solutions include both invasive and non-invasive techniques, using improvements in nanotechnology, biological treatments, and innovative delivery systems. The following paragraph clarifies these methodologies and the models used for evaluation.

Nanotechnology: Nanoparticles, liposomes, and dendrimers are used to encapsulate drugs, hence improving their translocation across the blood-brain barrier. These technologies enhance drug stability and

targeting efficacy, providing positive results in preclinical research. These systems can encapsulate therapeutic drugs, protecting them from degradation and improving their movement across the blood-brain barrier.

5.3 Toxicity assessment

The toxicity of the produced vectors was assessed by using different methods. In these methods, different concentrations of vectors were used on human BBB endothelial cells in a lab to see if they could harm the cells. The results from these assessments provide crucial insights into the safety and suitability of the vectors for drug delivery applications. These insights are essential for determining whether the vectors can be safely used in medical treatments, particularly in targeting the blood-brain barrier. Understanding their toxicity levels allows for the optimisation of vector formulations for both effective and safe drug delivery.

5.3.1 MTT assay

This study successfully generated vectors (liposomes) containing cell-penetrating peptides (CPPs) conjugated with fatty acids (lauric acid, myristic acid, and palmitic acid) and subsequently embedded them in liposomes as detailed in the previous chapter. This approach enhances the delivery of CPPs, improving their ability to penetrate cell membranes. By utilising fatty acids, the study optimises the stability and efficacy of the liposomal vectors embedded by cell penetrating triple peptide that contained two molecules of arginine and a lysine conjugated palmitic acid, lauric acid and myristic acid differently. Four different concentrations ($3.6x10^2$, $3.6x10^3$, $3.6x10^4$, and $3.6x10^5$ particles/mL) of these embedded liposomes were prepared and applied to human blood-brain barrier endothelial cells to evaluate their toxicity using the MTT assay. On the other hand the same concentrations of

embedded liposomes by ionic tripeptide conjugated fatty acids [$CH_3(CH_2)_{10}$CODDK, $CH_3(CH_2)_{12}$CODDK, $CH_3(CH_2)_{14}$CODDK] were applied. The varying concentrations of liposomes were tested to determine their impact on cell viability, providing insights into the potential safety of these delivery systems. This evaluation is crucial for assessing the feasibility of using liposomal vectors in therapeutic applications targeting the blood-brain barrier. The results indicated that liposomes embedded with cationic CPP-conjugated fatty acids showed minimal toxicity, maintaining cell viability over 95% for the peptide, including two arginine residues, one lysine residue, and three different fatty acids: palmitic acid, myristic acid, and lauric acid. (See Figures 5.1, 5.2, and 5.3.) This finding suggests that the specific composition of the liposomal vectors enhances their biocompatibility, making them promising candidates for targeted drug delivery. By ensuring high cell viability, these vectors can potentially minimise side effects when used in treatments aimed at the central nervous system.

The improved cell viability shown in the present research conforms with previous research indicating the biocompatibility of CPPs as delivery vectors. Porosk *et al.* (2019) demonstrated that increasing fatty acid length content in CPPs significantly increased siRNA transfection efficiency while minimising cytotoxicity. [224]

Rauch *et al*. (2023) similarly found that cell-penetrating peptides (CPPs) containing positively charged amino acids, such as arginine and lysine, significantly improved nucleic acid transport into cells while maintaining high cell viability. [225]

The use of palmitic acid, myristic acid, and lauric acid as coupling agents in our study confirms the idea that fatty acids might improve the stability and efficacy of CPP-based delivery systems. Previous studies indicate that incorporating fatty acids into CPPs reduces their hydrophilic properties and increases their electrostatic interaction with cell membranes, therefore increasing bioavailability and decreasing cytotoxicity. The results of this study support these conclusions since

the CPP-conjugated fatty acids in our liposomal formulations demonstrated improved biocompatibility and minimal toxicity. These results show that using cationic CPP-conjugated fatty acids not only makes drug delivery systems work better, but they also make them safer for possible drug delivery. Consequently, these findings highlight the promising role of fatty acids in optimising CPP-based formulations.

Furthermore, the MTT assay findings demonstrated that cell viability was above 95% at all applied concentrations of embedded liposomes on the blood-brain barrier endothelial cells. This indicates that the CPP-coupled fatty acids did not cause substantial cell death, even at high doses. This is especially crucial for potential therapeutic applications, simply because it confirms the safety and effectiveness of different concentrations for delivery vectors inside a biological system.

The results of this study further support the efficacy and safety of using CPPs in combination with fatty acids as delivery systems. A research study by Bangera *et al.* (2023) highlighted the numerous advantages of using CPPs for the delivery of drugs, particularly their ability to penetrate cell membranes and deliver therapeutic compounds with less cytotoxicity. The results of this research validate previous data and further demonstrate the potential of CPP-coupled fatty acids in therapeutic applications.[220]

According to the results, multiple research studies have shown differing levels of cytotoxicity linked to CPPs, depending upon their composition and the characteristics of the conjugated molecules. Timotievich *et. al.* (2023) observed that arginine-rich peptides (RRPs) facilitated high transmission levels with little toxicity, but other cell-penetrating peptides (CPPs) displayed higher toxicity levels. This highlights the need for optimising the composition of CPPs to improve their biocompatibility and efficacy for treatment.[226]

The results of this study improved that the cationic CPPs conjugated with fatty acids represent a potential drug delivery strategy. The

improved biocompatibility and minimal toxicity shown in the liposomal formulations indicate the possibility for safe and effective therapeutic applications.

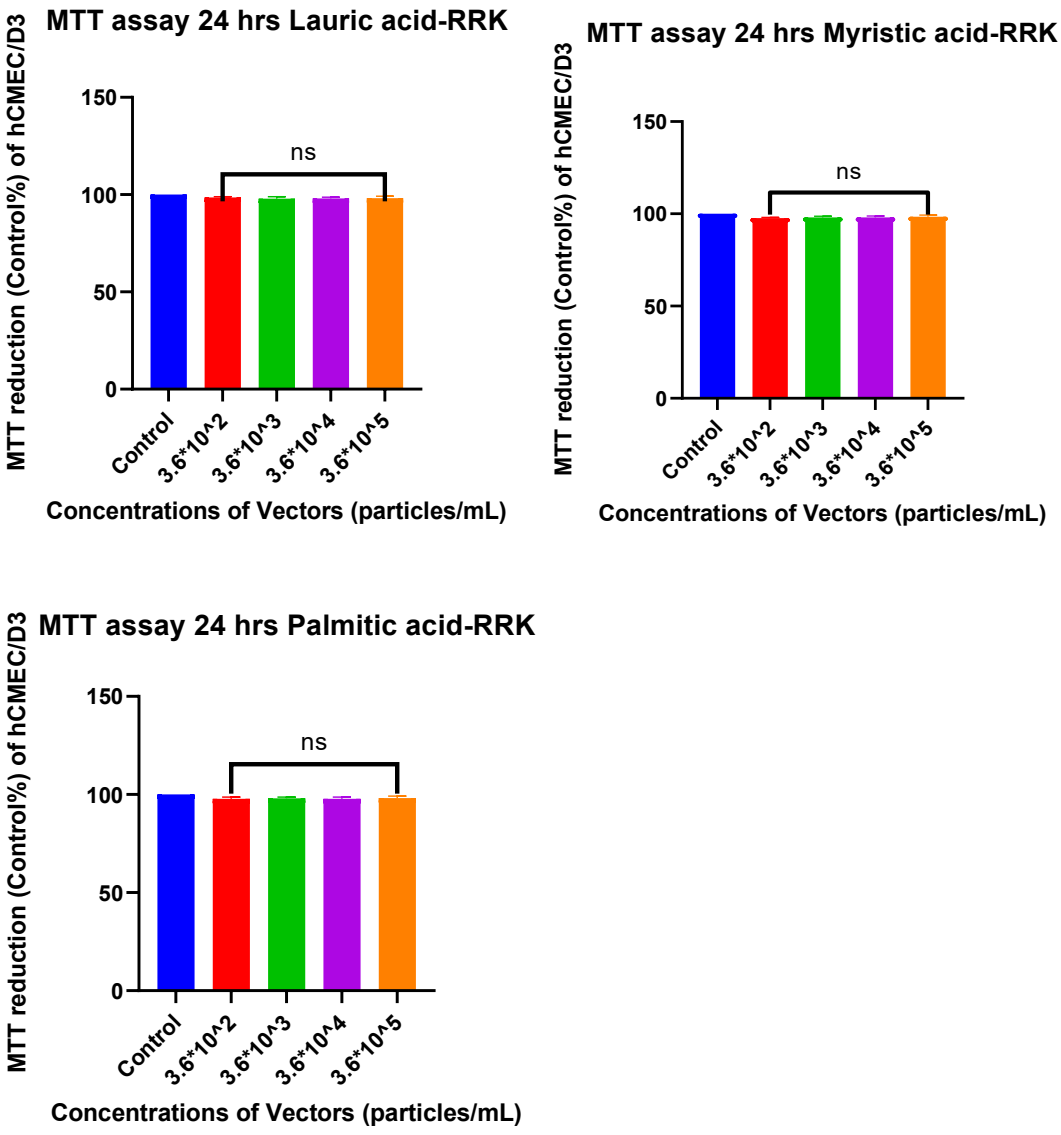

Figure 5.1: Shows that over 95% of the human blood-brain barrier endothelial cells (hCMEC/D3) were still alive 24 hours after being exposed to four different vector concentrations containing a triple peptide consisting of two arginine residues and one lysine residue, along with fatty acids (lauric acid, myristic acid, and palmitic acid).

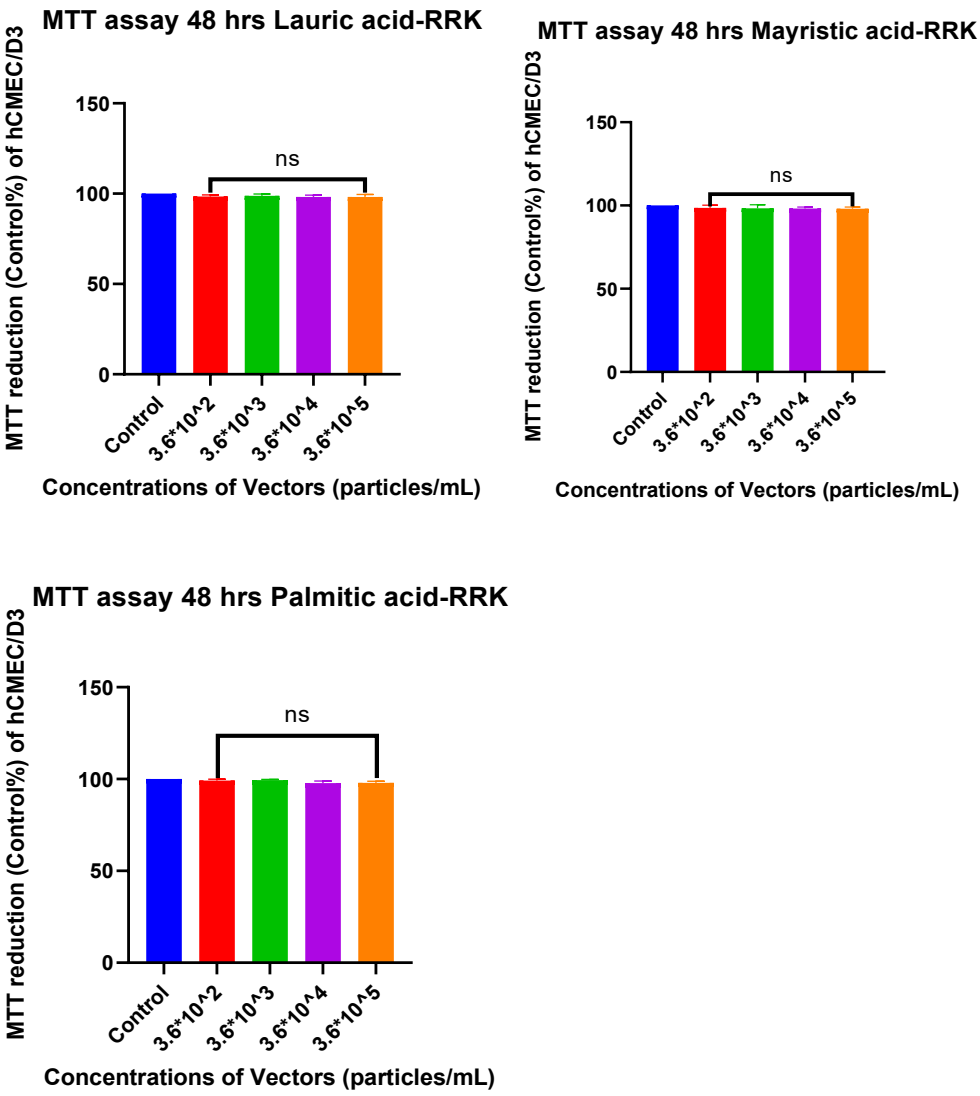

Figure 5.2: Demonstrates that more than 95% of the human blood-brain barrier endothelial cells (hCMEC/D3) were still alive 48 hours after being exposed to four different vector concentrations. The vectors were made up of a cationic triplet peptide with two arginine residues and one lysine residue, along with fatty acids such as lauric acid, myristic acid, and palmitic acid.

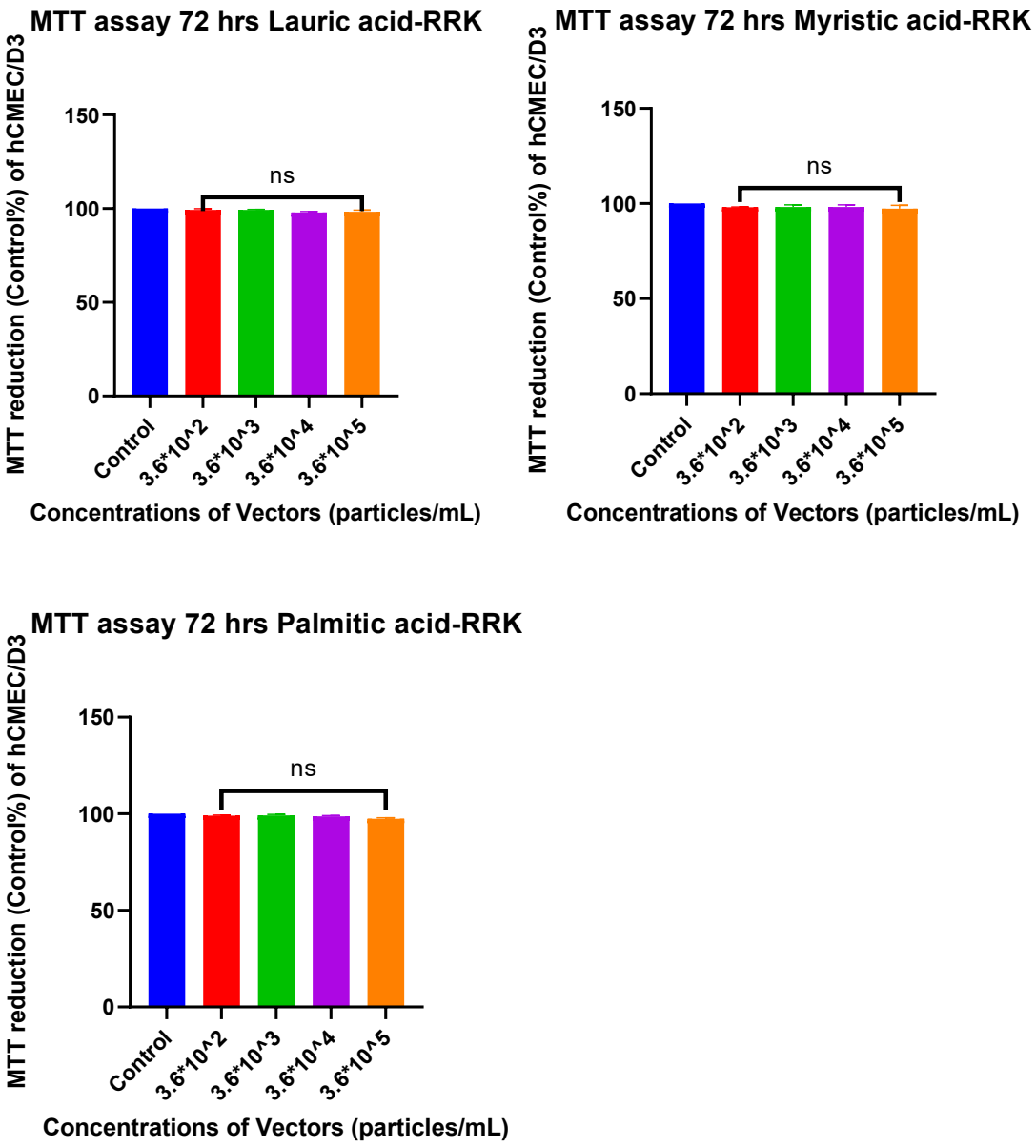

Figure 5.3: Illustrates that 72 hours after exposure to four different vector concentrations, more than 95% of the human blood-brain barrier endothelial cells (hCMEC/D3) remained alive. The vectors were embedded with a cationic triplet peptide that had two arginine residues and one lysine residue. Fatty acids such as lauric acid, myristic acid, and palmitic acid were also present.

5.4 Toxicity assessment of the ionic peptides

This study examines the cytotoxic effects of liposomes containing an ionic triple peptide consisting of two glutamic acid residues, one lysine residue, and palmitic acid on human blood-brain barrier (BBB) endothelial cells. Four different concentrations of liposomes were prepared, with 8,000 cells seeded in each well ($3.6x10^2$, $3.6x10^3$, $3.6x10^4$, and $3.6x10^5$ particles/well). The cytotoxicity was evaluated using the MTT assay.

Cell viability, assessed *via* the MTT assay, ranged from 60% to 70% after 24 hours at all concentrations, subsequently decreasing over time. After 48 hours, cell viability decreased to 40% to 50% and further declined to 20% to 30% after 72 hours, indicating moderate cytotoxicity (see Figure 5.4). The anionic peptides caused cell shrinkage, indicating their toxicity. Similar to cationic peptides, the ionic peptide was coupled with palmitic acid and embedded into liposomes.

The triple peptide possesses a net negative charge due to two glutamic acid residues, although the lysine residue partially decreased this charge. The cell membrane also carries a negative charge, leading to repulsion between the endothelial cells and the anionic triple peptide.

This study highlights the potential limitations of using negatively charged amino acids like glutamic acid in peptides. The observed moderate cytotoxicity indicates that interactions between a negatively charged peptide and the cell membrane may be less favourable than those involving positively charged peptides. This finding validates previous research indicating that the charge and hydrophobicity of cell-penetrating peptides (CPPs) are crucial for their interactions with cells.

In comparison, other researchers have investigated the application of liposomes for drug delivery across the blood-brain barrier (BBB). Studies demonstrate that liposomes can enhance the transport of therapeutic agents across the blood-brain barrier by targeting specific

receptors on endothelial cells, thereby increasing efficacy and reducing toxicity. [227]

Liposomal formulations have demonstrated the ability to circumvent active transporters at the blood-brain barrier, leading to substantial modifications in drug delivery mechanisms. [228] The cytotoxicity demonstrated in this study highlights the necessity of optimising the composition of CPPs to improve their biocompatibility and effectiveness.

The results indicate that liposomes are an efficient method for drug delivery across the blood-brain barrier; however, the specific composition of the encapsulated peptides is crucial for assessing their efficacy and cytotoxicity. Additional research is required to enhance these formulations for optimal therapeutic efficacy.

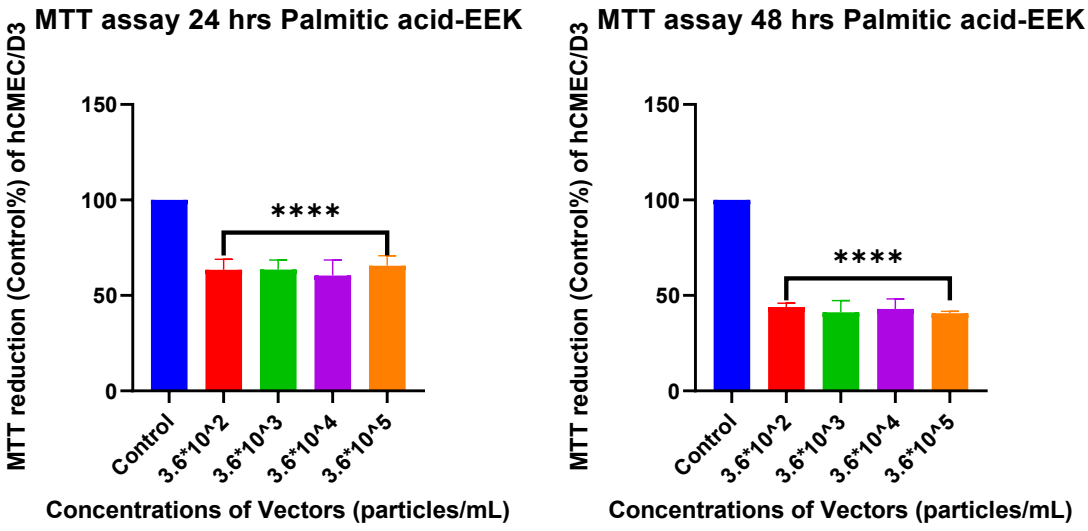

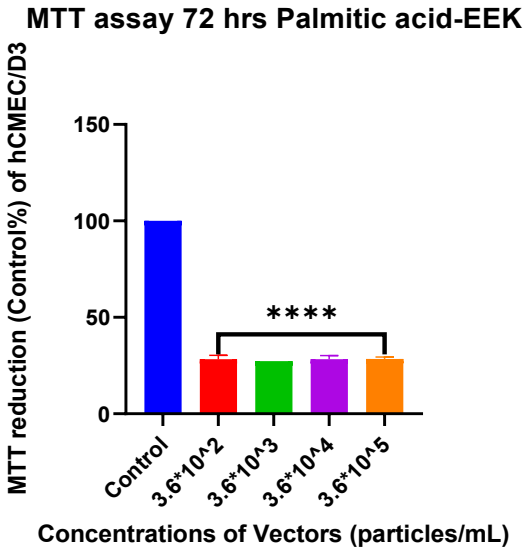

Figure 5.4: Illustrates the cytotoxicity of various liposome concentrations on the human blood-brain barrier endothelial cells (hCMEC/D3), embedded with ionic triple peptides consisting of two glutamic acid residues and one lysine residue, and coupled with fatty acids at different times: 24, 48, and 72 hours. It is evident that the cells' viability declined as the duration of exposure increased. This is because the net charge of the peptide was negative, and the cell membrane has a negative charge too; therefore, repulsion happened, and as a result, the cells died.

5.5 Applying vector to the BBB model

This study successfully produced vectors containing cell-penetrating peptides linked to fatty acids, embedded within liposomes. The primary objective was to evaluate the cytotoxicity of these functionalised liposomes (embedded tripeptide-fatty acids within the liposome) using the MTT assay on human endothelial cells. The results indicated that the vectors functionalised with cationic cell-penetrating tripeptides were biocompatible, as cell viability remained above 95%.

Following the confirmation of biocompatibility, different concentrations ($3.6x10^2$, $3.6x10^3$, $3.6x10^4$ particles/mL) of the functionalised vectors were prepared and embedded within liposomes. Two types of tripeptides conjugated to fatty acids were used: three cationic tripeptides conjugated fatty acids, $CH_3(CH_2)_{10}CORRK$ (lauric acid), $CH_3(CH_2)_{12}CORRK$ (myristic acid), and $CH_3(CH_2)_{14}CORRK$ (palmitic acid), and ionic tripeptides conjugated to palmitic acid ($CH_3(CH_2)_{14}CODDK$). L-carnosine (2.5 mg/mL) was encapsulated in the same liposomes embedded with these different tripeptides conjugated to fatty acids.

The fully functionalised vectors were applied to a modulated monolayer of BBB endothelial cells (hCMEC/D3) grown on an electrospinning nanofiber scaffold. The penetration of the encapsulated drug was monitored over 6 hours, related to the stability of the produced vectors was 7 hours, as mentioned in Chapter 3. Every hour, the eluent (250 µL) was replaced with fresh media, and the eluent was characterised by LC-MS to detect the penetrated drug (L-carnosine).

The results demonstrated that functionalised vectors could successfully permeate the drug (L-carnosine). L-carnosine was used as a drug example. The amount of transferred drug varied depending on the type of tripeptide and fatty acid conjugation. Vectors functionalised with cationic tripeptide-palmitic acid ($CH_3(CH_2)_{14}CORRK$) exhibited the highest drug penetration (see Figure 5.5), followed by those conjugated with myristic acid ($CH_3(CH_2)_{12}CORRK$) (see Figure 5.6) and lauric acid ($CH_3(CH_2)_{10}CORRK$) (see Figure 5.7). This is attributed to the positive charge of the peptide, consisting of two arginine and one lysine, which facilitates electrostatic interactions with the ionic groups (phosphate and sulphate groups) of the endothelial cells membrane. Additionally, the lipophilic properties of the fatty acids, which increase with the number of carbon atoms, further enhance drug penetration.

Conversely, vectors functionalised with ionic tripeptides conjugated to fatty acids showed minimal drug penetration. Despite being conjugated with the same fatty acid (palmitic acid), the tripeptide contained two ionic amino acids (aspartic acid) and one lysine, resulting in a net negative charge. The deprotonated carboxylic group of aspartic acid at physiological pH (7.4) led to repulsion between the ionic groups of the cell membrane and the functionalised vectors. (See Figure 5.8)

The results of this research have similarly explored the functionalisation of liposomes with CPPs and fatty acids to enhance their stability and drug delivery capabilities. For instance, a study by Bangera *et al.* highlighted the use of polymer-lipid hybrid nanoparticles (PLHNs) modified with CPPs for targeted drug delivery, demonstrating improved cellular uptake and therapeutic efficacy.[220] This aligns with the findings of the current study, which also observed enhanced stability and functionality of liposomes upon conjugation with CPPs and fatty acids.

Additionally, research by Ouyang *et al.* reviewed the progress in molecular dynamics simulations of CPP-membrane interactions, emphasising the importance of peptide-lipid interactions in enhancing CPP-mediated delivery.[221]

The current study's findings on the increased size and altered properties of functionalised liposomes are consistent with these observations, suggesting that peptide-lipid interactions play a crucial role in modulating liposome characteristics. Furthermore, recent advances in liposomal nanotechnology have led to the development of various liposomal formulations with enhanced functionalities, such as PEGylated liposomes and ligand-targeted liposomes.[229]

These advancements underscore the potential of liposome-based systems for targeted drug delivery, supporting this research's approach of using functionalised liposomes for BBB penetration.

In conclusion, the functionalisation of liposomes with cationic and ionic tripeptide-conjugated fatty acids enhances their stability and penetration ability, consistent with recent literature on CPP-based drug delivery systems. These findings contribute to the growing body of research on liposome functionalisation for improved therapeutic applications.

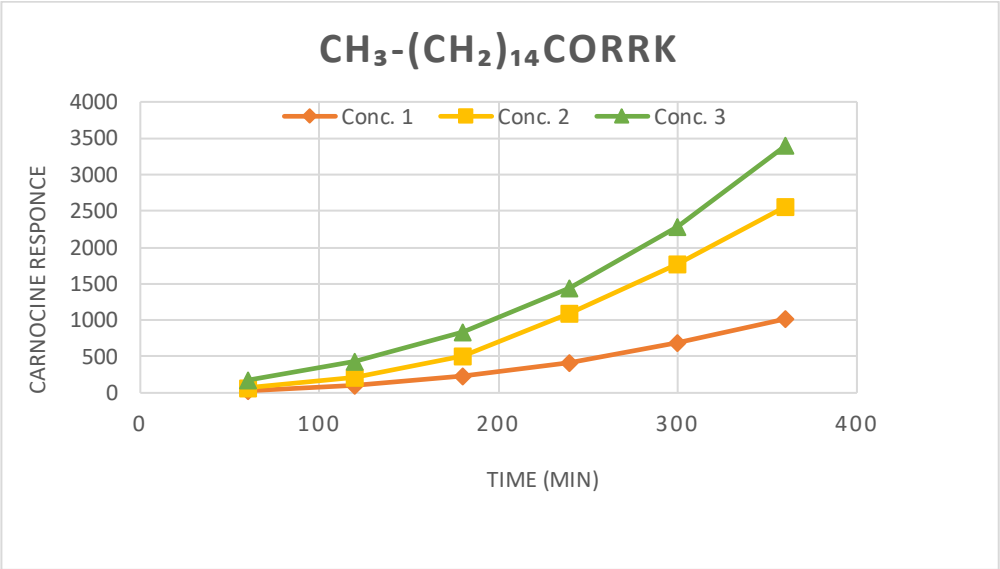

Figure 5. 5: Illustrates how L-carnosine penetrates the modulated BBB through functionalised vectors using cationic tripeptide-conjugated palmitic acid. (Three replicates).

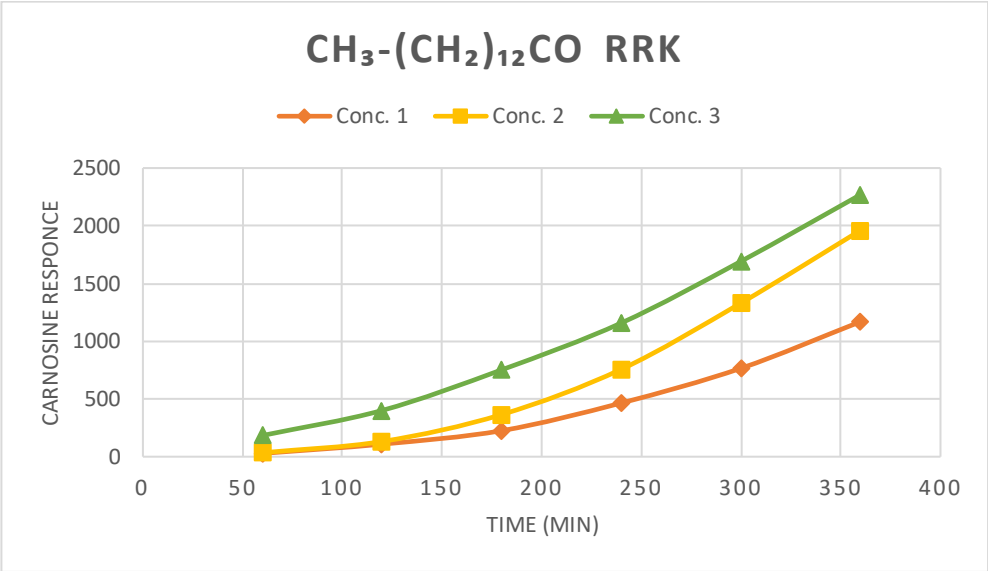

Figure 5. 6: Illustrates how L-carnosine penetrates the modulated BBB through functionalised vectors using cationic tripeptide-conjugated myristic acid. (Three replicates).

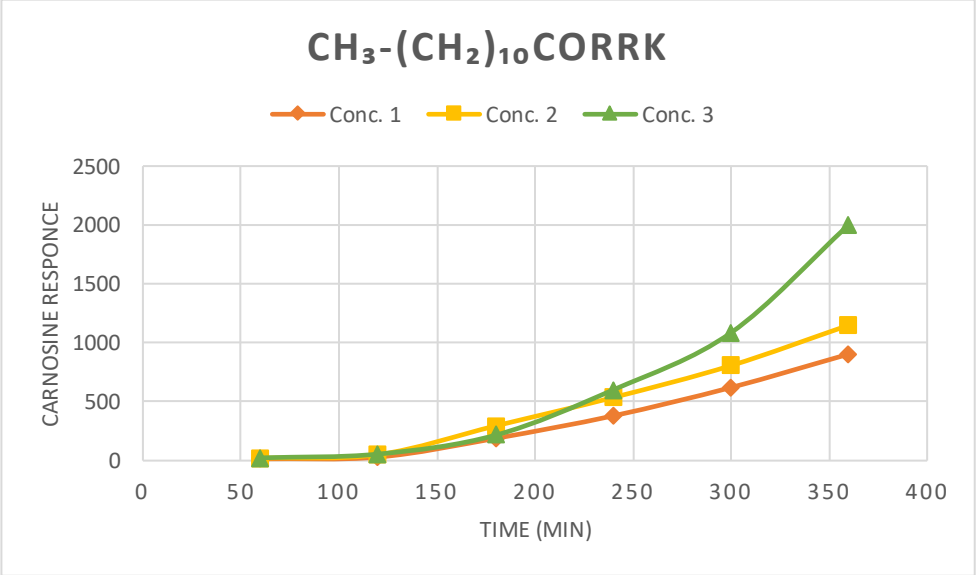

Figure 5. 7: Illustrates how L-carnosine penetrates the modulated BBB through functionalised vectors using cationic tripeptide-conjugated palmitic acid. (Three replicates).

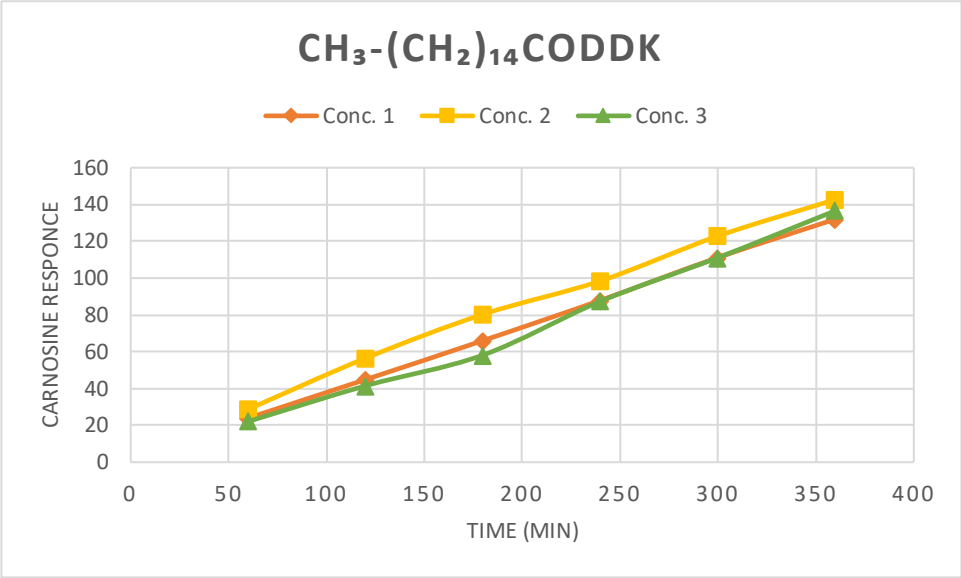

Figure 5. 8: Illustrates how L-carnosine penetrates the modulated BBB through functionalised vectors using cationic tripeptide-conjugated palmitic acid. (Three replicates)

5.6 Conclusion

This research shows that cell-penetrating peptides (CPPs) attached to fatty acids (lauric acid, myristic acid, and palmitic acid) and contained in liposomes can work well as biocompatible delivery vectors. When tested at different concentrations, liposomal formulations showed low toxicity and high cell viability in endothelial cells that line the blood-brain barrier. The results are in line with previous research, which showed that CPP-based delivery systems that include fatty acids are more stable, effective, and less harmful to cells.

Under physiological pH (*ca.* 7.4), the amino group at the end of the lysine side chain and guanidinium at the end arginine side chain can accept a proton (H^+), becoming NH_3^+. This protonation imparts a positive charge to lysine and arginine, enabling them to form electrostatic interactions with negatively charged molecules of the endothelial cell membrane. This interaction enhances the peptide's ability to cross the membrane, making it more effective in reaching its target within the cells. Ultimately, this strategic design allows for

improved therapeutic delivery and efficacy of the peptide. Lysine is essential for protein synthesis, enzyme function, and the production of hormones and antibodies. Additionally, it plays a crucial role in calcium absorption and collagen formation, which are important for brain health and function.[230] These functions highlight lysine's significance not only in basic biological processes but also in maintaining overall health, particularly in supporting cognitive functions. By facilitating these essential roles, lysine contributes to the body's ability to respond effectively to various physiological demands. Due to their highly penetrating character, attributed to their strong positive charge and high affinity for the ionic charge of the cell membrane, these peptides exhibit significant cell-penetrating capabilities. This means that the unique properties of these peptides allow them to easily enter cells, enhancing their potential therapeutic applications. Their ability to navigate cell membranes effectively makes them valuable in targeting and influencing cellular functions.

The results show that CPP-coupled fatty acids can be used in a variety of therapeutic settings and are both safe and effective as drug delivery systems. The research highlights the necessity of optimising the composition of vectors embedded with CPPs coupled with fatty acids to enhance their biocompatibility and treatment transfer efficacy.

The human blood-brain barrier endothelial cells (hCMEC/D3) became less viable over time as different concentrations of the vectors were added. This decline in cell viability suggests that the vectors may have a cytotoxic effect, which is important to evaluate when considering their potential therapeutic applications. Understanding this interaction is essential for optimising vector formulations for safe and effective use in targeting the blood-brain barrier. However, the ionic peptide that was used had two glutamic acid residues and one lysine residue. The presence of these specific amino acids may influence the interaction between the peptide and the cellular environment, potentially affecting

the vector's efficiency and toxicity. Therefore, examining the molecular composition of the peptide could provide insights into enhancing its delivery properties while minimising cytotoxicity. It was also linked to palmitic acid and then put inside the liposomes. The lysine residue reduced the negative charge of the glutamic acid residues, while the presence of palmitic acid enhanced their hydrophobicity. This alteration in charge and increased hydrophobicity can improve the stability and delivery of the peptide within liposomal structures. Consequently, these modifications could lead to more effective vector applications while reducing unwanted side effects. After putting it in the liposomes and putting it on the hCMEC/D3, the viability percentage went down. The rate was 60% after 24 hours, 40% after 48 hours, and 30% after 72 hours. These results proved that the ionic peptides, even coupled with fatty acids and embedded in the liposomes, are toxic to the endothelial cells. This decline in viability indicates that the ionic peptides may have detrimental effects on cell health despite their potential for enhancing drug delivery. Such toxicity must be carefully considered when evaluating the overall effectiveness of these vector applications in therapeutic settings.

Additionally, due to their acidic nature at the physiological pH (*ca.* 7.4), they acquire a negative charge. The blood-brain barrier makes it much harder for these negatively charged tripeptides, which are made up of ionic amino acids, to get to the brain compared to other tripeptides that contain cationic amino acids. This difficulty in crossing the BBB limits the availability of ionic tripeptides in the brain, potentially affecting their physiological roles.

Chapter 6: Conclusion

6.1 Conclusion:

The study was able to make liposomal vectors embedded with CPPs attached to fatty acids like lauric acid, myristic acid, and palmitic acid, and encapsulated with carnosine as a drug molecule.

Nanotechnology-based approaches, including using nanoparticles, liposomes, and cell-penetrating peptides, have shown promise in improving drug stability and targeting efficacy. Cell-penetrating peptides are a promising way to improve drug delivery across cellular membranes, especially when it comes to treating disorders of the central nervous system. This study showed that CPPs, specifically polyarginine peptides, may help move drug molecules, like carnosine, across the blood-brain barrier. The ability of CPPs to undergo receptor-independent cellular internalisation (electrostatic interaction) and their adaptability to different therapeutic settings underscore their versatility and potential to overcome biological barriers. Using CPPs in electrostatic interaction makes them even more useful for getting medicines across the BBB. This opens up new ways to treat neurological diseases like Alzheimer's and Parkinson's disease.

CPPs, particularly those containing cationic amino acids such as arginine and lysine, have demonstrated the ability to permeate the BBB *via* electrostatic interaction with the cell membrane. The electrostatic interactions between the positively charged peptides and the negatively charged endothelial cell membranes are crucial for this process. The study successfully synthesised and characterised several cationic peptides, confirming their potential for drug delivery applications. The study's findings align with previous research, confirming that fatty acid modifications improve the stability and permeability of CPPs, making them effective vectors for drug delivery. As a result, the modification of CPPs with fatty acids presents a

significant advancement in the field of drug delivery, providing a robust platform for the development of novel therapeutic strategies aimed at targeting the brain.

This research also explored the synthesis of ionic tripeptides as controls, revealing their inability to penetrate the BBB due to their negative charge. This finding underscores the importance of peptide charge in determining BBB permeability. The study also demonstrated the toxicity of ionic peptides, even when combined with fatty acids and embedded into liposomes. This shows how important it is to carefully consider peptide properties when designing drug delivery systems.

In addition, adding fluorophores to CPPs made it easier to see and track how peptides were distributed within endothelial cells, which gave us important information about how they moved.

Furthermore, using the microfluidic system to make liposomes allowed us to produce liposomes with stable and controlled sizes, which was proved by their low polydispersity (*ca.* 0.09), which made them even more useful as drug delivery vehicles. Dynamic light scattering and scanning electron microscopy confirmed that the liposomes, formed from a combination of L-phosphatidylcholine and cholesterol, were approximately 100 nm in size, and their polydispersity (*ca.* 0.1).

Also, this study proved that it is possible to put rhodamine B dye inside liposomes using a microfluidic system. This indicates the potential application of this method in drug encapsulation. Fluorescence microscopy validated the ability of the rhodamine B dye to move freely within liposomes and endothelial cells, underscoring its suitability for tracking and visualisation in biological environments, but it cannot be used instead of drugs to encapsulate into liposomes. Despite the successful encapsulation, the study discovered that the aqueous core of the liposomes was unable to effectively retain rhodamine B dye due to its small size and amphoteric properties, which caused it to move towards areas of its low concentration. This finding emphasises the

need for further optimisation of encapsulation techniques to enhance the stability and retention of therapeutic agents in liposomes.

This research explored the embedding of fluorophore-conjugated cell-penetrating peptides within liposomes. The fluorophore-CPP-fatty acid complexes were successfully synthesised and characterised, demonstrating clear fluorescence and proper embedding within the liposomes. The stability of these embedded liposomes was monitored, revealing a significant increase in size over time, which highlights the importance of optimising storage conditions to maintain liposome integrity.

Size exclusion chromatography was used to purify the fluorophore-CPP-fatty acid-embedded liposomes, ensuring the removal of unembedded molecules and contaminants. Fluorescence microscopy showed that these purified liposomes worked well when applied to endothelial cells. This suggests that CPPs could be used to deliver drugs across the BBB.

Non-invasive methods, like embedding cell-penetrating peptides within liposomes, provide additional pathways for drug delivery to the brain, with the aim of treating neurological diseases, particularly Alzheimer's. These systems protect therapeutic agents from degradation and facilitate their movement across the BBB, demonstrating positive results in preclinical studies.

Toxicity assessments using the MTT assay demonstrated minimal toxicity and high cell viability, confirming the biocompatibility of these vectors. Adding fatty acids to CPPs makes them more stable, bioavailable, and able to interact with cell membranes while lowering their cytotoxicity, which is in line with previous research.

However, the study also highlighted the limitations of using negatively charged peptides, such as those containing glutamic acid, which, according to the results of the MTT assay, exhibited moderate cytotoxicity due to repulsion between the negatively charged cell

membrane and the peptide. This underscores the importance of optimising peptide compositions to improve biocompatibility and efficacy.

In conclusion, this study has helped us learn more about how drugs get across the BBB. It shows that CPPs attached to fatty acids embedded in liposomes can be used as safe and effective delivery vectors.

6.2 Future work

Future studies should focus on optimising peptide properties, liposomes, and delivery methods to maximise efficacy and minimise toxicity, thereby facilitating the advancement of safe and effective drug delivery systems for clinical applications, especially for targeted drug delivery to the brain.

Subsequent research should focus on investigating the in vivo effectiveness and safety of these delivery vectors to enhance their therapeutic significance. (See Figure 6.1)

Focused ultrasound can achieve this by opening the BBB of the hippocampus, a specific location in the brain where the main reasons for Alzheimer's disease, which are plaques and tau protein grow.

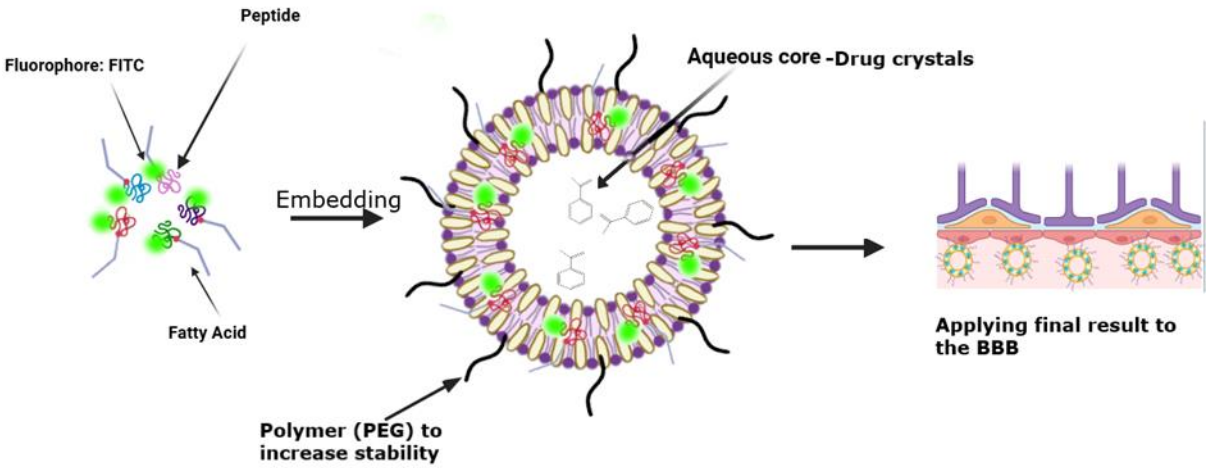

Figure 6.1: Illustrates an embedded liposome composed of peptide-fatty acid-fluorophore (FITC) directed at the blood-brain barrier. (The image created by BioRender.)

6.3 Reference

1 J. D. Steinmetz, K. M. Seeher, N. Schiess, E. Nichols, B. Cao, C. Servili, V. Cavallera, E. Cousin, H. Hagins, M. E. Moberg, M. L. Mehlman, Y. H. Abate, J. Abbas, M. A. Abbasi, M. Abbasian, H. Abbastabar, M. Abdelmasseh, M. Abdollahi, M. Abdollahi, M.-A. Abdollahifar, R. Abd-Rabu, D. M. Abdulah, A. Abdullahi, A. Abedi, V. Abedi, R. A. Abeldańo Zuńiga, H. Abidi, O. Abiodun, R. G. Aboagye, H. Abolhassani, V. Aboyans, W. A. Abrha, A. Abualhasan, E. Abu-Gharbieh, S. Aburuz, L. H. Adamu, I. Y. Addo, O. M. Adebayo, V. Adekanmbi, T. A. Adekiya, W. Adikusuma, Q. E. S. Adnani, S. Adra, T. Afework, A. A. Afolabi, A. Afraz, S. Afzal, S. Aghamiri, A. Agodi, W. Agyemang-Duah, B. O. Ahinkorah, A. Ahmad, D. Ahmad, S. Ahmad, A. M. Ahmadzade, A. Ahmed, A. Ahmed, H. Ahmed, J. Q. Ahmed, L. A. Ahmed, M. B. Ahmed, S. A. Ahmed, M. Ajami, B. Aji, O. Ajumobi, S. E. Akade, M. Akbari, H. Akbarialiabad, S. Akhlaghi, K. Akinosoglou, R. O. Akinyemi, M. Akonde, S. M. Al Hasan, F. Alahdab, T. M. A. AL-Ahdal, R. M. Al-amer, M. Albashtawy, M. T. AlBataineh, K. A. Aldawsari, H. Alemi, S. Alemi, A. M. Algammal, A. A. S. Al-Gheethi, F. A. N. Alhalaiqa, R. K. Alhassan, A. Ali, E. A. Ali, L. Ali, M. U. Ali, M. M. Ali, R. Ali, S. Ali, S. S. S. Ali, Z. Ali, S. M. Alif, Y. Alimohamadi, A. A. Aliyi, M. Aljofan, S. M. Aljunid, S. Alladi, J. U. Almazan, S. Almustanyir, B. Al-Omari, J. S. Alqahtani, I. Alqasmi, A. Y. Alqutaibi, R. Al-Shahi Salman, Z. Altaany, J. A. Al-Tawfiq, K. A. Altirkawi, N. Alvis-Guzman, Y. M. Al-Worafi, H. Aly, S. Aly, K. H. Alzoubi, R. Amani, A. Amindarolzarbi, S. Amiri, M. H. Amirzade-Iranaq, H. Amu, D. A. Amugsi, G. A. Amusa, J. Amzat, R. Ancuceanu, D. Anderlini, D. B. Anderson, C. L. Andrei, S. Androudi, D. Angappan, T. W. Angesom, A. Anil, A. Ansari-Moghaddam, R. Anwer, M. Arafat, A. Y. Aravkin, D. Areda, H. Ariffin, H. Arifin, M. Arkew, J. Ärnlöv, M. Arooj, A. A. Artamonov, K. D. Artanti, R. T. Aruleba, A. A. Asadi-

Pooya, T. F. Asena, M. Asghari-Jafarabadi, M. Ashraf, T. Ashraf, K. A. Atalell, S. S. Athari, B. T. T. Atinafu, P. Atorkey, M. M. W. Atout, A. Atreya, A. Aujayeb, A. Avan, B. P. Ayala Quintanilla, H. Ayatollahi, O. O. Ayinde, S. M. Ayyoubzadeh, S. Azadnajafabad, Z. Azizi, K. Azizian, A. Y. Azzam, M. Babaei, M. Badar, A. D. Badiye, S. Baghdadi, S. Bagherieh, R. Bai, A. A. Baig, S. Balakrishnan, S. Balalla, O. C. Baltatu, M. Banach, S. Bandyopadhyay, I. Banerjee, M. F. Baran, M. A. Barboza, M. Barchitta, M. Bardhan, S. L. Barker-Collo, T. W. Bärnighausen, A. Barrow, D. Bashash, H. Bashiri, H. A. Bashiru, A. Basiru, J. D. Basso, S. Basu, A.-M. M. Batiha, K. Batra, B. T. Baune, N. Bedi, A. Begde, T. Begum, B. Behnam, A. H. Behnoush, M. Beiranvand, Y. Béjot, A. Bekele, M. A. Belete, U. I. Belgaumi, M. Bemanalizadeh, R. G. Bender, B. Benfor, D. A. Bennett, I. M. Bensenor, B. Berice, P. J. G. Bettencourt, K. A. Beyene, A. Bhadra, D. S. Bhagat, K. Bhangdia, N. Bhardwaj, P. Bhardwaj, A. Bhargava, S. Bhaskar, A. N. Bhat, V. Bhat, G. K. Bhatti, J. S. Bhatti, R. Bhatti, A. Bijani, B. Bikbov, M. M. Bilalaga, A. Biswas, S. Bitaraf, V. R. Bitra, T. Bjørge, V. Bodolica, A. O. Bodunrin, A. Boloor, D. Braithwaite, C. Brayne, H. Brenner, A. Briko, M. L. Bringas Vega, J. Brown, C. M. Budke, D. Buonsenso, K. Burkart, R. A. Burns, Y. Bustanji, M. H. Butt, N. S. Butt, Z. A. Butt, L. S. Cabral, F. L. Caetano dos Santos, D. Calina, I. R. Campos-Nonato, C. Cao, H. Carabin, R. Cárdenas, G. Carreras, A. F. Carvalho, C. A. Castañeda-Orjuela, A. Casulli, F. Catalá-López, A. L. Catapano, A. Caye, L. Cegolon, M. Cenderadewi, E. Cerin, P. R. Chacón-Uscamaita, J. S. K. Chan, G. S. Chanie, J. Charan, V. K. Chattu, E. Chekol Abebe, H. Chen, J. Chen, G. Chi, F. Chichagi, S. B. Chidambaram, R. Chimoriya, P. R. Ching, A. Chitheer, Y. Y. Chong, H. Chopra, S. G. Choudhari, E. K. Chowdhury, R. Chowdhury, H. Christensen, D.-T. Chu, I. S. Chukwu, E. Chung, K. Coberly, A. Columbus, J. Comachio, J. Conde, P. A. Cortesi, V. M. Costa, R. A. S. Couto, M. H. Criqui, N. Cruz-Martins, M. A. Dabbagh Ohadi, S. Dadana, O. Dadras, X. Dai, Z. Dai, E. D’Amico,

H. A. Danawi, L. Dandona, R. Dandona, A. H. Darwish, S. Das, S. Das, A. M. Dascalu, N. R. Dash, M. Dashti, F. P. De la Hoz, A. de la Torre-Luque, D. De Leo, F. E. Dean, A. Dehghan, A. Dehghan, H. Dejene, D. Demant, A. K. Demetriades, S. Demissie, X. Deng, H. D. Desai, V. G. C. Devanbu, K. Dhama, S. D. Dharmaratne, M. Dhimal, D. Dias da Silva, D. Diaz, M. Dibas, D. D. Ding, M. Dinu, M. A. Dirac, M. Diress, T. C. Do, T. H. P. Do, K. D. K. Doan, M. Dodangeh, M. F. Doheim, K. G. Dokova, D. Dongarwar, H. L. Dsouza, J. Dube, S. Duraisamy, O. C. Durojaiye, S. Dutta, A. M. Dziedzic, H. A. Edinur, N. Eissazade, M. Ekholuenetale, T. C. Ekundayo, N. El Nahas, I. El Sayed, M. A. Elahi Najafi, I. Elbarazi, N. M. Elemam, F. J. Elgar, I. Y. Elgendy, H. R. Elhabashy, M. Elhadi, L. T. Elilo, R. G. Ellenbogen, O. A. A. Elmeligy, M. A. Elmonem, M. Elshaer, I. Elsohaby, M. Emamverdi, T. I. Emeto, M. Endres, C. I. Esezobor, S. Eskandarieh, A. Fadaei, A. F. Fagbamigbe, A. Fahim, A. Faramarzi, J. Fares, M. Farjoud Kouhanjani, A. Faro, F. Farzadfar, A. Fatehizadeh, M. Fathi, S. Fathi, S. A. F. Fatima, A. Feizkhah, S.-M. Fereshtehnejad, A. J. Ferrari, N. Ferreira, G. Fetensa, N. Firouraghi, F. Fischer, A. C. Fonseca, L. M. Force, A. Fornari, B. Foroutan, T. Fukumoto, M. A. Gadanya, A. M. Gaidhane, Y. Galali, N. Galehdar, Q. Gan, A. P. Gandhi, B. Ganesan, W. M. Gardner, N. Garg, S.-Y. Gau, R. K. Gautam, T. Gebre, M. Gebrehiwot, G. G. Gebremeskel, H. G. Gebreslassie, L. Getacher, B. Ghaderi Yazdi, F. Ghadirian, F. Ghaffarpasand, R. Ghanbari, M. Ghasemi, R. M. Ghazy, S. Ghimire, A. Gholami, A. Gholamrezanezhad, E. Ghotbi, S. Ghozy, A. Gialluisi, P. S. Gill, L. M. Glasstetter, E. V Gnedovskaya, A. Golchin, M. Golechha, P. Goleij, D. Golinelli, M. Gomes-Neto, A. C. Goulart, A. Goyal, R. J. Gray, M. Grivna, H. A. Guadie, B. Guan, G. Guarducci, S. Guicciardi, D. A. Gunawardane, H. Guo, B. Gupta, R. Gupta, S. Gupta, V. B. Gupta, V. K. Gupta, R. A. Gutiérrez, F. Habibzadeh, V. Hachinski, R. Haddadi, M. Hadei, N. R. Hadi, N. Haep, T. G. Haile, A. Haj-Mirzaian, B. J. Hall, R. Halwani, S. Hameed, M. Hamiduzzaman, A. Hammoud, H. Han,

N. Hanifi, G. J. Hankey, Md. A. Hannan, J. Hao, H. Harapan, H. E. Hareru, A. Hargono, N. I. Harlianto, J. M. Haro, N. N. Hartman, A. I. Hasaballah, F. Hasan, H. Hasani, M. Hasanian, A. Hassan, S. Hassan, S. Hassanipour, H. Hassankhani, M. B. Hassen, J. Haubold, S. I. Hay, K. Hayat, M. I. Hegazy, G. Heidari, M. Heidari, R. Heidari-Soureshjani, H. Hesami, K. Hezam, Y. Hiraike, H. J. Hoffman, R. Holla, K. P. Hopf, N. Horita, M. M. Hossain, Md. B. Hossain, S. Hossain, H. Hosseinzadeh, M. Hosseinzadeh, S. Hostiuc, C. Hu, J. Huang, Md. N. Huda, J. Hussain, N. R. Hussein, H.-H. Huynh, B.-F. Hwang, S. E. Ibitoye, M. Ilaghi, O. S. Ilesanmi, I. M. Ilic, M. D. Ilic, M. Immurana, F. Iravanpour, S. M. S. Islam, F. Ismail, H. Iso, G. Isola, M. Iwagami, C. C. D. Iwu, M. Iyer, A. Jaan, L. Jacob, F. Jadidi-Niaragh, M. Jafari, M. Jafarinia, A. Jafarzadeh, K. Jahankhani, N. Jahanmehr, H. Jahrami, A. Jaiswal, M. Jakovljevic, R. D. G. Jamora, S. Jana, N. Javadi, S. Javed, S. Javeed, S. K. Jayapal, S. Jayaram, H. Jiang, C. O. Johnson, W. D. Johnson, M. Jokar, J. B. Jonas, A. Joseph, N. Joseph, C. E. Joshua, M. Jürisson, A. Kabir, Z. Kabir, G. G. Kabito, V. Kadashetti, F. Kafi, R. Kalani, F. Kalantar, F. Kaliyadan, A. Kamath, S. Kamath, T. Kanchan, A. Kandel, H. Kandel, K. K. Kanmodi, M. Karajizadeh, J. Karami, S. D. Karanth, I. M. Karaye, A. Karch, A. Karimi, H. Karimi, A. Karimi Behnagh, H. Kasraei, N. J. Kassebaum, J. H. Kauppila, H. Kaur, N. Kaur, G. A. Kayode, F. Kazemi, L. Keikavoosi-Arani, C. Keller, M. Keykhaei, M. A. Khadembashiri, Y. S. Khader, M. A. Khafaie, H. Khajuria, A. Khalaji, F. Khamesipour, M. Khammarnia, M. Khan, M. A. Khan, Y. H. Khan, M. Z. Khan Suheb, S. Khanmohammadi, T. Khanna, K. Khatab, H. Khatatbeh, M. M. Khatatbeh, S. Khateri, M. N. Khatib, H. R. Khayat Kashani, M. S. Khonji, F. khorashadizadeh, M. Khormali, J. Khubchandani, S. Kian, G. Kim, J. Kim, M. S. Kim, Y. J. Kim, R. W. Kimokoti, A. Kisa, S. Kisa, M. Kivimäki, S. Kochhar, A.-A. Kolahi, K. N. Koly, F. Kompani, W. J. Koroshetz, S. Kosen, M. Kourosh Arami, A. Koyanagi, M. A. Kravchenko, K. Krishan, V. Krishnamoorthy, B.

Kuate Defo, M. A. Kuddus, A. Kumar, G. A. Kumar, M. Kumar, N. Kumar, N. B. Kumsa, S. Kundu, M. D. Kurniasari, D. Kusuma, A. Kuttikkattu, H. H. Kyu, C. La Vecchia, M. A. Ladan, C. Lahariya, T. Laksono, D. K. Lal, T. Lallukka, J. Lám, F. H. Lami, I. Landires, B. Langguth, S. Lasrado, K. Latief, K. Latifinaibin, K. M.-M. Lau, M. B. Laurens, B. K. Lawal, L. K. D. Le, T. T. T. Le, C. Ledda, M. Lee, S. Lee, S. W. Lee, W.-C. Lee, Y. H. Lee, M. Leonardi, T. L. Lerango, M.-C. Li, W. Li, V. S. Ligade, S. S. Lim, C. Linehan, C. Liu, J. Liu, W. Liu, C.-H. Lo, W. D. Lo, S. W. Lobo, G. Logroscino, G. Lopes, P. D. Lopukhov, L. Lorenzovici, S. Lorkowski, J. A. Loureiro, J. Lubinda, G. Lucchetti, R. Lutzky Saute, Z. F. Ma, M. Mabrok, M. Machoy, F. Madadizadeh, M. Magdy Abd El Razek, A. A. Maghazachi, N. Maghbouli, S. Mahjoub, M. Mahmoudi, A. Majeed, J. N. Malagón-Rojas, E. Malakan Rad, K. Malhotra, A. A. Malik, I. Malik, T. H. Mallhi, D. C. Malta, A. Manilal, V. Mansouri, M. A. Mansournia, B. P. Marasini, H. R. Marateb, S. F. Maroufi, J. Martinez-Raga, S. Martini, F. R. Martins-Melo, M. Martorell, W. März, R. R. Marzo, J. Massano, Y. Mathangasinghe, E. Mathews, R. J. Maude, A. Maugeri, P. K. Maulik, M. Mayeli, M. Mazaheri, C. McAlinden, J. J. McGrath, J. K. Meena, M. M. Mehndiratta, M. A. M. Mendez-Lopez, W. Mendoza, O. Mendoza-Cano, R. G. Menezes, M. Merati, A. Meretoja, A. Merkin, A. M. Mersha, T. Mestrovic, T. Mi, T. Miazgowski, I. M. Michalek, E. T. Mihretie, L. H. N. Minh, R. Mirfakhraie, A. Mirica, E. M. Mirrakhimov, M. Mirzaei, A. Misganaw, S. Misra, P. Mithra, B. A. Mizana, A. Mohamadkhani, N. S. Mohamed, E. Mohammadi, H. Mohammadi, S. Mohammadi, S. Mohammadi, M. Mohammadshahi, M. Mohammed, S. Mohammed, S. Mohammed, S. Mohan, H. Mojiri-forushani, N. Moka, A. H. Mokdad, S. Molinaro, H. Möller, L. Monasta, M. Moniruzzaman, F. Montazeri, M. Moradi, Y. Moradi, M. Moradi-Lakeh, P. Moraga, N. Morovatdar, S. D. Morrison, A. Mosapour, J. F. Mosser, E. Mossialos, M. Motaghinejad, P. Mousavi, S. E. Mousavi, S. Mubarik, L. Muccioli, F. Mughal, G. D. Mukoro, A. Mulita, F. Mulita, F. Musaigwa,

A. Mustafa, G. Mustafa, S. Muthu, A. J. Nagarajan, P. Naghavi, G. R. Naik, F. Nainu, T. S. Nair, H. H. R. Najmuldeen, N. Nakhostin Ansari, G. Nambi, H. Namdar Areshtanab, S. Nargus, B. R. Nascimento, A. Y. Naser, A. J. J. Nashwan, H. Nasoori, A. Nasreldein, Z. S. Natto, J. Nauman, B. P. Nayak, A. Nazri-Panjaki, M. Negaresh, H. Negash, I. Negoi, R. I. Negoi, S. M. Negru, S. A. Nejadghaderi, M. H. Nematollahi, O. D. Nesbit, C. R. J. Newton, D. H. Nguyen, H. T. H. Nguyen, H. Q. Nguyen, N.-T. T. Nguyen, P. T. Nguyen, V. T. Nguyen, R. K. Niazi, T. K. Nikolouzakis, V. Niranjan, L. A. Nnyanzi, E. A. Noman, N. Noroozi, B. Norrving, J. J. Noubiap, C. A. Nri-Ezedi, G. Ntaios, V. Nuńez-Samudio, D. Nurrika, B. Oancea, I. A. Odetokun, M. J. O'Donnell, R. E. Ogunsakin, J. O. Oguta, I.-H. Oh, H. Okati-Aliabad, S. R. Okeke, A. P. Okekunle, O. C. Okonji, P. G. Okwute, A. T. Olagunju, M. T. Olaiya, M. D. Olana, M. I. Olatubi, G. M. M. Oliveira, I. I. Olufadewa, B. O. Olusanya, A. Omar Bali, S. Ong, O. E. Onwujekwe, M. Ordak, A. U. Orji, D. V Ortega-Altamirano, U. L. Osuagwu, N. Otstavnov, S. S. Otstavnov, A. Ouyahia, M. O. Owolabi, M. P. P A, K. Pacheco-Barrios, J. R. Padubidri, P. K. Pal, P. N. Palange, C. Palladino, R. Palladino, R. F. Palma-Alvarez, F. Pan, D. Panagiotakos, S. Panda-Jonas, A. Pandey, A. Pandey, J. D. Pandian, H. U. Pangaribuan, I. Pantazopoulos, S. Pardhan, P. P. Parija, R. R. Parikh, S. Park, A. Parthasarathi, A. Pashaei, J. Patel, S. Patil, D. Patoulias, S. Pawar, P. Pedersini, U. Pensato, D. M. Pereira, J. Pereira, M. O. Pereira, M. F. P. Peres, N. Perico, S. Perna, I.-R. Petcu, F. E. Petermann-Rocha, H. T. Pham, M. R. Phillips, G. D. Pinilla-Monsalve, M. A. Piradov, E. Plotnikov, D. Poddighe, B. Polat, R. Poluru, C. D. Pond, G. R. Poudel, A. Pouramini, A. M. Pourbagher-Shahri, M. Pourfridoni, N. Pourtaheri, P. Y. Prakash, S. Prakash, V. Prakash, E. J. S. Prates, N. Pritchett, H. Purnobasuki, N. H. Qasim, I. Qattea, G. Qian, V. Radhakrishnan, P. Raee, H. Raeisi Shahraki, I. Rafique, A. Raggi, P. R. Raghav, M. M. Rahati, F. Rahim, Z. Rahimi, M. Rahimifard, M. O. Rahman, M. H. U. Rahman, M. Rahman, M. A.

Rahman, A. M. Rahmani, S. Rahmani, H. Rahmani Youshanlouei, M. Rahmati, S. Raj Moolambally, A. Rajabpour-Sanati, H. Ramadan, S. K. Ramasamy, P. Ramasubramani, S. Ramazanu, N. Rancic, I. R. Rao, S. J. Rao, D. Rapaka, V. Rashedi, A. M. Rashid, M.-M. Rashidi, M. Rashidi Alavijeh, A. Rasouli-Saravani, S. Rawaf, C. Razo, E. M. M. Redwan, A. Rekabi Bana, G. Remuzzi, N. Rezaei, N. Rezaei, N. Rezaei, M. Rezaeian, T. G. Rhee, A. Riad, S. R. Robinson, M. Rodrigues, J. A. B. Rodriguez, L. Roever, E. L. B. Rogowski, M. Romoli, L. Ronfani, P. Roy, K. Roy Pramanik, E. Rubagotti, M. A. Ruiz, T. C. Russ, K. S Sunnerhagen, A. M. A. Saad, Z. Saadatian, K. Saber, M. SaberiKamarposhti, S. Sacco, B. Saddik, E. Sadeghi, S. Sadeghian, U. Saeed, U. Saeed, M. Safdarian, S. Z. Safi, R. Sagar, D. Sagoe, F. Saheb Sharif-Askari, N. Saheb Sharif-Askari, A. Sahebkar, S. S. Sahoo, M. A. Sahraian, S. A. Sajedi, J. W. Sakshaug, M. A. Saleh, H. Salehi Omran, M. R. Salem, S. Salimi, H. Samadi Kafil, S. Samadzadeh, S. Samargandy, Y. L. Samodra, V. P. Samuel, A. M. Samy, N. Sanadgol, R. K. Sanjeev, F. Sanmarchi, D. F. Santomauro, I. N. Santri, M. M. Santric-Milicevic, A. Saravanan, A. Sarveazad, M. Satpathy, M. Saylan, M. Sayyah, N. Scarmeas, M. P. Schlaich, A. Schuermans, M. Schwarzinger, D. C. Schwebel, S. Selvaraj, A. K. Sendekie, P. Sengupta, S. Senthilkumaran, D. Serban, M. T. Sergindo, Y. Sethi, S. SeyedAlinaghi, A. Seylani, M. Shabani, M. Shabany, M. Shafie, S. Shahabi, A. Shahbandi, S. Shahid, F. Shahraki-Sanavi, H. R. Shahsavari, M. J. Shahwan, M. A. Shaikh, K. Shaji, S. Sham, A. T. T. Shama, M. A. Shamim, M. Shams-Beyranvand, M. A. Shamsi, M. Shanawaz, M. Sharath, S. Sharfaei, A. Sharifan, M. Sharma, R. Sharma, B. B. Shashamo, M. Shayan, R. A. Sheikhi, S. Shekhar, J. Shen, S. M. Shenoy, P. H. Shetty, D. S. Shiferaw, M. Shigematsu, R. Shiri, A. Shittu, K. M. Shivakumar, F. Shokri, S. Shool, S. A. Shorofi, S. Shrestha, A. B. Siankam Tankwanchi, E. E. Siddig, I. D. Sigfusdottir, J. P. Silva, L. M. L. R. Silva, E. Sinaei, B. B. Singh, G. Singh, P. Singh, S. Singh, S. B.

Sirota, S. Sivakumar, A. A. M. Sohag, R. Solanki, H. Soleimani, S. Solikhah, Y. Solomon, Y. Solomon, S. Song, Y. Song, H. Sotoudeh, M. Spartalis, B. A. Stark, J. R. Starnes, A. V Starodubova, D. J. Stein, T. J. Steiner, L. J. Stovner, M. Suleman, R. Suliankatchi Abdulkader, A. Sultana, J. Sun, D. Sunkersing, A. Sunny, H. Susianti, C. K. Swain, M. D. Szeto, R. Tabarés-Seisdedos, S. M. Tabatabaei, S. Tabatabai, M. Tabish, M. Taheri, A. Tahvildari, A. Tajbakhsh, M. Tampa, J. J. L. Tamuzi, K.-K. Tan, H. Tang, M. Tareke, I. U. Tarigan, N. Y. Tat, V. Y. Tat, R. Tavakoli Oliaee, S. M. Tavangar, A. Tavasol, Y. M. Tefera, A. Tehrani-Banihashemi, W. A. Temesgen, M.-H. Temsah, M. Teramoto, A. H. Tesfaye, E. G. Tesfaye, R. Tesler, O. Thakali, P. Thangaraju, R. Thapa, R. Thapar, N. K. Thomas, A. G. Thrift, J. H. V. Ticoalu, T. Tillawi, R. Toghroli, M. Tonelli, M. R. Tovani-Palone, E. Traini, N. M. Tran, N.-H. Tran, P. Van Tran, S. J. Tromans, T. C. Truelsen, T. T. T. T. Truyen, A. Tsatsakis, G. M. Tsegay, E. E. Tsermpini, A. R. Tualeka, D. G. Tufa, C. S. Ubah, A. J. Udoakang, I. Ulhaq, M. Umair, S. Umakanthan, K. K. Umapathi, B. Unim, B. Unnikrishnan, A. G. Vaithinathan, A. Vakilian, S. Valadan Tahbaz, R. Valizadeh, J. Van den Eynde, P. Vart, S. B. Varthya, T. J. Vasankari, S. Vaziri, B. Vellingiri, N. Venketasubramanian, G.-I. Verras, D. Vervoort, J. H. Villafańe, L. Villani, A. F. Vinueza Veloz, M. Viskadourou, S. K. Vladimirov, V. Vlassov, S. R. Volovat, L. T. Vu, I. S. Vujcic, B. Wagaye, Y. Waheed, W. Wahood, M. T. Walde, F. Wang, S. Wang, Y. Wang, Y.-P. Wang, M. Waqas, A. Waris, K. G. Weerakoon, R. G. Weintraub, A. H. Weldemariam, R. Westerman, J. L. Whisnant, D. P. Wickramasinghe, N. D. Wickramasinghe, B. Willekens, L. B. Wilner, A. S. Winkler, C. D. A. Wolfe, A.-M. Wu, S. Wulf Hanson, S. Xu, X. Xu, A. Yadollahpour, S. Yaghoubi, G. Yahya, K. Yamagishi, L. Yang, Y. Yano, Y. Yao, S. S. Yehualashet, A. Yeshaneh, M. Yesiltepe, S. Yi, A. Yiğit, V. Yiğit, D. K. Yon, N. Yonemoto, Y. You, M. Z. Younis, C. Yu, H. Yusuf, S. Zadey, M. Zahedi, F. Zakham, N. Zaki, A. Zali, G. Zamagni, R. Zand, G. G. Z. Zandieh, M. Zangiabadian, A.

Zarghami, M. S. Zastrozhin, M. G. M. Zeariya, Z. B. Zegeye, F. Zeukeng, C. Zhai, C. Zhang, H. Zhang, Y. Zhang, Z.-J. Zhang, H. Zhao, Y. Zhao, P. Zheng, H. Zhou, B. Zhu, A. Zhumagaliuly, M. Zielińska, Y. T. Zikarg, M. Zoladl, C. J. L. Murray, K. L. Ong, V. L. Feigin, T. Vos and T. Dua, Global, regional, and national burden of disorders affecting the nervous system, 1990–2021: a systematic analysis for the Global Burden of Disease Study 2021, *Lancet Neurol*, 2024, **23**, 344–381, DOI: 10.1016/ S1474-4422(24)00038-3.

2 S. U. Kim and J. de Vellis, Stem cell-based cell therapy in neurological diseases: A review, 2009, preprint, DOI: 10.1002/jnr.22054.

3 WHO, Intersectoral global action plan on epilepsy and other neurological disorders 2022-2031, https://iris.who.int/bitstream/handle/10665/371495/9789240076624-eng.pdf?sequence=1&isAllowed=y, (accessed 18 June 2024).

4 Alzheimer`s Society, The economic impact of dementia Module 1: Annual costs of dementia May 2024, https://www.alzheimers.org.uk/about-dementia/types-dementia/alzheimers-disease, (accessed 18 June 2024).

5 WHO, Optimizing brain health across the life course, https://www.who.int/publications/i/item/9789240054561, (accessed 19 June 2024).

6 V. L. Feigin, R. V. Krishnamurthi, A. M. Theadom, A. A. Abajobir, S. R. Mishra, M. B. Ahmed, K. H. Abate, M. A. Mengistie, T. Wakayo, F. Abd-Allah, A. M. Abdulle, S. F. Abera, K. E. Mohammed, G. Y. Abyu, S. W. Asgedom, T. M. Atey, B. D. Betsu, H. B. Mezgebe, K. B. Tuem, M. A. Woldu, A. N. Aichour, I. Aichour, M. T. Aichour, R. O. Akinyemi, S. Alabed, R. Al-Raddadi, N. Alvis-Guzman, A. T. Amare, H. Ansari, P. Anwari, J. Ärnlöv, S. Fereshtehnejad, E.

Weiderpass, R. Havmoeller, H. Asayesh, L. Avila-Burgos, E. F. G. A. Avokpaho, L. E. R. A. S. Afrique, M. R. Azarpazhooh, A. Barac, M. Barboza, S. L. Barker-Collo, T. Bärnighausen, M. S. Farvid, S. Mohammed, N. Bedi, E. Beghi, G. Giussani, D. A. Bennett, S. I. Hay, A. C. Goulart, I. S. Santos, I. M. Bensenor, P. A. Lotufo, A. Berhane, P. Jeemon, S. Bhaumik, L. Dandona, R. Dandona, G. A. Kumar, S. M. Birlik, S. Biryukov, D. Casey, K. J. Foreman, E. M. Goldberg, I. A. Khalil, H. H. Kyu, T. Manhertz, A. H. Mokdad, M. Naghavi, G. Nguyen, E. Nichols, M. Smith, C. J. L. Murray, G. A. Roth, J. D. Stanaway, T. Vos, R. G. Ellenbogen, M. Jakovljevic, D. L. Tirschwell, J. R. Zunt, D. J. Boneya, M. Hambisa, L. N. B. Bulto, H. Carabin, C. A. Castañeda-Orjuela, F. Catalá-López, R. Tabarés-Seisdedos, H. Chen, A. A. Chitheer, R. Chowdhury, H. Christensen, G. A. Deveber, S. D. Dharmaratne, H. P. Do, C. T. Nguyen, Q. L. Nguyen, T. H. Nguyen, V. M. Nong, K. Dokova, E. R. Dorsey, S. Eskandarieh, F. Fischer, A. Majeed, T. J. Steiner, S. Rawaf, R. Shakir, H. Shoman, J. M. Geleijnse, R. F. Gillum, P. N. Gona, H. C. Gugnani, R. Gupta, V. Hachinski, R. R. Hamadeh, G. J. Hankey, H. A. Hareri, P. Heydarpour, M. A. Sahraian, A. Kasaeian, R. Malekzadeh, G. Roshandel, S. G. Sepanlou, P. J. Hotez, M. Javanbakht, J. B. Jonas, Y. Kalkonde, A. Kandel, A. Karch, A. Kastor, M. Rahman, P. N. Keiyoro, Y. S. Khader, E. A. Khan, Y. Khang, A. T. A. Khoja, B. X. Tran, J. Khubchandani, D. Kim, Y. J. Kim, M. Kivimaki, Y. Kokubo, S. Kosen, M. Kravchenko, M. A. Piradov, Y. Y. Varakin, B. K. Defo, C. Kulkarni, R. Kumar, A. Larsson, P. M. Lavados, Y. Li, X. Liang, M. L. Liben, W. D. Lo, G. Logroscino, C. T. Loy, M. T. Mackay, A. Meretoja, C. E. I. Szoeke, H. M. Abd El Razek, L. G. Mantovani, J. Massano, M. Mazidi, C. McAlinden, S. Mehata, M. M. Mehndiratta, Z. A. Memish, W. Mendoza, G. A. Mensah, T. Wijeratne, T. R. Miller, N. Mohamed Ibrahim, A. Mohammadi, M. Moradi-Lakeh, I. M. Velasquez, K. I. Musa, J. W. Ngunjiri, D. N. A. Ningrum, B. Norrving, D. J. Stein, J. J. N. Noubiap, F. A. Ogbo, A. M. N. Renzaho, M. O. Owolabi, J. D.

Pandian, P. G. Parmar, D. M. Pereira, M. Petzold, M. R. Phillips, R. G. Poulton, F. Pourmalek, M. Qorbani, A. Rafay, R. K. Rai, S. Rajsic, A. Ranta, M. S. Rezai, E. Rubagotti, P. Sachdev, S. Safiri, R. Sahathevan, A. M. Samy, P. Santalucia, B. Sartorius, M. Satpathy, M. Sawhney, M. I. Saylan, M. A. Shaikh, M. Shamsizadeh, K. N. Sheth, M. Shigematsu, D. A. S. Silva, E. Sobngwi, L. A. Sposato, L. J. Stovner, L. J. Stovner, R. S. Abdulkader, D. Tanne, A. G. Thrift, R. Topor-Madry, T. Truelsen, K. N. Ukwaja, O. A. Uthman, T. Vasankari, N. Venketasubramanian, V. V. Vlassov, F. Wadilo, M. T. Wallin, R. Westerman, C. S. Wiysonge, C. D. Wolfe, D. Xavier, G. Xu, Y. Yano, H. H. Yimam, N. Yonemoto, C. Yu, Z. Zaidi and M. E. Zaki, Global, regional, and national burden of neurological disorders during 1990–2015: a systematic analysis for the Global Burden of Disease Study 2015, *Lancet Neurol*, DOI:10.1016/S1474-4422(17)30299-5.

7 G. Deuschl, E. Beghi, F. Fazekas, T. Varga, K. A. Christoforidi, E. Sipido, C. L. Bassetti, T. Vos and V. L. Feigin, The burden of neurological diseases in Europe: an analysis for the Global Burden of Disease Study 2017, *Lancet Public Health*, DOI:10.1016/S2468-2667(20)30190-0.

8 M. Su, T. Wang, C. Zou, K. Cao and F. Liu, Global, regional, and national burdens of Alzheimer's disease and other forms of dementia in the elderly population from 1999 to 2019: A trend analysis based on the Global Burden of Disease Study 2019, *Ibrain*, 2024, **10**, 488–499, DOI: 10.1002/ibra.12181.

9 Y. Huang, Y. Li, H. Pan and L. Han, Global, regional, and national burden of neurological disorders in 204 countries and territories worldwide, *J Glob Health*, DOI:10.7189/JOGH.13.04160.

10 D. Kumar, Y. Khader and N. Kumar Jha, *Global, regional, and national burden and attributable risk factors of neurological*

disorders: The Global Burden of Disease study 1990–2019, DOI: 10.3389/fpubh.2022.952161.

11 WHO, Global status report on the public health response to dementia, https://iris.who.int/bitstream/handle/10665/344701/9789240033245-eng.pdf?sequence=1, (accessed 19 June 2024).

12 B. O. Olusanya, A. C. Davis, D. Wertlieb, N. Y. Boo, M. K. C. Nair, R. Halpern, H. Kuper, C. Breinbauer, P. J. de Vries, M. Gladstone, N. Halfon, V. Kancherla, M. C. Mulaudzi, A. Kakooza-Mwesige, F. A. Ogbo, J. O. Olusanya, A. N. Williams, S. M. Wright, H. Manguerra, A. Smith, M. Echko, C. Ikeda, A. Liu, A. Millear, K. Ballesteros, E. Nichols, H. E. Erskine, D. Santomauro, Z. Rankin, M. Smith, H. A. Whiteford, H. E. Olsen and N. J. Kassebaum, Developmental disabilities among children younger than 5 years in 195 countries and territories, 1990–2016: a systematic analysis for the Global Burden of Disease Study 2016, *Lancet Glob Health*, 2018, **6**, e1100–e1121, DOI: 10.1016/S2214-109X(18)30309-7.

13 P. Seeman and N. Seeman, Alzheimer's disease: β-amyloid plaque formation in human brain, *Synapse*, 2011, **65**, 1289–1297, DOI: 10.1002/syn.20957.

14 R. C. Petersen and C. Kanow, *Early Diagnosis of Alzheimer's Disease: Is MCI Too Late? NIH Public Access*, 2009, vol. 6, DOI: 10.2174/156720509788929237.

15 P. Seeman and N. Seeman, Alzheimer's disease: β-amyloid plaque formation in human brain, *Synapse*, 2011, **65**, 1289–1297, DOI: 10.1002/syn.20957.

16 T. Mohamed, A. Shakeri and P. P. N. Rao, Amyloid cascade in Alzheimer's disease: Recent advances in medicinal chemistry, *Elsevier Masson SAS*, 2016, preprint, DOI: 10.1016/j.ejmech.2016.02.049.

17 Y. Huang and R. W. Mahley, Apolipoprotein E: Structure and function in lipid metabolism, neurobiology, and Alzheimer's diseases, *Academic Press Inc.*, 2014, preprint, DOI: 10.1016/j.nbd.2014.08.025.

18 Y. Huang and R. W. Mahley, Apolipoprotein E: Structure and function in lipid metabolism, neurobiology, and Alzheimer's diseases, *Academic Press Inc.*, 2014, preprint, DOI: 10.1016/j.nbd.2014.08.025.

19 J. Neugroschl and S. Wang, Alzheimer's disease: Diagnosis and treatment across the spectrum of disease severity, 2011, preprint, DOI: 10.1002/msj.20279.

20 R. Beisteiner, E. Matt, C. Fan, H. Baldysiak, M. Schönfeld, T. Philippi Novak, A. Amini, T. Aslan, R. Reinecke, J. Lehrner, A. Weber, U. Reime, C. Goldenstedt, E. Marlinghaus, M. Hallett and H. Lohse-Busch, Transcranial Pulse Stimulation with Ultrasound in Alzheimer's Disease—A New Navigated Focal Brain Therapy, *Advanced Science*, DOI:10.1002/advs.201902583.

21 S. Oshiro, M. S. Morioka and M. Kikuchi, Dysregulation of iron metabolism in Alzheimer's disease, Parkinson's disease, and amyotrophic lateral sclerosis, 2011, preprint, DOI: 10.1155/2011/378278.

22 R. Beisteiner, E. Matt, C. Fan, H. Baldysiak, M. Schönfeld, T. Philippi Novak, A. Amini, T. Aslan, R. Reinecke, J. Lehrner, A. Weber, U. Reime, C. Goldenstedt, E. Marlinghaus, M. Hallett and H. Lohse-Busch, Transcranial Pulse Stimulation with Ultrasound in Alzheimer's Disease—A New Navigated Focal Brain Therapy, *Advanced Science*, DOI:10.1002/advs.201902583.

23 A. C. Farr and M. P. Xiong, Challenges and Opportunities of Deferoxamine Delivery for Treatment of Alzheimer's Disease, Parkinson's Disease, and Intracerebral Hemorrhage, *American*

Chemical Society, 2021, preprint, DOI: 10.1021/acs.molpharmaceut.0c00474.

24 A. S. Schachter and K. L. Davis, Alzheimer's disease, *Dialogues Clin Neurosci*, 2000, **2**, 91–100, DOI: 10.31887/DCNS.2000.2.2/asschachter.

25 A. Eckert and L. Pagani, Amyloid-beta interaction with mitochondria, 2011, preprint, DOI: 10.4061/2011/925050.

26 A. K. Sahoo, J. Dandapat, U. C. Dash and S. Kanhar, Features and outcomes of drugs for combination therapy as multi-targets strategy to combat Alzheimer's disease, *Elsevier Ireland Ltd*, 2018, preprint, DOI: 10.1016/j.jep.2017.12.015.

27 J. Li, G. Wang, J. Liu, L. Zhou, M. Dong, R. Wang, X. Li, X. Li, C. Lin and Y. Niu, Puerarin attenuates amyloid-beta-induced cognitive impairment through suppression of apoptosis in rat hippocampus in vivo, *Eur J Pharmacol*, 2010, **649**, 195–201, DOI: 10.1016/j.ejphar.2010.09.045.

28 G. He, W. Luo, P. Li, C. Remmers, W. J. Netzer, J. Hendrick, K. Bettayeb, M. Flajolet, F. Gorelick, L. P. Wennogle and P. Greengard, Gamma-secretase activating protein is a therapeutic target for Alzheimer's disease, *Nature*, 2010, **467**, 95–98, DOI: 10.1038/nature09325.

29 H. He, W. Dong and F. Huang, *Anti-Amyloidogenic and Anti-Apoptotic Role of Melatonin in Alzheimer Disease*, 2010, vol. 8, DOI: 10.1007/s12035-024-04468-x.

30 C. Supnet and I. Bezprozvanny, Neuronal calcium signaling, mitochondrial dysfunction, and Alzheimer's disease, *IOS Press*, 2010, preprint, DOI: 10.3233/JAD-2010-100306.

31 E. Caballero, E. Hernando-Pérez, V. Tapias, M. Calvo-Rodríguez, C. Villalobos and L. Núñez, Amyloid Beta Oligomers-Induced Ca2+ Entry Pathways: Role of Neuronal Networks, NMDA

Receptors and Amyloid Channel Formation, *Biomedicines*, DOI:10.3390/biomedicines10051153.

32 A. D. C. Alonso, T. Zaidi, M. Novak, I. Grundke-Iqbal and K. Iqbal, *Hyperphosphorylation induces self-assembly of into tangles of paired helical filamentsstraight filaments*, 2001, DOI: 10.1073/pnas.121119298.

33 P. Zhang, S. Xu, Z. Zhu and J. Xu, Multi-target design strategies for the improved treatment of Alzheimer's disease, *Elsevier Masson SAS*, 2019, preprint, DOI: 10.1016/j.ejmech.2019.05.020.

34 F. Panza, V. Solfrizzi, D. Seripa, B. P. Imbimbo, M. Lozupone, A. Santamato, C. Zecca, M. R. Barulli, A. Bellomo, A. Pilotto, A. Daniele, A. Greco and G. Logroscino, Tau-Centric Targets and Drugs in Clinical Development for the Treatment of Alzheimer's Disease, *Hindawi Limited*, 2016, preprint, DOI: 10.1155/2016/3245935.

35 J. Avila, F. Wandosell and F. Hernández, Role of glycogen synthase kinase-3 in Alzheimer's disease pathogenesis and glycogen synthase kinase-3 inhibitors, 2010, preprint, DOI: 10.1586/ern.10.40.

36 M. Iba, J. L. Guo, J. D. McBride, B. Zhang, J. Q. Trojanowski and V. M. Y. Lee, Synthetic tau fibrils mediate transmission of neurofibrillary tangles in a transgenic mouse model of alzheimer's-like tauopathy, *Journal of Neuroscience*, 2013, **33**, 1024–1037, DOI: 10.1523/JNEUROSCI.2642-12.2013.

37 G. Shareena, D. Kumar and N. Thorat, in *Deciphering Drug Targets for Alzheimer's Disease*, 2023, DOI: 10.1007/978-981-99-2657-2_11.

38 M. Medina and J. Avila, Understanding the relationship between GSK-3 and Alzheimer's disease: A focus on how GSK-3 can

modulate synaptic plasticity processes, 2013, preprint, DOI: 10.1586/ern.13.39.

39 M. Llorens-Martín, J. Jurado, F. Hernández and J. Ávila, GSK-3β, a pivotal kinase in Alzheimer disease, 2014, preprint, DOI: 10.3389/fnmol.2014.00046.

40 B. Schaffer, M. Wiedau-Pazos and D. H. Geschwind, *Gene structure and alternative splicing of glycogen synthase kinase-3 beta (GSK-3b) in neural and non-neural tissues q*, DOI: 10.1016/S0378-1119(02)01092-2.

41 Y. Shen, M. Zhao, P. Zhao, L. Meng, Y. Zhang, G. Zhang, Y. Taishi and L. Sun, Molecular mechanisms and therapeutic potential of lithium in Alzheimer's disease: repurposing an old class of drugs, *Frontiers Media SA*, 2024, preprint, DOI: 10.3389/fphar.2024.1408462.

42 C. T. Mendes, F. B. Mury, E. De Sá Moreira, F. L. Alberto, O. V. Forlenza, E. Dias-Neto and W. F. Gattaz, Lithium reduces Gsk3b mRNA levels: Implications for Alzheimer Disease, *Eur Arch Psychiatry Clin Neurosci*, DOI:10.1007/s00406-008-0828-5.

43 J. Lewerenz and P. Maher, Chronic glutamate toxicity in neurodegenerative diseases-What is the evidence?, 2015, preprint, DOI: 10.3389/fnins.2015.00469.

44 A. Lau and M. Tymianski, Glutamate receptors, neurotoxicity and neurodegeneration, 2010, preprint, DOI: 10.1007/s00424-010-0809-1.

45 A. O. Egunlusi and J. Joubert, NMDA Receptor Antagonists: Emerging Insights into Molecular Mechanisms and Clinical Applications in Neurological Disorders, *Multidisciplinary Digital Publishing Institute (MDPI)*, 2024, preprint, DOI: 10.3390/ph17050639.

46 D. J. Newport, L. L. Carpenter, W. M. McDonald, J. B. Potash, M. Tohen and C. B. Nemeroff, Ketamine and other NMDA antagonists: Early clinical trials and possible mechanisms in depression, *American Psychiatric Association*, 2015, preprint, DOI: 10.1176/appi.ajp.2015.15040465.

47 C. Pușcașu, C. Chiriță, S. Negreș and N. M. Blebea, Exploring the Therapeutic Potential of N-Methyl-D-Aspartate Receptor Antagonists in Neuropathic Pain Management, *Multidisciplinary Digital Publishing Institute (MDPI)*, 2024, preprint, DOI: 10.3390/ijms252011111.

48 M. H. E. D. Moawad, I. Serag, I. M. Alkhawaldeh, A. Abbas, A. Sharaf, S. Alsalah, M. A. Sadeq, M. M. M. Shalaby, M. T. Hefnawy, M. Abouzid and M. Meshref, Exploring the Mechanisms and Therapeutic Approaches of Mitochondrial Dysfunction in Alzheimer's Disease: An Educational Literature Review, *Springer*, 2024, preprint, DOI: 10.1007/s12035-024-04468-y.

49 W. Wang, F. Zhao, X. Ma, G. Perry and X. Zhu, Mitochondria dysfunction in the pathogenesis of Alzheimer's disease: Recent advances, *BioMed Central Ltd.*, 2020, preprint, DOI: 10.1186/s13024-020-00376-6.

50 J. Krüger, R. Hinttala, K. Majamaa and A. M. Remes, *Mitochondrial DNA haplogroups in early-onset Alzheimer's disease and frontotemporal lobar degeneration*, 2010, DOI: 10.1186/1750-1326-5-8.

51 E. Akyuz, A. Arulsamy, F. S. Aslan, B. Sarisözen, B. Guney, A. Hekimoglu, B. N. Yilmaz, T. Retinasamy and M. F. Shaikh, An Expanded Narrative Review of Neurotransmitters on Alzheimer's Disease: The Role of Therapeutic Interventions on Neurotransmission, *Springer*, 2024, preprint, DOI: 10.1007/s12035-024-04333-y.

52 C. Wang, A. Nambiar, M. R. Strickland, C. Lee, S. Parhizkar, A. C. Moore, E. S. Musiek, J. D. Ulrich and D. M. Holtzman, APOE-ε4 synergizes with sleep disruption to accelerate Aβ deposition and Aβ-associated tau seeding and spreading, *Journal of Clinical Investigation*, DOI:10.1172/JCI169131.

53 S. D. Stites, N. M. Vogt, D. Blacker, M. Rumbaugh and M. W. Parker, Patients asking about APOE gene test results? Here's what to tell them, *Journal of Family Practice*, DOI:10.12788/jfp.0397.

54 N. Raza, A. Naseer, M. Tamoor and K. Zafar, Alzheimer Disease Classification through Transfer Learning Approach, *Diagnostics*, DOI:10.3390/diagnostics13040801.

55 N. I. on Aging (NIA), Alzheimer's Disease Genetics Fact Sheet, 2019, preprint, DOI: 10.1038/s42003-024-06242-1.

56 National Institutes of Health, Alzheimer's Disease Genetics Fact Sheet.

57 E. Greenfest-Allen, O. Valladares, P. P. Kuksa, P. Gangadharan, W. P. Lee, J. Cifello, Z. Katanic, A. B. Kuzma, N. Wheeler, W. S. Bush, Y. Y. Leung, G. Schellenberg, C. J. Stoeckert and L. S. Wang, NIAGADS Alzheimer's GenomicsDB: A resource for exploring Alzheimer's disease genetic and genomic knowledge, *Alzheimer's and Dementia*, DOI:10.1002/alz.13509.

58 C. Bellenguez, F. Küçükali, I. E. Jansen, L. Kleineidam, S. Moreno-Grau, N. Amin, A. C. Naj, R. Campos-Martin, B. Grenier-Boley, V. Andrade, P. A. Holmans, A. Boland, V. Damotte, S. J. van der Lee, M. R. Costa, T. Kuulasmaa, Q. Yang, I. de Rojas, J. C. Bis, A. Yaqub, I. Prokic, J. Chapuis, S. Ahmad, V. Giedraitis, D. Aarsland, P. Garcia-Gonzalez, C. Abdelnour, E. Alarcón-Martín, D. Alcolea, M. Alegret, I. Alvarez, V. Álvarez, N. J. Armstrong, A. Tsolaki, C. Antúnez, I. Appollonio, M. Arcaro, S. Archetti, A. A. Pastor, B. Arosio, L. Athanasiu, H. Bailly, N. Banaj, M. Baquero, S. Barral, A. Beiser, A. B. Pastor, J. E. Below, P. Benchek, L. Benussi, C. Berr,

C. Besse, V. Bessi, G. Binetti, A. Bizarro, R. Blesa, M. Boada, E. Boerwinkle, B. Borroni, S. Boschi, P. Bossù, G. Bråthen, J. Bressler, C. Bresner, H. Brodaty, K. J. Brookes, L. I. Brusco, D. Buiza-Rueda, K. Bûrger, V. Burholt, W. S. Bush, M. Calero, L. B. Cantwell, G. Chene, J. Chung, M. L. Cuccaro, Á. Carracedo, R. Cecchetti, L. Cervera-Carles, C. Charbonnier, H. H. Chen, C. Chillotti, S. Ciccone, J. A. H. R. Claassen, C. Clark, E. Conti, A. Corma-Gómez, E. Costantini, C. Custodero, D. Daian, M. C. Dalmasso, A. Daniele, E. Dardiotis, J. F. Dartigues, P. P. de Deyn, K. de Paiva Lopes, L. D. de Witte, S. Debette, J. Deckert, T. del Ser, N. Denning, A. DeStefano, M. Dichgans, J. Diehl-Schmid, M. Diez-Fairen, P. D. Rossi, S. Djurovic, E. Duron, E. Düzel, C. Dufouil, G. Eiriksdottir, S. Engelborghs, V. Escott-Price, A. Espinosa, M. Ewers, K. M. Faber, T. Fabrizio, S. F. Nielsen, D. W. Fardo, L. Farotti, C. Fenoglio, M. Fernández-Fuertes, R. Ferrari, C. B. Ferreira, E. Ferri, B. Fin, P. Fischer, T. Fladby, K. Fließbach, B. Fongang, M. Fornage, J. Fortea, T. M. Foroud, S. Fostinelli, N. C. Fox, E. Franco-Macías, M. J. Bullido, A. Frank-García, L. Froelich, B. Fulton-Howard, D. Galimberti, J. M. García-Alberca, P. García-González, S. Garcia-Madrona, G. Garcia-Ribas, R. Ghidoni, I. Giegling, G. Giorgio, A. M. Goate, O. Goldhardt, D. Gomez-Fonseca, A. González-Pérez, C. Graff, G. Grande, E. Green, T. Grimmer, E. Grünblatt, M. Grunin, V. Gudnason, T. Guetta-Baranes, A. Haapasalo, G. Hadjigeorgiou, K. L. Hamilton-Nelson, H. Hampel, O. Hanon, J. Hardy, A. M. Hartmann, L. Hausner, J. Harwood, S. Heilmann-Heimbach, S. Helisalmi, M. T. Heneka, I. Hernández, M. J. Herrmann, P. Hoffmann, C. Holmes, H. Holstege, R. H. Vilas, M. Hulsman, J. Humphrey, G. J. Biessels, X. Jian, C. Johansson, G. R. Jun, Y. Kastumata, J. Kauwe, P. G. Kehoe, L. Kilander, A. K. Ståhlbom, M. Kivipelto, A. Koivisto, J. Kornhuber, M. H. Kosmidis, W. A. Kukull, P. P. Kuksa, B. W. Kunkle, A. B. Kuzma, C. Lage, E. J. Laukka, L. Launer, A. Lauria, C. Y. Lee, J. Lehtisalo, O. Lerch, A. Lleó, W. Longstreth, O. Lopez, A. L. de Munain, S. Love, M. Löwemark, L.

Luckcuck, K. L. Lunetta, Y. Ma, J. Macías, C. A. MacLeod, W. Maier, F. Mangialasche, M. Spallazzi, M. Marquié, R. Marshall, E. R. Martin, A. M. Montes, C. M. Rodríguez, C. Masullo, R. Mayeux, S. Mead, P. Mecocci, M. Medina, A. Meggy, S. Mehrabian, S. Mendoza, M. Menéndez-González, P. Mir, S. Moebus, M. Mol, L. Molina-Porcel, L. Montrreal, L. Morelli, F. Moreno, K. Morgan, T. Mosley, M. M. Nöthen, C. Muchnik, S. Mukherjee, B. Nacmias, T. Ngandu, G. Nicolas, B. G. Nordestgaard, R. Olaso, A. Orellana, M. Orsini, G. Ortega, A. Padovani, C. Paolo, G. Papenberg, L. Parnetti, F. Pasquier, P. Pastor, G. Peloso, A. Pérez-Cordón, J. Pérez-Tur, P. Pericard, O. Peters, Y. A. L. Pijnenburg, J. A. Pineda, G. Piñol-Ripoll, C. Pisanu, T. Polak, J. Popp, D. Posthuma, J. Priller, R. Puerta, O. Quenez, I. Quintela, J. Q. Thomassen, A. Rábano, I. Rainero, F. Rajabli, I. Ramakers, L. M. Real, M. J. T. Reinders, C. Reitz, D. Reyes-Dumeyer, P. Ridge, S. Riedel-Heller, P. Riederer, N. Roberto, E. Rodriguez-Rodriguez, A. Rongve, I. R. Allende, M. Rosende-Roca, J. L. Royo, E. Rubino, D. Rujescu, M. E. Sáez, P. Sakka, I. Saltvedt, Á. Sanabria, M. B. Sánchez-Arjona, F. Sanchez-Garcia, P. S. Juan, R. Sánchez-Valle, S. B. Sando, C. Sarnowski, C. L. Satizabal, M. Scamosci, N. Scarmeas, E. Scarpini, P. Scheltens, N. Scherbaum, M. Scherer, M. Schmid, A. Schneider, J. M. Schott, G. Selbæk, D. Seripa, M. Serrano, J. Sha, A. A. Shadrin, O. Skrobot, S. Slifer, G. J. L. Snijders, H. Soininen, V. Solfrizzi, A. Solomon, Y. Song, S. Sorbi, O. Sotolongo-Grau, G. Spalletta, A. Spottke, A. Squassina, E. Stordal, J. P. Tartan, L. Tárraga, N. Tesí, A. Thalamuthu, T. Thomas, G. Tosto, L. Traykov, L. Tremolizzo, A. Tybjærg-Hansen, A. Uitterlinden, A. Ullgren, I. Ulstein, S. Valero, O. Valladares, C. Van Broeckhoven, J. Vance, B. N. Vardarajan, A. van der Lugt, J. Van Dongen, J. van Rooij, J. van Swieten, R. Vandenberghe, F. Verhey, J. S. Vidal, J. Vogelgsang, M. Vyhnalek, M. Wagner, D. Wallon, L. S. Wang, R. Wang, L. Weinhold, J. Wiltfang, G. Windle, B. Woods, M. Yannakoulia, H. Zare, Y. Zhao, X. Zhang, C. Zhu, M. Zulaica, J.

Laczo, V. Matoska, M. Serpente, F. Assogna, F. Piras, F. Piras, V. Ciullo, J. Shofany, C. Ferrarese, S. Andreoni, G. Sala, C. P. Zoia, M. Del Zompo, A. Benussi, P. Bastiani, M. Takalo, T. Natunen, T. Laatikainen, J. Tuomilehto, R. Antikainen, T. Strandberg, J. Lindström, M. Peltonen, R. Abraham, A. Al-Chalabi, N. J. Bass, C. Brayne, K. S. Brown, J. Collinge, D. Craig, P. Deloukas, N. Fox, A. Gerrish, M. Gill, R. Gwilliam, D. Harold, P. Hollingworth, J. A. Johnston, L. Jones, B. Lawlor, G. Livingston, S. Lovestone, M. Lupton, A. Lynch, D. Mann, B. McGuinness, A. McQuillin, M. C. O'Donovan, M. J. Owen, P. Passmore, J. F. Powell, P. Proitsi, M. Rossor, C. E. Shaw, A. D. Smith, H. Gurling, S. Todd, C. Mummery, N. Ryan, G. Lacidogna, A. Adarmes-Gómez, A. Mauleón, A. Pancho, A. Gailhajenet, A. Lafuente, D. Macias-García, E. Martín, E. Pelejà, F. Carrillo, I. S. Merlín, L. Garrote-Espina, L. Vargas, M. Carrion-Claro, M. Marín, M. Labrador, M. Buendia, M. D. Alonso, M. Guitart, M. Moreno, M. Ibarria, M. Periñán, N. Aguilera, P. Gómez-Garre, P. Cañabate, R. Escuela, R. Pineda-Sánchez, R. Vigo-Ortega, S. Jesús, S. Preckler, S. Rodrigo-Herrero, S. Diego, A. Vacca, F. Roveta, N. Salvadori, E. Chipi, H. Boecker, C. Laske, R. Perneczky, C. Anastasiou, D. Janowitz, R. Malik, A. Anastasiou, K. Parveen, C. Lage, S. López-García, A. Antonell, K. Y. Mihova, D. Belezhanska, H. Weber, S. Kochen, P. Solis, N. Medel, J. Lisso, Z. Sevillano, D. G. Politis, V. Cores, C. Cuesta, C. Ortiz, J. I. Bacha, M. Rios, A. Saenz, M. S. Abalos, E. Kohler, D. L. Palacio, I. Etchepareborda, M. Kohler, G. Novack, F. A. Prestia, P. Galeano, E. M. Castaño, S. Germani, C. R. Toso, M. Rojo, C. Ingino, C. Mangone, D. C. Rubinsztein, S. Teipel, N. Fievet, V. Deramerourt, C. Forsell, H. Thonberg, M. Bjerke, E. De Roeck, M. T. Martínez-Larrad, N. Olivar, N. Aguilera, A. Cano, P. Cañabate, J. Macias, O. Maroñas, R. Nuñez-Llaves, C. Olivé, E. Pelejá, A. D. Adarmes-Gómez, M. D. Alonso, G. Amer-Ferrer, M. Antequera, J. A. Burguera, F. Carrillo, M. Carrión-Claro, M. J. Casajeros, M. Martinez de Pancorbo, R. Escuela, L. Garrote-Espina, P. Gómez-

Garre, S. Hevilla, S. Jesús, M. A. L. Espinosa, A. Legaz, S. López-García, D. Macias-García, S. Manzanares, M. Marín, J. Marín-Muñoz, T. Marín, B. Martínez, V. Martínez, P. Martínez-Lage Álvarez, M. M. Iriarte, M. T. Periñán-Tocino, R. Pineda-Sánchez, D. Real de Asúa, S. Rodrigo, I. Sastre, M. P. Vicente, R. Vigo-Ortega, L. Vivancos, J. Epelbaum, D. Hannequin, D. campion, V. Deramecourt, C. Tzourio, A. Brice, B. Dubois, A. Williams, C. Thomas, C. Davies, W. Nash, K. Dowzell, A. C. Morales, M. Bernardo-Harrington, J. Turton, J. Lord, K. Brown, E. Vardy, E. Fisher, J. D. Warren, M. Rossor, N. S. Ryan, R. Guerreiro, J. Uphill, N. Bass, R. Heun, H. Kölsch, B. Schürmann, A. Lacour, C. Herold, J. A. Johnston, P. Passmore, J. Powell, Y. Patel, A. Hodges, T. Becker, D. Warden, G. Wilcock, R. Clarke, P. Deloukas, Y. Ben-Shlomo, N. M. Hooper, S. Pickering-Brown, R. Sussams, N. Warner, A. Bayer, I. Heuser, D. Drichel, N. Klopp, M. Mayhaus, M. Riemenschneider, S. Pinchler, T. Feulner, W. Gu, H. van den Bussche, M. Hüll, L. Frölich, H. E. Wichmann, K. H. Jöckel, M. Owen, S. Bahrami, I. Bosnes, P. Selnes, S. Bergh, A. Palotie, M. Daly, H. Jacob, A. Matakidou, H. Runz, S. John, R. Plenge, M. McCarthy, J. Hunkapiller, M. Ehm, D. Waterworth, C. Fox, A. Malarstig, K. Klinger, K. Call, T. Behrens, P. Loerch, T. Mäkelä, J. Kaprio, P. Virolainen, K. Pulkki, T. Kilpi, M. Perola, J. Partanen, A. Pitkäranta, R. Kaarteenaho, S. Vainio, M. Turpeinen, R. Serpi, T. Laitinen, J. Mäkelä, V. M. Kosma, U. Kujala, O. Tuovila, M. Hendolin, R. Pakkanen, J. Waring, B. Riley-Gillis, J. Liu, S. Biswas, D. Diogo, C. Marshall, X. Hu, M. Gossel, R. Graham, B. Cummings, S. Ripatti, J. Schleutker, M. Arvas, O. Carpén, R. Hinttala, J. Kettunen, A. Mannermaa, J. Laukkanen, V. Julkunen, A. Remes, R. Kälviäinen, J. Peltola, P. Tienari, J. Rinne, A. Ziemann, J. Waring, S. Esmaeeli, N. Smaoui, A. Lehtonen, S. Eaton, S. Lahdenperä, J. van Adelsberg, J. Michon, G. Kerchner, N. Bowers, E. Teng, J. Eicher, V. Mehta, P. Gormley, K. Linden, C. Whelan, F. Xu, D. Pulford, M. Färkkilä, S. Pikkarainen, A. Jussila, T. Blomster, M.

Kiviniemi, M. Voutilainen, B. Georgantas, G. Heap, F. Rahimov, K. Usiskin, T. Lu, D. Oh, K. Kalpala, M. Miller, L. McCarthy, K. Eklund, A. Palomäki, P. Isomäki, L. Pirilä, O. Kaipiainen-Seppänen, J. Huhtakangas, A. Lertratanakul, M. Hochfeld, N. Bing, J. E. Gordillo, N. Mars, M. Pelkonen, P. Kauppi, H. Kankaanranta, T. Harju, D. Close, S. Greenberg, H. Chen, J. Betts, S. Ghosh, V. Salomaa, T. Niiranen, M. Juonala, K. Metsärinne, M. Kähönen, J. Junttila, M. Laakso, J. Pihlajamäki, J. Sinisalo, M. R. Taskinen, T. Tuomi, B. Challis, A. Peterson, A. Chu, J. Parkkinen, A. Muslin, H. Joensuu, T. Meretoja, L. Aaltonen, J. Mattson, A. Auranen, P. Karihtala, S. Kauppila, P. Auvinen, K. Elenius, R. Popovic, J. Schutzman, A. Loboda, A. Chhibber, H. Lehtonen, S. McDonough, M. Crohns, D. Kulkarni, K. Kaarniranta, J. A. Turunen, T. Ollila, S. Seitsonen, H. Uusitalo, V. Aaltonen, H. Uusitalo-Järvinen, M. Luodonpää, N. Hautala, S. Loomis, E. Strauss, H. Chen, A. Podgornaia, J. Hoffman, K. Tasanen, L. Huilaja, K. Hannula-Jouppi, T. Salmi, S. Peltonen, L. Koulu, I. Harvima, Y. Wu, D. Choy, P. Pussinen, A. Salminen, T. Salo, D. Rice, P. Nieminen, U. Palotie, M. Siponen, L. Suominen, P. Mäntylä, U. Gursoy, V. Anttonen, K. Sipilä, J. W. Davis, D. Quarless, S. Petrovski, E. Wigmore, C. Y. Chen, P. Bronson, E. Tsai, Y. Huang, J. Maranville, E. Shaikho, E. Mohammed, S. Wadhawan, E. Kvikstad, M. Caliskan, D. Chang, T. Bhangale, S. Pendergrass, E. Holzinger, X. Chen, Å. Hedman, K. S. King, C. Wang, E. Xu, F. Auge, C. Chatelain, D. Rajpal, D. Liu, K. Call, T. he Xia, M. Brauer, M. Kurki, J. Karjalainen, A. Havulinna, A. Jalanko, P. Palta, P. della Briotta Parolo, W. Zhou, S. Lemmelä, M. Rivas, J. Harju, A. Lehisto, A. Ganna, V. Llorens, H. Laivuori, S. Rüeger, M. E. Niemi, T. Tukiainen, M. P. Reeve, H. Heyne, K. Palin, J. Garcia-Tabuenca, H. Siirtola, T. Kiiskinen, J. Lee, K. Tsuo, A. Elliott, K. Kristiansson, K. Hyvärinen, J. Ritari, M. Koskinen, K. Pylkäs, M. Kalaoja, M. Karjalainen, T. Mantere, E. Kangasniemi, S. Heikkinen, E. Laakkonen, C. Sipeky, S. Heron, A. Karlsson, D. Jambulingam, V. S. Rathinakannan, R. Kajanne, M. Aavikko, M. G.

Jiménez, P. della Briotta Parola, A. Lehistö, M. Kanai, M. Kaunisto, E. Kilpeläinen, T. P. Sipilä, G. Brein, G. Awaisa, A. Shcherban, K. Donner, A. Loukola, P. Laiho, T. Sistonen, E. Kaiharju, M. Laukkanen, E. Järvensivu, S. Lähteenmäki, L. Männikkö, R. Wong, H. Mattsson, T. Hiekkalinna, T. Paajanen, K. Pärn, J. Gracia-Tabuenca, E. Abner, P. M. Adams, A. Aguirre, M. S. Albert, R. L. Albin, M. Allen, L. Alvarez, L. G. Apostolova, S. E. Arnold, S. Asthana, C. S. Atwood, G. Ayres, C. T. Baldwin, R. C. Barber, L. L. Barnes, S. Barral, T. G. Beach, J. T. Becker, G. W. Beecham, D. Beekly, J. E. Below, P. Benchek, B. A. Benitez, D. Bennett, J. Bertelson, F. E. Margaret, T. D. Bird, D. Blacker, B. F. Boeve, J. D. Bowen, A. Boxer, J. Brewer, J. R. Burke, J. M. Burns, W. S. Bush, J. D. Buxbaum, N. J. Cairns, C. Cao, C. S. Carlson, C. M. Carlsson, R. M. Carney, M. M. Carrasquillo, S. Chasse, M. F. Chesselet, A. Chesi, N. A. Chin, H. C. Chui, S. Craft, P. K. Crane, D. H. Cribbs, E. A. Crocco, C. Cruchaga, M. Cullum, E. Darby, B. Davis, P. L. De Jager, C. DeCarli, J. DeToledo, M. Dick, D. W. Dickson, B. A. Dombroski, R. S. Doody, R. Duara, N. Ertekin-Taner, D. A. Evans, T. J. Fairchild, K. B. Fallon, M. R. Farlow, J. J. Farrell, V. Fernandez-Hernandez, S. Ferris, M. P. Frosch, B. Fulton-Howard, D. R. Galasko, A. Gamboa, M. Gearing, D. H. Geschwind, B. Ghetti, J. R. Gilbert, T. J. Grabowski, N. R. Graff-Radford, S. F. A. Grant, R. C. Green, J. H. Growdon, J. L. Haines, H. Hakonarson, J. Hall, R. L. Hamilton, O. Harari, L. E. Harrell, J. Haut, E. Head, V. W. Henderson, M. Hernandez, T. Hohman, L. S. Honig, R. M. Huebinger, M. J. Huentelman, C. M. Hulette, B. T. Hyman, L. S. Hynan, L. Ibanez, G. P. Jarvik, S. Jayadev, L. W. Jin, K. Johnson, L. Johnson, M. I. Kamboh, A. M. Karydas, M. J. Katz, J. A. Kaye, C. D. Keene, A. Khaleeq, R. Kim, J. Knebl, N. W. Kowall, J. H. Kramer, P. P. Kuksa, F. M. LaFerla, J. J. Lah, E. B. Larson, C. Y. Lee, E. B. Lee, A. Lerner, Y. Y. Leung, J. B. Leverenz, A. I. Levey, M. Li, A. P. Lieberman, R. B. Lipton, M. Logue, C. G. Lyketsos, J. Malamon, D. Mains, D. C. Marson, F. Martiniuk, D. C. Mash, E.

Masliah, P. Massman, A. Masurkar, W. C. McCormick, S. M. McCurry, A. N. McDavid, S. McDonough, A. C. McKee, M. Mesulam, J. Mez, B. L. Miller, C. A. Miller, J. W. Miller, T. J. Montine, E. S. Monuki, J. C. Morris, A. J. Myers, T. Nguyen, S. O'Bryant, J. M. Olichney, M. Ory, R. Palmer, J. E. Parisi, H. L. Paulson, V. Pavlik, D. Paydarfar, V. Perez, E. Peskind, R. C. Petersen, J. E. Phillips-Cremins, A. Pierce, M. Polk, W. W. Poon, H. Potter, L. Qu, M. Quiceno, J. F. Quinn, A. Raj, M. Raskind, E. M. Reiman, B. Reisberg, J. S. Reisch, J. M. Ringman, E. D. Roberson, M. Rodriguear, E. Rogaeva, H. J. Rosen, R. N. Rosenberg, D. R. Royall, M. A. Sager, M. Sano, A. J. Saykin, J. A. Schneider, L. S. Schneider, W. W. Seeley, S. H. Slifer, S. Small, A. G. Smith, J. P. Smith, Y. E. Song, J. A. Sonnen, S. Spina, P. S. George-Hyslop, R. A. Stern, A. B. Stevens, S. M. Strittmatter, D. Sultzer, R. H. Swerdlow, R. E. Tanzi, J. L. Tilson, J. Q. Trojanowski, J. C. Troncoso, D. W. Tsuang, O. Valladares, V. M. Van Deerlin, L. J. van Eldik, R. Vassar, H. V. Vinters, J. P. Vonsattel, S. Weintraub, K. A. Welsh-Bohmer, P. L. Whitehead, E. M. Wijsman, K. C. Wilhelmsen, B. Williams, J. Williamson, H. Wilms, T. S. Wingo, T. Wisniewski, R. L. Woltjer, M. Woon, C. B. Wright, C. K. Wu, S. G. Younkin, C. E. Yu, L. Yu, Y. Zhang, Y. Zhao, X. Zhu, H. Adams, R. O. Akinyemi, M. Ali, H. J. Aparicio, M. Bahadori, J. T. Becker, M. Breteler, D. Chasman, G. Chauhan, H. Comic, S. Cox, A. L. Cupples, G. Davies, C. S. DeCarli, M. G. Duperron, J. Dupuis, T. Evans, F. Fan, A. Fitzpatrick, A. E. Fohner, M. Ganguli, M. Geerlings, S. J. Glatt, H. M. Gonzalez, M. Goss, H. Grabe, M. Habes, S. R. Heckbert, E. Hofer, E. Hong, T. Hughes, T. F. Kautz, M. Knol, W. Kremen, P. Lacaze, J. Lahti, Q. Le Grand, E. Litkowski, S. Li, D. Liu, X. Liu, M. Loitfelder, A. Manning, P. Maillard, R. Marioni, B. Mazoyer, D. M. van Lent, H. Mei, A. Mishra, P. Nyquist, J. O'Connell, Y. Patel, T. Paus, Z. Pausova, K. Raikkonen-Talvitie, M. Riaz, S. Rich, J. Rotter, J. Romero, G. Roshchupkin, Y. Saba, M. Sargurupremraj, H. Schmidt, R. Schmidt, J. M. Shulman, J. Smith, H. Sekhar, R. Rajula, J. Shin,

J. Simino, E. Sliz, A. Teumer, A. Thomas, A. Tin, E. Tucker-Drob, D. Vojinovic, Y. Wang, G. Weinstein, D. Williams, K. Wittfeld, L. Yanek, Y. Yang, L. A. Farrer, B. M. Psaty, M. Ghanbari, T. Raj, P. Sachdev, K. Mather, F. Jessen, M. A. Ikram, A. de Mendonça, J. Hort, M. Tsolaki, M. A. Pericak-Vance, P. Amouyel, J. Williams, R. Frikke-Schmidt, J. Clarimon, J. F. Deleuze, G. Rossi, S. Seshadri, O. A. Andreassen, M. Ingelsson, M. Hiltunen, K. Sleegers, G. D. Schellenberg, C. M. van Duijn, R. Sims, W. M. van der Flier, A. Ruiz, A. Ramirez and J. C. Lambert, New insights into the genetic etiology of Alzheimer's disease and related dementias, *Nat Genet*, DOI:10.1038/s41588-022-01024-z.

59 M. Schreiber, T. D. Bird and D. W. Tsuang, Alzheimer's Disease Genetics, *Curr Behav Neurosci Rep*, DOI:10.1007/s40473-014-0026-x.

60 C. M. Karch, C. Cruchaga and A. M. Goate, Alzheimer's disease genetics: From the bench to the clinic, 2014, preprint, DOI: 10.1016/j.neuron.2014.05.041.

61 Y. P. Tang and E. S. Gershon, Genetic studies in Alzheimer's disease, *Dialogues Clin Neurosci*, 2003, **5**, 17–26, DOI: 10.31887/DCNS.2003.5.1/yptang.

62 X. Sun, W. D. Chen and Y. D. Wang, β-Amyloid: The key peptide in the pathogenesis of Alzheimer's disease, 2015, preprint, DOI: 10.3389/fphar.2015.00221.

63 D. Allan Butterfield and D. Boyd-Kimball, Oxidative Stress, Amyloid-β Peptide, and Altered Key Molecular Pathways in the Pathogenesis and Progression of Alzheimer's Disease, 2018, preprint, DOI: 10.3233/JAD-170543.

64 N. Dehghani, J. Bras and R. Guerreiro, How understudied populations have contributed to our understanding of Alzheimer's disease genetics, 2021, preprint, DOI: 10.1093/brain/awab028.

65 X. Li, J. Sundquist, B. Zöller and K. Sundquist, Dementia and Alzheimer's disease risks in patients with autoimmune disorders, *Geriatr Gerontol Int*, 2018, **18**, 1350–1355, DOI: 10.1111/ggi.13488.

66 C. Ho, C. Yeung, ; Shiu, L. A. Yeung and ; C Mary Schooling, *Association of autoimmune diseases with Alzheimer's disease: a Mendelian randomization study*, 2022, DOI: 10.1016/j.jpsychires.2022.09.052.

67 Y. R. Wang, X. Q. Zeng, J. Wang, C. J. Fowler, Q. X. Li, X. Le Bu, J. Doecke, P. Maruff, R. N. Martins, C. C. Rowe, C. L. Masters, Y. J. Wang and Y. H. Liu, Autoantibodies to BACE1 promote Aβ accumulation and neurodegeneration in Alzheimer's disease, *Acta Neuropathol*, 2024, **148**, 57, DOI: 10.1007/s00401-024-02814-x.

68 W. L. Klein, *A toxicity in Alzheimer's disease: globular oligomers (ADDLs) as new vaccine and drug targets*, 2002, vol. 41, DOI: 10.1016/S0197-0186(02)00050-5.

69 J. Wu and L. Li, Autoantibodies in Alzheimer's disease: Potential biomarkers, pathogenic roles, and therapeutic implications, *Nanjing Medical University and Chungbuk National University Press*, 2016, preprint, DOI: 10.7555/JBR.30.20150131.

70 N. Hansen, B. Malchow, I. Zerr, W. Stöcker, J. Wiltfang and C. Timäus, Neural cell-surface and intracellular autoantibodies in patients with cognitive impairment from a memory clinic cohort, *J Neural Transm*, DOI:10.1007/s00702-021-02316-0.

71 S. K. Garg, V. Vitvitsky, R. Albin and R. Banerjee, Astrocytic redox remodeling by amyloid beta peptide, *Antioxid Redox Signal*, 2011, **14**, 2385–2397, DOI:10.1089/ars.2010.3681.

72 H. S. Cho, L. K. Huang, Y. T. Lee, L. Chan and C. T. Hong, Suboptimal baseline serum vitamin B12 is associated with cognitive decline in people with alzheimer's disease undergoing cholinesterase inhibitor treatment, *Front Neurol*, DOI:10.3389/fneur.2018.00325.

73 S. Jatoi, D. A. Hafeez, S. U. Riaz, A. Ali, M. I. Ghauri and M. Zehra, Low Vitamin B12 Levels: An Underestimated Cause Of Minimal Cognitive Impairment And Dementia, *Cureus*, DOI:10.7759/cureus.6976.

74 M. Malakoutikhah, M. Teixidó and E. Giralt, Toward an optimal blood-brain barrier shuttle by synthesis and evaluation of peptide libraries, *J Med Chem*, 2008, **51**, 4881–4889, DOI: 10.1021/jm800156z.

75 Y. Yan, Y. Chen, Z. Liu, F. Cai, W. Niu, L. Song, H. Liang, Z. Su, B. Yu and F. Yan, Brain delivery of curcumin through low-intensity ultrasound-induced blood–brain barrier opening via lipid-plga nanobubbles, *Int J Nanomedicine*, 2021, **16**, 7433–7447, DOI: 10.2147/IJN.S327737.

76 B. Cheng, C. Bing and R. Chopra, The effect of transcranial focused ultrasound target location on the acoustic feedback control performance during blood-brain barrier opening with nanobubbles, *Sci Rep*, DOI:10.1038/s41598-019-55629-2.

77 H. Y. Huang, H. L. Liu, P. H. Hsu, C. S. Chiang, C. H. Tsai, H. S. Chi, S. Y. Chen and Y. Y. Chen, A multitheragnostic nanobubble system to induce blood-brain barrier disruption with magnetically guided focused ultrasound, *Advanced Materials*, 2015, **27**, 655–661, DOI: .

78 W. M. Pardridge, Blood-brain barrier delivery, 2007, preprint, DOI: 10.1016/j.drudis.2006.10.013.

79 R. K. Upadhyay, Drug delivery systems, CNS protection, and the blood brain barrier, *Hindawi Limited*, 2014, preprint, DOI: 10.1155/2014/869269.

80 M. Prinz, D. Erny and N. Hagemeyer, Ontogeny and homeostasis of CNS myeloid cells, *Nature Publishing Group*, 2017, preprint, DOI: 10.1038/ni.3703.

81 A. D. Greenhalgh, S. David and F. C. Bennett, Immune cell regulation of glia during CNS injury and disease, *Nature Research*, 2020, preprint, DOI: 10.1038/s41583-020-0263-9.

82 N. J. Abbott, L. Rönnbäck and E. Hansson, Astrocyte-endothelial interactions at the blood-brain barrier, 2006, preprint, DOI: 10.1038/nrn1824.

83 J. Bicker, G. Alves, A. Fortuna and A. Falcão, Blood-brain barrier models and their relevance for a successful development of CNS drug delivery systems: A review, *Elsevier B.V.*, 2014, preprint, DOI: 10.1016/j.ejpb.2014.03.012.

84 Y. Chen and L. Liu, Modern methods for delivery of drugs across the blood-brain barrier, 2012, preprint, DOI: 10.1016/j.addr.2011.11.010.

85 E. Sekerdag, in *Nanotechnology Methods for Neurological Diseases and Brain Tumors: Drug Delivery across the Blood-Brain Barrier*, Elsevier, 2017, pp. 93–102, DOI: 10.1016/B978-0-12-803796-6.00005-8.

86 K. E. Parrish, J. N. Sarkaria and W. F. Elmquist, Improving Drug Delivery to Primary and Metastatic Brain Tumors: Strategies to Overcome the Blood–Brain Barrier, *Clin Pharmacol Ther*, 2015, **97**, 336–346, DOI: 10.1002/cpt.71

87 E. Sekerdag, in *Nanotechnology Methods for Neurological Diseases and Brain Tumors: Drug Delivery across the Blood-Brain Barrier*, Elsevier, 2017, pp. 93–102, DOI: 10.1016 /B978-0-12-803796-6.00003-4.

88 C. Greene and M. Campbell, Tight junction modulation of the blood brain barrier: CNS delivery of small molecules, *Taylor and Francis Inc.*, 2016, preprint, DOI: 10.1080/21688370.2015.1138017.

89 W. M. Pardridge, Drug and gene targeting to the brain with molecular Trojan horses, 2002, preprint, DOI: 10.1038/nrd725.

90 E. A. Neuwelt, B. Bauer, C. Fahlke, G. Fricker, C. Iadecola, D. Janigro, L. Leybaert, Z. Molnár, M. E. O'Donnell, J. T. Povlishock, N. R. Saunders, F. Sharp, D. Stanimirovic, R. J. Watts and L. R. Drewes, Engaging neuroscience to advance translational research in brain barrier biology, 2011, preprint, DOI: 10.1038/nrn2995.

91 R. Daneman and M. Rescigno, The Gut Immune Barrier and the Blood-Brain Barrier: Are They So Different?, 2009, preprint, DOI: 10.1016/j.immuni.2009.09.012.

92 F. Odoardi, C. Sie, K. Streyl, V. K. Ulaganathan, C. Schläger, D. Lodygin, K. Heckelsmiller, W. Nietfeld, J. Ellwart, W. E. F. Klinkert, C. Lottaz, M. Nosov, V. Brinkmann, R. Spang, H. Lehrach, M. Vingron, H. Wekerle, C. Flügel-Koch and A. Flügel, T cells become licensed in the lung to enter the central nervous system, *Nature*, 2012, **488**, 675–679, DOI: 10.1038/nature11337.

93 S. Yamaguchi, S. Ito, T. Masuda, P.-O. Couraud and S. Ohtsuki, *Novel cyclic peptides facilitating transcellular blood-brain barrier*

transport of 1 macromolecules in vitro and in vivo 2 3, 2020, DOI: 10.1016/j.jconrel.2020.03.001.

94 Y. Chen and L. Liu, Modern methods for delivery of drugs across the blood-brain barrier, 2012, preprint, DOI: 10.1016/j.addr.2011.11.010.

95 A. Lalatsa, A. G. Schatzlein and I. F. Uchegbu, Strategies to deliver peptide drugs to the brain, *American Chemical Society*, 2014, preprint, DOI: 10.1021/mp400680d.

96 B. J. Andreone, B. W. Chow, A. Tata, B. Lacoste, A. Ben-Zvi, K. Bullock, A. A. Deik, D. D. Ginty, C. B. Clish and C. Gu, Blood-Brain Barrier Permeability Is Regulated by Lipid Transport-Dependent Suppression of Caveolae-Mediated Transcytosis, *Neuron*, 2017, **94**, 581-594.e5, DOI: 10.1016/j.neuron.2017.03.043.

97 K. Nagpal, S. K. Singh and D. N. Mishra, Drug targeting to brain: A systematic approach to study the factors, parameters and approaches for prediction of permeability of drugs across BBB, 2013, preprint, DOI: 10.1517/17425247.2013.762354.

98 W. A. Banks, Brain meets body: The blood-brain barrier as an endocrine interface, 2012, preprint, DOI: 10.1210/en.2012-1435.

99 X. Zhou, Q. R. Smith and X. Liu, Brain penetrating peptides and peptide–drug conjugates to overcome the blood–brain barrier and target CNS diseases, *John Wiley and Sons Inc*, 2021, preprint, DOI: 10.1002/wnan.1695.

100 X. Zhou, Q. R. Smith and X. Liu, Brain penetrating peptides and peptide–drug conjugates to overcome the blood–brain barrier and target CNS diseases, *John Wiley and Sons Inc*, 2021, preprint, DOI: 10.1002/wnan.1695.

101 M. H. Abraham, The factors that influence permeation across the blood-brain barrier, *Eur J Med Chem*, 2004, **39**, 235–240, DOI: 10.1016/j.ejmech.2003.12.004.

102 Y. Huang and L. Mucke, Alzheimer mechanisms and therapeutic strategies, *Elsevier B.V.*, 2012, preprint, DOI: 10.1016/j.cell.2012.02.040.

103 H. Lennernäs and E. Lundgren, Intestinal and blood-brain drug transport: Beyond involvement of a single transport function, *Elsevier Ltd*, 2004, preprint, DOI: 10.1016/j.ddtec.2004.11.010.

104 B. H. Wong, J. P. Chan, A. Cazenave-Gassiot, R. W. Poh, J. C. Foo, D. L. A. Galam, S. Ghosh, L. N. Nguyen, V. A. Barathi, S. W. Yeo, C. D. Luu, M. R. Wenk and D. L. Silver, Mfsd2a is a transporter for the essential ω-3 fatty acid docosahexaenoic acid (DHA) in eye and is important for photoreceptor cell development, *Journal of Biological Chemistry*, 2016, **291**, 10501–10514, DOI: 10.1074/jbc.M116.721340.

105 I. Brasnjevic, H. W. M. Steinbusch, C. Schmitz and P. Martinez-Martinez, Delivery of peptide and protein drugs over the blood-brain barrier, 2009, preprint, DOI: 10.1016/j.pneurobio.2008.12.002.

106 Y. Chen and L. Liu, Modern methods for delivery of drugs across the blood-brain barrier, 2012, preprint, DOI: 10.1016/j.addr.2011.11.010.

107 R. Zaragozá, Transport of Amino Acids Across the Blood-Brain Barrier, 2020, preprint, DOI: 10.3389/fphys.2020.00973.

108 V. M. Pulgar, Transcytosis to cross the blood brain barrier, new advancements and challenges, *Front Neurosci*, DOI:10.3389/fnins.2018.01019.

109 P. Bhatt and P. Narvekar, Challenges and Strategies for Drug Transport across the Blood Brain Barrier, *ARC Journal of Neuroscience*, 2018, **3**, 17–21, DOI: 10.20431/2456-057X.0303004.

110 A. S. Haqqani, K. Bélanger and D. B. Stanimirovic, Receptor-mediated transcytosis for brain delivery of therapeutics: receptor classes and criteria, *Frontiers in Drug Delivery*, DOI:10.3389/fddev.2024.1360302.

111 H. K. Alajangi, M. Kaur, A. Sharma, S. Rana, S. Thakur, M. Chatterjee, N. Singla, P. K. Jaiswal, G. Singh and R. P. Barnwal, Blood–brain barrier: emerging trends on transport models and new-age strategies for therapeutics intervention against neurological disorders, 2022, preprint, DOI: 10.1186/s13041-022-00937-4.

112 F. Hervé, N. Ghinea and J. M. Scherrmann, CNS delivery via adsorptive transcytosis, 2008, preprint, DOI: 10.1208/s12248-008-9055-2.

113 I. Brasnjevic, H. W. M. Steinbusch, C. Schmitz and P. Martinez-Martinez, Delivery of peptide and protein drugs over the blood-brain barrier, 2009, preprint, DOI: 10.1016/j.pneurobio.2008.12.002.

114 S. Bergmann, S. E. Lawler, Y. Qu, C. M. Fadzen, J. M. Wolfe, M. S. Regan, B. L. Pentelute, N. Y. R. Agar and C. F. Cho, Blood–brain-barrier organoids for investigating the permeability of CNS therapeutics, *Nat Protoc*, 2018, **13**, 2827–2843, DOI: 10.1038/s41596-018-0066-x.

115 B. Oller-Salvia, M. Sánchez-Navarro, E. Giralt and M. Teixidó, Blood-brain barrier shuttle peptides: An emerging paradigm for brain delivery, *Royal Society of Chemistry*, 2016, preprint, DOI: 10.1039/c6cs00076b.

116 B. Oller-Salvia, M. Sánchez-Navarro, E. Giralt and M. Teixidó, Blood-brain barrier shuttle peptides: An emerging paradigm for brain delivery, *Royal Society of Chemistry*, 2016, preprint, DOI: 10.1039/c6cs00076b.

117 E. M. Rhea, A. F. Logsdon, K. M. Hansen, L. M. Williams, M. J. Reed, K. K. Baumann, S. J. Holden, J. Raber, W. A. Banks and M. A. Erickson, The S1 protein of SARS-CoV-2 crosses the blood–brain barrier in mice, *Nat Neurosci*, 2021, **24**, 368–378, DOI:10.1038/s41593-020-00771-8.

118 F. González-Scarano and J. Martín-García, The neuropathogenesis of AIDS, 2005, preprint, DOI: 10.1038/nri1527.

119 S. Jain, V. Mishra, P. Singh, P. K. Dubey, D. K. Saraf and S. P. Vyas, RGD-anchored magnetic liposomes for monocytes/neutrophils-mediated brain targeting, *Int J Pharm*, 2003, **261**, 43–55, DOI: 10.1016/S0378-5173(03)00269-2.

120 T. F. Li, K. Li, Q. Zhang, C. Wang, Y. Yue, Z. Chen, S. J. Yuan, X. Liu, Y. Wen, M. Han, N. Komatsu, Y. H. Xu, L. Zhao and X. Chen, Dendritic cell-mediated delivery of doxorubicin-polyglycerol-nanodiamond composites elicits enhanced anti-cancer immune response in glioblastoma, *Biomaterials*, 2018, **181**, 35–52, DOI: 10.1016/j.biomaterials.2018.07.035.

121 R. Mooney, M. Hammad, J. Batalla-Covello, A. Abdul Majid and K. S. Aboody, Concise Review: Neural Stem Cell-Mediated Targeted Cancer Therapies, *John Wiley and Sons Ltd.*, 2018, preprint, DOI: 10.1002/sctm.18-0003.

122 M. Sarah, S. Bovenberg, M. H. Degeling and B. A. Tannous, Advances in stem cell therapy against gliomas, DOI:10.1016/j.molmed.

123 M. Demeule, A. Régina, J. Jodoin, A. Laplante, C. Dagenais, F. Berthelet, A. Moghrabi and R. Béliveau, *Drug transport to the brain: Key roles for the efflux pump P-glycoprotein in the blood-brain barrier*, DOI: 10.1016/S1537-1891(02)00201-X.

124 E. Gil-Martins, D. J. Barbosa, V. Silva, F. Remião and R. Silva, Dysfunction of ABC transporters at the blood-brain barrier: Role

in neurological disorders, *Elsevier Inc.*, 2020, preprint, DOI: 10.1016/j.pharmthera.2020.107554.

125 J. Ke, C. Yu, S. Li, Y. Hong, Y. Xu, K. Wang, T. Meng, Y. Ping, Q. Fu, H. Yuan and F. Hu, Combining Multifunctional Delivery System with Blood–Brain Barrier Reversible Opening Strategy for the Enhanced Treatment of Alzheimer's Disease, *Adv Healthc Mater*, DOI:10.1002/adhm.202302939.

126 X. Zhou, Q. R. Smith and X. Liu, Brain penetrating peptides and peptide–drug conjugates to overcome the blood–brain barrier and target CNS diseases, *John Wiley and Sons Inc*, 2021, preprint, DOI: 10.1002/wnan.1695.

127 M. Pirhaghi, F. Mamashli, F. Moosavi-Movahedi, P. Arghavani, A. Amiri, B. Davaeil, M. Mohammad-Zaheri, Z. Mousavi-Jarrahi, D. Sharma, Ü. Langel, D. E. Otzen and A. A. Saboury, Cell-Penetrating Peptides: Promising Therapeutics and Drug-Delivery Systems for Neurodegenerative Diseases, 2024, preprint, DOI: 10.1021/acs.molpharmaceut.3c01167.

128 H. Chen, A. A. Brayman, W. Kreider, M. R. Bailey and T. J. Matula, Observations of translation and jetting of ultrasound-activated microbubbles in mesenteric microvessels, *Ultrasound Med Biol*, 2011, **37**, 2139–2148, DOI: 10.1016/j.ultrasmedbio.2011.09.013.

129 I. de Cock, E. Zagato, K. Braeckmans, Y. Luan, N. de Jong, S. C. de Smedt and I. Lentacker, Ultrasound and microbubble mediated drug delivery: acoustic pressure as determinant for uptake via membrane pores or endocytosis, *J Control Release*, 2015, **197**, 20–28, DOI: 10.1016/j.jconrel.2014.10.031.

130 K. H. Song, B. K. Harvey and M. A. Borden, State-of-the-art of microbubble-assisted blood-brain barrier disruption, *Ivyspring International Publisher*, 2018, preprint, DOI: 10.7150/thno.26869.

131 A. Alonso, E. Reinz, J. W. Jenne, M. Fatar, H. Schmidt-Glenewinkel, M. G. Hennerici and S. Meairs, Reorganization of gap junctions after focused ultrasound blood-brain barrier opening in the rat brain, *Journal of Cerebral Blood Flow and Metabolism*, 2010, **30**, 1394–1402, DOI: 10.1038/jcbfm.2010.41.

132 B. Krasovitski and E. Kimmel, Shear stress induced by a gas bubble pulsating in an ultrasonic field near a wall, *IEEE Trans Ultrason Ferroelectr Freq Control*, 2004, **51**, 973–979, DOI: 10.1109/TUFFC.2004.1324401.

133 G. Samiotaki, F. Vlachos, Y. S. Tung and E. E. Konofagou, A quantitative pressure and microbubble-size dependence study of focused ultrasound-induced blood-brain barrier opening reversibility in vivo using MRI, *Magn Reson Med*, 2012, **67**, 769–777, DOI: 10.1002/mrm.23063..

134 K. H. Song, B. K. Harvey and M. A. Borden, State-of-the-art of microbubble-assisted blood-brain barrier disruption, *Ivyspring International Publisher*, 2018, preprint, DOI: 10.7150/thno.26869.

135 A. Rahman, M. A. Hossen, M. F. I. Chowdhury, S. Bari, N. Tamanna, S. S. Sultana, S. N. Haque, A. Al Masud and K. M. Saif-Ur-Rahman, Aducanumab for the treatment of Alzheimer's disease: a systematic review, 2023, preprint, DOI: 10.1111/psyg.12944.

136 A. Varadharajan, A. D. Davis, A. Ghosh, T. Jagtap, A. Xavier, A. J. Menon, D. Roy, S. Gandhi and T. Gregor, Guidelines for pharmacotherapy in Alzheimer's disease – A primer on FDA-approved drugs, 2023, preprint, DOI: 10.25259/JNRP_356_2023.

137 H. Sugimoto, Y. Iimura, Y. Yamanishi and K. Yamatsu, *Synthesis and Structure-Activity Relationships of Acetylcholinesterase Inhibitors: l-Benzyl-4-[(5,6-dimethoxy-l-oxoindan-2-yl)methyl]piperidine Hydrochloride and Related Compounds*, 1995, vol. 38, DOI: 10.1021/jm00024a009

138 R. Deshpande, Recent Advances in Approved, Withdrawn, Experimental and Investigational Drugs in Clinical Trials for Alzheimer's disease, *Medicinal & Analytical Chemistry International Journal*, DOI:10.23880/macij-16000174.

139 N. George, B. Al Sabahi, M. AbuKhader, K. Al Balushi, M. J. Akhtar and S. A. Khan, Design, synthesis and in vitro biological activities of coumarin linked 1,3,4-oxadiazole hybrids as potential multi-target directed anti-Alzheimer agents, *J King Saud Univ Sci*, DOI:10.1016/j.jksus.2022.101977.

140 M. S. Uddin, M. T. Kabir, P. Jeandet, B. Mathew, G. M. Ashraf, A. Perveen, M. N. Bin-Jumah, S. A. Mousa and M. M. Abdel-Daim, Novel anti-Alzheimer's therapeutic molecules targeting amyloid precursor protein processing, *Hindawi Limited*, 2020, preprint, DOI: 10.1155/2020/7039138.

141 C. G. Parsons, A. Stöffler and W. Danysz, Memantine: a NMDA receptor antagonist that improves memory by restoration of homeostasis in the glutamatergic system - too little activation is bad, too much is even worse, 2007, preprint, DOI: 10.1016/j.neuropharm.2007.07.013.

142 L. Devi and M. Ohno, Cognitive benefits of memantine in Alzheimer's 5XFAD model mice decline during advanced disease stages, *Pharmacol Biochem Behav*, 2016, **144**, 60–66, DOI: 10.1016/j.pbb.2016.03.002.

143 M. Pierre N. Tariot, M. Martin R. Farlow, M. George T. Grossberg, P. Stephen M. Graham, P. Scott McDonald and M. Ivan Gergel, *Memantine Treatment in Patients With Moderate to Severe Alzheimer Disease Already Receiving Donepezil*, Rochester, 2004, DOI: 10.1001/jama.291.3.317.

144 L. J6nsson, *Cost-Effectiveness of Memantine for Moderate to Severe Alzheimer's Disease in Sweden*, 2005, DOI: 10.1016/j.amjopharm.2005.05.002.

145 W. Wu, Y. Ji, Z. Wang, X. Wu, J. Li, F. Gu, Z. Chen and Z. Wang, The FDA-approved anti-amyloid-β monoclonal antibodies for the treatment of Alzheimer's disease: a systematic review and meta-analysis of randomized controlled trials, *BioMed Central Ltd*, 2023, preprint, DOI: 10.1186/s40001-023-01512-w.

146 R. Ali, G. Das Gupta and P. A. Chawla, Aducanumab: A new hope in Alzheimer's disease, *Health Sciences Review*, 2022, **4**, 100039, DOI: 10.1016/j.hsr.2022.100039.

147 S. Chowdhury and N. S. Chowdhury, Novel anti-amyloid-beta (Aβ) monoclonal antibody lecanemab for Alzheimer's disease: A systematic review, *Int J Immunopathol Pharmacol*, DOI:10.1177/03946320231209839.

148 L. Söderberg, M. Johannesson, P. Nygren, H. Laudon, F. Eriksson, G. Osswald, C. Möller and L. Lannfelt, Lecanemab, Aducanumab, and Gantenerumab — Binding Profiles to Different Forms of Amyloid-Beta Might Explain Efficacy and Side Effects in Clinical Trials for Alzheimer's Disease, *Neurotherapeutics*, 2023, **20**, 195–206, DOI:10.1007/s13311-022-01308-6 .

149 H. A. Blair, Lecanemab in Alzheimer's disease: a profile of its use, *Drugs and Therapy Perspectives*, DOI:10.1007/s40267-024-01108-2.

150 E. R. Schiller, B. D. Silverglate and G. T. Grossberg, Profiling lecanemab as a treatment option for Alzheimer's disease, *Taylor and Francis Ltd.*, 2024, preprint, DOI: 10.1080/14737175.2024.2333970.

151 A. C. Morocho López, A. A. Salgado Feijoo and V. E. Briones Morales, Eficacia y potencial de Donanemab: Nuevo Tratamiento Aprobado para el Alzheimer, *Ciencia Latina Revista Científica Multidisciplinar*, 2024, **8**, 2316–2328, DOI: 10.37811/cl_rcm.v8i5.

152 T. Song, Y. Wang, B. D. Silverglate and G. T. Grossberg, Pharmacokinetic evaluation of donanemab for the treatment of Alzheimer's, *Taylor and Francis Ltd.*, 2024, preprint, DOI: 10.1080/17425255.2024.2357637.

153 J. T. Groves, Membrane Mechanics in Living Cells, *Cell Press*, 2019, preprint, DOI: 10.1016/j.devcel.2018.12.011.

154 J. Xie, Y. Bi, H. Zhang, S. Dong, L. Teng, R. J. Lee and Z. Yang, Cell-Penetrating Peptides in Diagnosis and Treatment of Human Diseases: From Preclinical Research to Clinical Application, *Frontiers Media S.A.*, 2020, preprint, DOI: 10.3389/fphar.2020.00697.

155 G. Sharma, A. Modgil, C. Sun and J. Singh, Grafting of cell-penetrating peptide to receptor-targeted liposomes improves their transfection efficiency and transport across blood-brain barrier model, *J Pharm Sci*, 2012, **101**, 2468–2478, DOI: 10.1002/jps.23152.

156 N. Schmidt, A. Mishra, G. H. Lai and G. C. L. Wong, Arginine-rich cell-penetrating peptides, 2010, preprint, DOI: 10.1016/j.febslet.2009.11.046,
DOI: :10.1016/j.febslet.2009.11.046.

157 Y. Zhai, S. Li, H. Wang and Y. Shan, Revealing the dynamic mechanism of cell-penetrating peptides across cell membranes at the single-molecule level, *J Mater Chem B*, 2024, **12**, 5589–5593, DOI: 10.1039/d4tb00522h.

158 E. D. Timotievich, I. P. Shilovskiy and M. R. Khaitov, Cell-Penetrating Peptides as Vehicles for Delivery of Therapeutic Nucleic Acids. Mechanisms and Application in Medicine, 2023, preprint, DOI: 10.1134/S0006297923110111.

159 M. Dowaidar, Uptake pathways of cell-penetrating peptides in the context of drug delivery, gene therapy, and vaccine development, *Cell Signal*, DOI:10.1016/j.cellsig.2024.111116.

160 P. Patel, K. Benzle, D. Pei and G. L. Wang, Cell-penetrating peptides for sustainable agriculture, *Elsevier Ltd*, 2024, preprint, DOI: 10.1016/j.tplants.2024.05.011, DOI: 10.1016/j.tplants.2024.05.011.

161 I. Ruseska and A. Zimmer, Internalization mechanisms of cell-penetrating peptides, *Beilstein Journal of Nanotechnology*, 2020, **11**, 101–123, DOI: 10.3762/bjnano.11.10.

162 C. Zheng, C. Ma, E. Bai, K. Yang and R. Xu, *Transferrin and cell-penetrating peptide dual-functioned liposome for targeted drug delivery to glioma*, 2015, vol. 8, DOI: 10.1016/j.foodchem.2023.137228.

163 J. Cheng, B. A. Teply, I. Sherifi, J. Sung, G. Luther, F. X. Gu, E. Levy-Nissenbaum, A. F. Radovic-Moreno, R. Langer and O. C. Farokhzad, Formulation of functionalized PLGA-PEG nanoparticles for in vivo targeted drug delivery, *Biomaterials*, 2007, **28**, 869–876, DOI: 10.1016/j.biomaterials.2006.09.047.

164 G. Kibria, H. Hatakeyama, N. Ohga, K. Hida and H. Harashima, Dual-ligand modification of PEGylated liposomes shows better cell selectivity and efficient gene delivery, *Journal of Controlled Release*, 2011, **153**, 141–148, DOI: 10.1016/j.jconrel.2011.03.012.

165 J. Li, X. Zhang, M. Wang, X. Li, H. Mu, A. Wang, W. Liu, Y. Li, Z. Wu and K. Sun, Synthesis of a bi-functional dendrimer-based nanovehicle co-modified with RGDyC and TAT peptides for neovascular targeting and penetration, *Int J Pharm*, 2016, **501**, 112–123, DOI: 10.1016/j.ijpharm.2016.01.068.

166 P. Agrawal, S. Bhalla, S. S. Usmani, S. Singh, K. Chaudhary, G. P. S. Raghava and A. Gautam, CPPsite 2.0: A repository of experimentally validated cell-penetrating peptides, *Nucleic Acids Res*, 2016, **44**, D1098–D1103, DOI: 10.1093/nar/gkv1266.

167 D. Derossit, M. H. Joliott, G. Chassaingl and M. Prochiantztn, *THE JDWRXAL OF BioLoCteAL CHEIMMTRY The Third Helix of the Antennapedia Homeodornain Translocates through Biological ~ e m b r a n e s ~*, 1994, vol. 269, DOI: 10.1016/S0021-9258(17)34080-2.

168 L. M. Traub, Tickets to ride: Selecting cargo for clathrin-regulated internalization, 2009, preprint, DOI: 10.1038/nrm2751.

169 E. Vivès, P. Brodin and B. Lebleu, A truncated HIV-1 Tat protein basic domain rapidly translocates through the plasma membrane and accumulates in the cell nucleus, *Journal of Biological Chemistry*, 1997, **272**, 16010–16017, DOI: 10.1074/jbc.272.25.16010.

170 M. Kristensen, H. Franzyk, M. T. Klausen, A. Iversen, J. S. Bahnsen, R. B. Skyggebjerg, V. Foderà and H. M. Nielsen, Penetratin-Mediated Transepithelial Insulin Permeation: Importance of Cationic Residues and pH for Complexation and Permeation, *AAPS Journal*, 2015, **17**, 1200–1209, DOI: 10.1208/s12248-015-9747-3.

171 G. Sharma, S. Lakkadwala, A. Modgil and J. Singh, The role of cell-penetrating peptide and transferrin on enhanced delivery of drug to brain, *MDPI AG*, 2016, preprint, DOI: 10.3390/ijms17060806.

172 C. F. Cho, J. M. Wolfe, C. M. Fadzen, D. Calligaris, K. Hornburg, E. A. Chiocca, N. Y. R. Agar, B. L. Pentelute and S. E. Lawler, Blood-brain-barrier spheroids as an in vitro screening platform for brain-penetrating agents, *Nat Commun*, DOI:10.1038/ncomms15623.

173 H. Yan and F. E. Chen, Recent Progress in Solid-Phase Total Synthesis of Naturally Occurring Small Peptides, *John Wiley and Sons Inc*, 2022, preprint, DOI: 10.1002/adsc.202200079.

174 Walker, J. M. "Methods in Molecular BiologyTM Series Editor." *Life Sci* 531 (2009): 588. DOI: 10.1016/j.foodchem.2023.137228.

175 E. P. Aparna and K. S. Devaky, Advances in the Solid-Phase Synthesis of Pyrimidine Derivatives, *ACS Comb Sci*, 2019, **21**, 35–68, DOI: 10.1021/acscombsci.8b00172.

176 E. A. Reynoso-Soto and I. A. Rivero, *Synthesis of Peptides Histamine H2 Receptors in Solid-Phase Assisted by Microwave*, 2010, vol. 54, DOI: 10.3389/fphar.2015.00286.

177 G. Sabatino, A. D'Ercole, L. Pacini, M. Zini, A. Ribecai, A. Paio, P. Rovero and A. M. Papini, An Optimized Scalable Fully Automated Solid-Phase Microwave-Assisted cGMP-Ready Process for the Preparation of Eptifibatide, *Org Process Res Dev*, 2021, **25**, 552–563, DOI: 10.1021/acs.oprd.0c00490.

178 W. M. Hussein, M. Skwarczynski and I. Toth, *Peptide Synthesis Methods and Protocols Methods in Molecular Biology 2103*, DOI: 10.1007/978-1-0716-0227-0.

179 E. A. Reynoso-Soto and I. A. Rivero, *Synthesis of Peptides Histamine H2 Receptors in Solid-Phase Assisted by Microwave*, 2010, vol. 54, DOI: 10.3390/micro3040058.

180 P. V Ingle, K. G. Rathod, B. S. Gayke, G. K. Balaiya, P. B. Divekar and M. R. Waje, *ADVANCEMENTS AND CHALLENGES IN DRUG DELIVERY SYSTEMS A COMPREHENSIVE REVIEW*, 2024, vol. 12, DOI: 10.1186/1556-276X-8-102.

181 Mohammad Shoaib Shaikh Hamid, Pooja R. Hatwar, Ravindrakumar L. Bakal and Nitin B. Kohale, A comprehensive review on Liposomes: As a novel drug delivery system, *GSC*

Biological and Pharmaceutical Sciences, 2024, **27**, 199–210, DOI: 10.30574/gscbps.

182 M. Luo, B. D. Oomah, W. Akoetey, Y. Zhang, H. Daneshfozoun and F. Hosseinian, Liposomes as sustainable delivery systems in food, cosmetic, and pharmaceutical applications, *John Wiley and Sons Inc*, 2024, preprint, DOI: 10.1002/aocs.12907.

183 Rupali A. Mendake, Pooja R. Hatwar, Ravindrakumar L. Bakal, Kanchan A. Hiwe and Supriya S. Barewar, Advance and opportunities in nanoparticle drug delivery for central nervous system disorders: A review of current advances, *GSC Biological and Pharmaceutical Sciences*, 2024, **27**, 044–058, DOI: 10.30574/gscbps.2024.27.3.0222.

184 C. Chai and J. Park, Food liposomes: Structures, components, preparations, and applications, *Elsevier Ltd*, 2024, preprint, DOI: 10.1016/j.foodchem.2023.137228.

185 P. Nakhaei, R. Margiana, D. O. Bokov, W. K. Abdelbasset, M. A. Jadidi Kouhbanani, R. S. Varma, F. Marofi, M. Jarahian and N. Beheshtkhoo, Liposomes: Structure, Biomedical Applications, and Stability Parameters With Emphasis on Cholesterol, *Frontiers Media SA*, 2021, preprint, DOI: 10.3389/fbioe.2021.705886.

186 P. Santhosh, J. Genova, A. Iglič, V. Kralj-Iglič and N. P. Ulrih, Influence of cholesterol on bilayer fluidity and size distribution of liposomes, *Comptes Rendus de L'Academie Bulgare des Sciences*, 2020, **73**, 949–958, DOI: 10.7546/CRABS.2020.07.07.

187 K. A. Melzak, S. A. Melzak, E. Gizeli and J. L. Toca-Herrera, Cholesterol organization in phosphatidylcholine liposomes: A surface plasmon resonance study, *Materials*, 2012, **5**, 2306–2325, DOI: 10.3390/ma5112306.

188 S. Huláková, J. Gallová and F. Devínsky, Cholesterol protects phosphatidylcholine liposomes from N,N-dimethyl-1-

dodecanamine N-oxide influence, *Acta Chim Slov*, 2015, **62**, 420–427, DOI: 10.17344/acsi.2014.750.

189 L. W. Allahou, S. Y. Madani and A. Seifalian, Investigating the Application of Liposomes as Drug Delivery Systems for the Diagnosis and Treatment of Cancer, *Hindawi Limited*, 2021, preprint, DOI: 10.1155/2021/3041969.

190 T. Subramani and H. Ganapathyswamy, An overview of liposomal nano-encapsulation techniques and its applications in food and nutraceutical, *Springer*, 2020, preprint, DOI: 10.1007/s13197-020-04360-2.

191 L. Sercombe, T. Veerati, F. Moheimani, S. Y. Wu, A. K. Sood and S. Hua, Advances and challenges of liposome assisted drug delivery, *Frontiers Media S.A.*, 2015, preprint, DOI: 10.3389/fphar.2015.00286.

192 D. Powers and N. Nosoudi, Liposomes; from synthesis to targeting macrophages, *Biomedical Research*, DOI:10.35841/biomedicalresearch.30-19-058.

193 G. Bozzuto and A. Molinari, Liposomes as nanomedical devices, *Dove Medical Press Ltd.*, 2015, preprint, DOI: 10.2147/IJN.S68861.

194 A. Akbarzadeh, R. Rezaei-Sadabady, S. Davaran, S. W. Joo, N. Zarghami, Y. Hanifehpour, M. Samiei, M. Kouhi and K. Nejati-Koshki, Liposome: Classification, preparation, and applications, *Nanoscale Res Lett*, DOI:10.1186/1556-276X-8-102.

195 A. Bezelya, B. Küçüktürkmen and A. Bozkır, Microfluidic Devices for Precision Nanoparticle Production, *Multidisciplinary Digital Publishing Institute (MDPI)*, 2023, preprint, DOI: 10.3390/micro3040058.

196 G. Buttitta, S. Bonacorsi, C. Barbarito, M. Moliterno, S. Pompei, G. Saito, I. Oddone, G. Verdone, D. Secci and S. Raimondi,

Scalable microfluidic method for tunable liposomal production by a design of experiment approach, *Int J Pharm*, DOI:10.1016/j.ijpharm.2024.124460.

197 S. Lindsay, O. Tumolva, T. Khamiakova, H. Coppenolle, M. Kovarik, S. Shah, R. Holm and Y. Perrie, Can We Simplify Liposome Manufacturing Using a Complex DoE Approach?, *Pharmaceutics*, 2024, **16**, 1159, DOI: 10.3390/pharmaceutics16091159.

198 D. L. Vázquez-Durán, A. Ortega and A. Rodríguez, Amino Acid Transporters Proteins Involved in the Glutamate-Glutamine Cycle and Their Alterations in Murine Models of Alzheimer's Disease, *Springer*, 2024, preprint, DOI: 10.1007/s12035-024-03966-3.

199 M. K. F. Cox, E. R. Hascup, A. Bartke and K. N. Hascup, Friend or Foe? Defining the Role of Glutamate in Aging and Alzheimer's Disease, *Frontiers Media S.A.*, 2022, preprint, DOI: 10.3389/fragi.2022.929474.

200 V. N. Bukke, M. Archana, R. Villani, A. D. Romano, A. Wawrzyniak, K. Balawender, S. Orkisz, S. Beggiato, G. Serviddio and T. Cassano, The dual role of glutamatergic neurotransmission in Alzheimer's disease: From pathophysiology to pharmacotherapy, *MDPI AG*, 2020, preprint, DOI: 10.3390/ijms21207452.

201 D. Oh, A. Nasrolahi Shirazi, K. Northup, B. Sullivan, R. K. Tiwari, M. Bisoffi and K. Parang, Enhanced cellular uptake of short polyarginine peptides through fatty acylation and cyclization, *Mol Pharm*, DOI:10.1021/mp500203e.

202 K. Langel, S. Lindberg, D. Copolovici, P. Arukuusk, R. Sillard and Ü. Langel, Novel fatty acid modifications of transportan 10, *Int J Pept Res Ther*, 2010, **16**, 247–255, DOI: 10.1007/s10989-010-9224-x.

203 M. Cavaco, P. Fraga, J. Valle, R. D. M. Silva, L. Gano, J. D. G. Correia, D. Andreu, M. A. R. B. Castanho and V. Neves, Molecular

determinants for brain targeting by peptides: a meta-analysis approach with experimental validation, *Fluids Barriers CNS*, DOI:10.1186/s12987-024-00545-5.

204 S. M. Ghorai, A. Deep, D. Magoo, C. Gupta and N. Gupta, Cell-Penetrating and Targeted Peptides Delivery Systems as Potential Pharmaceutical Carriers for Enhanced Delivery across the Blood–Brain Barrier (BBB), *Multidisciplinary Digital Publishing Institute (MDPI)*, 2023, preprint, DOI: 10.3390/pharmaceutics15071999.

205 K. Langel, S. Lindberg, D. Copolovici, P. Arukuusk, R. Sillard and Ü. Langel, Novel fatty acid modifications of transportan 10, *Int J Pept Res Ther*, 2010, **16**, 247–255, DOI: 10.1007/s10989-010-9224-x.

206 W. Pham, M. F. Kircher, R. Weissleder and C. H. Tung, Enhancing membrane permeability by fatty acylation of oligoarginine peptides, *ChemBioChem*, 2004, **5**, 1148–1151, DOI: 10.1002/cbic.200400063.

207 M. M. Patel and B. M. Patel, Crossing the Blood–Brain Barrier: Recent Advances in Drug Delivery to the Brain, *CNS Drugs*, 2017, **31**, 109–133.

208 F. Zakany, I. M. Mándity, Z. Varga, G. Panyi, P. Nagy and T. Kovacs, Effect of the Lipid Landscape on the Efficacy of Cell-Penetrating Peptides, *Multidisciplinary Digital Publishing Institute (MDPI)*, 2023, preprint, DOI: 10.3390/cells12131700.

209 G. Donadio, R. Di Martino, R. Oliva, L. Petraccone, P. Del Vecchio, B. Di Luccia, E. Ricca, R. Isticato, A. Di Donato and E. Notomista, A new peptide-based fluorescent probe selective for zinc(II) and copper(II), *J Mater Chem B*, 2016, **4**, 6979–6988, DOI: 10.1039/c6tb00671j.

210 G. Buttitta, S. Bonacorsi, C. Barbarito, M. Moliterno, S. Pompei, G. Saito, I. Oddone, G. Verdone, D. Secci and S. Raimondi,

Scalable microfluidic method for tunable liposomal production by a design of experiment approach, *Int J Pharm*, DOI:10.1016/j.ijpharm.2024.124460.

211 A. Pittiu, M. Pannuzzo, L. Casula, R. Pireddu, D. Valenti, M. C. Cardia, F. Lai, A. Rosa, C. Sinico and M. Schlich, Production of liposomes by microfluidics: The impact of post-manufacturing dilution on drug encapsulation and lipid loss, *Int J Pharm*, DOI:10.1016/j.ijpharm.2024.124641.

212 S. Lindsay, O. Tumolva, T. Khamiakova, H. Coppenolle, M. Kovarik, S. Shah, R. Holm and Y. Perrie, Can We Simplify Liposome Manufacturing Using a Complex DoE Approach?, *Pharmaceutics*, 2024, **16**, 1159, DOI: 10.3390/pharmaceutics16091159.

213 T. Yamada and H. Suzuki, Microfluidics-based stable production of monodisperse giant unilamellar vesicles by oil-phase removal from double emulsion, *J Liposome Res*, DOI:10.1080/08982104.2024.2420337.

214 D. Carugo, E. Bottaro, J. Owen, E. Stride and C. Nastruzzi, Liposome production by microfluidics: Potential and limiting factors, *Sci Rep*, DOI:10.1038/srep25876.

215 A. Giannopoulos-Dimitriou, A. Saiti, A. Petrou, I. S. Vizirianakis and D. G. Fatouros, in *Liposomes in Drug Delivery: What, where, how and when to Deliver*, Elsevier, 2024, pp. 89–121, DOI: 10.1016/B978-0-443-15491-1.00022-5.

216 H. Nsairat, A. A. Ibrahim, A. M. Jaber, S. Abdelghany, R. Atwan, N. Shalan, H. Abdelnabi, F. Odeh, M. El-Tanani and W. Alshaer, Liposome bilayer stability: emphasis on cholesterol and its alternatives, *Taylor and Francis Ltd.*, 2024, preprint, DOI: 10.1080/08982104.2023.2226216.

217 P. Chowdhary, L. Mahalakshmi, S. Dutta, J. A. Moses and C. Anandharamakrishnan, in *Liposomal Encapsulation in Food*

Science and Technology, Elsevier, 2022, pp. 223–237, DOI: 10.1016/B978-0-12-823935-3.00014-X.

218 J. Shi, D. Zhao, X. Li, F. Ding, X. Tang, N. Liu, H. Huang and C. Liu, The conjugation of rhodamine B enables carrier-free mitochondrial delivery of functional proteins, *Org Biomol Chem*, 2020, **18**, 6829–6839, DOI: 10.1039/D0OB01305F.

219 P. K. Walhout, Z. He, B. Dutagaci, G. Nawrocki and M. Feig, Molecular Dynamics Simulations of Rhodamine B Zwitterion Diffusion in Polyelectrolyte Solutions, *Journal of Physical Chemistry B*, 2022, **126**, 10256–10272, DOI: 10.1021/acs.jpcb.2c06281.

220 P. D. Bangera, D. D. Kara, K. Tanvi, V. K. Tippavajhala and M. Rathnanand, Highlights on Cell-Penetrating Peptides and Polymer-Lipid Hybrid Nanoparticle: Overview and Therapeutic Applications for Targeted Anticancer Therapy, *Springer Science and Business Media Deutschland GmbH*, 2023, preprint, DOI: 10.1208/s12249-023-02576-x.

221 J. Ouyang, Y. Sheng and W. Wang, Recent Advances of Studies on Cell-Penetrating Peptides Based on Molecular Dynamics Simulations, *MDPI*, 2022, preprint, DOI: 10.3390/cells11244016.

222 Z. Cheng, H. Huang, M. Yin and H. Liu, Applications of liposomes and lipid nanoparticles in cancer therapy: current advances and prospects, *Exp Hematol Oncol*, 2025, **14**, 11, DOI: 10.1186/s40164-025-00602-1.

223 H. Yu, Y. Wang, Y. Chen, M. Cui, F. Yang, P. Wang and M. Ji, Transmissible H-aggregated NIR-II fluorophore to the tumor cell membrane for enhanced PTT and synergistic therapy of cancer, *Nano Converg*, DOI:10.1186/s40580-022-00352-4.

224 L. Porosk, P. Arukuusk, K. Põhako, K. Kurrikoff, K. Kiisholts, K. Padari, M. Pooga and Ü. Langel, Enhancement of siRNA

transfection by the optimization of fatty acid length and histidine content in the CPP, *Biomater Sci*, 2019, **7**, 4363–4374, DOI: 10.1039/c9bm00688e.

225 L. Rauch-Wirth, A. Renner, K. Kaygisiz, T. Weil, L. Zimmermann, A. A. Rodriguez-Alfonso, D. Schütz, S. Wiese, L. Ständker, T. Weil, D. Schmiedel and J. Münch, Optimized peptide nanofibrils as efficient transduction enhancers for in vitro and ex vivo gene transfer, *Front Immunol*, DOI:10.3389/fimmu.2023.1270243.

226 E. D. Timotievich, I. P. Shilovskiy and M. R. Khaitov, Cell-Penetrating Peptides as Vehicles for Delivery of Therapeutic Nucleic Acids. Mechanisms and Application in Medicine, 2023, preprint, DOI: 10.1134/S0006297923110111.

227 S. Mondal and S. Ghosh, Liposome-Mediated Anti-Viral Drug Delivery Across Blood–Brain Barrier: Can Lipid Droplet Target Be Game Changers?, *Springer*, 2024, preprint, DOI: 10.1007/s10571-023-01443-4.

228 F. Juhairiyah and E. C. M. de Lange, Understanding Drug Delivery to the Brain Using Liposome-Based Strategies: Studies that Provide Mechanistic Insights Are Essential, *Springer Science and Business Media Deutschland GmbH*, 2021, preprint, DOI: 10.1208/s12248-021-00648-z.

229 D. M. Anwar, H. Y. Hedeya, S. H. Ghozlan, B. M. Ewas and S. N. Khattab, Surface-modified lipid-based nanocarriers as a pivotal delivery approach for cancer therapy: application and recent advances in targeted cancer treatment, *Springer Science and Business Media Deutschland GmbH*, 2024, preprint, DOI: 10.1186/s43088-024-00566-x.

230 R. Zaragozá, Transport of Amino Acids Across the Blood-Brain Barrier, *Frontiers Media S.A.*, 2020, preprint, DOI: 10.3389/fphys.2020.00973.